RENORMALIZATION GROUP APPROACH TO DENSE BARYONIC MATTER

Matthias Drews
October, 2014

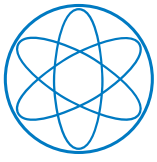

Technische Universität München

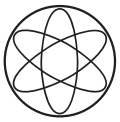

Technische Universität München
Physik Department
Institut für Theoretische Physik T39
Univ.-Prof. Dr. Wolfram Weise

RENORMALIZATION GROUP APPROACH TO DENSE BARYONIC MATTER

Matthias Johannes Drews, M. Sc.

Vollständiger Abdruck der von der Fakultät für Physik der Technischen Universität München zur Erlangung des akademischen Grades eines

Doktors der Naturwissenschaften (Dr. rer. nat.)

genehmigten Dissertation.

Vorsitzender:		Univ.-Prof. Dr. Stephan Paul
Prüfer der Dissertation:	1.	Univ.-Prof. Dr. Wolfram Weise (em.)
	2.	Univ.-Prof. Dr. Nora Brambilla

Die Dissertation wurde am 02.10.2014 bei der Technischen Universität München eingereicht und durch die Fakultät für Physik am 11.11.2014 angenommen.

This work has been supported by the BMBF, the Excellence cluster “Origin and Structure of the Universe”, the Fondazione Bruno Kessler, the TUM Graduate School, and the Wilhelm und Else Heraeus-Stiftung.

ABSTRACT

This work investigates a chiral nucleon-meson model, which is suited to analyze chiral symmetry breaking and the thermodynamics of nuclear matter at the same time. We go beyond the mean-field approximation by including pionic fluctuations in a non-perturbative way with methods of the functional renormalization group. Within the model, we can exclude a chiral phase transition for temperatures below 100 MeV and densities below about twice the nuclear saturation density. Furthermore, we extend the model to asymmetric nuclear matter and therefore obtain a description for the interior of neutron stars.

ZUSAMMENFASSUNG

In dieser Arbeit untersuchen wir ein chirales Nukleon-Meson-Modell, welches sowohl chirale Symmetriebrechung als auch die Thermodynamik von Kernmaterie beschreiben kann. Wir gehen über die Mean-Field-Näherung hinaus und berücksichtigen Pionfluktuationen auf nichtperturbative Weise im Rahmen der funktionalen Renormierungsgruppe. Innerhalb des Modells kann für Temperaturen unterhalb von 100 MeV und Dichten unter etwa der zweifachen nuklearen Sättigungsdichte ein chiraler Phasenübergang ausgeschlossen werden. Darüber hinaus weiten wir das Modell auf asymmetrische Kernmaterie aus und erhalten damit eine Beschreibung für das Innere von Neutronensternen.

PUBLICATIONS

The text of this thesis contains material which has previously been published in the articles listed below.

M. Drews, T. Hell, B. Klein, and W. Weise, "Thermodynamic phases and mesonic fluctuations in a chiral nucleon-meson model", *Phys. Rev. D.* **88** (2013) 096011, arXiv:1308.5596,

M. Drews, T. Hell, B. Klein, and W. Weise, "Dense nucleonic matter and the renormalization group", *EPJ web conf.* **66** (2014) 04008, arXiv:1307.6973,

M. Drews, W. Weise, "Functional renormalization group approach to neutron matter", *Phys. Lett. B* **738** (2014) 187–190, arXiv:1404.0882.

ACKNOWLEDGMENTS

In the first place, I would like to express my gratitude to Prof. Dr. Wolfram Weise for giving me the opportunity to write my thesis in his group. He was always open for inspiring discussions and for sharing his profound insights on nuclear physics with a former string theorist. I would further like to thank him for offering me the possibility to participate in numerous conferences all over the world and for initiating my six-months stay at the ECT* in beautiful Trento, Italy.

I am thankful to Kenji Fukushima for inviting me to the Yukawa Institute in Kyoto for a very instructive three-weeks visit in 2011. I further thank Kouji Kashiwa for inviting me to a joyful visit at the Brookhaven National Laboratory on Long Island in 2012. I also wish to thank the members of the ECT* for their warm welcome during my stay in Trento.

It is a pleasure to thank Prof. Dr. Norbert Kaiser for his helpful advice on all sorts of conceptional and practical issues during my research. I am very grateful to Thomas Hell for his support and his collaboration. Moreover, I am glad to thank my office mates, Robert Lang and Alexander Laschka, for the friendly atmosphere, which made me enjoy my stay at the TUM. I am very grateful to all my current and former colleagues at T39, in particular Michael Altenbuchinger, Nino Bratovic, Maximilian Duell, Salvatore Fiorilla, Lisheng Geng, Jeremy Holt, Bertram Klein, Stefan Petschauer, Paul Springer and Corbinian Wellenhofer for a nice and inspiring environment, many enlightening conversations on physics and for shared hours outside the office.

A very special place is reserved for my thanks to Kathrin Helmsauer for her love and support.

Last, but not least, I am indebted to express my deepest gratitude to my family for their permanent support during all these years, which made this thesis possible.

CONTENTS

1

INTRODUCTION

In January 1932, Lev Landau theorized [1] about the interior of heavy stars, a place characterized by "a violation of the law of energy", where "the laws of ordinary quantum mechanics break down", and "the density of matter becomes so great that atomic nuclei come in close contact, forming one gigantic nucleus". Whereas the two former conclusions might sound a bit premature from today's perspective, the "gigantic nucleus" is often understood as a first description of a neutron star. Remarkably, Landau's paper was developed independently and even before[1] the detection of the neutron by James Chadwick in February 1932 [3]. It took another two years until Walter Baade and Fritz Zwicky constructed the first models of neutron stars built out of actual neutrons, without altering quantum mechanics and the conservation of energy [4–7].

These days we are again in a situation where the smoke starts to clear. In the past, high-precision measurements of neutron-star masses were relatively sparse. Consequently, the interior of a neutron star was up for speculation, and a plethora of theories based on all kinds of exotic matter was on the market. But after the discovery of neutron stars as heavy as twice the mass of the sun [8, 9], paired with an extreme accuracy, theoretical considerations are strongly constrained. It turns out that conventional models – working with nucleon and meson rather than quark degrees of freedom – are in agreement with all constraints. More exotic models are either ruled out or require a substantial amount of fine tuning.

In the present thesis, we study a generalized linear sigma model of nucleons (protons and neutrons), interacting through exchange of pions and other boson fields. We include fluctuation effects in the framework of the functional renormalization group in a systematic non-perturbative way. The thermodynamic equation of state obtained in this model can be taken to describe the interior of neutron stars. This allows us to compare our results with state-of-the-art approaches such as chiral effective field theory, quantum Monte-Carlo calculations, or phenomenological models.

One aspect of the strong force as described by Quantum Chromodynamics (QCD) is chiral symmetry. At small baryon chemical potential chiral symmetry is restored at high temperatures in a crossover and not in a true phase transition. In contrast, the situation at higher baryon chemical potentials remains unclear. Many models predict a first-order transition that ends in a second-order critical endpoint. A lot of theoretical and experimental effort is put into the determination of the critical endpoint, whose existence would be a landmark in the phase-diagram of QCD. However, it is far from certain whether such a critical point exists. While we certainly cannot definitely answer this question within our model, we can still exclude the appearance of a chiral first-order phase transition in a broad region.

Another aspect of our approach concerns the question of chiral restoration in the context of neutron matter at low temperatures, which is also relevant for the description of neutron

1 See Ref. [2] for the historical backgrounds, in particular how the paper on neutron stars possibly saved Landau's life.

stars. The chiral condensate is an order parameter of chiral restoration. In chiral effective field theory it was observed that the chiral condensate in symmetric nuclear matter is stabilized at higher densities [10–13]. An important role is played by two-pion exchange processes and repulsive three-body forces, including the appearance of a virtual Δ-isobar and the action of the Pauli principle in the nucleon Fermi sea. Unfortunately, no such stabilizing mechanism is known for pure neutron matter. The condensate decreases almost linearly as a function of density [14, 15]. Already at about two to three times nuclear saturation density, the condensate drops below 20 percent of its vacuum value. These findings raise a principal question about the applicability of any chiral approach to neutron matter at higher densities. We will argue that a non-perturbative treatment of pionic fluctuations, as it is done in this work in the context of a chiral nucleon-meson model, can indeed stabilize the condensate up to much higher densities.

The thesis is organized as follows: First, in Chapter 2, we give an introduction into the many facets of QCD as the theory of strong interactions, inasmuch as they are relevant to this work. The low-energy behavior of QCD is governed by two important properties, namely confinement and chiral symmetry breaking. The symmetries and symmetry breaking patterns are investigated in detail. We extend the discussion to finite temperatures and densities, and elaborate on different approaches to study the phases of QCD. We particularly focus on cold and dense nuclear matter and its characteristic liquid-gas transition.

In Chapter 3, we take one step back and look deeper at the underlying formalism of quantum field theories. A special role is played by the low-energy effective action, as it contains the whole information about thermal and quantum fluctuations and therefore provides us with the full low-energy theory. Out of a number of approaches to compute the effective action, we focus on the functional renormalization group (FRG), which is based on an action that interpolates between the quantum action of the microscopic theory and the low-energy effective action.

Chapter 4 combines the concepts of the functional renormalization group with hadronic physics. Cold and dense matter is described in the framework of a chiral nucleon-meson model, with baryons interacting via exchange of pions and other boson fields. First, experimental and observational constraints from nuclear physics are discussed and the parameters are adjusted accordingly. After a mean-field study, the bosonic fluctuations are included within the FRG framework. The properties of symmetric nuclear matter are investigated and compared with calculations from different approaches. The model is extended to account for asymmetric nuclear matter and the liquid-gas transition is studied, as the matter under consideration becomes more and more neutron rich. In the final section, neutron star matter is analyzed. The corresponding equation of state is taken as a model for the interior of a neutron star. The mass-radius relation is analyzed, in particular with regard to the observational constraints.

Chapter 5 is reserved for a summary and an outlook to further research.

2

FROM GAUGE THEORIES TO NUCLEAR MATTER

Only four fundamental forces describe physical phenomena from subatomic scales up to astronomic distances. In the order of increasing strength, these forces are gravity, the weak force, electromagnetism, and the strong force. There exists a unified formalism – namely gauge theory – which underlies all forces. The reason why gauge theory is so important lies in the way how it combines the principle of locality with the freedom to choose a reference frame [16].

The underlying gauge theory of the strong force is Quantum Chromodynamics (QCD). A wide range of phenomena, reaching from the early universe, to nuclear physics and the interior of dense stars, is governed by QCD. The aim of this first chapter is to give a broad overview of the properties of QCD, in particular at finite temperature and density.

2.1 GRAVITY

To begin with, we will briefly illustrate the concept of gauge theories in the case of general relativity (GR). All concepts can then be applied *mutatis mutandis* to QCD as well. Our main motivation is to understand the underlying equations that describe the interior of a neutron star from a gravitational perspective. The task of nuclear physics is then to provide a good description of matter that can be fed into the equations.

To keep the main discussion short, all relevant concepts and objects that are mentioned in this overview are explained in more detail in Appendix A.2.1.

Space-time is modeled by a $(3+1)$-dimensional manifold, where at each point of the manifold a reference frame can be chosen freely. It is convenient to glue a copy of flat Minkowski space locally to each point. A change of reference frame is given by an element of the restricted Lorentz group $\mathrm{SO}^+_\uparrow(3,1)$, which acts by matrix multiplication on vectors in the internal Minkowski space. The manifold itself also comes with a notion of a local linearization, namely the tangent space. The tangent space and the internal Minkowski space can be identified with the help of the **vierbein** (or moving frame) e^I_μ, which converts space-time indices μ into Minkowski indices I. Moreover, the vierbein induces a curved metric $g_{\mu\nu}$ on the manifold from the internal flat Minkowski metric η_{IJ}.

Observers at different locations can make different choices of reference frames, but in the end, they want to collate their measurements. To that end, the **spin connection** $\omega_\mu{}^I{}_J$ allows to compare vectors X^I defined in the local Minkowski spaces. The covariant derivative of X^I is given by

$$D_\mu X^I = (\delta^I{}_J\,\partial_\mu + \omega_\mu{}^I{}_J) X^J\,. \tag{2.1}$$

Its first part describes how X^I changes as a function of space-time and its second part describes how the internal Minkowski spaces are rotated relative to each other. The vector X^I is said to be parallely transported if its covariant derivative vanishes along the path. A different choice of local reference frame is made by rotating the vierbein e by

an infinitesimal Lorentz transformation, h, which is an element of the Lie algebra $\mathfrak{so}(3,1)$ with coordinates $h_I{}^J$. Under this **gauge transformation** the connection changes as

$$\omega \to h(d+\omega)h^{-1}\,, \tag{2.2}$$

where d denotes the exterior derivative. Furthermore, the connection gives rise to the curvature tensor

$$\Omega = d\omega + \omega \wedge \omega\,, \tag{2.3}$$

where $\wedge$ denotes the wedge-product. In local coordinates, Ω has components $\Omega_{\mu\nu}{}^I{}_J$, with two internal and two space-time indices[2]. The dynamics of classical Einstein gravity can be described by the Palatini action, S_{P}, as defined in the appendix. An action for the matter part,

$$S_{\mathrm{matter}} = \int d^4x\, \mathcal{L}_{\mathrm{m}}\,, \tag{2.4}$$

is added to the Palatini action. The energy-momentum tensor,

$$T^{\mu\nu} = \frac{2}{\sqrt{-g}}\frac{\partial \mathcal{L}_{\mathrm{m}}}{\partial g_{\mu\nu}}\,, \tag{2.5}$$

follows directly from the matter action. A variation of the full action $S_{\mathrm{P}} + S_{\mathrm{matter}}$ with respect to e and ω yields **Einstein's field equations** (see, e.g., [17]):

$$R_{\mu\nu} - \frac{1}{2}g_{\mu\nu}R = 8\pi G T_{\mu\nu}\,, \tag{2.6}$$

where the Ricci tensor has components $R_{\mu\nu} = g_{\nu\rho}\,\eta^{JK}\,e^{\sigma}_{K}\,e^{\rho}_{I}\,\Omega_{\mu\sigma}{}^I{}_J$ and the Ricci scalar is $R = g^{\mu\nu}R_{\mu\nu}$.

We are mainly interested in neutron stars. The interior of a non-rotating neutron star is modeled by a perfect fluid, characterized only by its pressure p, its energy density ϵ and its four-velocity u_μ. The energy-momentum tensor takes the simple form

$$T_{\mu\nu} = \epsilon\, u_\mu u_\nu + p(g_{\mu\nu} + u_\mu u_\nu)\,. \tag{2.7}$$

We restrict ourselves to static, spherically symmetric solutions that only depend on a radial coordinate, r. With an appropriate ansatz for the vierbein, one quickly computes the connection ω, the curvature Ω, and solves Einstein's equations (see [18] for a derivation). As a consequence of Birkhoff's theorem [19], the exterior of the neutron star is described by the Schwarzschild solution. The interior is given by the solutions to the **Tolman–Oppenheimer–Volkoff** (TOV) equations [20–22]

$$\begin{aligned}\frac{dp(r)}{dr} &= -\frac{G}{r^2}\Big(\epsilon(r)+p(r)\Big)\Big(m(r)+4\pi r^3 p(r)\Big)\left(1-\frac{2Gm(r)}{r}\right)^{-1}\,,\\ \frac{dm(r)}{dr} &= 4\pi r^2 \epsilon(r)\,.\end{aligned} \tag{2.8}$$

The first equation is a generalization of the classical equation for hydrostatic equilibrium, obtained in the Newtonian limit $2Gm(r)/r \ll 1$ and $p \ll \epsilon$:

$$\frac{dp(r)}{dr} = -\frac{G\,\epsilon(r)\,m(r)}{r^2}\,. \tag{2.9}$$

2 If the internal indices are converted into space-time indices with the vierbein, one gets the Riemann curvature tensor with components $R_{\mu\nu}{}^\rho{}_\sigma$. The components are related to each other by the Bianchi identities.

The radius R of the neutron star is defined as the value of r where the energy density of the neutron star dropped to the surface energy density, i.e., $\epsilon(R) = \epsilon_s$. There are two different definitions of the mass of a star. First, the radial direction can be measured with the metric entry $g_{rr} = (1 - 2Gm(r)/r)^{-1/2}$, giving rise to the proper mass,

$$M_p = 4\pi \int_0^R \frac{dr\, r^2}{\sqrt{1 - \frac{2Gm(r)}{r}}}\, \epsilon(r)\,, \tag{2.10}$$

which includes the gravitational binding energy. The observable mass of the neutron star,

$$M = 4\pi \int_0^R dr\, r^2 \epsilon(r)\,, \tag{2.11}$$

is the difference of proper mass and gravitational binding energy, i.e., $M = M_p - E_B$. It is the observable mass and not the proper mass that enters the Schwarzschild metric in the exterior of the neutron star, therefore only the observable mass can be measured at a far distance. If we speak of the mass of the neutron star, we always mean the observable mass M from now on.

From the TOV equations it is clear that the mass and radii of neutron stars can be computed, once the relation between pressure and energy density is known. This equation of state can only be computed within a microscopic theory of the strong force, which is QCD. It is based on a generalization of gauge theories to more general internal spaces, which was first proposed in 1954 by Chen Ning Yang and Robert Mills [23].

2.2 QUANTUM CHROMODYNAMICS

In **Yang–Mills theory**, the gauge group is no longer the Lorentz group, but a non-abelian Lie group, here taken to be $\mathrm{SU}(N)$, where N is some natural number. At each point of space-time a copy of $\mathbb{C}^N$ is attached, where $\mathrm{SU}(N)$ acts via matrix multiplication. Just like in gravity, at each point the orientation in the internal space can be chosen freely. To compare vectors in the internal space, an analogy of the spin connection must be defined, namely the Yang–Mills connection ${A_\mu}^I{}_J = A^a_\mu (T^a)^I{}_J$, where $(T^a)^I{}_J$ are the generators of the Lie algebra $\mathfrak{su}(N)$. The indices I, J are now purely internal and no longer connected to space-time, even their multiplicity differs. Consequently, there is no analog of the vierbein. The corresponding covariant derivative in the fundamental representation[3] is defined in analogy to (2.1) as

$$D_\mu = \partial_\mu - igA^a_\mu T^a\,, \tag{2.12}$$

where g is the coupling constant of the Yang-Mills theory. The connection transforms under a **gauge transformation** $h \in \mathfrak{su}(N)$ in the internal space as

$$A_\mu \to h \left(\tfrac{i}{g}\partial_\mu + A_\mu\right) h^{-1}\,, \tag{2.13}$$

similarly to Eq. (2.2). In analogy to Eq. (2.3), one defines the curvature

$$G = dA - igA \wedge A\,, \tag{2.14}$$

which is called the field strength of the theory. In local coordinates, G has components

$$G^a_{\mu\nu} = \partial_\mu A^a_\nu - \partial_\nu A^a_\mu + g f^{abc} A^b_\mu A^c_\nu\,, \tag{2.15}$$

3 For a different representation R, replace the generators T^a with the generators T^a_R of R.

where f^{abc} are the structure constants of SU(N). **Quantum Chromodynamics** (QCD) is based on an SU(N) Yang–Mills-theory, where N is the number of colors, $N = N_c = 3$. The Lie algebra $\mathfrak{su}(3)_c$ of the color gauge group SU$(3)_c$ is generated by $T^a = \frac{\lambda^a}{2}$, where λ^a are the eight Gell-Mann matrices. The connection A therefore has components A^a_μ, with $a = 1, \dots 8$. They are identified as the gauge bosons of the theory, the **gluons**. The gauge bosons couple to **quark** fields, ψ, that transform in the fundamental representation. This means that under a local gauge transformation $h \in \mathfrak{su}(3)_c$, the quarks transform as $\psi \to h\psi$. The quarks come in $N_f = 6$ different flavors, namely up, down, strange, charm, bottom, and top, with masses m_f. The dynamics of QCD follows from its Lagrangian

$$\mathcal{L}_{\text{QCD}} = \sum_{f=1}^{N_f} \bar{\psi}_f (i\gamma^\mu D_\mu - m_f)\psi_f - \frac{1}{4} G^a_{\mu\nu} G^{a\mu\nu} \,, \tag{2.16}$$

where γ^μ are the Dirac matrices defined in Appendix A.1. One is often interested in composite operators, for instance the product of two fields at different space-time points. However, since the relative phase is not physical, this is not a gauge invariant object. Instead, operators are connected via **Wilson lines**, defined as the path-ordered product

$$\mathcal{W}(x, y, \gamma) = \mathcal{P} \exp\left(ig \int_\gamma dx^\mu \, A_\mu \right) , \tag{2.17}$$

where γ is a path connecting x and y. Composite operators, like finite-size quark-antiquark, baryon type or glue configurations can then be defined in a gauge-invariant way:

$$\begin{aligned} \mathcal{O}_1 &= \bar{\psi}(x)\, \mathcal{W}(x, y, \gamma)\, \psi(y) \,, \\ \mathcal{O}_2 &= \epsilon^{abc} [\mathcal{W}(u, x, \gamma_1)\psi(x)]^a [\mathcal{W}(u, y, \gamma_2)\psi(y)]^b [\mathcal{W}(u, z, \gamma_3)\psi(z)]^c \,, \\ \mathcal{O}_3 &= \text{Tr}\, F_{\mu\nu}(x)\, \mathcal{W}(x, y, \gamma)\, F^{\mu\nu}(y) \,. \end{aligned} \tag{2.18}$$

In the next sections, we will discuss the properties of QCD in more detail.

2.3 ASYMPTOTIC FREEDOM AND CONFINEMENT

QCD is characterized by two complimentary properties, namely asymptotic freedom at high energies and confinement in the low energy regime, a behavior that does not appear in any abelian four-dimensional theory. In 1973, Gross, Wilczek [24,25], and Politzer [26,27] computed the change of the QCD analog of the fine structure constant, $\alpha_s = g^2/4\pi$, as the renormalization scale μ_R is varied in the $\overline{\text{MS}}$-renormalization scheme. They found a logarithmic decrease of α_s for increasing scales,

$$\alpha_s(\mu_R) = \frac{4\pi}{\beta_0 \log \frac{\mu_R^2}{\Lambda^2_{\overline{\text{MS}}}}} \,, \qquad \beta_0 = \frac{1}{3}(11 N_c - 2 N_f) > 0 \,, \tag{2.19}$$

where $\Lambda_{\overline{\text{MS}}} \simeq 200$–$300$ MeV [28] denotes the scale where a perturbative calculation diverges. Consequently, QCD is **asymptotically free** at high energies.

On the other side, low energy QCD – or, equivalently, QCD at large distances – is not accessible by perturbative calculations. A non-perturbative approach is **lattice QCD** [29], where on a finite lattice an action is formulated, which approaches QCD in the infinite-volume limit. Quarks are located on the lattice sites, and gluons link different sites similar to the Wilson lines (2.17). Path-integrals then can be computed using Monte Carlo techniques.

In nature, free quarks and gluons are not observed, and the hadron spectrum consists only of color-neutral particles, a property which is called **color confinement**. There are numerous and often complimentary explanations for confinement (see, e.g., [30] for an overview).

- A flux tube connects a quark and an anti-quark inside a meson. If one tries to separate the two constituents, the size of the flux tube and consequently the energy of the system rise linearly. It costs an infinite amount of energy to separate the quark from the anti-quark. At some point, the flux tube will break and additional mesons are generated. Indications for such a behavior are the Regge trajectories in the resonance spectrum, which can be explained in a string-like picture.

- It is instructive to study the operator $\mathcal{O}_1$ defined in Eq. (2.18), where γ now is a spatial path which connects a quark with an anti-quark at a distance r at a given time t, in the limit of infinitely heavy masses. The correlator $\langle \mathcal{O}_1^\dagger(t)\, \mathcal{O}_1(0)\rangle$ can be computed on a lattice in Euclidean time. For large times t, the minimum-energy state is singled out, since all higher states are exponentially suppressed and one can show that the r-dependent potential equals

$$V(r) = -\lim_{t\to\infty} \frac{d}{dt} \log \langle \mathcal{O}_1^\dagger(t)\, \mathcal{O}(0)\rangle \ . \tag{2.20}$$

  On the other hand, $\langle \mathcal{O}_1^\dagger(t)\, \mathcal{O}_1(0)\rangle$ is proportional to the expectation value of the Wilson loop,

$$W(\gamma) = \big\langle \operatorname{Tr} \mathcal{W}(0,0,\gamma)\big\rangle \,, \tag{2.21}$$

  for a rectangular path γ of side length r and t. Combining the two results above yields $W(\gamma) \sim \exp(-V(r)t)$. Therefore, a lattice gauge theory calculation of the expectation value of the Wilson loop allows us to deduce the potential $V(r)$ of a pair of a static heavy quark and an antiquark. Indeed, lattice calculations (see, e.g., [31]) show that the potential rises linearly for larger distances, which is a signal of confinement, as described. At finite temperatures, a Wilson line wrapping around the imaginary time direction is called a Polyakov loop. The expectation value of the Polyakov loop is an order parameter for the breaking of the so-called center symmetry, which is related to confinement. Strictly speaking, this is only true in the pure gauge theory or in the limit of infinitely heavy quarks. The expectation value of the Polyakov loop is still useful for small non-vanishing quark masses as a measure for statistical confinement. However, the characteristic clustering property of confinement cannot be achieved this way.

- A concept which goes back to 't Hooft, Polyakov and Mandelstam [32–35] is to understand confinement as a "dual" Meißner effect [36]. In the Bardeen–Cooper–Schrieffer theory of superconductors, Cooper pairs of electrically charged electrons form a condensate. If a hypothetical magnetic monopole is inserted into the condensate, its magnetic flux is confined to tubes as a consequence of the Meißner effect. In QCD, the role of electric and magnetic fields is interchanged, hence the name "dual" superconductor. In 1994, monopole (and dyon) condensation was analytically proven to be responsible for confinement and the emergence of a mass gap in $\mathcal{N} = 2$ supersymmetric Yang–Mills theory in the seminal papers by Seiberg and Witten [37,38]. The proof, however, strongly relies on the large symmetry of the theory. In QCD, one has to rely on lattice calculations and various simulations indeed indicate a monopole dominance [39–43].

- A different confinement mechanism due to 't Hooft are center vortices [44, 45], topological objects which populate the vacuum with Wilson lines intersecting with them. The vortex picture is closely related to monopole condensation: monopoles can end on vortices, such that vortices can be considered as flux tubes between monopoles and anti-monopoles.
- In the Kugo–Ojima [46] and Gribov–Zwanziger [47, 48] scenarios, color confinement is explained by a suppression of the gluons and an enhancement of the ghosts in the infrared. Progress in this direction was made in Dyson–Schwinger calculations in Landau gauge [49], in the framework of the functional renormalization group [50], and on the lattice [51–55]. It was argued [56] that the critical exponents of the gluon and ghost propagators in the IR determine the minima of the Polyakov potential.

After the discussion of the implications of local gauge symmetries, we now turn to the global symmetries of QCD.

2.4 GLOBAL SYMMETRIES

We have seen that as a consequence of confinement, quarks and gluons are not the right degrees of freedom in the low-energy regime. In addition to the local gauge theory, QCD possesses also a number of global symmetries. Weinberg's famous "theorem" [57] states that the low-energy effective theory is given by the most general Lagrangian consistent with the underlying symmetries, where the free parameters have to be determined from experiments. Therefore, a good knowledge of the global symmetries is crucial to understand QCD at low energies.

First of all, as a quantum field theory, QCD is invariant under Poincaré transformations, which implies invariance under simultaneous charge, parity, and time transformations (CPT) [58]. In principle, CP could be broken if the **theta term**,

$$\mathcal{L}_\theta = -\frac{\theta}{64\pi^2}\epsilon^{\mu\nu\rho\sigma}G^a_{\mu\nu}G^a_{\rho\sigma}\,, \tag{2.22}$$

is added to the Lagrangian. The theta term does not require a (local) metric tensor and only depends on the (global) topology of the gauge field configurations. It turns out that the vacuum structure of QCD is non-trivial and a θ dependence is a natural consequence of instanton configurations.

Instantons are gauge configurations in the Euclidean, Wick-rotated version of QCD [59–61] and can be interpreted as tunneling processes in the WKB formalism [62] between different topologically non-equivalent vacua. Instantons are truly non-perturbative effects which do not appear in perturbation theory around the trivial vacuum. A more detailed description is given in Appendix A.2.2, where it is shown that any gauge configuration can be classified by an integer, the so-called winding number

$$n = \frac{g^2}{64\pi^2}\int d^4x\;\epsilon^{\mu\nu\rho\sigma}G^a_{\mu\nu}G^a_{\rho\sigma}\,. \tag{2.23}$$

In each sector, characterized by a fixed winding number, there is a gauge configuration that minimizes the Yang–Mills action in Euclidean space, namely the (anti-)self-dual[4] configuration, which satisfies $G^a_{\mu\nu} = \pm\frac{1}{2}\epsilon_{\mu\nu\rho\sigma}G^{a,\rho\sigma}$, for positive and negative winding numbers,

4 There are no self-dual solutions in Lorentzian signature in $3+1$ dimensions, which is why one has to look at Euclidean space.

respectively. These configurations are called (multi-)**instantons** with winding number n, and were first constructed for $n = 1$ by Belavin, Polyakov, Schwartz, and Tyupkin [59]. A complete classification of instantons in a general framework was later obtained through the ADHM construction[5] [64]. From the self-duality relation follows that the contribution of an instanton configuration with winding number n to the Euclidean path integral is proportional to $\exp(-8\pi^2|n|/g^2)$ and depends non-analytically on g.

In the path integral, all fluctuations around instanton configurations with an arbitrary winding number n are included. The cluster decomposition principle implies [65] that these configurations contribute with a weight factor $\mathrm{e}^{i\theta n}$ to the path integral, which leads to the non-trivial theta vacuum. Equivalently, one can add the theta term (2.22) to the Lagrangian.

The value of θ is a free parameter of the theory and has to be fixed empirically. An upper limit from dipole moments [66] is $|\theta| < 10^{-10}$. The unexpected smallness of θ was dubbed the **strong CP problem**. An elegant solution by Peccei and Quinn [67, 68] is to add a new $U(1)_{\mathrm{PQ}}$ symmetry to the theory. In this way, θ turns into a dynamical field, the axion, whose potential is minimized at $\theta = 0$. In principle, another solution would be a massless quark, because in this case θ could be rotated away. However, the quark-masses of the lightest quarks in the $\overline{\mathrm{MS}}$ scheme at a renormalization scale of $\mu_R = 2\,\mathrm{GeV}$ are [28]

$$m_u = 2.3^{+0.7}_{-0.5}\,\mathrm{MeV}\,, \quad m_d = 4.8^{+0.7}_{-0.3}\,\mathrm{MeV}\,, \quad m_s = 95^{+5}_{-5}\,\mathrm{MeV}\,. \tag{2.24}$$

These masses are non-vanishing, which excludes this particular solution of the strong CP problem. Nevertheless, they are very small compared to QCD scales which are of the order 1 GeV, for instance a few times $\Lambda_{\overline{\mathrm{MS}}}$, or $4\pi f_\pi$, where f_π is the decay constant of the pion. It is therefore often fruitful to study QCD in the massless limit. In the following, we will for simplicity only consider the two lightest quarks, the up and the down quark. It is useful to decompose the quark field into left- and right-handed fields,

$$\psi_R = \frac{1}{2}(1+\gamma_5)\psi\,, \quad \psi_L = \frac{1}{2}(1-\gamma_5)\psi\,, \tag{2.25}$$

where γ_5 is defined in Appendix A.1. In terms of these new fields, the quark-part of the QCD Lagrangian (2.16) with vanishing masses is diagonal: $\bar\psi_R i\gamma^\mu D_\mu \psi_R + \bar\psi_L i\gamma^\mu D_\mu \psi_L$. The massless QCD Lagrangian then possesses an enlarged symmetry under rotations in flavor space, namely invariance under the symmetry group $\mathrm{U}(2)_L \times \mathrm{U}(2)_R$. The full symmetry group is not preserved by the quantization procedure, but only a subgroup $\mathrm{U}(1)_V \times \mathrm{SU}(2)_V$. In the following, we will discuss the symmetries and symmetry breaking patterns in more detail. The full symmetry group can be decomposed into four subgroups:

1. **Singlet vector symmetry**, $U(1)_V$:

$$\psi \to \mathrm{e}^{i\alpha}\,\psi\,, \quad \bar\psi \to \bar\psi\,\mathrm{e}^{-i\alpha}\,. \tag{2.26}$$

   The corresponding Noether current is $V^\mu = \bar\psi\gamma^\mu\psi$, and the respective charge is the baryon number $Q^V = \int d^3x\; \psi^\dagger\psi$, which is also conserved after the quantization procedure.

2. **Singlet axial symmetry**, $U(1)_A$:

$$\psi \to \mathrm{e}^{i\alpha\gamma_5}\,\psi\,, \quad \bar\psi \to \bar\psi\,\mathrm{e}^{i\alpha\gamma_5}\,. \tag{2.27}$$

5 Instantons were consequently also studied extensively in differential geometry. For instance, Simon Donaldson won the Fields medal for his contributions to the classifications of four-manifolds with the help of self-dual connections [63].

In this case, the Noether current is $A^\mu = \bar\psi\gamma^\mu\gamma_5\psi$ and the corresponding axial charge is given by $Q^A = \int d^3x\ \psi^\dagger\gamma_5\psi$. It turns out that the path-integral measure is not invariant under an axial $U(1)_A$ symmetry transformation, but transforms as [69,70]

$$\mathcal{D}\psi\,\mathcal{D}\bar\psi \to \mathcal{D}\psi\,\mathcal{D}\bar\psi\ \exp\left(-\alpha\frac{ig^2}{32\pi^2}\int d^4x\ \epsilon^{\mu\nu\rho\sigma}G^a_{\mu\nu}G^a_{\rho\sigma}\right). \tag{2.28}$$

By itself, this unusual transformation behavior does not break the axial symmetry, in particular as the integrand in the exponent is a total derivative, as is shown in Appendix A.2.2. However, we have also seen that instanton configurations decay slowly enough at large distances, such that the integral is non-vanishing. Consequently, the $U(1)_A$ symmetry is said to be **anomalously broken**. As a consequence, the η'-meson is no longer a (quasi-)Goldstone boson, which explains its large mass.

3. Symmetry under **axial vector transformations** (which do not form a group):

$$\psi \to \mathrm{e}^{-i\frac{1}{2}\boldsymbol{\alpha}\cdot\boldsymbol{\tau}\gamma_5}\,\psi\,, \quad \bar\psi \to \bar\psi\,\mathrm{e}^{-i\frac{1}{2}\boldsymbol{\alpha}\cdot\boldsymbol{\tau}\gamma_5}\,, \tag{2.29}$$

where $\boldsymbol{\tau} = (\tau^1,\tau^2,\tau^3)$ are the Pauli matrices defined in Appendix A.1. Associated with this symmetry are the axial currents $A^\mu_i = \bar\psi\gamma^\mu\gamma_5\frac{\tau^i}{2}\psi$ with the corresponding charges $Q^A_i = \int d^3x\ \psi^\dagger\gamma_5\frac{\tau^i}{2}\psi$. The invariance under axial transformation is called **chiral symmetry** (although this expression is also often used for the full symmetry). Whereas the QCD Lagrangian is invariant under chiral symmetry, the QCD ground state is not invariant. The symmetry is said to be **spontaneously broken** and the ground state of QCD is in the **Nambu–Goldstone phase**. If instead the true ground state was in the **Wigner–Weyl phase** with unbroken symmetry, there would be a degeneracy in the hadron spectrum between positive and negative parity states, which is not observed in nature. Chiral symmetry breaking is associated with an order parameter, the **chiral** or **quark condensate**, defined as

$$\langle\bar\psi\psi\rangle = \langle\bar u u + \bar d d\rangle = i\int d^4x\,\mathrm{Tr}\,S(x,x)\,, \tag{2.30}$$

where $S(x,y) = -i\,\langle 0|\mathcal{T}\psi(x)\bar\psi(y)|0\rangle$ is the quark propagator. The chiral condensate, $\langle\bar\psi\psi\rangle = \langle\bar\psi_L\psi_R + \bar\psi_R\psi_L\rangle$, mixes right- and left-handed components and therefore a non-vanishing condensate breaks chiral symmetry. In Euclidean time (see Appendix A.1.4 for the conventions), the quark fields can be decomposed in terms of eigenfunctions of the Dirac operator in a given gauge field configuration A, i.e.,

$$i\gamma^\mu_{\mathrm{E}}D^{\mathrm{E}}_\mu\psi_\lambda = \lambda\psi_\lambda\,. \tag{2.31}$$

Expressed in these eigenfunctions, the quark propagator is

$$S(x,y) = -\sum_\lambda\frac{\psi_\lambda(x)\,\psi^\dagger_\lambda(y)}{im+\lambda}\,. \tag{2.32}$$

Because γ^{E}_5 anti-commutes with $\gamma^\mu_{\mathrm{E}}D^{\mathrm{E}}_\mu$, eigenfunctions occur in pairs, namely if ψ_λ has eigenvalue λ, then $\gamma^{\mathrm{E}}_5\psi_\lambda$ has eigenvalue $-\lambda$. The eigenvalues are distributed according to the spectral density $\rho(\lambda)$, which is therefore an even function of λ. Since the eigenfunctions are normalized, the quark condensate in the field configuration A is

$$\begin{aligned}\langle\bar\psi\psi\rangle_A &= \int d\lambda\ \rho(\lambda)\frac{-i}{im+\lambda} = -\int d\lambda\ \rho(\lambda)\left(\frac{m}{m^2+\lambda^2}+i\frac{\lambda}{m^2+\lambda^2}\right)\\ &\xrightarrow{m\to 0} -\int d\lambda\ \rho(\lambda)\left(\pi\delta(\lambda)+i\,\mathrm{PV}\,\frac{1}{\lambda}\right) = -\pi\rho(0)\,.\end{aligned} \tag{2.33}$$

In the last step, the contribution from the principal value vanishes, because $\rho(\lambda)$ is an even function. The equation (2.33) is called the **Banks–Casher relation** [71] and shows the connection between chiral symmetry breaking and quarks with $\lambda \simeq 0$. Let us define the index of the Dirac operator as the number of left-handed zero modes, n_L, minus the number of right-handed zero modes, n_R. The Atiyah-Singer index theorem [72] relates the index of the Dirac operator (i.e., a locally defined object) to the second Chern class (i.e., a globally defined object, which is simply the winding number),

$$n_L - n_R = \frac{g^2}{64\pi^2} \int d^4x \, \epsilon^{\mu\nu\rho\sigma} G^a_{\mu\nu} G^a_{\rho\sigma} = n \,. \tag{2.34}$$

Since instantons are related to zero-mode quarks via the index theorem, the instanton liquid model can explain the generation of a condensate by a delocalization of these zero-modes (see [73, 74] for numerical studies). Chiral symmetry is restored, once the zero-mode zone disappears [75], and whether chiral symmetry is broken or not depends crucially on the topological density of the instantons.

Through the triangle diagrams, instantons with winding number n change the axial charge by a factor $\Delta Q^A = 2N_f n$, where we have restored the explicit dependence on N_f. For $n = 1$, non-local $2N_f$-quark interactions are generated, as was first discussed by 't Hooft [76].

4. **Vector symmetry**, $\mathrm{SU}(2)_V$ (isospin symmetry):

$$\psi \to \mathrm{e}^{-i\frac{1}{2}\boldsymbol{\alpha}\cdot\boldsymbol{\tau}} \psi \,, \quad \bar{\psi} \to \bar{\psi}\, \mathrm{e}^{i\frac{1}{2}\boldsymbol{\alpha}\cdot\boldsymbol{\tau}} \,. \tag{2.35}$$

The corresponding isovector currents are $V_i^\mu = \bar{\psi}\gamma^\mu \frac{\tau^i}{2}\psi$ and the respective vector charges are $Q_i^V = \int d^3x \, \psi^\dagger \frac{\tau^i}{2}\psi$. As a consequence of the **Vafa–Witten theorem** [77], the $\mathrm{SU}(2)_V$ symmetry cannot be spontaneously broken. Similarly to the derivation of the Banks–Casher relation, we compute a corresponding order parameter, which is in this case the condensate

$$\begin{aligned} \langle \bar{u}u - \bar{d}d \rangle_A &= \int d\lambda \, \rho(\lambda) \left[\frac{-i}{im_u + \lambda} - \frac{-i}{im_d + \lambda} \right] \\ &= (m_d - m_u) \int d\lambda \, \rho(\lambda) \frac{1}{(im_u + \lambda)(im_d + \lambda)} \,. \end{aligned}$$

The integrand has poles at $-im_u$ and $-im_d$. Because the Dirac operator is Hermitian, the integration over λ extends only over real values. Consequently, the integral is non-singular as $m_u \to m_d$, and the condensate vanishes. The vector symmetry cannot be broken.

We have seen that the $U(1)_A$ symmetry is broken by quantum effects and the chiral symmetry is broken spontaneously in the QCD ground state. In total, the original $\mathrm{U}(2)_L \times \mathrm{U}(2)_R$ symmetry is broken down to a $\mathrm{U}(1)_V \times \mathrm{SU}(2)_V$ subgroup. In addition, the finite quark masses, $M = \mathrm{diag}(m_u, m_d)$, introduce an explicit symmetry breaking effect. The divergences of the currents in the presence of massive quarks is

$$\begin{aligned} &\partial_\mu V^\mu = 0 \,, && \partial_\mu A^\mu = 2i\bar{\psi} M \gamma_5 \psi + \frac{g^2}{16\pi^2} \epsilon^{\mu\nu\rho\sigma} G^a_{\mu\nu} G^a_{\rho\sigma} \,, \\ &\partial_\mu V_i^\mu = i\bar{\psi}\Big[M, \frac{\tau^i}{2}\Big]\psi \,, && \partial_\mu A_i^\mu = i\bar{\psi}\Big\{M, \frac{\tau^i}{2}\Big\}\gamma_5\psi \,, \end{aligned} \tag{2.36}$$

where $\{\cdot,\cdot\}$ is the anti-commutator. The vector current V_i^μ is not conserved for $m_u \neq m_d$.

We will now discuss in more detail the consequences of a spontaneously broken chiral symmetry. Goldstone's theorem [78, 79] tells us that for any spontaneously broken symmetry, there is a corresponding massless Goldstone boson. The axial charges do not leave the vacuum invariant but instead generate new states $Q_i^A\,|0\rangle$, which are identified as pseudoscalar mesons, the **pions**. As a consequence of explicit chiral symmetry breaking, the pions are not exactly massless and are called pseudo-Goldstone bosons. Nevertheless, the explicit symmetry breaking is small and from the approximate chiral symmetry alone it is possible to derive several low energy theorems. Let $|\pi_i(p)\rangle$ denote a normalized one-pion state with momentum p. The state $A_i^\mu(x)\,|0\rangle$ has non-vanishing overlap with the pions,

$$\langle 0|A_i^\mu(x)|\pi_j(p)\rangle = ip^\mu f_0 \delta_{ij}\,\mathrm{e}^{-ipx}\ . \tag{2.37}$$

The momentum dependence is a consequence of Lorentz symmetry. Moreover, f_0 denotes the **pion decay constant** in the chiral limit, which differs from the physical pion decay constant[6],

$$f_\pi = (92.21 \pm 0.02 \pm 0.14)\,\mathrm{MeV}\ \ [28]\,, \tag{2.38}$$

only by corrections of the order of the quark masses. We will evaluate $\langle 0\,|\,[Q_1^A,\,\partial_\mu A_1^\mu]\,|\,0\rangle$ at $t=0$ in two different ways. First, with Eq. (2.36) we find

$$\begin{aligned}\langle\,0\,|\,[Q_1^A,\,\partial_\mu A_1^\mu]\,|\,0\,\rangle &= \langle\,0\,|\,[Q_1^A,\,i\bar\psi\{M,\frac{\tau^1}{2}\}\gamma_5\psi]\,|\,0\,\rangle \\ &= i(m_u+m_d)\,\langle\,0\,|\,[Q_1^A,\,\bar\psi\,\frac{\tau^1}{2}\,\gamma_5\psi]\,|\,0\,\rangle = -\frac{i}{2}(m_u+m_d)\,\langle\bar\psi\psi\rangle\ ,\end{aligned} \tag{2.39}$$

where the last equation can be computed from $Q_1^A = \int d^3x\ \psi^\dagger\gamma_5\frac{\tau^1}{2}\psi$ together with the equal-time fermion anticommutation rules. Second, we insert a set of pion states into $\langle 0\,|\,[Q_1^A,\,\partial_\mu A_1^\mu]\,|\,0\rangle$. The hypothesis of a **partially conserved axial current** states that this forms already a complete set, i.e.,

$$1 \to \int \frac{d^3p}{2E_p(2\pi)^3}\,|\pi_i(p)\rangle\ \langle\pi_i(p)|\ , \tag{2.40}$$

if inserted into the commutator. As a consequence of Eq. (2.37) together with the relation $\langle 0|Q_i^A|\pi_j(p)\rangle = i\delta_{ij}f_\pi E_p(2\pi)^3\delta^{(3)}(\boldsymbol{p})$ at $t=0$, we find

$$\langle\,0\,|\,[Q_1^A,\,\partial_\mu A_1^\mu]\,|\,0\,\rangle = if_\pi^2 E^2_{\boldsymbol{p}=0} = if_\pi^2 m_\pi^2\,. \tag{2.41}$$

A comparison of Eqs. (2.39) and (2.41) yields the **Gell-Mann–Oakes–Renner** (GOR) relation [80],

$$2m_\pi^2 f_\pi^2 = -(m_u+m_d)\,\langle\bar\psi\psi\rangle\ , \tag{2.42}$$

which is valid up to corrections of the order $m_{u,d}^2$. As the quark masses depend on the renormalization scale, so does the quark condensate, and only the product is invariant under the renormalization group. The GOR relation is tested extremely well on the lattice [81]. It connects properties of quarks, i.e., QCD degrees of freedom, with properties of the pions, which dominate the low energy regime. The chiral condensate can be deduced from the quark masses, or from the lattice [82]. At a renormalization scale in the GeV range, the condensate is of the order $-1.8\,\mathrm{fm}^{-3}$.

Having discussed the low-energy properties of QCD, we will turn to non-vanishing temperatures and densities in the next section.

6 The pion decay constant is determined from the decays $\pi^- \to \mu^-\bar\nu_\mu$ and $\pi^- \to \mu^-\bar\nu_\mu\gamma$. The first error is due to the uncertainty of the matrix element $|V_{ud}|$ of the CKM-matrix, and the second error is due to higher-order corrections.

2.5 QCD AT FINITE TEMPERATURE AND DENSITY

We have seen that the most important characteristics of low-energy QCD are color confinement and chiral symmetry breaking. Both properties are lost at high temperature, at high densities, or in strong magnetic fields. In order to gain a solid understanding of such diverse phenomena as the early universe, heavy-ion collisions, or neutron stars, it is therefore crucial to understand QCD quantitatively and qualitatively at finite temperatures and chemical potentials (see [83] for a recent survey).

2.5.1 *Heavy-ion collisions*

At very high temperatures, the QCD coupling is small and thus perturbative QCD is applicable. The dominant degrees of freedom are quarks and gluons and the system is described as a **quark-gluon plasma** (QGP). It is believed that at the four main experiments at the Relativistic Heavy Ion Collider (RHIC) in Brookhaven (namely STAR [84], PHENIX [85], PHOBOS [86], and BRAHMS [87]) a state dominated by quarks and gluons was produced. In the recent years a "standard model" of heavy-ion collisions emerged [88–90], which in many ways parallels the big-bang standard model in cosmology (see Table 1). The colliding objects move at a relativistic speed and are strongly Lorentz-contracted along the collision axis. The initial state is characterized by the energy and the centrality of the collision. After the initial collision, a hot and dense fireball is created, which thereupon undergoes a rapid expansion. The initial state is far from equilibrium and the pre-equilibrium phase is commonly described by classical Yang-Mills dynamics. After a time of only about $\tau = 1\,\mathrm{fm}$, the system is expected to reach thermal equilibrium, at least locally. The main motivation for this assumption is the tremendous success of phenomenological descriptions based on local equilibrium. An initial density profile is chosen to characterize the system after local equilibration. Different descriptions exist, such as MC-Glauber, MC-KLN and IP-Glasma models. The subsequent stage up to about $\tau = 10\,\mathrm{fm}$ can be described by relativistic viscous hydrodynamics [91]. Because the final density profile depends on the initial density profile, which differs slightly from collision to collision, there are event-by-event fluctuations. Moreover, the centrality of the collision influences the initial state. A study of anisotropies allows us to infer properties of the QGP produced during the earliest stages of the collision. Dissipative forces can smear out anisotropies, most importantly being the ratio of shear viscosity η and entropy density s of the QGP. If η/s was too large, the anisotropies would disappear and all information about the initial profile gets lost. For a given initial density profile, the ratio η/s is fitted to the experimental data on the elliptic flow v_2 as well as higher anisotropic flows v_n [92]. It turns out that the elliptic flow is unexpectedly large and therefore η/s is very small. For Au+Au collisions at RHIC, one finds [93, 94]

$$\frac{\eta}{s} \simeq 1.5 \cdot \frac{1}{4\pi}\,. \tag{2.43}$$

In addition, the IP-Glasma model based on the color-glass-condensate model seems to be singled out by experiments, since it is the only approach which can reproduce all measured anisotropies [95]. The ratio η/s is not constant but depends on the temperature. The Au+Au collisions conducted at the ALICE and ATLAS experiments at the LHC probe the QGP at large temperatures. Consequently, one finds a larger value for $\eta/s \simeq 2.5/4\pi$ [96]. Even at these higher temperatures η/s is still very close to the bound $1/(4\pi) \simeq 0.08$, which was derived in the context of the AdS/CFT duality and is expected to hold for all

heavy-ion collisions	cosmological evolution
hot fireball: pressure-driven expansion	space-time: gravity-driven Hubble expansion
hadrosynthesis, chemical freeze-out	primordial nucleosynthesis
kinetical freeze-out	recombination
detected hadron abundances	observed cosmic microwave background
initial density fluctuations leading to	initial density fluctuations leading to
• event-by-event fluctuations	• large-scale structure of the universe,
• anisotropic flow	• deviations from isotropy in the cosmic microwave background.

Table 1: A comparison of different stages in heavy-ion collisions and in cosmology.

reasonable gauge theories with gravity duals [97]. The quark gluon plasma is therefore strongly coupled (sQGP) and behaves like an almost perfect fluid.

Finally, after the time-span τ of about 10 fm, the temperature drops down to about 160 MeV. Matter starts to hadronize and **chemical freeze-out** sets in, which implies that the ratios of the particle species are fixed from now on. After chemical freeze-out the hadrons still scatter elastically until the temperature drops further and these interactions cease as well. After the **kinetical freeze-out**, the particles propagate freely and can be measured in the detectors.

At chemical freeze-out, the system can be described as a grand-canonical ensemble of hadrons and resonances in equilibrium [98], including particles up to masses of about 2 GeV. To account for the finite width of the resonances, one integrates over the mass, distributed according to a Breit-Wigner function. Elastic interactions are included in a simplified way by hard-core repulsion, implemented as an excluded volume correction, similar to a van-the-Waals gas. The main assumptions of this **hadron-resonance gas (HRG) model** is that the medium is at equilibrium, that hadronization of all particles takes place at the same time, and that the in-medium masses of the hadrons do not differ a lot from their vacuum values. The only free parameters of the model are the temperature T and the baryon chemical potential μ at freeze-out. They are adjusted to the ratios of hadron yields[7] by minimizing the χ^2 distribution. The model is remarkably successful in reproducing the ratios of measured particle yields [99, 100].

The HRG model works very well; however, it would certainly be desirable to compute the freeze-out temperatures directly from QCD. In recent years, it became possible to perform such calculations for small chemical potentials in lattice QCD, where one studies ratios of cumulants of conserved charge fluctuations and determines in this way the freeze-out line. In the limited range of small μ accessible to lattice computations, the results are in agreement with the HRG calculations [101, 102].

Numerous experiments at different energies were analyzed, from AGS, SIS, and SPS to the RHIC (see [103] for a review). Each collision energy corresponds to a particular freeze-out temperature and baryon chemical potential. For small energies, initial nucleons are dominant, and the baryon chemical potential is large. Higher energies correspond to

7 Taking ratios of yields instead of yields eliminates the size of the fireball as an additional parameter.

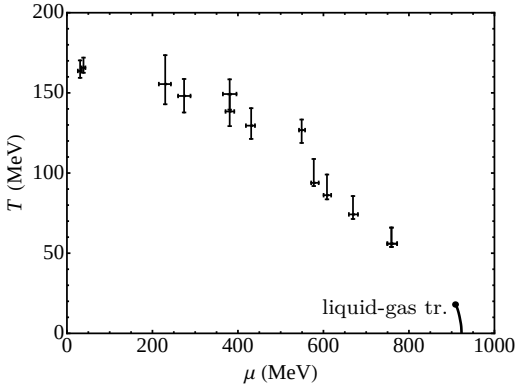

Figure 1: Chemical freeze-out points from the hadron-resonance gas model [100]. The freeze-out curve points towards the nuclear liquid-gas transition in the lower right-hand corner.

smaller baryon chemical potentials, where newly produced hadrons dominate, with pions being the most abundant species. At the same time, higher energies allow to test higher temperatures. By varying the energy, one scans the freeze-out line in a T–μ diagram. Some of the freeze-out points obtained from such a hadron-resonance gas analysis are shown in Fig. 1. It is remarkable that if one follows the freeze-out line to higher baryon chemical potentials, i.e., smaller energy, one ends up in a region very close to the nuclear liquid-gas phase transition. This observation turns out to be important if one connects the freeze-out line to chiral restoration. We will turn to this point in the next section.

2.5.2 *Chiral restoration*

Heavy-ion experiments revealed a new kind of matter at high temperatures, the strongly coupled quark-gluon plasma. Together with deconfinement, chiral symmetry is also restored. At zero chemical potential, both events are not phase transitions but crossovers, which means that the respective order parameters are smooth functions of T. The pseudo-critical temperature of the **chiral restoration**, T_c, is defined as the highest peak in the susceptibility of the chiral condensate (the point of strongest descent of the condensate). This temperature is nowadays well determined from different lattice calculations, with comparable values

$$\begin{aligned} T_c &= 154(9)\,\text{MeV} \qquad \text{HotQCD [104]}\,, \\ T_c &= 147\text{–}157\,\text{MeV} \qquad \text{Wuppertal-Budapest [105]}\,. \end{aligned} \tag{2.44}$$

Remarkably, this temperature turns out to be very close to the chemical freeze-out temperature, T_f, at zero baryon chemical potential. At small chemical potentials, it was argued that only close to T_c it is possible to maintain chemical equilibrium [106]. If the temperature of the system is below the QCD pseudo-critical crossover temperature, the dominating interaction is two-particle hadron scattering and it was estimated that these processes alone cannot establish chemical equilibrium of (multi-)strange hadrons fast enough. Multi-hadron processes are suppressed by a high power of the density and cannot contribute. However, close to the pseudo-critical temperature, the density increases dramatically and multi-hadron processes become dominant. These collective excitations are able to thermalize the system fast enough. A detailed comparison of different freeze-out criteria is found in Ref. [107].

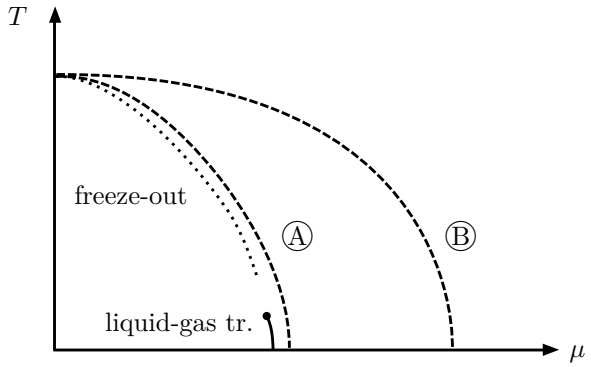

Figure 2: Two possible chiral restoration lines: In scenario A the entanglement between chiral restoration and chemical freeze-out (dotted line) holds for larger chemical potentials as well, whereas in scenario B the two lines are clearly separated.

The success of the hadron-resonance gas model further tells us that chemical freeze-out should occur in the hadronic phase, i.e., $T_f \leq T_c$. The latest calculations on the lattice [108] and in the hadron-resonance gas model [109] indeed predict a smaller freeze-out temperature than earlier works, in agreement with $T_f \leq T_c$.

A natural question is whether this connection between chemical freeze-out and chiral restoration holds as well for larger chemical potentials. If this was the case, as is shown in scenario A in Fig. 2, chiral symmetry would get restored very close to the nuclear liquid-gas transition. This would be problematic, because we have no experimental implications that chiral symmetry is restored in nuclear matter at relatively low densities.

An important finding is that at least for small chemical potentials the pseudo-critical temperatures of chiral restoration and deconfinement are closely intertwined. In principle, it is possible that these lines diverge for larger chemical potentials. It was conjectured that there might exist an exotic state, the **quarkyonic phase** [110], where the degrees of freedom are still confined, but which differs from ordinary nuclear matter by a large baryon number density and energy density that can be traced back to the quark constituents. Chiral symmetry might already be restored, but this does not have to be the case. It was argued that the chemical freeze-out curve can be explained by quarkyonic matter [111]. At low baryon chemical potentials, the baryon density is relatively small and Goldstone bosons are the dominant degrees of freedom. The transition can then be estimated to occur close to the Hagedorn temperature, where the dual resonance model breaks down. For small baryon densities, this temperature does not vary a lot, such that the freeze-out curve is almost horizontal. For higher densities (such as predicted in quarkyonic matter), baryons dominate. The Hagedorn spectrum is now balanced by a Boltzmann factor, which depends on μ. As a result, the freeze-out curve decreases almost linearly. Mean-field studies of quark-meson or NJL models indeed show a phase with confined degrees of freedom but where chiral symmetry is already restored. In contrast, if a μ-dependent Polyakov-loop potential is used in a functional renormalization group approach, this phase is absent [112, 113]. Further possible scenarios for high-density QCD phases, which are frequently discussed in the literature are inhomogeneous phases, such as pion or kaon condensates [114, 115].

At very large chemical potentials, perturbative methods are applicable. The two-quark state can be decomposed as $3 \otimes 3 = 6 \oplus \overline{3}$, where the sextet is always repulsive, while the anti-triplet becomes attractive via one-gluon exchange. Similarly to electro-magnetic superconductivity, Cooper pairs can form and a diquark condensate is formed. The diquark

condensate has color and flavor indices and therefore the local color symmetry is hidden and the global flavor symmetry is broken. A **color-superconducting phase** is expected.

One important problem in QCD phase-diagram studies concerns the order of the chiral restoration transition. All we know is that at zero chemical potential there is no phase transition but rather a rapid crossover. At larger chemical potentials, the restoration could in principle be of first order. The first-order line then ends in a second-order **critical endpoint** (CEP). The CEP would be a landmark in the QCD phase-diagram and lots of theoretical and experimental effort is therefore devoted to the search of the CEP. However, it is not clear at all if it exists. There are numerous different approaches to study chiral restoration, which can be roughly divided in what we will call "small-μ" and "small-T" approaches.

1. **Small-μ approaches.** In principle, **lattice QCD** has the advantage that it does not rely on any particular model assumptions. It would therefore be desirable to compute the pseudo-critical temperature T_c as a function of the chemical potential on the lattice. Unfortunately, lattice computations at large chemical potentials are not possible because of the sign problem: the weighting factor is highly oscillatory and a Monte-Carlo treatment of the path integral breaks down. Several approaches were developed to extend lattice QCD to finite μ. Examples are reweighting, Taylor expanding in μ, and the continuation to imaginary chemical potentials [116–119]. In general, lattice calculations are still restricted by the sign problem to $\mu/3T < 1$ and cannot be trusted for large chemical potentials. Moreover, possible phase transitions are connected with divergences and all approaches circumventing the sign problem break down. Nevertheless, one can compute the curvatures κ_f and κ_c of the freeze-out curve and chiral-restoration curve, respectively, for small μ, with

$$\frac{T_{f,c}(\mu)}{T_{f,c}(0)} = 1 - \kappa_{f,c}\left(\frac{\mu}{3T_{f,c}}\right)^2 + \mathcal{O}(\mu^4/T_{f,c}^4)\,. \tag{2.45}$$

The curvatures obtained by lattice calculations are

$$\begin{aligned} \kappa_f &= 0.21(2) && [107], \\ \kappa_c &= 0.059(2)(4) && [120], \\ \kappa_c &= 0.059(18) && [121]. \end{aligned} \tag{2.46}$$

The curvature of the chemical freeze-out line is about a factor four larger than the curvature of the chiral restoration curve. This indicates a divergence of the curves as in scenario B in Fig. 2, already at small chemical potentials.

A study of the critical endpoint in lattice QCD is more involved because of the sign problem. Some insight can be gained by varying the quark masses [122]. The order of the phase transition depends on these quark masses. A useful approach is to study the order of the chiral restoration as function of the light-quark mass $m_u = m_d$ and the strange quark mass m_s. As noted above, at the physical point one finds a crossover at $\mu = 0$. In contrast, if the quark masses were smaller, there would be a first-order phase transition [123]. On the boundary between these two regions in the mass-plane, the transition is of second order. Consequently, it is fruitful to study how this boundary region (the so-called critical surface) changes as a function of the chemical potential. A lattice simulation at an imaginary chemical potential was performed at relatively large quark masses. One observes that the critical surface shrinks [124]. This means that the physical point stays in the crossover region and

does not get closer to the boundary, which would exclude a critical endpoint for physical quark masses.

A different conclusion was drawn from recent studies using **Dyson–Schwinger equations**. A chiral CEP is found at a relatively high temperature $T = 100\,\mathrm{MeV}$ and a critical quark chemical potential in the range $\mu_q = 170$–$190\,\mathrm{MeV}$ [125, 126].

Chiral restoration at larger chemical potentials can be studied in QCD-type models that take chiral symmetry into account. The **Nambu–Jona-Lasinio model** [127, 128] (NJL model) was inspired by the Bardeen–Cooper–Schrieffer theory of superconductors. It describes quark-type (quasi-)particles that interact via four-fermion couplings [129]. The model does not include confinement, a short-coming that can be overcome by coupling it to the Polyakov loop potential [130–137] (PNJL model). The existence of a critical point cannot definitely be proven nor disproven in these models. The strength of vector interactions and the 't Hooft coupling (which accounts for the axial $\mathrm{U}(1)_A$ anomaly) play an important role, and whether the CEP exists depends sensitively on their values. This can be shown in the NJL model [138–140], in the local PNJL model [141, 142] as well as in a nonlocal PNJL model [143]. In addition, the vector interaction also determines crucially the curvature of the critical surface in these models [144].

The **chiral quark-meson (QM) model** couples quarks in a chirally invariant way to a scalar, σ, and pionic degrees of freedom [145–147]. Statistical confinement can be included by using the Polyakov-quark-meson model (PQM model [112, 148]). It was found that the endpoint moves to smaller temperatures if the mass of the σ is increased. In particular, if the mass is large enough, no CEP is found [149]. Likewise, if the μ-dependence of the Polyakov loop (as derived from pure Yang-Mills theory) is included in the model, the CEP moves to smaller temperatures [149].

At high baryon chemical potentials and small temperatures, baryons are the dominant degrees of freedom. It is unlikely that a model built upon quark-type particles – like the PQM model or PNJL model – can be applied within this region. Nucleons play an important role and can substantially enhance the density and pressure as compared to quark models, as was shown in Ref. [150]. As a result, the transition to the quark-dominated phase is typically predicted at too low densities as compared to more realistic models.

Another finding is that fluctuations beyond the mean-field approximation are very important. If they are included properly, the critical endpoint appears at smaller temperatures and larger chemical potentials. This effect already appears if back-reactions are taken into account in the PQM model [112]. Similar effects are observed if bosonic fluctuations are treated in the framework of the functional renormalization group [113, 151–153]. No critical endpoint exists within the range of applicability of the model. It is therefore not enough to stay in the mean-field approximation. Fluctuations can make a difference and have to be properly accounted for.

2. **Small-T approaches.** A different route to gain insight into chiral restoration and chemical freeze-out is to start with what we know from nuclear physics at small temperatures and high densities. Models based on hadronic degrees of freedom are adjusted to reproduce the empirically given data. One of the earliest models for the nuclear interactions was developed by Hideki Yukawa in 1935 [154]. In his theory, a scalar field is the carrier of the force between nuclei. Later it was realized that the long-range force is governed by pion exchange, which is a pseudo-scalar. At

smaller distances other more massive mesons become important, such as the $\omega(782)$ and $\rho(770)$ mesons. **One-boson exchange models** were extended substantially, starting in the 60s (see [155] for a review). An important ingredient of these models is the scalar-isoscalar σ or $f_0(500)$ field introduced by Johnson and Teller in 1955 [156]. If one analyses the $I = 0$ s-wave in pion-pion scattering, one indeed finds a pole. However, its location is at $\sqrt{s} \sim (500 - i\,300)$ MeV [157,158]. It has a large imaginary part – which would correspond to a decay width of $\Gamma \simeq 600\,\text{MeV}$ – and therefore is not a resonance. In fact, it does not even have a Breit-Wigner shape, and is certainly not a particle. The boson σ that appears in boson-exchange models should therefore rather be considered as an effective field which parametrizes part of the medium-range interactions.

Dense matter can be studied in **relativistic mean-field models**, which are generalizations of the Walecka model [159]. Some of the exchange bosons acquire expectation values, whose dependence on temperature and density can then be derived.

All these models do not take chiral symmetry into account. After the discovery of chiral symmetry, the field σ was combined with the pions into a four-vector which transforms under the chiral symmetry group $\text{SU}(2)_L \times \text{SU}(2)_R \cong \text{SO}(4)$. One gets the **linear sigma model** derived by Gell-Mann and Lévy in 1960 [160]. Because the σ does not correspond to a physical particle, it is desirable to eliminate it from the theory. At low energies and temperatures, the pionic fluctuations should dominate and the σ can be integrated out by making it infinitely heavy. One arrives at the **non-linear sigma model**, which contains pion fields only. A systematic way to include higher pionic interactions was finally introduced by Weinberg [57]. The crucial point is that both the relevant momenta p and the pion mass m_π are small compared to the chiral scale $\Lambda_\chi \simeq 1\,\text{GeV}$. This provides us with a natural power counting scheme, where p/Λ_χ and m_π/Λ_χ serve as expansion parameters. The mass of the lowest excited state of the nucleon, the $\Delta(1232)$ resonance, is only $293\,\text{MeV} \simeq 2m_\pi$ larger than the mass of the nucleon. It is therefore often useful to include this mass difference also in the set of small scales, in order to improve the convergence behavior. Weinberg argued that all possible terms are allowed in the Lagrangian at a given order, as long as they respect the symmetries of the underlying theory. The **chiral effective field theory (ChEFT)** obtained in this way [161] therefore is the low-energy theory of QCD (for reviews consult [162–164]).

At zero temperature and at the chemical potential $\mu = 923\,\text{MeV}$, there exists a first-order **liquid-gas phase transition** from the vacuum state to nuclear matter. The region in the phase diagram around the liquid-gas phase transition at finite densities and temperatures can be studied in in-medium ChEFT (see [165] for a recent review).

The approach we will use in this thesis is based on a chiral version of the boson-exchange model [150, 166]. Like in the linear sigma model, a four-vector $(\sigma, \boldsymbol{\pi})$ couples to the nucleon and accounts for long- and medium-range interactions. The short-range interactions are modeled by an exchange of vector bosons. Because of the chiral nature of the model, it is possible to study both the liquid-gas transition and chiral restoration. This **chiral nucleon-meson (ChNM) model** has been studied so far only in the mean-field approximation. Because we know that fluctuations – especially those involving pions – have an important effect on chiral restoration, it is necessary to include fluctuations beyond the mean-field approximation, which will be the focus of the present work. All parameters of the models will be adjusted to the empirical data we have concerning nuclear matter, which will be discussed next.

2.6 NUCLEAR MATTER

Nuclear matter is an idealized system of infinite extent, subject only to the strong force. Its properties can be deduced from an extrapolation of empirical data of nuclei. An important property of nuclei is saturation. For sufficiently large nuclei, the radius scales with the number of nucleons, A, as

$$R \simeq A^{1/3} r_0 \,, \tag{2.47}$$

where the empirical charge radius r_0 is about 1 fm. Therefore, the charge density saturates for large nucleon numbers, which is a consequence of the finite range of the nucleon-nucleon interactions. An analysis of the charge distribution via electron-nucleon scattering revealed that a large number of nuclei can be described by the charge distribution [167]

$$n_{\text{charge}}(r) = \frac{n_0}{1 + \mathrm{e}^{(r-R)/a}} \,, \tag{2.48}$$

where $a \simeq 0.5\,\text{fm}$. In particular, the central density $(A/Z)n_0$ is constant for each nucleus, where Z is the number of protons. Empirically, one finds for the **nuclear saturation density** the value

$$n_0 = 0.16\,\text{fm}^{-3} \,. \tag{2.49}$$

In the liquid-drop model, the masses of nuclei are determined by the **semi-empirical mass formula** (or Bethe-Weizsäcker formula)

$$M = Z m_p + (A - Z) m_n - E_{\text{B}} \,, \tag{2.50}$$

where the **binding energy** is

$$E_{\text{B}} = a_{\text{V}} A - a_{\text{S}} A^{2/3} - a_{\text{C}} \frac{Z^2}{A^{1/3}} - a_{\text{A}} \frac{(A-2Z)^2}{A} - a_{\text{P}} \frac{\lambda}{A^{3/4}} \,, \tag{2.51}$$

for constants a_{V}, a_{S}, a_{C}, a_{A}, and a_{P}. We discuss the individual terms in the following. Because of the saturation property, a nucleus behaves similar to a liquid drop. The nuclear force is short-ranged, so in a good approximation nucleons only interact with their nearest neighbors. Hence, the main contribution to the binding energy comes from the volume term proportional to the nucleon number or volume $A \sim R^3$. Nucleons on the surface can only interact with other nucleons inside the nucleus. The binding energy therefore has to be corrected by a term proportional to the surface area $4\pi R^2 \sim A^{2/3}$. The surface term can also be written in the form

$$E_{\text{B, surface}} = -4\pi R^2 \Sigma \,, \tag{2.52}$$

where Σ denotes the **surface tension**. The third term in the binding energy stems from a Coulomb interaction of the protons proportional to $Z^2 R^{-1} \sim Z^2 A^{-1/3}$. The fourth term is the **symmetry energy** (also called asymmetry energy), which takes into account that nuclei prefer to have $N \simeq Z$ because of Pauli blocking, where N is the neutron number. The last term is the pairing energy, where $\lambda = 1$ for odd-odd, $\lambda = 0$ for even-odd, and $\lambda = -1$ for even-even nuclei, which follows from an analysis of possible beta-decays in the shell model. The dependence on A is found empirically[8]. The parameters are fitted to the available data. For the infinite system of nuclear matter, one studies the energy

8 Other dependencies are also found in the literature, for instance $A^{-1/2}$.

per particle E/A in the limit $A \to \infty$. Only the volume term and the symmetry term contribute.

The degree of isospin asymmetry can be characterized by the **proton fraction**,

$$x = \frac{Z}{A} = \frac{n_p}{n_p + n_n}\,, \tag{2.53}$$

where n_p and n_n are the proton and neutron density, respectively. Symmetric nuclear matter is characterized by $x = 0.5$, whereas pure neutron matter corresponds to $x = 0$. The x-dependence of the energy per particle can be approximated by a parabolic expansion around symmetric nuclear matter, i.e.,

$$\frac{E}{A}(n, x) = \frac{E}{A}(n, 0.5) + S(n)\,(1 - 2x)^2 + \dots\,. \tag{2.54}$$

The energy per particle of symmetric matter at saturation density can be obtained from an extrapolation of the binding energy of heavy nuclei to the thermodynamic limit. One finds [168]

$$\frac{E}{A}(n_0, 0.5) = -16.0(1)\,\mathrm{MeV}\,. \tag{2.55}$$

Under the assumption that terms beyond the quadratic approximation can be neglected, the density-dependent symmetry energy $S(n)$ is the difference between the energy per particle of pure neutron matter and symmetric nuclear matter for a given density, n. Close to saturation density, we can expand

$$S(n) = E_{\mathrm{sym}} + \frac{L}{3}(n - n_0) + \dots\,. \tag{2.56}$$

The leading term is the **symmetry energy**, as in the liquid-drop model. It is a measure of the cost to convert symmetric nuclear matter to pure neutron matter at saturation density. The **L-parameter** describes how this quantity changes if the density is increased. These parameters are important, because they can be constrained by empirical data. For neutron-rich nuclei the radius of the neutron distribution is larger than that of the protons. If a neutron is not located in the core but in the skin, the surface tension increases. A reduction in symmetry energy can compensate this effect. If the L-parameter (i.e., the difference between symmetry energy in the center at higher density and at the surface at lower density) is larger than the surface tension, it is energetically favorable to have a thicker neutron-skin. A measurement of the neutron-skin thickness can therefore limit the L-parameter. Other constraints can be obtained from heavy-ion collisions, dipole polarizabilities, giant and pygmy dipole resonance energies, as well as from fitting nuclear masses [169–171]. Combining all the constraints yields the following limits:

$$\begin{aligned} &29\,\mathrm{MeV} \le E_{\mathrm{sym}} \le 33\,\mathrm{MeV}\,,\\ &40\,\mathrm{MeV} \le L \le 62\,\mathrm{MeV}\,. \end{aligned} \tag{2.57}$$

After this concise overview of QCD and nuclear physics, we want to study the nucleon-meson model as a useful description of dense matter. Before we can come to this point, we have to develop the theoretical background needed to include fluctuations beyond the mean-field approximation, which will be done in the next chapter.

3

CONCEPTS OF THE RENORMALIZATION GROUP

Classically, the solutions of the equations of motions are well-determined paths. In contrast, in quantum mechanics all paths are allowed. Each path is weighted by a factor $\exp(iS)$, where S denotes the action of the path. The solution of a quantum field theory in the path-integral picture consists of a complete summation over all possible field configurations with the respective measure. All information is finally encoded in a low-energy effective action. In the following, we will present a modern approach to compute the effective action, namely the functional renormalization group. The extension to finite temperatures and chemical potentials is discussed.

3.1 THE EFFECTIVE ACTION

Nowadays, most quantum field theories are understood as effective theories. The theory is modeled to describe nature in a certain range of momenta, or, equivalently, at certain length scales. Accordingly, effective field theories naturally come with a certain cutoff scale, Λ. In quantum electrodynamics, for instance, if one tries to push the cut-off scale Λ to infinity, one either generates a non-physical Landau-ghost [172], or ends up with a trivial free theory. Scalar ϕ^4 theory is quite likely plagued by the same triviality problem and does not exist without a cut-off scale [173]. Only in asymptotically free non-abelian gauge theories the cutoff can in principle be pushed to infinity. In the following, we will study theories defined at a scale Λ. The theory consists of a certain number of degrees of freedom – the quantum fields – and a Lagrangian $\mathcal{L}$, which encodes the dynamics. The fields can consist of bosonic degrees of freedom, φ, as well as fermionic ones, ψ and $\bar{\psi}$. The momentum dependence will in the following be denoted by a subscript, i.e.,

$$\varphi_p \equiv \varphi(p)\,, \quad \psi_p \equiv \psi(p)\,, \quad \bar{\psi}_p \equiv \bar{\psi}(p)\,. \tag{3.1}$$

It is useful to combine the bosonic and fermionic fields into a vector

$$\xi_p = \begin{pmatrix} \varphi_p \\ \psi_p \\ \bar{\psi}^T_{-p} \end{pmatrix}\,, \quad \xi^T_p := (\xi^T)_{-p} = (\varphi_{-p}\,,\ \psi^T_{-p}\,,\ \bar{\psi}_p). \tag{3.2}$$

In order to keep the equations readable, we adopt in the following DeWitt's condensed notation [174]. A quantum field $\eta^a(x)$ is then simply denoted by η^I, where now I stands for space-time coordinates x as well as external indices a. Moreover, the product of two fields $\tilde{\chi}$ and χ is defined as

$$\tilde{\chi}\chi \equiv \tilde{\chi}_I \chi^I = \sum_a \int d^4x\ \tilde{\chi}^a(x)\ \chi^a(x) = \sum_a \int \frac{d^4p}{(2\pi)^4}\ \tilde{\chi}^a(-p)\ \chi^a(p)\,. \tag{3.3}$$

The **partition function** $Z[J]$ and the **Schwinger functional** (or energy functional) $W[J]$ depend on the external sources $J = (j, \bar{\eta}, \eta^T)^T$. They are defined as

$$Z[J] = \mathrm{e}^{-iW[J]} = \int \mathcal{D}\xi \ \mathrm{e}^{i\int d^4x\, \mathcal{L}+iJ^T\xi} \,. \tag{3.4}$$

In the spirit of Feynman's path-integral formalism, the partition function is a sum over all possible field configurations, weighted with the respective measure. The expectation value of an operator $\mathcal{O}$ (which can contain fields and its derivatives) is in the presence of external charges J given by

$$\langle \mathcal{O} \rangle_J = \frac{1}{Z[J]} \int \mathcal{D}\xi \ \mathcal{O}\, \mathrm{e}^{i\int d^4x\, \mathcal{L}+iJ^T\xi} \,. \tag{3.5}$$

For $n \geq 3$, the Schwinger functional W it is the generating functional of all connected correlation functions, i.e.,

$$\left. \frac{\delta^n W[J]}{i\delta J_{i_1}^T(x_1) \cdots i\delta J_{i_n}^T(x_n)} \right|_{J=0} = i \langle \xi_{i_1}(x_1) \cdots \xi_{i_n}(x_n) \rangle_{\text{conn}} \,. \tag{3.6}$$

Moreover, the propagator $D_i(x, y)$ of ξ_i is the connected two-point function and given by a second derivative

$$\left. \frac{\delta^2 W[J]}{i\delta J_i^T(x_1)\ i\delta J_i(x_2)} \right|_{J=0} = iD_i(x_1, x_2) \,. \tag{3.7}$$

Therefore, the Schwinger functional contains all information of the quantum field theory. In the presence of a small coupling, W can be computed in a perturbative way with the help of Feynman diagrams. However, at a strong coupling, or in the vicinity of phase changes, such as those in QCD at finite temperature and chemical potential, no such expansion parameter exists. A non-perturbative computation is required.

Instead of computing the partition function directly, which is a function of external charges, it is fruitful to to change variables. The new variables are the expectation values of the quantum fields ξ in a background source J, the **classical fields**

$$\Phi_i(x) = \langle \xi_i(x) \rangle_J = -\frac{\delta W[J]}{\delta J_i^T(x)} \,. \tag{3.8}$$

The components of the classical fields in momentum space are in analogy to Eq. (3.2) defined as

$$\Phi_p = \begin{pmatrix} \phi_p \\ \Psi_p \\ \bar{\Psi}_{-p}^T \end{pmatrix} \,, \quad \Phi_p^T \equiv (\Phi^T)_{-p} = (\phi_{-p}\,,\ \Psi_{-p}^T\,,\ \bar{\Psi}_p). \tag{3.9}$$

The change of variables is realized by a Legendre transformation of the Schwinger functional,

$$\Gamma[\Phi] = -W[J] - J^T\Phi \,, \tag{3.10}$$

which is the Φ-dependent **(quantum) effective action**. From the definition of the effective action directly follow the quantum equations of motion,

$$\frac{\delta\Gamma[\Phi]}{\delta\Phi_i(x)} = -J_i^T(x) \,. \tag{3.11}$$

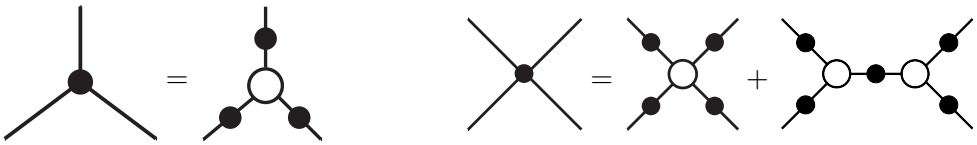

Figure 3: Relation between connected diagrams (full dots) and 1PI diagrams (open circles), in the case of three-point correlators (left-hand side) and four-point correlators (right-hand side).

In the absence of external sources, the right-hand side vanishes. Therefore, one important feature of the effective action is that it is minimized by the classical field configuration $\Phi(x)$. From topological considerations, there sometimes exist configurations that are space-time dependent. Important examples are solitons, monopoles, domain walls, and cosmic strings. Nevertheless, the minimizing field configuration often is homogeneously distributed, i.e., $\Phi(x) \equiv \Phi = \text{const.}$, one example being the chiral condensate in nuclear matter. In this case, the effective action factors, i.e.,

$$\Gamma[\Phi] = -(VT) \cdot U(\Phi)\,, \tag{3.12}$$

where $U(\Phi)$ is the **(quantum) effective potential**, and (VT) is a four-dimensional volume factor, time T times spatial volume V. In this case, Γ is no longer a functional, but only a function, which often leads to tremendous simplifications, as we will see below.

A second important property of the effective action Γ is that it also serves as a generating functional. Whereas the Schwinger functional W gave us all connected diagrams, the effective action Γ generates all one-particle irreducible (1PI) diagrams. These diagrams cannot be split into two by cutting a single line. For $n \geq 3$, the 1PI diagrams are the n-th moments of Γ,

$$\frac{\delta^n \Gamma[\Phi]}{\delta\Phi_{i_1}(x_1)\cdots\delta\Phi_{i_n}(x_n)} = -i\langle \xi_{i_1}(x_1)\cdots\xi_{i_n}(x_n)\rangle_{\text{1PI}}\,. \tag{3.13}$$

The connected n-point functions can be written in terms of 1PI-functions and connected m-point functions with $m < n$. The respective diagrams for $n = 3$ and $n = 4$ are shown in Fig. 3. Moreover, the second derivative of the effective action with respect to the fields is the inverse propagator,

$$\frac{\delta^2 \Gamma[\Phi]}{\delta\Phi_i^T(x_1)\;\delta\Phi_i(x_2)} = iD_i^{-1}(x_1, x_2)\,, \tag{3.14}$$

which follows from Eq. (3.7) and the identity

$$\int d^4z\; \frac{\delta^2 W[\Phi]}{\delta J_i^T(x_1)\;\delta J_i(z)}\;\frac{\delta^2 \Gamma[\Phi]}{\delta\Phi_i^T(z)\;\delta\Phi_i(x_2)} = \delta(x_1 - x_2)\,. \tag{3.15}$$

In other words, the quantum effective action already contains all correlation functions at tree-level. It is the low-energy action with all quantum fluctuations integrated out. If the effective action is known, the low-energy theory is completely solved, and therefore it is of great interest to know efficient methods to compute the effective action. In the presence of a small coupling (such as the coupling strength or $1/N_c$ in the large-N_c limit) the theory can be treated perturbatively. Then, up to one-loop order, the effective action can be computed (see, e.g., [65]) as

$$\Gamma[\Phi] = S[\Phi] + \frac{i}{2}\,\text{Tr}\log\frac{\delta^2 S}{\delta\Phi^2} + \text{higher order}. \tag{3.16}$$

In the next section, we will extend the concepts above to finite temperatures.

3.2 FINITE TEMPERATURE

Thermodynamics and quantum field theory in the path-integral formalism are conceptually very similar (see the textbooks [175, 176]). In statistical mechanics, a system in thermal equilibrium is described by the grand-canonical partition function

$$Z_{\rm gc} = \mathrm{Tr}\, \mathrm{e}^{-\beta(H-\mu N)}\,, \tag{3.17}$$

where H is the Hamiltonian and N the particle number operator. The inverse temperature $\beta = 1/T$ and the chemical potential μ are introduced as Lagrange multipliers which ensure the conservation of energy and particle number. The grand-canonical potential is formally very similar to the partition function (3.4) of a quantum field theory, with the inverse temperature playing the role of time. In the Matsubara formalism, a thermal field theory can be obtained by Wick rotating the time dimension, $t = x^0 \to -i\tau = -ix^4_{\rm E}$. The time integral $\int dt$ is replaced by an integral over τ. The τ-dimension is compactified on a circle with radius β. The (anti-)commutation relations imply that bosonic fields φ are periodic while fermionic fields ψ are antiperiodic, i.e.,

$$\varphi(\boldsymbol{x},\beta) = \varphi(\boldsymbol{x},0)\,, \quad \psi(\boldsymbol{x},\beta) = -\psi(\boldsymbol{x},0)\,. \tag{3.18}$$

As follows from a Fourier analysis, the corresponding momenta in the finite τ-direction are discrete, i.e., $p_4 \to -\omega_l$, where ω_l with $l \in \mathbb{Z}$ are the **Matsubara frequencies**,

$$\begin{aligned} &\omega_l = 2l\pi T\,, && \text{for bosons,} \\ &\omega_l = (2l+1)\pi T\,, && \text{for fermions.} \end{aligned} \tag{3.19}$$

Therefore, the four-dimensional momentum integral at zero temperature is replaced by a three-dimensional integral and a summation over Matsubara frequencies:

$$\int \frac{d^4p}{(2\pi)^4} \quad \to \quad T\sum_{\omega_l} \int \frac{d^3p}{(2\pi)^3}\,. \tag{3.20}$$

We are finally interested in theories containing fermions ψ interacting with scalar fields φ via a Yukawa interaction of strength g_φ and with a massive vector field A via a covariant derivative $D_\mu = \partial_\mu - ig_A A_\mu$. The most general action needed in the present context is in Minkowskian signature given by

$$S_{\rm M} = \int d^4x \,\Big[\bar\psi(i\gamma^\mu D_\mu - g_\varphi\varphi)\psi + \frac{1}{2}\partial_\mu\varphi\,\partial^\mu\varphi - U(\varphi) - \frac{1}{4}F_{\mu\nu}F^{\mu\nu} + \frac{m_A^2}{2}A_\mu A^\mu\Big], \tag{3.21}$$

where $F_{\mu\nu}$ is the field strength of the (possibly non-abelian) field A_μ and $U(\phi)$ is a potential, which contains powers of ϕ and its derivatives. As shown in more detail in Appendix A.1, the Minkowski action is turned into a Euclidean action

$$\begin{aligned} S_{\rm E} = \int_0^\beta d\tau \int d^3x_{\rm E} \,\Big[&\bar\psi(\gamma^\mu_{\rm E} D^{\rm E}_\mu + g_\varphi\varphi)\psi + \frac{1}{2}\partial^{\rm E}_\mu\varphi\,\partial^\mu_{\rm E}\phi + U(\varphi) \\ &+ \frac{1}{4}F_{\mu\nu}F^{\mu\nu} + \frac{m_A^2}{2}A^{\rm E}_\mu A^\mu_{\rm E}\Big]. \end{aligned} \tag{3.22}$$

The definition of the Euclidean objects, $\gamma^\mu_{\rm E}$, $\partial^{\rm E}_\mu$, and $A^{\rm E}_\mu$ can also be found in the appendix. As in statistical mechanics, a chemical potential μ for the fermionic modes is introduced as a Lagrange parameter corresponding to the conserved particle number,

$$N = \int d^3x\, \psi^\dagger(x)\,\psi(x) = \int d^3x\, \bar\psi(x)\,\gamma^0\,\psi(x)\,. \tag{3.23}$$

As a consequence, a term $\beta\mu N$ is added to the exponent in the path integral. Altogether, the partition function in Minkowskian signature at $T = 0$ and $\mu = 0$, which is given by

$$Z_{\mathrm{M}}[J_i] = \int \mathcal{D}\psi\, \mathcal{D}\psi^\dagger\, \mathcal{D}\varphi\, \exp\Big(iS_{\mathrm{M}} + iJ^T\xi\Big), \tag{3.24}$$

transforms into a partition function in Euclidean space at finite temperature T and chemical potential μ, given by

$$Z_{\mathrm{M}}[J_i, T, \mu] = \int \mathcal{D}\psi\, \mathcal{D}\psi^\dagger\, \mathcal{D}\varphi\, \exp\Big(- S_{\mathrm{E}} + \int_0^\beta d\tau \int d^3x\, \mu\psi^\dagger\psi + J^T\xi\Big). \tag{3.25}$$

In complete analogy to the vacuum field theory, one can derive an effective action in the presence of temperature and chemical potentials. Since the theory is defined in Euclidean space, the definitions differ by several factors of i and -1 as compared to the vacuum field theory. The Schwinger functional $W_{\mathrm{E}}[J, T, \mu]$ is the logarithm of the partition function, i.e.,

$$\mathrm{e}^{W_{\mathrm{E}}[J,T,\mu]} = Z_{\mathrm{E}}[J, T, \mu]\,. \tag{3.26}$$

The expectation value of ξ in the background of the source J defines the classical field

$$\Phi_i(x) = \langle \xi_i(x)\rangle_{J,T,\mu} = \frac{\delta W_{\mathrm{E}}[J, T, \mu]}{\delta J_i^T(x)}\,. \tag{3.27}$$

The propagator can be derived from the Schwinger functional via

$$\left.\frac{\delta^2 W_{\mathrm{E}}[J, T, \mu]}{\delta J_i^T(x_1)\, \delta J_i(x_2)}\right|_{J=0} = D_i(x_1, x_2)\,. \tag{3.28}$$

The effective action is the Legendre transform of the Schwinger functional,

$$\Gamma_{\mathrm{E}}[\Phi, T, \mu] = -W_{\mathrm{E}}[J, T, \mu] + J^T\,\Phi\,, \tag{3.29}$$

which implies the quantum equations of motion

$$\frac{\delta\Gamma_{\mathrm{E}}[\Phi, T, \mu]}{\delta\Phi_i(x)} = J_i^T(x)\,. \tag{3.30}$$

The inverse propagator is given by

$$\frac{\delta^2\Gamma_{\mathrm{E}}[\Phi, T, \mu]}{\delta\Phi_i^T(x_1)\, \delta\Phi_i(x_2)} = D_i^{-1}(x_1, x_2)\,. \tag{3.31}$$

As in the vacuum case, for spatially constant solutions Φ of the quantum equations of motion (such as the chiral condensate), the effective actions simplifies to

$$\Gamma_{\mathrm{E}}[\Phi, T, \mu] = (\beta V)\cdot U_{\mathrm{E}}(\Phi, T, \mu)\,, \tag{3.32}$$

where βV is the Euclidean volume. Again, the effective potential $U_{\mathrm{E}}(\Phi, T, \mu)$ is only a function of Φ and no longer a functional. Let $\Phi_{\mathrm{min}}(T, \mu)$ be the minimum of the potential U at a given temperature and chemical potential. If the potential is evaluated at its minimum and the external sources are set to zero, the partition function takes the simple form

$$Z_{\mathrm{E}}(T, \mu) = \mathrm{e}^{-\beta V\, U_{\mathrm{gc}}(T,\mu)}\,, \tag{3.33}$$

where U_{gc} is the **grand-canonical potential**,

$$U_{\mathrm{gc}}(T,\mu) = U\big(\Phi_{\mathrm{min}}(T,\mu),T,\mu\big)\,. \tag{3.34}$$

Equation (3.33) is identified as the grand-canonical partition function of a system in thermodynamic equilibrium. All thermodynamic observables can be computed from the corresponding grand-canonical potential U_{gc}. In particular, the pressure p, the fermion density n, the entropy density s, and the energy density ϵ, are given by

$$\begin{aligned} p &= -U_{\mathrm{gc}}(T,\mu)\,, \qquad & n &= -\frac{\partial U_{\mathrm{gc}}(T,\mu)}{\partial \mu}\,, \\ s &= -\frac{\partial U_{\mathrm{gc}}(T,\mu)}{\partial T}\,, & \epsilon &= -p + \mu n + T s\,. \end{aligned} \tag{3.35}$$

So far, we have only defined the effective action but we have not yet shown any practical way how to compute the effective action efficiently. We will turn to this point in the next section.

3.3 EXACT RENORMALIZATION GROUP EQUATIONS

Often, a perturbative computation of the effective action is not feasible. As we have seen in Sec. 2.3, this is the case in QCD at low energies, as the coupling grows too large and perturbation theory breaks down. Further obstacles to perturbation theory are phase transitions, such as the nuclear liquid-gas transition. The correlation length of effective (quasi-)particles becomes large as compared to the characteristic distance between the microscopic objects of the theory. If this is the case, interactions spread over the medium and collective effects dominate.

3.3.1 *Wilson's RG and Polchinski's RG*

New non-perturbative approaches became possible through Wilson's understanding of the renormalization group [177] (see [178] for a short historical overview). In perturbative field theory, one tries to integrate out all momentum scales at once. In general, this leads to divergences both in the infrared and in the ultraviolet regime, which have to be regulated in some way. We have however seen that we usually deal with effective theories, defined at a certain momentum scale Λ. Wilson's idea was to study how a theory changes if the momentum scale is lowered to a new scale $c\Lambda$, with $c < 1$. His proposal was to integrate out momentum shells, i.e., all contributions to the path integral with $c\Lambda < |p| < \Lambda$. After a rescaling procedure, a new effective theory results, now at a scale $c\Lambda$. In principle, all operators allowed by the underlying symmetries have to be included. Their respective couplings are changing according to the renormalization group equations. In this way, new operators naturally appear in the Lagrangian. This procedure is often numerically more stable and easier to solve than a perturbative calculation. Most importantly, it is a completetly non-perturbative approach and does not depend on any small couplings.

There are several different implementations of Wilson's idea to compute the effective action, which are sometimes collectively called **exact renormalization group equations** (ERGE). The first one, **Wilson's ERGE**, implements the idea of momentum shells in a direct way. Let us rewrite the partition function in Euclidean space as

$$Z = \int [\mathcal{D}\xi]_{|p|<\Lambda}\ \mathrm{e}^{-S_\Lambda[\xi]} = \int [\mathcal{D}\xi]_{|p|<c\Lambda} \int [\mathcal{D}\xi]_{c\Lambda<|p|<\Lambda}\ \mathrm{e}^{-S_\Lambda[\xi]}\,, \tag{3.36}$$

where the path integral measure over the fields was split according to the contributing momentum scales. If one now defines

$$\mathrm{e}^{-S_{c\Lambda}[\xi]} \equiv \int [\mathcal{D}\xi]_{c\Lambda<|p|<\Lambda} \ \mathrm{e}^{-S_{\Lambda}[\xi]} \,, \tag{3.37}$$

then the partition function reads

$$Z = \int [\mathcal{D}\xi]_{|p|<c\Lambda} \ \mathrm{e}^{-S_{c\Lambda}[\xi]} \ . \tag{3.38}$$

The path integral has the same structure as in Eq. (3.36). However, the momenta of the fields contributing to the partition function are now restricted to the range $|p| < c\Lambda$. What is described in this way is the flow of the action in the space of all possible actions, sometimes called **theory space**.

Wilson's ERGE is straightforward to write down, but almost impossible to tackle numerically. In general, non-local interactions are generated and a derivative expansion is not possible. An improvement is **Polchinski's ERGE** as proposed in Ref. [179]. The idea of Polchinksi was to replace the sharp momentum cutoff by a softer one (see [180] for a review). He added a **regulator term**,

$$\Delta S_k[\xi] = \frac{1}{2} \xi^T R_k \, \xi \,, \tag{3.39}$$

to the action, where R_k is a regulator function and k is a renormalization scale with the dimension of a momentum. The renormalization scale plays the role of an intrinsic resolution length $\sim k^{-1}$. The action then is k-dependent, i.e.,

$$S_k^{\mathrm{Pol}}[\xi, J] = S_k^{\mathrm{Pol}}[\xi] + \Delta S_k[\xi] - J^T \xi \,. \tag{3.40}$$

This action gives rise to the following definition of a partition function:

$$Z_k^{\mathrm{Pol}}[J] = \int \mathcal{D}\xi \, \mathrm{e}^{-S_k^{\mathrm{Pol}}[\xi, J]} \ . \tag{3.41}$$

The regulator function as introduced by Polchinski has to satisfy three conditions:

1. First, R_k is supposed to regularize the theory in the infrared regime. Therefore, it must be positive for small momenta, i.e.,

$$\lim_{p^2/k^2 \to 0} R_k(p^2) > 0 \,. \tag{3.42}$$

2. Next, R_k has to vanish for $k \to 0$, i.e.,

$$\lim_{k^2/p^2 \to 0} R_k(p^2) = 0 \,. \tag{3.43}$$

   In this way, it is ensured that the partition function Z_k reduces to the full low-energy partition function as k goes to zero.

3. Finally, for $k \to \Lambda$, the regulator function has to be large. In this way, one recovers the bare action as the starting point at $k = \Lambda$.

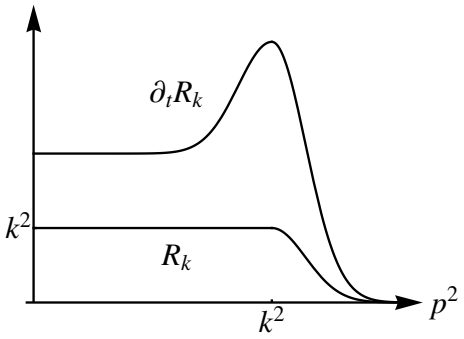

Figure 4: Typical behaviour of the regulator function R_k and its derivative $\partial_t R_k = k\partial_k R_k$.

The regulator therefore typically looks like the one in Fig. 4. Modes with squared momentum below k^2 are equipped with an effective squared mass $m^2 \sim k^2$. Higher momentum modes are not altered, and the regulator vanishes. The exact form of the regulator function is in principle arbitrary. The flow in theory space will change, but the endpoint in the limit $k \to 0$ will be the same. In practice, approximations must be made, and also the endpoint in theory space will depend on the specific choice of the regulator function.

We now turn to the determination of $S_k^{\mathrm{Pol}}[\xi]$. The renormalization group procedure consists of a rewriting of the path integral as the momentum scale is lowered. In the spirit of Wilson's integration over momentum shells, its value should not depend on the renormalization scale k. Therefore, $\frac{\partial Z_k^{\mathrm{Pol}}}{\partial k} = 0$. This conditions allows us to solve for $S_k^{\mathrm{Pol}}[\xi]$. Its evolution as k is lowered is described by Polchinski's equation [179]

$$\frac{\partial S_k^{\mathrm{Pol}}[\xi]}{\partial k} = \frac{1}{2}\frac{\delta S_k^{\mathrm{Pol}}[\xi]}{\delta \xi}\cdot\frac{\partial R_k^{-1}}{\partial k}\cdot\frac{\delta S_k^{\mathrm{Pol}}[\xi]}{\delta \xi} - \frac{1}{2}\,\mathrm{Tr}\left(\frac{\partial R_k^{-1}}{\partial k}\frac{\delta^2 S_k^{\mathrm{Pol}}[\xi]}{\delta \xi^2}\right). \tag{3.44}$$

3.3.2 *The functional RG*

Polchinski's ERGE deals directly with the partition function in the path integral formalism. It turns out that it is numerically and conceptually easier to consider the effective action instead. This is the so-called **functional renormalization group** (FRG) approach. For numerous reviews we refer for instance to Refs. [181–189]. Instead of Eq. (3.40), one defines

$$S_k[\xi, J] = S[\xi] + \Delta S_k[\xi] - J^T\xi\,, \tag{3.45}$$

where the k-dependent action $S_k^{\mathrm{Pol}}[\xi]$ was replaced by the classical action $S[\xi]$ and $\Delta S_k[\xi]$ is defined as in Eq. (3.39). The regulator term R_k has to satisfy the same conditions as above on page 29. The construction of the k-dependent effective action parallels the discussion leading to Eq. (3.10). The partition function is

$$Z_k[J] = \mathrm{e}^{W_k[J]} = \int \mathcal{D}\xi\, \mathrm{e}^{-S_k[\xi,J]}\,. \tag{3.46}$$

The classical field,

$$\Phi = \frac{\delta W_k[J]}{\delta J^T} = \langle\xi\rangle_J\,, \tag{3.47}$$

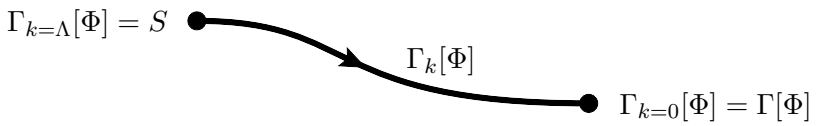

Figure 5: The flow of the effective action Γ_k in the infinite-dimensional "theory space", spanned by all operators allowed by the symmetries. The dynamics as a function of the renormalization scale k is governed by the flow equation.

is computed from the Schwinger functional $W_k[J]$. The **k-dependent effective action** is defined as a slight modification of the Legendre transformation[9]. If $\widetilde{\Gamma}_k[\Phi]$ denotes the Legendre transform of $W_k[J]$, then

$$\Gamma_k[\Phi] = \widetilde{\Gamma}_k[\Phi] - \Delta S_k[\Phi] = -W_k[J] + \Phi^T J - \frac{1}{2}\Phi^T R_k \Phi. \tag{3.48}$$

The action Γ_k is designed in such a way that it interpolates between the microscopic action (for $k = \Lambda$) and the full quantum effective action (in the limit $k \to 0$), as illustrated in Fig. 5.

One defines the derivatives of the effective action with respect to the fields (with the short-hand notation $\delta_{\Phi_p} \equiv \frac{\delta}{\delta \Phi_p}$) as follows:

$$\Gamma_k^{(n,m)}(p_1, \ldots, p_n, q_1, \ldots, q_m) \equiv \overrightarrow{\delta}_{\Phi^T_{p_1}} \cdots \overrightarrow{\delta}_{\Phi^T_{p_n}} \Gamma_k \overleftarrow{\delta}_{\Phi_{q_1}} \cdots \overleftarrow{\delta}_{\Phi_{q_m}} . \tag{3.49}$$

For the flow equation, the second derivative of the effective action is needed, which is the following matrix (in what is sometimes called "superspace"):

$$\Gamma_k^{(1,1)}(p,p') = \overrightarrow{\delta}_{\Phi^T_p} \Gamma_k \overleftarrow{\delta}_{\Phi_{p'}} = \begin{pmatrix} \overrightarrow{\delta}_{\phi_{-p}} \Gamma_k \overleftarrow{\delta}_{\phi_{p'}} & \overrightarrow{\delta}_{\phi_{-p}} \Gamma_k \overleftarrow{\delta}_{\Psi_{p'}} & \overrightarrow{\delta}_{\phi_{-p}} \Gamma_k \overleftarrow{\delta}_{\bar{\Psi}^T_{-p'}} \\ \overrightarrow{\delta}_{\Psi^T_{-p}} \Gamma_k \overleftarrow{\delta}_{\phi_{p'}} & \overrightarrow{\delta}_{\Psi^T_{-p}} \Gamma_k \overleftarrow{\delta}_{\Psi_{p'}} & \overrightarrow{\delta}_{\Psi^T_{-p}} \Gamma_k \overleftarrow{\delta}_{\bar{\Psi}^T_{-p'}} \\ \overrightarrow{\delta}_{\bar{\Psi}_p} \Gamma_k \overleftarrow{\delta}_{\phi_{p'}} & \overrightarrow{\delta}_{\bar{\Psi}_p} \Gamma_k \overleftarrow{\delta}_{\Psi_{p'}} & \overrightarrow{\delta}_{\bar{\Psi}_p} \Gamma_k \overleftarrow{\delta}_{\bar{\Psi}^T_{-p'}} \end{pmatrix} . \tag{3.50}$$

With these definitions we can now write down the **flow equation** for the effective action Γ_k as it was first deduced by Christof Wetterich [190]:

$$k\frac{\partial \Gamma_k[\Phi]}{\partial k} = \frac{1}{2}\,\mathrm{Tr}\left[k\frac{\partial R_k}{\partial k} \cdot \left(\Gamma_k^{(1,1)}[\Phi] + R_k\right)^{-1}\right] = \frac{1}{2}$$

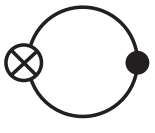

. (3.51)

Wetterich's flow equation relates the change of the k-dependent effective action to a one-loop diagram. In general, the flow equation is a functional differential equation, because Φ can depend on space-time coordinates as well. In the pictorial version on the right-hand side, the line with the dot denotes a full propagator, whereas the cross denotes the insertion of the regulator function $k\frac{\partial R_k}{\partial k}$. The trace goes over internal and space-time indices. Moreover, it extends over the bosonic and fermionic subspaces as indicated in the structure of the matrix (3.50). It is understood that the fermionic subspace comes with an additional minus sign (sometimes called "supertrace").

9 The modification is needed in order to establish the connection between Γ_k and the microscopic action S in the limit $k \to \Lambda$.

As compared to the path integral formalism, a formulation in terms of differential equations has numerical advantages. Differential equations are often easier to implement and are considerably more stable. Furthermore, the flow equations are invariant under all symmetries of the underlying theory, which is not always the case in a Wilsonian-type block spin approach. This feature is particularly important in the case of gauge theories. As compared to Polchinski's equation, the FRG equations can be understood more intuitively in terms of loop diagrams.

The flow equation can be proven as follows: First, the quantum equations of motion at the scale k derived from the original (unmodified) effective action defined in Eq. (3.48) are

$$J = \overrightarrow{\delta}_{\Phi^T} \widetilde{\Gamma}_k[\Phi] = \overrightarrow{\delta}_{\Phi^T} \Gamma_k[\Phi] + R_k\Phi = \Gamma_k^{(1,0)}[\Phi] + R_k\Phi\,. \tag{3.52}$$

Moreover, the full k-dependent propagator D_k can be expressed in terms of the effective action from the following consideration:

$$\left.\begin{aligned} \frac{\delta J}{\delta\Phi} &\overset{(3.52)}{=} \Gamma_k^{(1,0)}[\Phi] \overleftarrow{\delta}_\Phi + R_k = \Gamma_k^{(1,1)}[\Phi] + R_k \\ \frac{\delta\Phi}{\delta J} &\overset{(3.47)}{=} \frac{\delta^2 W_k[J]}{\delta J^T\,\delta J} \overset{(3.28)}{=} D_k. \end{aligned}\right\} \Longrightarrow D_k = \left(\Gamma_k^{(1,1)}[\Phi] + R_k\right)^{-1}. \tag{3.53}$$

Note that the term R_k originates from the modified Legendre transformation (3.48). In terms of the unmodified Legendre transformation $\widetilde{\Gamma}_k$ we re-derive the formula (3.31):

$$D_k = \left(\Gamma_k^{(1,1)}[\Phi] + R_k\right)^{-1} = \left(\widetilde{\Gamma}_k^{(1,1)}[\Phi]\right)^{-1}. \tag{3.54}$$

The computation of the flow of Γ_k is now straightforward:

$$\begin{aligned} \frac{\partial\Gamma_k[\Phi]}{\partial k} &\overset{(3.48)}{=} -\left(\frac{\partial W_k}{\partial k}\right)[J] \underbrace{-\frac{\delta W_k[J]}{\delta J}\cdot\frac{\partial J}{\partial k} + \frac{\partial J}{\partial k}\cdot\Phi^T}_{=0} - \frac{1}{2}\Phi^T\frac{\partial R_k}{\partial k}\Phi \\ &\overset{(3.46)}{=} \frac{1}{2}\left\langle \xi^T\frac{\partial R_k}{\partial k}\,\xi\right\rangle - \frac{1}{2}\Phi^T\frac{\partial R_k}{\partial k}\Phi = \frac{1}{2}\frac{\partial R_k}{\partial k}\cdot\frac{\delta^2 W_k[J]}{\delta J^T\,\delta J} \\ &\overset{(3.53)}{=} \frac{1}{2}\frac{\partial R_k}{\partial k}\cdot\left(\Gamma_k^{(1,1)}[\Phi] + R_k\right)^{-1}. \end{aligned} \tag{3.55}$$

The formula includes – hidden in the DeWitt notation – a trace over internal, "superspace", and space-time indices. If we write down the trace explicitly, we arrive at the flow equation (3.51).

The k-dependent effective action interpolates as desired between microscopic and quantum effective action, which can be seen as follows:

1. By expanding the action around the classical (background) field Φ, it is easy to derive from Eq. (3.48) that

$$\mathrm{e}^{-\Gamma_k[\Phi]} = \int \mathcal{D}\xi\, \mathrm{e}^{-S[\Phi+\xi] + \frac{\delta\Gamma_k}{\delta\Phi}\xi - \frac{1}{2}\xi R_k\xi}\,. \tag{3.56}$$

   For $k = \Lambda$, the regulator function R_k is required to be large. Consequently, $-\frac{1}{2}\xi R_k\xi$ leads to a delta-functional $\delta[\xi]$. Only the classical field configuration contributes to the path integral and therefore $\Gamma_k[\Phi] \xrightarrow{k\to\Lambda} S[\Phi]$. The regulator equips all particles with large effective masses. Consequently, all fluctuations around the classical field configuration are highly suppressed and only the classical configuration can contribute.

2. In the opposite limit, when $k \to 0$, the regulator term vanishes. All modes are fully integrated out, so $\Gamma_k \to \widetilde{\Gamma}_k \to \Gamma$.

In general, the effective action contains all possible operators that respect the symmetries of the underlying theory. The relative strength of these operators is then computed by Wetterich's flow equation. In this way, one gets an infinite tower of coupled equations. Similar to the Dyson-Schwinger equations it is not feasible to compute an infinite number of differential equations. It is therefore important to truncate the set of flow equations in such a way that the most relevant operators are kept. In the **derivative expansion** [191], only powers of derivatives of the fields up to a certain order are kept. All higher derivative couplings are ignored. This approach is often combined with an expansion in powers of the fields. The derivative expansion provides a useful scheme that allows systematic improvement by going to higher orders. In practice, most calculations work at leading order in the derivative expansion. It is instructive to first study a $O(N)$-symmetric model with scalars ϕ_i, $i = 1, \ldots, N$. The square of the fields that is invariant under $O(N)$ transformations is denoted as $\chi = \frac{1}{2}\phi^a\phi^a$. To leading order in the derivative expansion, the effective action has the form [192]

$$\Gamma_k = \int d^4x \left[\frac{1}{2} Z_k(\chi)\, \partial_\mu \phi^a\, \partial^\mu \phi^a + \frac{1}{4} Y_k(\chi)\, \partial_\mu \chi\, \partial^\mu \chi + U_k(\chi)\right]. \tag{3.57}$$

A non-trivial wave-function renormalization Z_k leads to an anomalous dimension. If $Z_k \equiv 1$ and $Y_k \equiv 0$, one speaks of the **local potential approximation** (LPA, [193]). A study of an $O(N)$ model indeed indicates that the anomalous dimension is negligible [194]. In the LPA, it is possible to derive an optimized regulator function [195]. The **Litim regulator functions** for bosonic and fermionic fields take the simple form

$$\begin{aligned} R_k^{\text{bos}} &= p^2\, r_{\text{bos}} \equiv (k^2 - p^2) \cdot \theta(k^2 - p^2)\,, \\ R_k^{\text{fer}} &= \begin{pmatrix} 0 & ip_\mu (\gamma_{\text{E}}^\mu)^T \\ ip_\mu \gamma_{\text{E}}^\mu & 0 \end{pmatrix} r_{\text{fer}} \equiv \begin{pmatrix} 0 & ip_\mu (\gamma_{\text{E}}^\mu)^T \\ ip_\mu \gamma_{\text{E}}^\mu & 0 \end{pmatrix} \left(\sqrt{\tfrac{k^2}{p^2}} - 1\right) \cdot \theta(k^2 - p^2). \end{aligned} \tag{3.58}$$

The role of the regulator can be understood very intuitively in this case. On the one hand, its appearance in the full loop in the denominator acts as an IR cutoff: For small momentum modes with $p^2 < k^2$, the squared momentum gets replaced by the larger regulator scale k^2. Even massless fluctuations acquire a finite effective mass and are therefore smoothed out. On the other hand, the regulator insertion $k\frac{dR_k}{dk}$ in the nominator regulates in the ultraviolet regime, and modes with $p^2 > k^2$ do not contribute to the flow. The flow equation therefore is manifestly both UV and IR finite.

The Litim regulator is optimal in the sense that it maximizes the denominator,

$$\min_{q^2 \geq 0} \left[\overrightarrow{\delta}_{\Phi_q^T} \Gamma_k \overleftarrow{\delta}_{\Phi_q} + R_k(q^2)\right] = Ck^2 > 0\,. \tag{3.59}$$

The existence of a gap $C > 0$ is necessary in order for the flow to be finite. The maximum is achieved for a regulator that renders the left-hand side momentum independent. Together with the constraints on R_k stated on page 29, the regulator then is uniquely fixed. Moreover, it can be shown that this choice of regulator leads to the fastest decoupling of heavy modes [195].

At finite temperatures, the time integral is converted into a sum over Matsubara frequencies according to Eq. (3.20). The inverse temperature acts already as an UV regulator in the imaginary-time direction. The sum over Matsubara frequencies converges and the

regulator function R_k only has to act on the three-momenta. The regulator takes the form [196, 197]

$$\begin{aligned} R_k^{\text{bos}} &= p^2\, r_{\text{bos}} = (k^2 - |\boldsymbol{p}|^2) \cdot \theta(k^2 - |\boldsymbol{p}|^2)\,, \\ R_k^{\text{fer}} &= \begin{pmatrix} 0 & ip_i(\gamma_{\text{E}}^i)^T \\ ip_i\gamma_{\text{E}}^i & 0 \end{pmatrix} r_{\text{fer}} = \begin{pmatrix} 0 & ip_i(\gamma_{\text{E}}^i)^T \\ ip_i\gamma_{\text{E}}^i & 0 \end{pmatrix} \left(\sqrt{\tfrac{k^2}{|\boldsymbol{p}|^2}} - 1\right) \cdot \theta(k^2 - |\boldsymbol{p}|^2)\,. \end{aligned} \tag{3.60}$$

Because of the structure of the regulators, the dependence on three-momenta is eliminated and only an integral over a theta-function remains. Then it is often possible to perform the Matsubara sum, and the flow equation can be written down analytically.

3.4 NUMERICAL EVALUATION

In the following, different strategies are examined to numerically compute Wetterich's equation. Only the leading-order in the derivative expansion in the local potential approximation is discussed. Even in this case, there are infinitely many operators that are allowed and therefore an infinite system of coupled differential equations has to be solved. One possible truncation is to **Taylor expand** the potential up to a certain order around the renormalization- scale dependent minimum. We again study the $O(N)$ model from Eq. (3.57) (with $Z_k \equiv 1$ and $Y_k \equiv 0$). The ansatz for the effective potential is

$$U_k(\chi) = \sum_{n=1}^{N_{\max}} \frac{a_{n,k}}{n!} (\chi - \chi_{0,k})^n\,. \tag{3.61}$$

The right-hand side of the flow equation (3.51) can also be expanded in a power series around $\chi_{0,k}$. Comparing the coefficients of both sides leads to flow equations for the couplings $a_{n,k}$ and the minimum $\chi_{0,k}$. The convergence of the expansion can be checked by going to higher orders, i.e., by increasing $N_{\max}$.

The Taylor-expansion method is numerically fast. Moreover, the flow equations can be interpreted in a pictorial way, which highlights the underlying physics. We will come back to this point, once we derived the flow equations for the ChNM model. A big drawback, however, is that the method relies on the existence of a unique minimum. Problems occur if the underlying theory shows a first-order phase transition. At a phase transition, the minimum of the potential is discontinuous and it is no longer possible to expand around a global minimum $\chi_{0,k}$. The Taylor expansion method therefore breaks down at first-order transitions, such as the liquid-gas transition.

A different approach that also works for first-order transitions is the **grid method** of Ref. [198]. On the χ-axis, a total of $N_\#$ grid points, χ_i, are chosen. The grid points are distributed with constant spacing, $d = \chi_{i+1} - \chi_i$. Around each of these grid poins, a local effective potential $U_{k,i}$ is defined on the interval $\chi_i - \frac{d}{2} \leq \chi \leq \chi_i + \frac{d}{2}$. Each potential is expanded up to the third power in χ (i.e., sixth powers in the fields) around its respective grid point, i.e.,

$$U_{k,i}(\chi) = \sum_{n=0}^{3} \frac{a_i^{(n)}(k)}{n!} (\chi - \chi_i)^n\,. \tag{3.62}$$

The full effective potential $U_k(\chi)$ is then obtained by gluing together these piecewise defined potentials. The flow equations for $a_i^{(0)}(k)$ is given by Wetterich's equation evaluated

at χ_i. Because Wetterich's equation involves the second derivative of the potential with respect to the fields, the flow equation will be a function f that involves first and second derivatives of the potential with respect to χ. The flow equation for $a_i^{(1)}(k)$ is obtained by differentiating the flow equation for $a_i^{(0)}(k)$ with respect to χ. The system of differential equations is

$$\begin{aligned}\partial_k a_i^{(0)}(k) &= f\big(k, \chi_i, a_i^{(1)}(k), a_i^{(2)}(k)\big),\\ \partial_k a_i^{(1)}(k) &= (\partial_\chi f)\big(k, \chi_i, a_i^{(1)}(k), a_i^{(2)}(k), a_i^{(3)}(k)\big).\end{aligned} \tag{3.63}$$

This is a system of $2N_\#$ uncoupled differential equations, because the equation at grid point i contains no information about the neighboring grid points. However, there are $4N_\#$ unknowns and the system is underdetermined. The potentials at different grid points must be matched in some way. The grand canonical potential is continuous and continuously differentiable, therefore the potential $U_k(\chi)$ and its derivative $U_k^{(1)}(\chi)$ have to be continuous as well, as a consequence of the Gibbs-Duhem relation. Hence, the functions $U_{k,i}(\chi)$ and $U_{k,i}^{(1)}(\chi)$ are matched between two grid points, where both local potentials are defined. In total, there are $2(N_\# - 1)$ matching conditions. To get a closed system of equations, two more equations are needed. We additionally match the second derivative $U_{k,i}^{(2)}(\chi)$ for the outmost grid points between $i = 1$ and $i = 2$, as well as between $i = N_\# - 1$ and $i = N_\#$. In total, all matching conditions are

$$\begin{aligned}&\sum_{n=0}^{3} \frac{1}{n!}\left(\frac{d}{2}\right)^n \Big(a_i^{(n)}(k) - (-1)^n a_{i+1}^{(n)}(k)\Big) = 0\,, \text{ for } i = 1, \dots, N_\# - 1\,,\\ &\sum_{n=0}^{2} \frac{1}{n!}\left(\frac{d}{2}\right)^n \Big(a_i^{(n+1)}(k) - (-1)^n a_{i+1}^{(n+1)}(k)\Big) = 0\,, \text{ for } i = 1, \dots, N_\# - 1\,,\\ &\sum_{n=0}^{1} \frac{1}{n!}\left(\frac{d}{2}\right)^n \Big(a_i^{(n+2)}(k) - (-1)^n a_{i+1}^{(n+2)}(k)\Big) = 0\,, \text{ for } i = 1 \text{ and } N_\# - 1\,.\end{aligned} \tag{3.64}$$

The set of constraint equations can be written as a system of linear equations,

$$A \begin{pmatrix} a_1^{(0)}(k) \\ \vdots \\ a_{N_\#}^{(0)}(k) \\ a_1^{(1)}(k) \\ \vdots \\ a_{N_\#}^{(1)}(k) \end{pmatrix} = B \begin{pmatrix} a_1^{(2)}(k) \\ \vdots \\ a_{N_\#}^{(2)}(k) \\ a_1^{(3)}(k) \\ \vdots \\ a_{N_\#}^{(3)} \end{pmatrix}, \tag{3.65}$$

where A and B are $(2N_\# \times 2N_\#)$-matrices. The matrices A and B are complicated for larger values of $N_\#$ and we will not write them down explicitly. However, a computer algebra system easily inverts the matrix B. The second and third derivatives of the potential, $a_i^{(2)}(k)$ and $a_i^{(3)}(k)$, can then be expressed as functions of zeroth and first derivatives, $a_i^{(0)}(k)$ and $a_i^{(1)}(k)$, respectively. We call the functions g_i and h_i respectively, for each $i = 1, \dots, N_\#$:

$$\begin{aligned}a_i^{(2)}(k) &= g_i\big(\{a_j^{(0)}(k),\, a_j^{(1)}(k)\}_{j=1,\dots,N_\#}\big),\\ a_i^{(3)}(k) &= h_i\big(\{a_j^{(0)}(k),\, a_j^{(1)}(k)\}_{j=1,\dots,N_\#}\big).\end{aligned} \tag{3.66}$$

The functions g_i and h_i depend only linearly on its arguments. The coefficient take their maximal values for the grid-point itself, $j = i$, and adjacent grid points, whereas the influence of more distant grid-points decreases drastically. The $2N_\#$ functions g_i and h_i allow us to eliminate $a_i^{(2)}(k)$ and $a_i^{(3)}(k)$ from the flow equations (3.63). A set of coupled differential equations for $a_i^{(0)}(k)$ and $a_1^{(1)}(k)$ is the result, which can be solved with efficient numerical routines, like Runge-Kutta algorithms. As an initial condition we must provide the potential and its first derivative at the UV scale, i.e., $a_i^{(n)}(\Lambda_{\mathrm{UV}})$, for $n = 1, 2$ and $i = 1, \ldots, N_\#$.

Theoretically, the equations are integrated from $k = \Lambda$ down to $k = 0$. It is in practice not possible to integrate down to $k = 0$. The reason is that the effective action becomes convex, which results in numerical instabilities. If the infrared cutoff k_{IR} is chosen small enough, the location of the minimum does not change anymore and the physical predictions are left unaltered.

The grid method has the great advantage that it determines the potential not only around its minimum as in the Taylor-expansion method, but globally as a function of χ. The downside is that the numerical evaluation is considerably more costly as compared to the Taylor expansion. Nevertheless, because we want to study first-order phase transitions, we will use the grid method for explicit calculations.

We have now set the stage for a proper treatment of fluctuations and can turn to physical applications.

4

FUNCTIONAL RENORMALIZATION GROUP APPROACH TO A CHIRAL NUCLEON-MESON MODEL

We introduce the chiral nucleon-meson model in detail. First, we show how the parameters are adjusted to hadron properties and nuclear physics constraints. Then, the methods of the previous chapter are applied, and the model is investigated in the setup of the functional renormalization group. Symmetric matter is studied, as well as asymmetric matter. Finally, neutron stars are discussed.

4.1 THE CHIRAL NUCLEON-MESON MODEL

One of our aims is to study the chiral restoration at higher chemical potentials and small temperatures. We want to start from the nuclear liquid-gas transition, because then the parameters can be fitted to well-known data. We therefore study a model based on the relevant degrees of freedom within that region. Close to the liquid-gas phase transition, these are nucleons, which are interacting via exchange of effective bosons. To study chiral restoration, chiral symmetry is to be included in the nucleon-model from the beginning. The neutrons and protons are combined into an isospin doublet, $\psi = (\psi_a)_{a=1,2} = (\psi_p,\ \psi_n)^T$, that transforms in the fundamental representation of SU(2). The long-range attractive part of the nucleon-nucleon interaction is modeled by the (2×2)-matrix

$$\Phi = \frac{1}{\sqrt{2}}(\sigma + i\boldsymbol{\pi} \cdot \boldsymbol{\tau}) \tag{4.1}$$

that transforms in the $(\frac{1}{2}, \frac{1}{2})$ representation of the chiral symmetry group $\mathrm{SU}(2)_L \times \mathrm{SU}(2)_R$. Here, $\boldsymbol{\tau}$ are the Pauli matrices in flavor space (see Appendix A.1). The repulsive short-distance foce is included via four-fermion vector-isoscalar interactions $(\bar{\psi}\gamma_\mu\psi)\,(\bar{\psi}\gamma^\mu\psi)$ and vector-isovector interactions $(\bar{\psi}\gamma_\mu\boldsymbol{\tau}\psi) \cdot (\bar{\psi}\gamma^\mu\boldsymbol{\tau}\psi)$. A Hubbard-Stratonovich transformation replaces the four-point interaction with effective vector-bosons, the vector-isoscalar field ω_μ and the vector-isovector field $\boldsymbol{\rho}_\mu$. The field strength tensors are given by

$$\begin{aligned} F^{(\omega)}_{\mu\nu} &= \partial_\mu\omega_\nu - \partial_\nu\omega_\mu\,, \\ \boldsymbol{F}^{(\rho)}_{\mu\nu} &= \partial_\mu\boldsymbol{\rho}_\nu - \partial_\nu\boldsymbol{\rho}_\mu - g_\rho\boldsymbol{\rho}_\mu \times \boldsymbol{\rho}_\nu\,. \end{aligned} \tag{4.2}$$

In Minkowski space-time, the Lagrangian of the **chiral nucleon-meson (ChNM) model** is given by

$$\begin{aligned}\mathcal{L}_{\mathrm{M}} = {}& \bar{\psi}_a i\gamma^\mu \partial_\mu \psi_a + \frac{1}{2}\,\mathrm{Tr}\,\partial\Phi\,\partial\Phi^\dagger - \mathcal{U}_{\mathrm{mic}}(\Phi,\Phi^\dagger) \\ & - \frac{1}{4}F^{(\omega)}_{\mu\nu}F^{(\omega)\mu\nu} - \frac{1}{4}\boldsymbol{F}^{(\rho)}_{\mu\nu}\cdot\boldsymbol{F}^{(\rho)\mu\nu} + \frac{1}{2}m_\omega^2\omega_\mu\omega^\mu + \frac{1}{2}m_\rho^2\boldsymbol{\rho}_\mu\cdot\boldsymbol{\rho}^\mu \\ & - \sqrt{2}\bar{\psi}_a\left[\frac{1}{2}(1+\gamma_5)\big(g_s\Phi_{ab} + g_\omega\gamma^\mu\omega_\mu\delta_{ab} + g_\rho\gamma^\mu\rho^i_\mu\tau^i_{ab}\big)\right]\psi_b \\ & - \sqrt{2}\bar{\psi}_a\left[\frac{1}{2}(1-\gamma_5)\big(g_s(\Phi^\dagger)_{ab} + g_\omega\gamma^\mu\omega_\mu\delta_{ab} + g_\rho\gamma^\mu\rho^i_\mu\tau^i_{ab}\big)\right]\psi_b.\end{aligned} \tag{4.3}$$

The symmetry group $\mathrm{SU}(2)_L \times \mathrm{SU}(2)_R$ is a double cover of SO(4), which induces a Lie algebra isomorphism $\mathfrak{su}(2)_L \times \mathfrak{su}(2)_R \cong \mathfrak{so}(4)$. Therefore, an equivalent description can be given in terms of a four-component field $\phi = (\sigma, \boldsymbol{\pi})$ instead of the field Φ. Its square,

$$\chi = \frac{1}{2}\phi^2 = \frac{1}{2}(\sigma^2 + \boldsymbol{\pi}^2)\,, \tag{4.4}$$

is invariant under chiral SO(4) transformations. In this new notation, the Lagrangian reads:

$$\begin{aligned}\mathcal{L}_{\mathrm{M}} = {}& \bar{\psi}\Big[i\gamma^\mu\partial_\mu - g_s(\sigma + i\gamma_5\boldsymbol{\pi}\cdot\boldsymbol{\tau}) - \gamma^\mu(g_\omega\omega_\mu + g_\rho\boldsymbol{\rho}_\mu\cdot\boldsymbol{\tau})\Big]\psi \\ & + \frac{1}{2}\partial_\mu\sigma\,\partial^\mu\sigma + \frac{1}{2}\partial_\mu\boldsymbol{\pi}\cdot\partial^\mu\boldsymbol{\pi} - \mathcal{U}_{\mathrm{mic}}(\boldsymbol{\pi},\sigma) \\ & - \frac{1}{4}F^{(\omega)}_{\mu\nu}F^{(\omega)\mu\nu} - \frac{1}{4}\boldsymbol{F}^{(\rho)}_{\mu\nu}\cdot\boldsymbol{F}^{(\rho)\mu\nu} + \frac{1}{2}m_\omega^2\omega_\mu\omega^\mu + \frac{1}{2}m_\rho^2\boldsymbol{\rho}_\mu\cdot\boldsymbol{\rho}^\mu\,.\end{aligned} \tag{4.5}$$

Finite temperatures and chemical potentials require a modification. In the Matsubara formalism, space-time is Wick-rotated to Euclidean space. The time-component is rotated as $x^0 \to -i\tau$. The τ-dimension is compactifed on a circle, such that τ is restricted to $[0,\beta]$ with inverse temperature $\beta = 1/T$. Hence, the time-integral is replaced by $-i\int_0^\beta d\tau$. The bosons and fermions are periodic or anti-periodic, respectively, under a shift $\tau \to \tau + \beta$. As we have seen in Sec. 3.2, the Minkowski-space action $S_{\mathrm{M}} = \int d^4x\,\mathcal{L}_{\mathrm{M}}$ is transformed into a Euclidean action $S_{\mathrm{E}} = \int_0^\beta d\tau \int d^3x\,\mathcal{L}_{\mathrm{E}}$ with

$$\begin{aligned}\mathcal{L}_{\mathrm{E}} = {}& \bar{\psi}\Big[\gamma^\mu_{\mathrm{E}}\partial^{\mathrm{E}}_\mu + g_s(\sigma + i\gamma_5\boldsymbol{\pi}\cdot\boldsymbol{\tau}) - i\gamma^\mu(g_\omega\omega^{\mathrm{E}}_\mu + g_\rho\boldsymbol{\rho}^{\mathrm{E}}_\mu\cdot\boldsymbol{\tau})\Big]\psi \\ & + \frac{1}{2}\partial^{\mathrm{E}}_\mu\sigma\,\partial^\mu_{\mathrm{E}}\sigma + \partial^{\mathrm{E}}_\mu\boldsymbol{\pi}\cdot\partial^\mu_{\mathrm{E}}\boldsymbol{\pi} + \mathcal{U}_{\mathrm{mic}}(\boldsymbol{\pi},\sigma) \\ & + \frac{1}{4}F^{(\omega)}_{\mu\nu}F^{(\omega)\mu\nu} + \frac{1}{4}\boldsymbol{F}^{(\rho)}_{\mu\nu}\cdot\boldsymbol{F}^{(\rho)\mu\nu} + \frac{1}{2}m_\omega^2\omega^{\mathrm{E}}_\mu\omega^\mu_{\mathrm{E}} + \frac{1}{2}m_\rho^2\boldsymbol{\rho}^{\mathrm{E}}_\mu\cdot\boldsymbol{\rho}^\mu_{\mathrm{E}}\,.\end{aligned} \tag{4.6}$$

The definition of the Euclidean gamma matrices, γ^μ_{E}, derivatives, $\partial^{\mathrm{E}}_\mu$, and vector fields, ω^{E}_μ and $\boldsymbol{\rho}^{\mathrm{E}}_\mu$, is found in Appendix A.1.

Baryon-number conservation is guaranteed by a Lagrange parameter, the baryon chemical potential, μ. As in Sec. 3.2, in the path integral formalism the exponent picks up an additional term $-\mu\int_0^\beta d\tau\int d^3x\,\psi^\dagger\psi$ proportional to the baryon number.

For isospin asymmetric matter, an additional chemical potential can be introduced that breaks isospin symmetry. We will outline two ways to introduce a second chemical potential.

1. **Isospin chemical potential**. The ChNM model is invariant under rotations in isospin-3 direction, which are given by

$$\psi \to \mathrm{e}^{i\theta\tau^3}\,\psi\,, \quad \psi^\dagger \to \mathrm{e}^{-i\theta\tau^3}\,\psi\,, \quad \pi_\pm \equiv \pi_1 \pm i\pi_2 \to \mathrm{e}^{\mp 2\theta i}\,\pi_\pm\,. \tag{4.7}$$

The corresponding Noether current is

$$J^3_\mu = \bar\psi\tau^3\gamma_\mu\psi + i(\pi_-\partial_\mu\pi_+ - \pi_+\partial_\mu\pi_-) = \bar\psi\tau^3\gamma_\mu\psi + 2(\pi_2\partial_\mu\pi_1 - \pi_1\partial_\mu\pi_2)\,. \tag{4.8}$$

The isospin chemical potential is most easily introduced in the Hamiltonian formalism, as outlined in [176] in the context of Bose-Einstein condensation. The conjugate fields to $\pi_{1,2}$ are $\eta_{1,2} = \frac{\partial\pi_{1,2}}{\partial t}$. The conserved charge is the integral over space of the zero component of J^3_μ,

$$Q = \int d^3x\,\left(\psi^\dagger\tau^3\psi + 2\pi_2\eta_1 - 2\pi_1\eta_2\right). \tag{4.9}$$

The relevant part of the Hamiltonian of the ChNM model needed in the present context is

$$\mathcal{H} = \frac{1}{2}\eta_1^2 + \frac{1}{2}\eta_2^2 + (\boldsymbol{\nabla}\pi_1)^2 + (\boldsymbol{\nabla}\pi_2)^2 + U(\pi_1^2+\pi_2^2) + \dots\,, \tag{4.10}$$

where all terms that do not depend on $\pi_{1,2}$ are not written down explicitly. The isospin chemical potential μ_I is introduced as the Lagrange multiplier that ensures charge conservation. Let $\{\xi_i\}$ be the collection of all fields ψ, σ, $\boldsymbol{\pi}$, ω, and $\boldsymbol{\rho}$. In the path integral formalism, the partition function is

$$\begin{aligned} Z^{(\mathrm{iso})}_\mathrm{E}[J] = \int \mathcal{D}\eta_1\,\mathcal{D}\eta_2 \int \mathcal{D}\pi_1\,\mathcal{D}\pi_2\,(\cdots)\,\exp\Bigg\{ \int_0^\beta d\tau \\ \times \Bigg[\int d^3x\Big(i\eta_1\frac{\partial\pi_1}{\partial\tau} + i\eta_2\frac{\partial\pi_2}{\partial\tau} + \dots - \mathcal{H} + \sum_i J_i\xi^i\Big) - \mu_\mathrm{I}Q\Bigg]\Bigg\}, \end{aligned} \tag{4.11}$$

where again all fields other than $\pi_{1,2}$ are not written down explicitly. The conjugate momenta η_1 and η_2 appear only quadratically and can be integrated out. The result can be written as

$$\begin{aligned} Z^{(\mathrm{iso})}_\mathrm{E}[J] = \int \mathcal{D}\pi_1\,\mathcal{D}\pi_2\,(\cdots)\,\exp\Bigg\{ -\int_0^\beta d\tau \int d^3x \\ \times \Bigg[\frac{1}{2}\left((\partial_\mu + 2\mu_\mathrm{I}\delta_{\mu 0})\pi_+\right)\left((\partial_\mu - 2\mu_\mathrm{I}\delta_{\mu 0})\pi_-\right) + \dots + \mu_\mathrm{I}\psi^\dagger\tau^3\psi - \sum_i J_i\eta^i\Bigg]\Bigg\}. \end{aligned} \tag{4.12}$$

The omitted terms in the exponent essentially give the Lagrangian (4.3), only with the kinetic terms of the fields π_1 and π_2 omitted.

If all fields are again written down explicitly, the full partition function is

$$
\begin{aligned}
Z_{\mathrm{E}}^{(\mathrm{iso})}[J] = \int \mathcal{D}\psi\, \mathcal{D}\psi^\dagger\, \mathcal{D}\sigma\, \mathcal{D}\boldsymbol{\pi}\, \mathcal{D}\omega\, \mathcal{D}\boldsymbol{\rho}\, \exp\Bigg\{ - \int_0^\beta d\tau \int d^3x \\
\times \Big[\bar{\psi} \Big[\gamma_{\mathrm{E}}^\mu \partial_\mu^{\mathrm{E}} + g_s(\sigma + i\gamma_5 \boldsymbol{\pi}\cdot\boldsymbol{\tau}) + \gamma^\mu(\delta_\mu^4 \mu + \delta_\mu^4 \mu_{\mathrm{I}} \tau^3 - i g_\omega \omega_\mu^{\mathrm{E}} - i g_\rho \boldsymbol{\rho}_\mu^{\mathrm{E}} \cdot \boldsymbol{\tau}) \Big] \psi \\
+ \frac{1}{4} F_{\mu\nu}^{(\omega)} F^{(\omega)\mu\nu} + \frac{1}{4} \boldsymbol{F}_{\mu\nu}^{(\rho)} \cdot \boldsymbol{F}^{(\rho)\mu\nu} + \frac{1}{2} m_\omega^2 \omega_\mu^{\mathrm{E}} \omega_{\mathrm{E}}^\mu + \frac{1}{2} m_\rho^2 \boldsymbol{\rho}_\mu^{\mathrm{E}} \cdot \boldsymbol{\rho}_{\mathrm{E}}^\mu \\
+ \frac{1}{2} \partial_\mu^{\mathrm{E}} \sigma\, \partial_{\mathrm{E}}^\mu \sigma + \frac{1}{2} \partial_\mu^{\mathrm{E}} \pi_0\, \partial_{\mathrm{E}}^\mu \pi_0 + \frac{1}{2} \big((\partial_\mu^{\mathrm{E}} + 2\mu_{\mathrm{I}} \delta_\mu^4) \pi_+ \big) \big((\partial_{\mathrm{E}}^\mu - 2\mu_{\mathrm{I}} \delta_4^\mu) \pi_- \big) \\
+ \mathcal{U}_{\mathrm{mic}}(\boldsymbol{\pi}, \sigma) - \sum_i J_i \eta^i \Big] \Bigg\},
\end{aligned}
\tag{4.13}
$$

where it is implicitly understood that the fields obey the respective boundary conditions. Note that simply adding a term $\mu_{\mathrm{I}} Q$ to the action does not give the right expression. The term $2\mu_{\mathrm{I}}^2 \pi_+ \pi_-$ is not obtained in this way and only follows from the proper derivation as outlined above.

2. **Proton and neutron chemical potentials**. Another possibility is to introduce a chemical potential which only couples to the charge

$$
Q = \int d^3x\; \psi^\dagger \tau^3 \psi\,, \tag{4.14}
$$

which is the difference of proton and neutron number. This chemical potential together with the baryon chemical potential can be replaced by chemical potentials μ_p and μ_n which couple to proton and neutron number, respectively. Projectors on proton and neutron states are defined as

$$
P_p = \begin{pmatrix} 1 & \\ & 0 \end{pmatrix}, \quad P_n = \begin{pmatrix} 0 & \\ & 1 \end{pmatrix}. \tag{4.15}
$$

The partition function gets an additional factor $\exp(\beta\mu_p N_p + \beta\mu_n N_n)$, where

$$
N_p = \int d^3x\; \psi^\dagger P_p \psi = \int d^3x\; \psi_p^\dagger \psi_p\,, \quad N_n = \int d^3x\; \psi^\dagger P_n \psi = \int d^3x\; \psi_n^\dagger \psi_n\,. \tag{4.16}
$$

The partition function at finite temperature and chemical potential then is

$$
\begin{aligned}
Z_{\mathrm{E}}[J] = \int \mathcal{D}\psi\, \mathcal{D}\psi^\dagger\, \mathcal{D}\sigma\, \mathcal{D}\boldsymbol{\pi}\, \mathcal{D}\omega\, \mathcal{D}\boldsymbol{\rho}\, \exp\Bigg\{ - \int_0^\beta d\tau \int d^3x \\
\times \Big[\bar{\psi} \Big[\gamma_{\mathrm{E}}^\mu \partial_\mu^{\mathrm{E}} + g_s(\sigma + i\gamma_5 \boldsymbol{\pi}\cdot\boldsymbol{\tau}) + \gamma^\mu(\delta_\mu^4 \mu_p P_p + \delta_\mu^4 \mu_n P_n - i g_\omega \omega_\mu^{\mathrm{E}} - i g_\rho \boldsymbol{\rho}_\mu^{\mathrm{E}} \cdot \boldsymbol{\tau}) \Big] \psi \\
+ \frac{1}{4} F_{\mu\nu}^{(\omega)} F^{(\omega)\mu\nu} + \frac{1}{4} \boldsymbol{F}_{\mu\nu}^{(\rho)} \cdot \boldsymbol{F}^{(\rho)\mu\nu} + \frac{1}{2} m_\omega^2 \omega_\mu^{\mathrm{E}} \omega_{\mathrm{E}}^\mu + \frac{1}{2} m_\rho^2 \boldsymbol{\rho}_\mu^{\mathrm{E}} \cdot \boldsymbol{\rho}_{\mathrm{E}}^\mu \\
+ \frac{1}{2} \partial_\mu^{\mathrm{E}} \sigma\, \partial_{\mathrm{E}}^\mu \sigma + \frac{1}{2} \partial_\mu^{\mathrm{E}} \boldsymbol{\pi} \cdot \partial_{\mathrm{E}}^\mu \boldsymbol{\pi} + \mathcal{U}_{\mathrm{mic}}(\boldsymbol{\pi}, \sigma) - \sum_i J_i \eta^i \Big] \Bigg\}.
\end{aligned}
\tag{4.17}
$$

In the absence of a term which explicitly breaks isospin symmetry, the model only depends on the square $\chi = \frac{1}{2}(\sigma^2 + \boldsymbol{\pi}^2)$. The charge (4.9) corresponds to isospin-3 rotations that involve the pionic fields $\pi_{1,2}$. In consequence, the partition function (4.13) is no longer invariant under the full isospin group SO(4). Instead, the isospin chemical potential breaks the group down to an $\mathrm{SO}(2) \times \mathrm{SO}(2)$ subgroup. The invariant squares transforming under this subgroup are

$$\chi_1 = \frac{1}{2}(\pi_1^2 + \pi_2^2)\,, \quad \chi_2 = \frac{1}{2}(\pi_3^2 + \sigma^2)\,. \tag{4.18}$$

A non-vanishing value of χ_1 is identified as a pion condensate. The model with isospin-chemical potential is substantially harder to solve in the framework of the functional renormalization group as will be explained, once the flow equations are derived. We will therefore study the second variant, although it does not fully take the isospin symmetry into account. We will also comment on the justification of this approximation later on.

4.2 MEAN-FIELD APPROXIMATION

In general, a full solution of the path integral (4.17) is not feasible. Moreover, the microscopic potential U_{mic} is not known *a priori*. In a first approximation to the full problem, all bosonic fields are replaced by their (temperature and density-dependent) expectation values and are treated as background fields. This is called the **mean-field approximation**. Only rotationally invariant solutions are considered. Therefore, all spatial components of the vector bosons ω_i and $\boldsymbol{\rho}_i$ vanish in the mean-field approximation. Instead of using the Euclidean four-component of the vector fields it is advantageous to work with the Minkowskian zero-component. As explained in Appendix A.1, the reason is that the expectation value of the zero-components are real in contrast to the Euclidean fields. Hence, ω^4 is replaced by $-i\omega^0$ and $\boldsymbol{\rho}^4$ by $-i\boldsymbol{\rho}^0$.

In general, isospin symmetry can be broken for asymmetric matter. A possible consequence is a pion-condensate, which was studied in the framework of the functional renormalization group for two-color QCD [199] and also in the quark-meson model [200]. In this thesis, we assume that the pion condensate vanishes, i.e., $\boldsymbol{\pi} = 0$. The only isospin-symmetry breaking is introduced by different chemical potentials for protons and neutrons, as well as a possible non-vanishing mean field of the ρ-boson in isospin-3 direction, $\rho_0^3(x)$. To sum up, the only fields that can get an expectation value are $\sigma(x)$, $\omega_0(x)$ and $\rho_3^0(x)$. In thermodynamic equilibrium, only spatially constant fields are considered. The mean-field values of the vector bosons enter the partition function in the same way as the chemical potentials. It therefore is reasonable to introduce effective chemical potentials,

$$\begin{aligned} \mu_{p,\mathrm{eff}} &= \mu_p - g_\omega \omega_0 - g_\rho \rho_0^3\,, \\ \mu_{n,\mathrm{eff}} &= \mu_n - g_\omega \omega_0 + g_\rho \rho_0^3\,, \end{aligned} \tag{4.19}$$

which the nucleons experience in the presence of bosonic background fields. The mean field of the σ-boson equips the nucleons with a mass term, namely

$$m = g_s \sigma\,. \tag{4.20}$$

In the mean-field approximation, the partition function evaluated at vanishing sources takes the form

$$Z_{\mathrm{E}} = \int \mathcal{D}\psi\, \mathcal{D}\psi^{\dagger}\, \exp\Bigg\{ - \int_0^{\beta} d\tau \int d^3x \\ \times \Big[\bar{\psi}\Big[\gamma_{\mathrm{E}}^{\mu}\partial_{\mu}^{\mathrm{E}} + m + \gamma^4(\mu_{p,\mathrm{eff}}P_p + \mu_{n,\mathrm{eff}}P_n)\Big]\psi - \frac{1}{2}m_{\omega}^2\omega_0^2 - \frac{1}{2}m_{\rho}^2(\rho_0^3)^2 + U_{\sigma}(\sigma)\Big]\Bigg\}. \tag{4.21}$$

The σ-potential U_σ partially parameterizes the effects of the vacuum fluctuations of pions and the σ-field. For fixed, space-time independent bosonic fields, the potential U_σ and the mass terms factor out and give a contribution $\exp\{-\beta V \cdot U_{\mathrm{B}}(\sigma, \omega_0, \rho_0^3)\}$, where we defined the bosonic potential

$$U_{\mathrm{B}}(\sigma, \omega_0, \rho_0^3) = -\frac{1}{2}m_{\omega}^2\omega_0^2 - \frac{1}{2}m_{\rho}^2(\rho_0^3)^2 + U_{\sigma}(\sigma)\,. \tag{4.22}$$

The remaining nucleon fields appear only quadratically. As a consequence, the path integral can be performed and the partition function is

$$\log Z_E = \log\det D - \beta V \cdot U_{\mathrm{B}}(\sigma, \omega_0, \rho_0^3) = \mathrm{Tr}\log D - \beta V \cdot U_{\mathrm{B}}(\sigma, \omega_0, \rho_0^3)\,, \tag{4.23}$$

where the operator D is easiest computed in momentum space, which according to Eq. (3.20) splits into an integral over three-momenta and a sum over the Matsubara frequencies, $\omega_l^{(p)} = (2l+1)\pi T$ and $\omega_l^{(n)} = (2l+1)\pi T$, for protons and neutrons, respectively. Then D takes the form (see, e.g., [176])

$$D = -\beta\big[(\omega_l^{(p)} + i\mu_{p,\mathrm{eff}})P_p + (\omega_l^{(n)} + i\mu_{n,\mathrm{eff}})P_n - i\gamma^0\gamma^i p_i - im\gamma^0\big]. \tag{4.24}$$

First, the determinant over Dirac and isospin indices is computed and then, after applying Eq. (4.23), the trace over momenta is taken. With the definition $E = \sqrt{\boldsymbol{p}^2 + m^2}$, one finds

$$\begin{aligned}\mathrm{Tr}\log D &= 2V \sum_{i=p,n}\sum_{l=-\infty}^{\infty}\int \frac{d^3p}{(2\pi)^3}\log\Big[\beta^2\big((\omega_l^{(i)} + i\mu_{i,\mathrm{eff}})^2 + E^2\big)\Big] \\ &= V\sum_{i=p,n}\sum_{l=-\infty}^{\infty}\sum_{r=\pm1}\int\frac{d^3p}{(2\pi)^3}\log\Big[(2l+1)^2\pi^2 + \beta^2(E - r\mu_{i,\mathrm{eff}})^2\Big] \\ &= V\sum_{i=p,n}\sum_{l=-\infty}^{\infty}\sum_{r=\pm1}\int\frac{d^3p}{(2\pi)^3}\Bigg\{\log\big[1 + (2l+1)^2\pi^2\big] \\ &\qquad + \int_1^{\beta^2(E-r\mu_{i,\mathrm{eff}})^2}\frac{dx^2}{x^2 + (2l+1)^2\pi^2}\Bigg\}.\end{aligned} \tag{4.25}$$

The first term does not depend on the temperature or the chemical potentials. It therefore gives a (divergent) contribution that can be absorbed into the potential $U_\sigma(\sigma)$. The summation over l can be performed for the integrand of the last term. The sum has poles at $l = -\frac{1}{2} \pm i\frac{x}{2\pi}$. The identity

$$\sum_{l=-\infty}^{\infty} f(l) = -\pi \sum_{\text{res. } a_i} \mathrm{Res}(f, a_i)\cdot\cot(\pi a_i)\,, \tag{4.26}$$

yields that the summation equals

$$-\pi\cdot\frac{1}{2\pi}\cdot\frac{\cot(-\frac{\pi}{2}+i\frac{x}{2})}{2ix}-\pi\cdot\frac{1}{2\pi}\cdot\frac{\cot(-\frac{\pi}{2}-i\frac{x}{2})}{-2ix}=\frac{1}{x}\cdot\left(\frac{1}{2}-\frac{1}{\mathrm{e}^x+1}\right). \tag{4.27}$$

The x-integral now can be performed. Again, terms independent of the temperature and the chemical potentials are dropped. It remains

$$\begin{aligned}\operatorname{Tr}\log D &= 2V\sum_{i=p,n}\int\frac{d^3p}{(2\pi)^3}\left\{\beta E+\sum_{r=\pm1}\log\left[1+\mathrm{e}^{-\beta(E-r\mu_{i,\mathrm{eff}})}\right]\right\}\\ &= 2V\sum_{i=p,n}\int\frac{d\Omega\,dp}{(2\pi)^3}\left\{p^2\beta E-\sum_{r=\pm1}\frac{1}{3}p^3\,\frac{\partial}{\partial p}\log\left[1+\mathrm{e}^{-\beta(E-r\mu_{i,\mathrm{eff}})}\right]\right\}\\ &= 2\beta V\sum_{i=p,n}\int\frac{d^3p}{(2\pi)^3}\left\{E+\sum_{r=\pm1}\frac{p^2}{3E}n_{\mathrm{F}}(E-r\mu_{i,\mathrm{eff}})\right\},\end{aligned} \tag{4.28}$$

where the second line follows from an integration by parts and the Fermi distribution n_{F} is defined in Appendix A.1. The first contribution to Eq. (4.28) does not depend on the temperature and is quadratically divergent. However, it does depend on the field σ, and can be identified as a Hartree term, which takes fermionic vacuum fluctuations into account. In the older literature, the Hartree term was often ignored, and therefore one sometimes speaks of the "extended mean-field (eMF) approximation" if it is included. We will not make such a distinction and always include the Hartree term. A first proper treatment of this term in the context of the quark-meson model was done by Skokov *et al.* [201], which we will briefly reproduce. First, notice that the three-dimensional integral can be turned into a four-dimensional integral, namely,

$$\begin{aligned}\int\frac{d^4p}{(2\pi)^4}\log\frac{p^2+m^2}{p^2} &= \lim_{\Lambda\to\infty}\int_{-\Lambda}^{\Lambda}\frac{dp_0}{2\pi}\int\frac{d^3p}{(2\pi)^3}\log\frac{p_0^2+E^2}{p_0^2+\boldsymbol{p}^2}\\ &= \lim_{\Lambda\to\infty}\int\frac{d^3p}{(2\pi)^3}\frac{1}{2\pi}\cdot\left(4E\arctan\frac{\Lambda}{E}-4|\boldsymbol{p}|\arctan\frac{\Lambda}{|\boldsymbol{p}|}+2\Lambda\log\frac{E^2+\Lambda^2}{\boldsymbol{p}^2+\Lambda^2}\right)\\ &= \int\frac{d^3p}{(2\pi)^3}E+C\,,\end{aligned} \tag{4.29}$$

where C is an (infinitely large) constant that can be dropped. The four-dimensional integral over the logarithm can be computed in dimensional regularization. Set $d=4-2\epsilon$ and let Λ be an arbitrary momentum scale. Then

$$\begin{aligned}\int\frac{d^3p}{(2\pi)^3}E &= \Lambda^{2\epsilon}\int\frac{d^dp}{(2\pi)^d}\log\frac{p^2+m^2}{p^2}=\Lambda^{2\epsilon}\int_0^{m^2}d\widetilde{m}^2\int\frac{d^dp}{(2\pi)^d}\frac{1}{p^2+\widetilde{m}^2}\\ &= \Lambda^{2\epsilon}\int_0^{m^2}d\widetilde{m}^2\frac{\Gamma(1-\frac{d}{2})\,\Gamma(\frac{d}{2})}{(4\pi)^{d/2}\,\Gamma(1)\,\Gamma(\frac{d}{2})}(\widetilde{m}^2)^{-(1-d/2)}\\ &= -\frac{m^4}{32\pi^2}\left(\frac{1}{\epsilon}+\frac{3}{2}-\gamma_{\mathrm{E}}-\log\frac{4\pi m^2}{\Lambda^2}\right),\end{aligned} \tag{4.30}$$

where γ_{E} is the Euler-Mascheroni constant. If the counterterm

$$\delta\mathcal{L}=-\frac{(g_s\sigma)^4}{8\pi^2}\left(\frac{1}{\epsilon}+\frac{3}{2}-\gamma_{\mathrm{E}}-\log 4\pi\right) \tag{4.31}$$

is added to the Lagrangian, the contribution of the Hartree term to $\log Z_{\mathrm{E}}$ is

$$\beta V \cdot \frac{m^4}{8\pi^2} \log \frac{m^2}{\Lambda^2} = \beta V \cdot \frac{(g_s\sigma)^4}{8\pi^2} \log \frac{(g_s\sigma)^2}{\Lambda^2} \,. \tag{4.32}$$

Because this term depends only on the bosonic fields, we will include this term (divided by $-\beta V$) in the bosonic potential $U_{\mathrm{B}}(\sigma, \omega_0, \rho_0^3)$.

From Eq. (4.23) and recalling the discussion that lead to Eq. (3.32), the **mean-field potential** is defined as

$$\boxed{U_{\mathrm{MF}}(T, \mu_p, \mu_n, \sigma, \omega_0, \rho_0^3) = U_{\mathrm{F}}(T, \mu_p, \mu_n, \sigma, \omega_0, \rho_0^3) + U_{\mathrm{B}}(\sigma, \omega_0, \rho_0^3) \,,} \tag{4.33}$$

where the **fermionic potential** is given by

$$\begin{aligned} \boxed{U_{\mathrm{F}}(T, \mu, \sigma, \omega_0, \rho_0^3) &= -\frac{2}{\beta} \sum_{i=p,n} \sum_{r=\pm 1} \int \frac{d^3p}{(2\pi)^3} \log \left[1 + \mathrm{e}^{-\beta(E - r\mu_{i,\mathrm{eff}})}\right] \\ &= -2 \sum_{i=p,n} \sum_{r=\pm 1} \int \frac{d^3p}{(2\pi)^3} \frac{p^2}{3E} n_{\mathrm{F}}(E - r\mu_{i,\mathrm{eff}}) \,.} \end{aligned} \tag{4.34}$$

Next, we turn to the description of the bosonic potential $U_{\mathrm{B}}(\sigma, \omega_0, \rho_0^3)$. Let us restore the pion fields for a moment. If chiral symmetry is unbroken, the chiral part of the potential, $U_{\mathrm{B}}^{(\chi)}$ depends only on the invariant square, $\chi = \frac{1}{2}(\sigma^2 + \boldsymbol{\pi}^2)$. At $T = 0$ and $\mu_p = \mu_n = 0$, the potential can be expanded up to order $N_{\max}$ around the vacuum expectation values of the fields, namely

$$\sigma = \sigma_0 \,, \quad \boldsymbol{\pi} = 0 \,. \tag{4.35}$$

The corresponding invariant square is denoted as $\chi_0 = \frac{1}{2}\sigma_0^2$. In addition, the contribution from the Hartree term (4.32) is included with $\sigma^2 \to 2\chi$. Moreover, chiral symmetry is explicitly broken by a linear term in σ, which slightly distorts the potential towards the σ-direction. The complete ansatz for the **bosonic potential** is

$$\boxed{U_{\mathrm{B}}(\sigma, \boldsymbol{\pi}, \omega_0, \rho_0^3) = -\frac{1}{2} m_\omega^2 \omega_0^2 - \frac{1}{2} m_\rho^2 (\rho_0^3)^2 + U_{\mathrm{B},\chi}(\chi) + c(\sigma_0 - \sigma) \,,} \tag{4.36}$$

where

$$U_{\mathrm{B},\chi}(\chi) = \sum_{n=0}^{N_{\max}} \frac{a_n}{n!} (\chi - \chi_0)^n - \frac{g_s^4 \chi^2}{2\pi^2} \log \frac{2 g_s^2 \chi}{\Lambda^2} \,. \tag{4.37}$$

The derivatives of $U_{\mathrm{B},\chi}$ with respective to the field χ are denoted by primes, e.g.,

$$U'_{\mathrm{B},\chi}(\chi) = \frac{\partial U_{\mathrm{B},\chi}(\chi)}{\partial \chi} \,. \tag{4.38}$$

The parameters of the model are fixed by three considerations. First, in vacuum, i.e., at $T = 0$ and $\mu_n = \mu_p = 0$, the potential has to reproduce the low-energy theorems. More parameters are fitted to the liquid-gas phase transition of nuclear matter. Finally, the equation of state of pure neutron matter gives one further constraint. We will discuss each of these constraints in the following.

4.2.1 *Vacuum constraints*

Constraints in vacuum include low-energy theorems, the pion decay constant, $f_\pi = 93\,\mathrm{MeV}$, and the pion mass, $m_\pi = 139\,\mathrm{MeV}$.

1. The minimum of the potential is fixed by low-energy theorems in vacuum. Under an infinitesimal axial vector transformation (2.29), the fields transform as

$$\psi \to (1 - i\frac{1}{2}\boldsymbol{\alpha}\cdot\boldsymbol{\tau}\gamma_5)\psi\,, \qquad \pi^i \to \pi^i + \sigma\alpha^i\,, \qquad \sigma \to \sigma - \pi^i\alpha_i\,. \tag{4.39}$$

The axial vector current, A_i^μ, can be read off by making $\boldsymbol{\alpha}$ dependent on space-time. Terms only depending on $\sigma^2 + \boldsymbol{\pi}^2$ are invariant, while

$$\begin{aligned}\bar\psi\Big[i\gamma^\mu\partial_\mu + g_s(\sigma + i\gamma_5\boldsymbol{\pi}\cdot\boldsymbol{\tau})\Big]\psi \;\to\; &\bar\psi\Big[i\gamma^\mu\partial_\mu + g_s(\sigma + i\gamma_5\boldsymbol{\pi}\cdot\boldsymbol{\tau})\Big] - \\ &- \underbrace{\Big(\bar\psi\gamma^\mu\gamma_5\frac{\tau^i}{2}\psi + \sigma\partial^\mu\pi_i - \pi_i\partial^\mu\sigma\Big)}_{A_i^\mu}\,\partial_\mu\alpha^i.\end{aligned} \tag{4.40}$$

The last term of the of the axial current A_i^μ can be neglected as compared to the other two terms, if we expand around the expectation values $\langle\sigma\rangle = \sigma_0$ and $\langle\boldsymbol{\pi}\rangle = 0$. The divergence of the axial current is given by

$$\partial_\mu A_i^\mu = \sigma_0\partial_\mu\partial^\mu\pi_i + \ldots = \sigma_0 m_\pi^2\pi_i + \ldots\,, \tag{4.41}$$

where we omitted terms involving the nucleons and wrote down only the projection on the pion fields. The same quantity can be computed from Eq. (2.37), namely

$$\partial_\mu A_i^\mu = f_\pi m_\pi^2\pi_i + \ldots\,, \tag{4.42}$$

where again only the projection on the pion fields is written down. Comparing the two expressions, we find that the vacuum expectation value of σ equals the pion decay constant,

$$\sigma_0 = f_\pi. \tag{4.43}$$

2. The masses of the fields are determined by the second derivatives of the potential with respect to the fields $\phi = (\phi^a) = (\sigma, \boldsymbol{\pi})$, evaluated at the vacuum expectation values. They are therefore given by the matrix

$$M^a{}_b = \frac{\partial U_\mathrm{B}}{\partial\phi_a\partial\phi^b} = U'_{\mathrm{B},\chi}(\chi)\cdot\delta^a{}_b + U''_{\mathrm{B},\chi}(\chi)\,\phi^a\,\phi_b\,. \tag{4.44}$$

This matrix can be diagonalized with respect to the eigenvalues

$$\lambda_0 = U'_{\mathrm{B},\chi}(\chi) + 2\chi\,U''_{\mathrm{B},\chi}(\chi)\,, \quad \lambda_{1,2,3} = U'_{\mathrm{B},\chi}(\chi)\,. \tag{4.45}$$

The latter are eigenvalues because

$$\begin{aligned}\det\Big(M^a{}_b - U'_{\mathrm{B},\chi}(\chi)\,\delta^a{}_b\Big) &= \det U''_{\mathrm{B},\chi}(\chi)\,\phi^a\,\phi_b \\ &= \det U''_{\mathrm{B},\chi}(\chi)\begin{pmatrix}\phi^0\phi^T\\ \vdots\\ \phi^3\phi^T\end{pmatrix} = \det\begin{pmatrix}\phi^T\\ \vdots\\ \phi^T\end{pmatrix}\cdot\prod_a U''_{\mathrm{B},\chi}(\chi)\,\phi^a = 0.\end{aligned} \tag{4.46}$$

The corresponding eigenvectors are

$$\ker \begin{pmatrix} \phi^T \\ \phi^T \\ \phi^T \\ \phi^T \end{pmatrix} = \left\langle \begin{pmatrix} -\phi_1 \\ \phi_0 \\ 0 \\ 0 \end{pmatrix}, \begin{pmatrix} -\phi_2 \\ 0 \\ \phi_0 \\ 0 \end{pmatrix}, \begin{pmatrix} -\phi_3 \\ 0 \\ 0 \\ \phi_0 \end{pmatrix} \right\rangle . \tag{4.47}$$

The orthogonal vector is ϕ with eigenvalue $U'_{\mathrm{B},\chi}(\chi) + 2\chi U''_{\mathrm{B},\chi}(\chi)$. The masses of the three pions and the σ-boson are therefore given by

$$m_\pi^2 = U'_{\mathrm{B},\chi}(\chi_0)\,, \qquad m_\sigma^2 = U'_{\mathrm{B},\chi}(\chi_0) + 2\chi U''_{\mathrm{B},\chi}(\chi_0)\,. \tag{4.48}$$

Another way to prove these equations is to expand the potential around $\chi = \chi_0$ and to explicitly compute the potential up to quadratic order in the fields.

3. The pressure has to vanish in vacuum, i.e., the potential is zero at its minimum. This yields the conditions

$$U_{\mathrm{B}}(f_\pi, \mathbf{0}, 0, 0) = 0\,, \qquad \frac{\partial U_{\mathrm{B},\chi}}{\partial \sigma}(f_\pi, \mathbf{0}, 0, 0) = 0\,. \tag{4.49}$$

4. The coupling constant g_s is fixed by the nucleon mass, since in vacuum the coupling to the σ-field, $\bar\psi g_s \sigma_0 \psi = \bar\psi g_s f_\pi \psi$, provides a mass term and therefore

$$g_s = \frac{m_{\mathrm{N}}}{f_\pi} = 10.1\,, \tag{4.50}$$

where $m_{\mathrm{N}} = 939\,\mathrm{MeV}$ is the nucleon mass.

The ansatz for the **chirally invariant part of the baryon potential** satisfying the above constraints (4.48) and (4.49) is

$$\begin{aligned} U_{\mathrm{B},\chi}(\chi) = {} & \frac{g_s^4}{8\pi^2} f_\pi^4 \log \frac{\frac{1}{2} f_\pi^2}{\chi} + \left[m_\pi^2 + \frac{g_s^4}{4\pi^2} f_\pi^2 \left(1 + 2 \log \frac{\frac{1}{2} f_\pi^2}{\chi} \right) \right] (\chi - \chi_0) \\ & + \frac{1}{2} \left[\frac{m_\sigma^2 - m_\pi^2}{f_\pi^2} + \frac{g_s^4}{2\pi^2} \left(3 + 2 \log \frac{\frac{1}{2} f_\pi^2}{\chi} \right) \right] (\chi - \chi_0)^2 \\ & + \sum_{n=3}^{N_{\max}} \frac{a_n}{n!} (\chi - \chi_0)^n\,, \end{aligned} \tag{4.51}$$

given that the symmetry breaking constant is

$$c = m_\pi^2 f_\pi\,. \tag{4.52}$$

Note that the renormalization scale, Λ, from the regularization of the Hartree term disappeared from the mean-field potential, as it should [201]. Moreover, the potential is finite in the limit $\chi \to 0$ as the logarithmic terms cancel.

The potential is expanded in powers of χ up to order $N_{\max} = 4$. The remaining free parameters are m_σ, a_3, a_4, m_ω, m_ρ, g_ω, and g_ρ.

4.2.2 *Constraints from the liquid-gas phase transition*

The expectation values of the bosonic fields have been taken to be constant so far. For each value of T, μ_n, and μ_p, these expectation values are determined in such a way that the most dominant contribution to the path integral is selected, which is the one that minimizes the mean-field potential U_{MF}. The respective solutions are marked by a bar:

$$\bar{\sigma}(T,\mu_p,\mu_n)\,, \quad \bar{\omega}_0(T,\mu_p,\mu_n)\,, \quad \bar{\rho}_0^3(T,\mu_p,\mu_n)\,. \tag{4.53}$$

Comparing with Eq. (3.34), if the mean-field potential is evaluated at these values, one obtains the grand-canonical potential,

$$U_{\mathrm{gc}}(T,\mu_p,\mu_n) = U_{\mathrm{MF}}(T,\mu_p,\mu_n,\bar{\sigma}(T,\mu_p,\mu_n),\bar{\omega}_0(T,\mu_p,\mu_n),\bar{\rho}_0^3(T,\mu_p,\mu_n))\,. \tag{4.54}$$

It is useful to define the following field-dependent functions:

$$\begin{aligned}
n_n(T,\mu_p,\mu_n,\sigma,\omega_0,\rho_0^3) &= -\frac{\partial U_{\mathrm{MF}}}{\partial \mu_n} = 2\int \frac{d^3p}{(2\pi)^3}\Big[n_{\mathrm{F}}(E-\mu_{n,\mathrm{eff}}) - n_{\mathrm{F}}(E+\mu_{n,\mathrm{eff}})\Big]\,,\\
n_p(T,\mu_p,\mu_n,\sigma,\omega_0,\rho_0^3) &= -\frac{\partial U_{\mathrm{MF}}}{\partial \mu_p} = 2\int \frac{d^3p}{(2\pi)^3}\Big[n_{\mathrm{F}}(E-\mu_{p,\mathrm{eff}}) - n_{\mathrm{F}}(E+\mu_{p,\mathrm{eff}})\Big]\,,\\
n_s(T,\mu_p,\mu_n,\sigma,\omega_0,\rho_0^3) &= \frac{\partial U_{\mathrm{MF}}}{\partial m}\\
&= \sum_{i=p,n} 2\int \frac{d^3p}{(2\pi)^3}\frac{m}{E}\Big[n_{\mathrm{F}}(E-\mu_{i,\mathrm{eff}}) + n_{\mathrm{F}}(E+\mu_{i,\mathrm{eff}})\Big]\,.
\end{aligned} \tag{4.55}$$

When evaluated at the minimum (4.53), they yield according to Eq. (3.35) the neutron, proton, and scalar density, respectively.

The minimization of the potential with respect to ω_0 is

$$\begin{aligned}
&\frac{\partial U_{\mathrm{MF}}}{\partial \omega_0}(T,\mu_p,\mu_n,\bar{\sigma},\bar{\omega}_0,\bar{\rho}_0^3) = 0\,,\\
\Rightarrow\quad & 0 = -m_\omega^2\bar{\omega}_0 - \frac{\partial}{\partial\omega_0}\left\{\frac{2}{\beta}\sum_{i=p,n}\sum_{r=\pm1}\int\frac{d^3p}{(2\pi)^3}\log\left[1+\mathrm{e}^{-\beta(E-r\mu_{i,\mathrm{eff}})}\right]\right\}\\
\Rightarrow\quad & \bar{\omega}_0 = \frac{g_\omega}{m_\omega^2}\sum_{i=p,n}\frac{2}{\beta}\int\frac{d^3p}{(2\pi)^3}\sum_{r=\pm1}\frac{\partial}{\partial\mu_{i,\mathrm{eff}}}\log\left[1+\mathrm{e}^{-\beta(E-r\mu_{i,\mathrm{eff}})}\right]\\
&\qquad = \frac{g_\omega}{m_\omega^2}\sum_{i=p,n}2\int\frac{d^3p}{(2\pi)^3}\Big[n_{\mathrm{F}}(E-\mu_{i,\mathrm{eff}}) - n_{\mathrm{F}}(E+\mu_{i,\mathrm{eff}})\Big]\\
&\qquad = \frac{g_\omega}{m_\omega^2}\Big[n_p(T,\mu_p,\mu_n,\bar{\sigma},\bar{\omega}_0,\bar{\rho}_0^3) + n_n(T,\mu_p,\mu_n,\bar{\sigma},\bar{\omega}_0,\bar{\rho}_0^3)\Big].
\end{aligned} \tag{4.56}$$

Likewise, the minimization conditions with respect to ρ_0^3 and σ can be computed. We define the quantities

$$G_\omega = \frac{g_\omega^2}{m_\omega^2}\,, \qquad G_\rho = \frac{g_\rho^2}{m_\rho^2}\,, \tag{4.57}$$

which are the coupling strengths of the original vector-isoscalar interactions $(\bar{\psi}\gamma_\mu\psi)\,(\bar{\psi}\gamma^\mu\psi)$ and vector-isovector interactions $(\bar{\psi}\gamma_\mu\boldsymbol{\tau}\psi)\cdot(\bar{\psi}\gamma^\mu\boldsymbol{\tau}\psi)$. The resulting set of **mean-field equations** is

$$\boxed{\begin{aligned} g_\omega\bar{\omega}_0 &= G_\omega\Big[n_p(T,\mu_p,\mu_n,\bar{\sigma},\bar{\omega}_0,\bar{\rho}_0^3)+n_n(T,\mu_p,\mu_n,\bar{\sigma},\bar{\omega}_0,\bar{\rho}_0^3)\Big],\\ g_\rho\bar{\rho}_0^3 &= G_\rho\Big[n_p(T,\mu_p,\mu_n,\bar{\sigma},\bar{\omega}_0,\bar{\rho}_0^3)-n_n(T,\mu_p,\mu_n,\bar{\sigma},\bar{\omega}_0,\bar{\rho}_0^3)\Big],\\ \frac{\partial U_{\mathrm{B}}}{\partial\sigma}(\bar{\sigma},\bar{\omega}_0,\bar{\rho}_0^3) &= -g_s\; n_s(T,\mu_p,\mu_n,\bar{\sigma},\bar{\omega}_0,\bar{\rho}_0^3)\,. \end{aligned}} \tag{4.58}$$

The ω_0-field adjusts itself in such a way that it is proportional to the baryon density (proton plus neutron density), whereas the ρ_0^3-field is proportional to the difference of proton and neutron density.

In a first step, we study isospin-symmetric nuclear matter, characterized by equal chemical potentials $\mu \equiv \mu_n = \mu_p$, which implies equal neutron and proton densities. The expectation value of the ρ-boson vanishes and therefore the ρ-boson does not contribute in this case. Isospin-symmetric nucular matter is characterized by a first-order liquid-gas phase transition at vanishing temperature. Most of the remaining model parameters are adjusted as to provide a good description of the liquid-gas transition.

1. The chemical potential is the change of energy, when an additional particle is added. The liquid-gas phase transition therefore sets in at a critical chemical potential which equals the difference of nucleon mass and binding energy,

$$\mu_c = m_{\mathrm{N}} - E_{\mathrm{B}} = 939\,\mathrm{MeV} - 16\,\mathrm{MeV} = 923\,\mathrm{MeV}. \tag{4.59}$$

There are three scales $m_{\mathrm{N}} > \mu_c > m_{\mathrm{L}}$ involved, where the latter is the **Landau mass**. It is the effective mass associated with a pseudo-particle excitation at the Fermi surface. The Fermi momentum, $p_{\mathrm{F}} = 290\,\mathrm{MeV}$, can be computed from the nuclear saturation density $n_0 = \frac{4}{6\pi^2}p_{\mathrm{F}}^3 = 0.16\,\mathrm{fm}^{-3}$. The liquid-gas phase transition manifests itself in the mean-field potential by two degenerate minima, one located at the vacuum value $\sigma = f_\pi$ and a newly appearing second minimum at a smaller value σ_c. In particular, the nucleon in the liquid phase is described by an effective in-medium mass $g_s\sigma_c$. The Landau mass is then given by

$$m_{\mathrm{L}} = \sqrt{p_{\mathrm{F}}^2 + g_s^2\sigma_c^2}\,. \tag{4.60}$$

The Landau mass is equal to the effective chemical potential at the second minimum at σ_c. From the mean-field equations (4.58) one finds

$$m_{\mathrm{L}} = \mu_c - g_\omega\bar{\omega}_{0,c} = \mu_c - G_\omega(n_p+n_n) = \mu_c - G_\omega n_0\,, \tag{4.61}$$

where $\bar{\omega}_{0,c}$ is the expectation value of ω_0 at σ_c. This condition fixes the coupling

$$G_\omega = \frac{\mu_c - m_{\mathrm{L}}}{n_0}\,. \tag{4.62}$$

The value of the Landau mass (or, equivalently in our model, the effective in-medium nucleon mass) is not precisely known. As in Ref. [166] we fix $m_{\mathrm{L}} = 0.8\,m_{\mathrm{N}}$. Then

$$G_\omega = 5.71\,\mathrm{fm}^2\,, \quad \sigma_c = 69.8\,\mathrm{MeV}\,. \tag{4.63}$$

It turns out that if the vector fields are treated as background fields, the theory does not depend on the Yukawa coupling and the mass separately, but only on the ratio $G_\omega = g_\omega^2/m_\omega^2$. One way to see this, is to observe that the mean field equations are invariant under the rescaling transformation

$$m_\omega \to \lambda m_\omega\,, \quad \omega_0 \to \omega_0/\lambda\,, \quad g_\omega \to \lambda g_\omega\,, \tag{4.64}$$

for any positive λ. In the absence of a kinetical term, the overall factorization of ω_0 is not determined. The physically meaningful combination which is invariant under this symmetry is the field $g_\omega\omega_0$. In terms of this new field, one already sees at the level of the Lagrangian (4.3), but also explicitly in the mean-field equations (4.58) that the theory depends only on G_ω. If the vector boson is allowed to fluctuate, the overall normalization of ω_0 is fixed, and the mass becomes an independent parameter. After this clarification, for the sake of concreteness and in order to be comparable to the literature, we choose $m_\omega = 783\,\mathrm{MeV}$, which is the mass of the physical omega meson. This fixes

$$g_\omega = 9.5\,, \quad \omega_{0,c} = -18\,\mathrm{MeV}\,. \tag{4.65}$$

2. The remaining parameters are m_σ, a_3, a_4, g_ρ, and m_ρ. Two parameters are fixed in order to reproduce the liquid-gas phase transition. We have just seen that at $T = 0$ and $\mu = \mu_c$ the potential develops a second minimum at $\sigma = \sigma_c$. The condition of two degenerate minima is

$$\begin{aligned} &\frac{\partial U_{\mathrm{MF}}}{\partial\sigma}(0,\mu_c,\mu_c,\sigma_c,\omega_{0,c},0) = 0\,,\\ &U_{\mathrm{MF}}(0,\mu_c,\mu_c,\sigma_c,\omega_{0,c},0) = U_{\mathrm{MF}}(0,\mu_c,\mu_c,f_\pi,0,0) = 0\,. \end{aligned} \tag{4.66}$$

The negative of the mean-field potential evaluated at its minimum yields the pressure. The second condition tells us that at μ_c both the vacuum and nuclear matter have vanishing pressure and can coexist. The two conditions allow us to solve for $a_3(m_\sigma)$ and $a_4(m_\sigma)$, such that only the σ-mass m_σ remains as a free parameter. The solution is

$$\begin{aligned} a_3 &= -2.70\cdot 10^{-1}\ \mathrm{MeV}^{-2} + 4.40\cdot 10^{-7}\, m_\sigma^2\ \mathrm{MeV}^{-4}\,,\\ a_4 &= -2.24\cdot 10^{-4}\ \mathrm{MeV}^{-4} + 5.54\cdot 10^{-10}\, m_\sigma^2\ \mathrm{MeV}^{-6}\,. \end{aligned} \tag{4.67}$$

The most important inputs from nuclear matter are the **compression modulus**,

$$K = 9n\left(\frac{dn}{d\mu}\right)^{-1}\,, \tag{4.68}$$

and the **surface tension** of a nuclear droplet. We will now recall Coleman's computation of the surface tension in field theory in a thin-wall approximation [202]. Let us start with pure vacuum. At the phase transition, bubbles appear in the surrounding vacuum. A single bubble can be described as a time-independent field configuration, $\sigma(r)$, that depends only on the radius r. Outside the bubble, the σ-field takes the value f_π, whereas inside the bubble, $\sigma = \sigma_c$, the value of nuclear matter. Only in a small transition region $\sigma(r)$ is varying. Let R be radius of the bubble, implicitly defined by

$$\sigma(R) = \frac{1}{2}(f_\pi + \sigma_c)\,. \tag{4.69}$$

The thin-wall approximation states that the region where $\sigma(r)$ is varying is much smaller than R. The action of the field configuration is

$$S = 4\pi \int dr\, r^2 \left[\frac{1}{2} \left(\frac{d\sigma}{dr} \right)^2 + U_{\mathrm{MF}}(\sigma) \right], \tag{4.70}$$

and the classical field equation obtained from the action is

$$\frac{d^2\sigma}{dr^2} + \frac{2}{r} \frac{d\sigma}{dr} = \frac{dU_{\mathrm{MF}}}{d\sigma}\,. \tag{4.71}$$

In the wall region, the second term is negligible, because we assume that R is large. The remaining equation is a typical soliton-like equation and can be written as

$$\frac{d}{d\sigma} \left[\frac{1}{2} \left(\frac{d\sigma}{dr} \right)^2 - U_{\mathrm{MF}}(\sigma) \right] = 0\,. \tag{4.72}$$

An integration, together with the boundary condition at $r = \infty$ gives

$$\frac{1}{2} \left(\frac{d\sigma}{dr} \right)^2 - U_{\mathrm{MF}}(\sigma) = -U_{\mathrm{MF}}(f_\pi) = 0\,. \tag{4.73}$$

The action S is a measure of the energy from the non-trivial configuration. Outside the bubble, the integrand vanishes, because in this region $U_{\mathrm{MF}}(\sigma) = U_{\mathrm{MF}}(f_\pi) = 0$ and $\sigma(r)$ is constant. The integration over the interior delivers the contribution from the volume term. The integration over the wall-region separating the two phases gives the contribution of the surface energy. We can approximate $r \simeq R$ in this region. With the help of Eq. (4.73) we obtain for this integration region

$$S_{\mathrm{surface}} = 4\pi R^2 \int_{\sigma_c}^{f_\pi} d\sigma \frac{d\sigma}{dr} = 4\pi R^2 \int_{\sigma_c}^{f_\pi} d\sigma \sqrt{2U_{\mathrm{MF}}(\sigma)}\,. \tag{4.74}$$

Comparing with Eq. (2.52) we find the surface tension of the nuclear droplet in our model,

$$\Sigma = \int_{\sigma_c}^{f_\pi} d\sigma \sqrt{2U_{\mathrm{MF}}(\sigma)}\,. \tag{4.75}$$

The surface tension indicates how strongly the minima at the liquid-gas transition are separated. According to Eq. (4.75), it measures the thickness of the potential barrier between the two minima, so if the surface tension is large, the liquid phase and the gas phase are well separated. If the temperature is increased, the potential well between the two minima and therefore also the surface tension decrease. In addition, the two minima approach each other. At the critical point of the liquid-gas phase transition, the minima are degenerate and the surface tension goes to zero. The droplets of nuclear matter are no longer held together by the surface tension and they completely melt away. Accordingly, liquid and gas phases are no longer distinguishable. Therefore, the position of the critical endpoint is sensitive to the initial input value of Σ at $T = 0$. The larger the value of the surface tension, the more temperature is needed to melt the nucleons. The empirical value of the surface tension deduced from the semi-empirical mass-formula (2.50) is $\Sigma = 1.11\,\mathrm{MeV\ fm^{-2}}$. This value can be obtained by the choice

$$m_\sigma = 880\,\mathrm{MeV}\,. \tag{4.76}$$

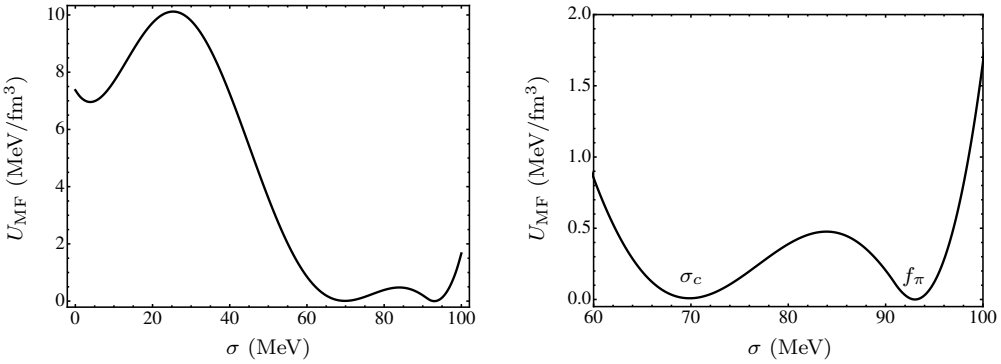

Figure 6: The mean-field potential of symmetric nuclear matter at $T = 0$ and $\mu = \mu_c$.

As already mentioned, we stress that the σ-boson in our model only parameterizes part of the unresolved short-distance interaction. It does not correspond to the pole in the pion-pion scattering amplitude, which cannot be treated as a particle.

The higher Taylor coefficients of the χ-expansion associated with this particular σ-mass follow from Eq. (4.67)

$$a_3 = 6.87 \cdot 10^{-2}\,\mathrm{MeV}^{-2}\,, \quad a_4 = 2.05 \cdot 10^{-4}\,\mathrm{MeV}^{-4}\,. \tag{4.77}$$

The compression modulus comes out as

$$K = 290\,\mathrm{MeV}\,, \tag{4.78}$$

slightly larger than the empirical value $K = 240(30)\,\mathrm{MeV}$.

For vanishing temperature, the mean-field potential is shown for $\mu = \mu_c$ in Fig. 6. The minimum at $\sigma = \sigma_c$ corresponds to nuclear matter, the minimum at $\sigma = f_\pi$ to the vacuum state.

4.2.3 *Constraints from pure neutron matter*

Next, asymmetric matter is studied in the ChNM model. The chemical potentials of neutrons and protons are now different. Because neutron and proton densities also are different, the expectation value of the ρ-field is non-vanishing. Consequently, the parameters g_ρ and m_ρ contribute and have to be fixed. We fit their values to the equation of state of pure neutron matter, characterized by a vanishing proton density. The function n_p defined in Eq. (4.55) is therefore set to zero. Since $\mu_{p,\mathrm{eff}}$ is positive, the integrand,

$$n_{\rm F}(E - \mu_{p,\mathrm{eff}}) - n_{\rm F}(E + \mu_{p,\mathrm{eff}}) = \frac{1}{\mathrm{e}^{\beta(E-\mu_{p,\mathrm{eff}})}+1} - \frac{1}{\mathrm{e}^{\beta(E+\mu_{p,\mathrm{eff}})}+1}\,, \tag{4.79}$$

is non-negative and vanishes only for $\mu_{p,\mathrm{eff}} = 0$. Hence, the chemical potential of the proton is determined as a function of the expectation values of the vector bosons as

$$\mu_p = g_\omega \omega_0 + g_\rho \rho_0^3\,. \tag{4.80}$$

The mean-field equations (4.58) with $n_p = 0$ imply a direct proportionality of $\bar{\omega}_0$ and $\bar{\rho}_0^3$, namely

$$g_\rho \bar{\rho}_0^3 = -\frac{G_\rho}{G_\omega}\, g_\omega \bar{\omega}_0\,, \tag{4.81}$$

and the expectation value $\bar{\rho}_0^3$ can be eliminated in favor of $\bar{\omega}_0$. The neutron effective chemical potential is therefore given by

$$\mu_{n,\mathrm{eff}} = \mu_n - g_\omega \omega_0 \left(1 + \frac{G_\rho}{G_\omega}\right). \tag{4.82}$$

The only free parameters are the temperature T and the neutron chemical potential μ_n. The remaining two mean-field equations can be solved under the constraints (4.80), (4.81), and (4.82) for ω_0 and σ.

At zero temperature, the neutron and scalar density can be computed analytically. Two possible cases have to be considered.

1. $\mu_{n,\mathrm{eff}} < m$. The Fermi distribution in the integrand of U_F defined in Eq. (4.34) turns into a step function $\theta(\mu_{n,\mathrm{eff}} - \sqrt{p^2+m^2})$, which vanishes identically for all momenta. Only the bosonic part contributes to the mean-field potential, i.e.,

   $$U_\mathrm{MF} = U_\mathrm{B}\,. \tag{4.83}$$

   The mean field equations simplify to

   $$\bar{\omega}_0 = 0\,, \qquad \frac{\partial U_\mathrm{B}}{\partial \sigma}(\bar{\sigma}, 0, 0) = 0\,. \tag{4.84}$$

2. $\mu_{n,\mathrm{eff}} \geq m$. The step function provides now an upper cutoff for the momenta and the Fermi sea of the nucleons is filled. The mean-field potential is

   $$\begin{aligned} U_\mathrm{MF} &= U_\mathrm{B} - \frac{1}{\pi^2}\int_0^{\sqrt{\mu_{n,\mathrm{eff}}^2 - m^2}} dp\, \frac{p^4}{3\sqrt{p^2+m^2}} \\ &= U_\mathrm{B} + \frac{1}{24\pi^2}\Big[\mu_{n,\mathrm{eff}}(5m^2 - 2\mu_{n,\mathrm{eff}}^2)\sqrt{\mu_{n,\mathrm{eff}}^2 - m^2} \\ &\qquad - 3m^4 \log\frac{\mu_{n,\mathrm{eff}} + \sqrt{\mu_{n,\mathrm{eff}}^2 - m^2}}{m}\Big]. \end{aligned} \tag{4.85}$$

   The resulting mean-field equations then are

   $$\begin{aligned} g_\omega \bar{\omega}_0 &= \frac{G_\omega}{\pi^2}\int_0^{\sqrt{\mu_{n,\mathrm{eff}}^2 - m^2}} dp\, p^2 = \frac{G_\omega}{3\pi^2}(\mu_{n,\mathrm{eff}}^2 - m^2)^{3/2}\,, \\ \frac{\partial U_\mathrm{B}}{\partial \sigma}(\bar{\sigma}, \bar{\omega}_0, \bar{\rho}_0^3) &= -\frac{g_s}{\pi^2}\int_0^{\sqrt{\mu_{n,\mathrm{eff}}^2 - m^2}} dp\, \frac{m\,p^2}{\omega} \\ &= -\frac{g_s}{2\pi^2}\left(m\,\mu_{n,\mathrm{eff}}\sqrt{\mu_{n,\mathrm{eff}}^2 - m^2} - m^3 \log\frac{\mu_{n,\mathrm{eff}} + \sqrt{\mu_{n,\mathrm{eff}}^2 - m^2}}{m}\right), \end{aligned} \tag{4.86}$$

   where it is implicitly understood that m and $\mu_{n,\mathrm{eff}}$ have to be evaluated at the minimum $\bar{\sigma}$, $\bar{\omega}_0$, and $\bar{\rho}_0^3$.

For a given μ_n, the mean-field equations are solved. According to Eq. (4.54), the grand-canonical potential is the mean-field potential evaluated at the minimum $\bar{\sigma}$, $\bar{\omega}_0$, and $\bar{\rho}_0^3$. We suppress the field-dependence of the quantities in our notation. In the following, all

quantities are implicitly evaluated at the minimum. From the grand-canonical potential, the energy density (3.35) follows, namely

$$\begin{aligned}\epsilon &= U_{\mathrm{MF}} + \mu_n\, n_n \\ &= U_{\mathrm{B}} + \frac{1}{24\pi^2}\Big[(5m^2\,\mu_{n,\mathrm{eff}} - 2\mu_{n,\mathrm{eff}}^3 + 8\mu_n\,\mu_{n,\mathrm{eff}}^2 - 8\mu_n\,m^2)\sqrt{\mu_{n,\mathrm{eff}}^2 - m^2} \\ &\qquad\qquad - 3m^4 \log\frac{\mu_{n,\mathrm{eff}} + \sqrt{\mu_{n,\mathrm{eff}}^2 - m^2}}{m}\Big]\,.\end{aligned} \tag{4.87}$$

The energy per particle is given by

$$\begin{aligned}\frac{E}{A} &= \frac{\epsilon}{n_n} - m_{\mathrm{N}} = \frac{U_{\mathrm{MF}}}{n_n} + \mu_n - m_{\mathrm{N}} \\ &= \frac{U_{\mathrm{B}}}{n_n} + \frac{1}{8}\Big[\frac{5m^2\,\mu_{n,\mathrm{eff}} - 2\mu_{n,\mathrm{eff}}^3 + 8\mu_n\,\mu_{n,\mathrm{eff}}^2 - 8\mu_n\,m^2}{\mu_{n,\mathrm{eff}}^2 - m^2} \\ &\qquad\qquad - \frac{3m^4}{(\mu_{n,\mathrm{eff}}^2 - m^2)^{3/2}} \log\frac{\mu_{n,\mathrm{eff}} + \sqrt{\mu_{n,\mathrm{eff}}^2 - m^2}}{m}\Big] - m_{\mathrm{N}}\,.\end{aligned} \tag{4.88}$$

In Eq. (2.54) we gave an expression for the energy per particle, which in the case of pure neutron matter at saturation density reads

$$\frac{E}{A}(n_0, 0) = \frac{E}{A}(n_0, 0.5) + E_{\mathrm{sym}}\,. \tag{4.89}$$

If we take $E_{\mathrm{sym}} = 32\,\mathrm{MeV}$, we find the energy per particle of pure neutron matter at n_0, namely

$$\frac{E}{A}(n_0, 0) = 16\,\mathrm{MeV}. \tag{4.90}$$

All remaining parameters can now be fixed. First, the expectation values $\bar{\sigma}$ and $\bar{\omega}_0$ can be computed as follows:

$$\begin{aligned} & n_n = \frac{1}{3\pi^2}(\mu_{n,\mathrm{eff}}^2 - (g_s\bar{\sigma})^2)^{3/2} = n_0\,, \\ \Rightarrow\quad & \bar{\sigma} = \frac{1}{g_s}\sqrt{\mu_{n,\mathrm{eff}}^2 - (3\pi^2 n_0)^{2/3}}\,, \qquad g_\omega\bar{\omega}_0 = G_\omega n_n = G_\omega n_0\,. \end{aligned} \tag{4.91}$$

The free variables μ_n and G_ρ have to be fixed in order to reproduce (4.90) together with

$$\frac{\partial U_{\mathrm{MF}}}{\partial\sigma} = 0\,. \tag{4.92}$$

The solution is found for $\mu_n = 985\,\mathrm{MeV}$ and for the coupling

$$G_\rho = 1.07\,\mathrm{fm}^2\,. \tag{4.93}$$

Again, we stress that only the ratio $G_\rho = g_\rho^2/m_\rho^2$ enters the model in the mean-field approximation. We fix $m_\rho = m_\omega$ to make the model comparable to the literature. With this choice, the coupling of the ρ-field is given by

$$g_\rho = 4.12\,. \tag{4.94}$$

All mean-field parameters are summed up in Table 2. The model is completely determined and can be studied by varying T, μ_p, and μ_n. We will first discuss the extension beyond the mean-field approximation and then compare the results directly to the mean-field calculations.

$a_3\,(\mathrm{MeV}^{-2})$	$a_4\,(\mathrm{MeV}^{-4})$	$m_\sigma\,(\mathrm{MeV})$	g_s	$G_\omega\,(\mathrm{fm}^2)$	$G_\rho\,(\mathrm{fm}^2)$
$6.87 \cdot 10^{-2}$	$2.05 \cdot 10^{-4}$	880	10.1	5.71	1.07

Table 2: List of all mean-field parameters.

4.3 WETTERICH'S FLOW EQUATION

Fluctuations can be included in the framework of the functional renormalization group. The k-dependent effective action is treated up to first order in the derivative expansion (see Eq. (3.57)), and in the local potential approximation, i.e., with $Z_k \equiv 1$ and $Y_k \equiv 0$. Moreover, the influence of a running of the Yukawa couplings is expected to be small, as is known from explicit computations in the quark-meson model [203]. The Yukawa couplings g_s, g_ω, and g_ρ are therefore taken to be constants. We define the following matrix of chemical potentials

$$\boldsymbol{\mu} = \mu_p P_p + \mu_n P_n = \begin{pmatrix} \mu_p & \\ & \mu_n \end{pmatrix} . \tag{4.95}$$

The ansatz for the **effective action** Γ_k in the ChNM model in four-dimensional Euclidean space-time is given by

$$\begin{aligned} \Gamma_k = \int d^4x \, \Big\{ & \bar{\psi}\Big[\gamma^\mu_{\mathrm{E}}\partial^{\mathrm{E}}_\mu + g_s(\sigma + i\gamma_5\,\boldsymbol{\pi}\cdot\boldsymbol{\tau}) + \gamma^0\boldsymbol{\mu} - i\gamma^\mu(g_\omega\,\omega^{\mathrm{E}}_\mu + g_\rho\,\boldsymbol{\rho}^{\mathrm{E}}_\mu\cdot\boldsymbol{\tau})\Big]\psi \\ & + \frac{1}{2}\partial^{\mathrm{E}}_\mu\sigma\;\partial^\mu_{\mathrm{E}}\sigma + \partial^{\mathrm{E}}_\mu\boldsymbol{\pi}\cdot\partial^\mu_{\mathrm{E}}\boldsymbol{\pi} + U_k(T,\mu_p,\mu_n,\boldsymbol{\pi},\sigma,\omega_\mu,\boldsymbol{\rho}_\mu) \\ & + \frac{1}{4}F^{(\omega)}_{\mu\nu}F^{(\omega)\mu\nu} + \frac{1}{4}\boldsymbol{F}^{(\rho)}_{\mu\nu}\cdot\boldsymbol{F}^{(\rho)\mu\nu}\Big\}, \end{aligned} \tag{4.96}$$

where U_k is the k-dependent effective potential that contains bosonic interactions and the mass terms of the vector bosons. It is important to stress that the fields that appear in the effective action are not the quantum fields of the initial action. Instead, they are the "classical" fields at the scale k as defined in Eq. (3.47). In the limit $k \to 0$ they are exactly the classical fields (3.8) of the low-energy theory. Strictly speaking, the fields that appear in the Lagrangian (4.3) of the underlying theory are the fields ξ of Sec. 3.1, whereas the fields in the effective action above correspond to the fields Φ. We do not want to blow up the notation by introducing new labels, but the distinction should be kept in mind.

The nucleons are allowed to fluctuate around the Fermi surface. The vector bosons, in contrast, are heavier than the relevant scales. Therefore, the ω and the ρ fields can be included as non-fluctuating background fields, so we will treat them in the mean-field approximation. As discussed in Appendix A.1, the Euclidean expectation values of the vector fields are purely imaginary. It is therefore convenient to work with the real vector-field components in Minkowski-space. Hence, $\omega_{\mathrm{E},4}$ and $\rho^3_{\mathrm{E},4}$ are replaced by $-i\omega_0$ and $-i\rho^3_0$, respectively. The effective action simplifies to

$$\begin{aligned} \Gamma_k = \int d^4x \, \Big\{ & \bar{\psi}\Big[\gamma^\mu_{\mathrm{E}}\partial^{\mathrm{E}}_\mu + g_s(\sigma + i\gamma_5\,\boldsymbol{\pi}\cdot\boldsymbol{\tau}) + \gamma^0(\boldsymbol{\mu} - g_\omega\,\omega_0 - g_\rho\,\rho^3_0\,\tau^3)\Big]\psi \\ & + \frac{1}{2}\partial^{\mathrm{E}}_\mu\sigma\;\partial^\mu_{\mathrm{E}}\sigma + \partial^{\mathrm{E}}_\mu\boldsymbol{\pi}\cdot\partial^\mu_{\mathrm{E}}\boldsymbol{\pi} + U_k(T,\mu_p,\mu_n,\boldsymbol{\pi},\sigma,\omega_0,\rho^3_0)\Big\}. \end{aligned} \tag{4.97}$$

In analogy to the mean-field potential (4.36), the ansatz for the **effective potential** U_k is

$$\begin{aligned} U_k(T,\mu_p,\mu_n,\boldsymbol{\pi},\sigma,\omega_0,\rho_0^3) = &-\frac{1}{2}m_\omega^2\omega_0^2 - \frac{1}{2}m_\rho^2(\rho_0^3)^2 \\ &+ U_{k,\chi}(T,\mu_p,\mu_n,\chi,\omega_0,\rho_0^3) + m_\pi^2 f_\pi(f_\pi-\sigma)\,. \end{aligned} \tag{4.98}$$

The chiral potential $U_{k,\chi}$ can be Taylor expanded around χ_0. The non-analytic term in the mean-field potential originates from a Hartree term that is automatically included in the RG treatment. Therefore, the ansatz for $U_{k,\chi}$ is

$$U_{k,\chi}(T,\mu_p,\mu_n,\chi,\omega_0,\rho_0^3) = \sum_n \frac{a_{n,k}(T,\mu_p,\mu_n,\omega_0,\rho_0^3)}{n!}(\chi-\chi_0)^n\,. \tag{4.99}$$

In thermodynamics, we are finally interested in homogeneous fields. The volume factors out and the left-hand-side of Wetterich's equation (3.51) turns into a flow for the effective potential,

$$\frac{\partial\Gamma_k}{\partial k} = \beta V\cdot\frac{\partial U_{k,\chi}(T,\mu_p,\mu_n,\chi,\omega_0,\rho_0^3)}{\partial k}\,. \tag{4.100}$$

The computation of the right-hand side of the flow equation is slightly technical and therefore performed in Appendix A.3. The Bose distribution n_B and the Fermi distribution n_F are defined in Appendix A.1. **Wetterich's flow equation** for the ChNM model is given by

$$\begin{aligned} k\frac{\partial U_{k,\chi}}{\partial k}(T,\mu_p,\mu_n,\chi,\omega_0,\rho_0^3) &= f_U(T,\mu_p,\mu_n,\chi,\omega_0,\rho_0^3)\,, \\ f_U(T,\mu_p,\mu_n,\chi,\omega_0,\rho_0^3) &= \frac{1}{2}\;\; + \;\; \frac{1}{2} \\ &= \frac{k^5}{12\pi^2}\Bigg\{\frac{1+2n_\mathrm{B}(E_\sigma)}{E_\sigma} + \frac{3[1+2n_\mathrm{B}(E_\pi)]}{E_\pi} \\ &\qquad - \sum_{i=n,p}\frac{4[1-\sum_{r=\pm1}n_\mathrm{F}(E_\mathrm{N}-r\mu_{i,\mathrm{eff}})]}{E_\mathrm{N}}\Bigg\}, \end{aligned} \tag{4.101}$$

with

$$\begin{aligned} &E_\pi^2 = k^2+m_\pi^2\,, \qquad E_\sigma^2 = k^2+m_\sigma^2\,, \qquad E_\mathrm{N}^2 = k^2+m_\mathrm{N}^2\,, \\ &m_\pi^2 = U'_{k,\chi}(\chi)\,, \qquad m_\sigma^2 = U'_{k,\chi}(\chi)+2\chi\,U''_{k,\chi}(\chi)\,, \qquad m_\mathrm{N}^2 = 2g_s^2\chi\,, \\ &\mu_{p,\mathrm{eff}} = \mu_p - g_\omega\omega_0 - g_\rho\rho_0^3\,, \qquad \mu_{n,\mathrm{eff}} = \mu_n - g_\omega\omega_0 + g_\rho\rho_0^3\,. \end{aligned}$$

The different contributions to the flow equation can be given a physical interpretation. The σ field, the pions and the nucleons enter all with their respective multiplicity. The nucleons come with an additional minus sign from the trace in the fermionic loop. All particles enter with a vacuum piece and a Bose or Fermi distribution, respectively, which vanishes in the limit $T=\mu=0$. Next, we will elucidate the connection to in-medium propagators.

4.3.1 *Taylor-expansion method*

Because of the first-order liquid-gas phase transition, the minimum of the potential as a function of σ is discontinuous. As we have seen in Sec. 3.4, the flow equation has to be solved on a grid in σ (or χ). But before we turn to the actual evaluation of the flow equation, it is nevertheless useful to study the Taylor expanded flow equations, even though this approach works only away from the phase transition. Starting from the ansatz (4.99), the flow equations for the couplings can be computed directly from the full flow equation as

$$k\frac{\partial a_{n,k}}{\partial k} = k\frac{\partial}{\partial k}\left.\frac{\partial^n U_{k,\chi}}{\partial^n \chi}\right|_{\chi=\chi_0} = \left.\frac{\partial^n f_U}{\partial \chi^n}\right|_{\chi=\chi_0} . \tag{4.102}$$

To get a better physical understanding, it is useful to study the expression for f_U with the Matsubara sums not yet performed. As shown in Appendix A.3,

$$f_U = l_0^{\mathrm{bos}}(E_\pi) + l_0^{\mathrm{bos}}(E_\sigma) - \sum_{i,n,p} l_0^{\mathrm{fer}}(E_{\mathrm{N}}, \mu_{i,\mathrm{eff}}) , \tag{4.103}$$

where the threshold functions are defined as

$$\begin{aligned} l_0^{\mathrm{bos}}(E) &= \frac{k^5}{6\pi^2} T \sum_l \frac{1}{\omega_l^2 + E^2} , & \omega_l &= 2l\pi T , \\ l_0^{\mathrm{fer}}(E,\mu) &= \frac{k^5}{6\pi^2} T \sum_l \frac{1}{(\omega_l + i\mu)^2 + E^2} , & \omega_l &= (2l+1)\pi T . \end{aligned} \tag{4.104}$$

Instead of the Matsubara formalism one can work in the real-time formalism (which is however practically more difficult) by replacing

$$\frac{1}{\omega_l^2 + |\boldsymbol{p}|^2 + m^2} \to \frac{i}{p^2 - m^2 + i\epsilon} + \frac{2\pi}{\mathrm{e}^{\beta|p_0|} - 1}\delta(p^2 - m^2) , \tag{4.105}$$

in the case of bosons, as is shown for instance in Ref. [176]. We have defined $p^2 = p_0^2 - |\boldsymbol{p}|^2$. The Matsubara sum is then replaced by an integral over p_0. For fermions, the fields double in real-time formalism, and correspondence is in general more difficult. However, in the case of vanishing temperature the same results can be obtained from a calculation in real time, using the propagator

$$D_F = (p_\mu \gamma^\mu + m)\left[\frac{i}{p^2 - m^2 + i\epsilon} - 2\pi\,\theta(p_0)\cdot\theta(k_f - |\boldsymbol{p}|)\cdot\delta(p^2 - m^2)\right] . \tag{4.106}$$

The first term is identified as the vacuum propagator. The second term is an **in-medium insertion** as a result of the Fermi sea, filled up to $k_f = \sqrt{\mu^2 - m^2}$, which accounts for Pauli-blocking effects. In the non-relativistic limit, an equivalent description of the propagator is given by

$$D_F = \frac{i\theta(k_f - |\boldsymbol{p}|)}{p_0 - \frac{p^2}{2m} - i\epsilon} + \frac{i\theta(|\boldsymbol{p}| - k_f)}{p_0 - \frac{p^2}{2m} + i\epsilon} . \tag{4.107}$$

The first expression corresponds to propagating particles, the second to holes. All **particle-hole excitations** are therefore naturally included in the FRG framework. We can now

give a physical interpretation of the flow equations. First, look at the flow of the zero-component, i.e., the pressure, which is given by

$$k\frac{\partial a_{0,k}}{\partial k} = f_U|_{\chi=\chi_0} = \frac{1}{2}$$  $$+\ \frac{1}{2}$$  . (4.108)

Note that the interpretation of the loops is different from that in the full flow equation. Here, the loops are evaluated at the minimum χ_0, whereas in the flow equation, the loops still depend on χ as a free parameter and therefore determine the potential for all values of χ. If we replace the propagator by the free one, this is just the leading order in thermal perturbation theory. Note, however, that here we make use of the full propagator, and the equation is exact.

In a similar way, the flow equations for the higher order couplings can be obtained. From Eq. (4.102) we must differentiate with respect to the fields χ, and new propagators are generated this way. The new equations can be understood in terms of diagrams: Differentiating with respect to χ corresponds to "pulling out" legs from the loops in all possible ways. For $a_{2,k}$ we can write

$$k\frac{\partial a_{2,k}}{\partial k} =$$ 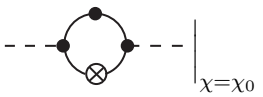 $$+$$ 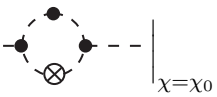 $$-\ \frac{1}{2}$$  . (4.109)

We can also understand these results in a more formal way. One can take functional derivatives of Wetterich's flow equation with respect to the field χ to get the flow equation of n-point functions. For instance, taking one derivative gives the flow equation of the one-point function

$$k\frac{\partial \Gamma_k^{(1,0)}}{\partial k} = -\frac{1}{2}\,\mathrm{Tr}\left[k\frac{\partial R_k}{\partial k}\cdot\left(\Gamma_k^{(1,1)}+R_k\right)^{-1}\cdot\Gamma^{(2,1)}\cdot\left(\Gamma_k^{(1,1)}+R_k\right)^{-1}\right]. \tag{4.110}$$

Pictorially we can write this equation as

$$k\frac{\partial}{\partial k}$$ $$= -\frac{1}{2}$$ 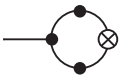 . (4.111)

The solid lines represent all possible fields in the theory (bosons and fermions). The cross on the right-hand side is the regulator insertion $k\frac{\partial R_k}{\partial k}$. The full propagators correspond to $(\Gamma_k^{(1,1)}+R_k)^{-1}$, and $\Gamma^{(2,1)}$ is the full three-point coupling. Taking one further derivative with respect to χ gives the flow of the two-point function,

$$\begin{aligned} k\frac{\partial \Gamma_k^{(1,1)}}{\partial k} &= -\frac{1}{2}\,\mathrm{Tr}\left[k\frac{\partial R_k}{\partial k}\cdot\left(\Gamma_k^{(1,1)}+R_k\right)^{-1}\cdot\Gamma^{(2,2)}\cdot\left(\Gamma_k^{(1,1)}+R_k\right)^{-1}\right] \\ &\quad + \mathrm{Tr}\left[k\frac{\partial R_k}{\partial k}\cdot\left(\Gamma_k^{(1,1)}+R_k\right)^{-1}\cdot\Gamma^{(2,1)}\cdot\left(\Gamma_k^{(1,1)}+R_k\right)^{-1}\cdot\Gamma^{(2,1)}\cdot\left(\Gamma_k^{(1,1)}+R_k\right)^{-1}\right]. \end{aligned} \tag{4.112}$$

Again, the pictorial representation is straightforward:

$$k\frac{\partial}{\partial k}$$  $$= -\frac{1}{2}$$  $$+$$  . (4.113)

As is clear from the formulas or the pictorial representation, the flow equation for an n-point coupling requires information about the $n+1$ and $n+2$-point couplings as well. As a consequence, an infinite number of coupled equations must be solved. The flow equations bear a resemblance to **Dyson-Schwinger equations**. One difference is that the FRG equations contain only full propagators and n-point functions, whereas also bare couplings enter the Dyson-Schwinger equations. In both approaches, the set of equations has to be truncated in order to do numerical calculations.

For boson-exchange models it is common to make a different ansatz. Instead of the Taylor expansion (4.99) around the fixed value $\chi_0 = \frac{1}{2}f_\pi^2$, it is more useful to expand around a k-dependent minimum $\chi_{0,k}$. The potential is defined as

$$U_{k,\chi}^{\text{Taylor}}(T,\mu_p,\mu_n,\chi,\omega_0,\rho_0^3) = \sum_n \frac{a_{n,k}(T,\mu_p,\mu_n,\omega_0,\rho_0^3)}{n!}(\chi-\chi_{0,k})^n\,. \tag{4.114}$$

Not all coefficients are independent. The coefficient $a_{1,k}$ can be fixed by requiring that $\chi_{0,k}$ is the minimum of $U_{k,\chi}^{\text{Taylor}}$ for all k. The flow of the couplings can be determined as follows:

$$k\frac{da_{n,k}}{dk} = k\frac{d}{dk}\frac{\partial^n U_{k,\chi}^{\text{Taylor}}}{\partial\chi^n}\bigg|_{\chi=\chi_0}\,. \tag{4.115}$$

The right-hand side can then be computed using the identity

$$k\frac{d}{dk}\frac{\partial U_{k,\chi}^{\text{Taylor}}}{\partial\chi} = k\frac{\partial}{\partial k}\frac{\partial U_{k,\chi}^{\text{Taylor}}}{\partial\chi} + \frac{\partial^2 U_{k,\chi}^{\text{Taylor}}}{\partial\chi\,\partial\chi_{0,k}}\frac{\partial\chi_{0,k}}{\partial k}\,, \tag{4.116}$$

and similar for higher χ-derivatives, together with the flow equation (4.101). For concreteness, we expand up to power $n=2$ in $\chi-\chi_{0,k}$. The full set of flow equations is then

$$\begin{aligned}
k\frac{d\chi_{0,k}}{dk} &= -\frac{2}{m_\pi^2 f_\pi \chi_{0,k}^{-3/2} + 2a_{2,k}}\frac{\partial f_U}{\partial\chi}\bigg|_{\chi=\chi_0}\,,\\
k\frac{da_{0,k}}{dk} &= \frac{m_\pi^2 f_\pi}{\sqrt{2\chi_{0,k}}}\,k\frac{d\chi_{0,k}}{dk} + f_U|_{\chi=\chi_0}\,,\\
k\frac{da_{2,k}}{dk} &= \frac{\partial^2 f_U}{\partial\chi^2}\bigg|_{\chi=\chi_0}\,.
\end{aligned} \tag{4.117}$$

After this short digression we will now turn back to the evaluation of the flow equations and discuss the role of the vector fields in more detail.

4.3.2 *Flow equations for the vector fields*

As discussed, the vector fields ω and ρ parameterize part of the nucleonic short-range interactions. Consequently, their masses are large compared to the relevant scales, and they are treated as constant background fields. The values ω_0 and ρ_0^3 are adjusted in such a way that the effective potential (4.98) is minimized. In principle, the flow equations have to be solved for a certain number of values (ω_0,ρ_0^3) distributed over a suitable range, which is numerically costly. It is therefore desirable to eliminate the background fields as free parameters. Background fields $\omega_{0,k}(\chi)$ and $\rho_{0,k}^3(\chi)$ are introduced, which depend both on the flow parameter k and the chiral field χ. Their values are adjusted in such a way

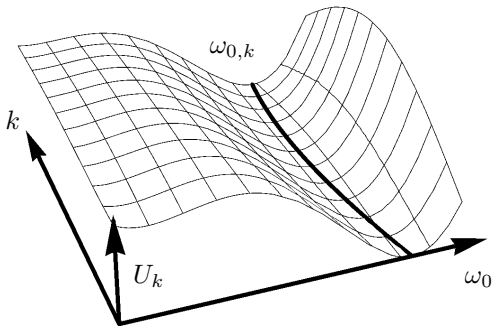

Figure 7: Two-dimensional slice (with the χ and ρ_0^3 directions not shown for simplicity): the potential is minimized at each k as a function of ω_0. The solution is $\omega_{0,k}$. Instead of finding the constant ω_0 that minimizes the potential at $k = 0$, one determines the minimum at each renormalization scale k.

that at each scale k and value of χ the full effective potential is minimized as a function of ω_0 and ρ_0^3. The corresponding equations are

$$\begin{aligned}\frac{\partial}{\partial y}\Big[U_{k,\chi}(T,\mu_p,\mu_n,\chi,y,\rho_{0,k}^3(\chi)) - \frac{1}{2}m_\omega^2 y^2\Big]\Big|_{y=\omega_{0,k}(\chi)} &= 0\,,\\ \frac{\partial}{\partial z}\Big[U_{k,\chi}(T,\mu_p,\mu_n,\chi,\omega_{0,k}(\chi),z) - \frac{1}{2}m_\rho^2 z^2\Big]\Big|_{z=\rho_{0,k}^3(\chi)} &= 0\,.\end{aligned} \tag{4.118}$$

A visualization is given in Fig. 7, where only two dimensions are shown and the dependence on ρ_0^3 is neglected for reasons of visualizability. The flow equation for $\omega_0(k)$ can be rewritten more explicitly using Wetterich's equation (4.101)

$$\frac{\partial}{\partial y}\Big[\int_\Lambda^k dp\,\frac{\partial}{\partial p}U_{p,\chi}(T,\mu_p,\mu_n,\chi,y,\rho_{0,k}(\chi)) - \frac{1}{2}m_\omega^2 y^2\Big]\Big|_{y=\omega_{0,k}(\chi)} = 0\,, \tag{4.119}$$

with the solution

$$\begin{aligned}\omega_{0,k}(\chi) = -\frac{1}{3\pi^2 m_\omega^2}\int_k^\Lambda dp\,\frac{p^4}{E_\mathrm{N}}\sum_{r=\pm1}\frac{\partial}{\partial y}\Big[&n_\mathrm{F}(E_\mathrm{N} - r(\mu_p - g_\omega y - g_\rho\rho_{0,k}^3(\chi)))\\ &+ n_\mathrm{F}(E_\mathrm{N} - r(\mu_n - g_\omega y + g_\rho\rho_{0,k}^3(\chi)))\Big]\Big|_{y=\omega_{0,k}(\chi)}.\end{aligned} \tag{4.120}$$

The y-derivative can be replaced by a derivative with respect to the chemical potential. We define the k- and χ-dependent effective chemical potentials,

$$\begin{aligned}\mu_{p,\mathrm{eff},k}(\chi) &= \mu_p - g_\omega\omega_{0,k}(\chi) - g_\rho\rho_{0,k}^3(\chi)\,,\\ \mu_{n,\mathrm{eff},k}(\chi) &= \mu_n - g_\omega\omega_{0,k}(\chi) + g_\rho\rho_{0,k}^3(\chi)\,.\end{aligned} \tag{4.121}$$

The **k-dependence of the ω-boson** is then given by the solution of the integral equation

$$\boxed{\begin{aligned}g_\omega\omega_{0,k}(\chi) = \frac{G_\omega}{3\pi^2}\int_k^\Lambda dp\,\frac{p^4}{E_\mathrm{N}}\sum_{r=\pm1}\frac{\partial}{\partial\mu}\Big[&n_\mathrm{F}(E_\mathrm{N} - r\mu)\Big|_{\mu=\mu_{p,\mathrm{eff},k}(\chi)}\\ &+n_\mathrm{F}(E_\mathrm{N} - r\mu)\Big|_{\mu=\mu_{n,\mathrm{eff},k}(\chi)}\Big]\end{aligned}} \tag{4.122}$$

The flow equation for $\rho_0^3(k)$ can be derived in exactly the same way. The only difference is that by replacing the y-derivative with a μ-derivative, the Fermi distribution that contains the neutron chemical potential picks up an additional minus sign. With this taken into account we arrive at the **flow equation for the ρ_0^3 background field**:

$$\boxed{g_\rho \rho_{0,k}^3(\chi) = \frac{G_\rho}{3\pi^2}\int_k^\Lambda dp\, \frac{p^4}{E_\mathrm{N}} \sum_{r=\pm 1} \frac{\partial}{\partial \mu}\Big[n_\mathrm{F}(E_\mathrm{N} - r\mu)\Big|_{\mu=\mu_{p,\mathrm{eff},k}(\chi)} - n_\mathrm{F}(E_\mathrm{N} - r\mu)\Big|_{\mu=\mu_{n,\mathrm{eff},k}(\chi)}\Big].} \tag{4.123}$$

The k-dependent fields $\omega_{0,k}(\chi)$ and $\rho_{0,k}^3(\chi)$ are inserted into the effective potential. Applying equation (4.118) allows us to rewrite the minimizing condition for U_k as

$$\begin{aligned} & k\frac{\partial U_k}{\partial k}(T,\mu_p,\mu_n,\sigma,\boldsymbol{\pi},\omega_{0,k}(\chi),\rho_{0,k}^3(\chi)) \\ &\quad = \Big\{ k\frac{\partial U_{k,\chi}}{\partial k}(T,\mu_p,\mu_n,\chi,y,z) \\ &\qquad + \frac{\partial}{\partial y}\Big[U_{k,\chi}(T,\mu_p,\mu_n,\chi,y,z) - \frac{1}{2}m_\omega^2 y^2\Big]\cdot k\frac{\partial \omega_{0,k}(\chi)}{\partial k} \\ &\qquad + \frac{\partial}{\partial z}\Big[U_{k,\chi}(T,\mu_p,\mu_n,\chi,y,z) - \frac{1}{2}m_\rho^2 z^2\Big]\cdot k\frac{\partial \rho_{0,k}^3(\chi)}{\partial k}\Big\}\Big|_{y=\omega_{0,k}(\chi),\, z=\rho_{0,k}^3(\chi)} \\ &\quad = k\frac{\partial U_{k,\chi}}{\partial k}(T,\mu_p,\mu_n,\chi,y,z)\Big|_{y=\omega_{0,k}(\chi),\, z=\rho_{0,k}^3(\chi)}. \end{aligned} \tag{4.124}$$

If one finally uses Eq. (4.101), **Wetterich's flow equation** is transformed into

$$\boxed{k\frac{\partial U_{k,\chi}}{\partial k}(T,\mu_p,\mu_n,\chi,\omega_{0,k}(\chi),\rho_{0,k}^3(\chi)) = f_U(T,\mu_p,\mu_n,\chi,\omega_{0,k}(\chi),\rho_{0,k}^3(\chi))\,.} \tag{4.125}$$

Note that the flow equation for $\omega_{0,k}(\chi)$ can be rewritten after an integration by parts and with help of $\frac{\partial}{\partial\mu} \to -r\frac{E_\mathrm{N}}{p}\cdot\frac{\partial}{\partial p}$ as

$$\begin{aligned} g_\omega \omega_{0,k}(\chi) = {} & \frac{G_\omega}{\pi^2}\int_k^\Lambda dp\, p^2 \sum_{i=p,n}\Big[n_\mathrm{F}(E_\mathrm{N} - \mu_{i,\mathrm{eff},k}(\chi)) - n_\mathrm{F}(E_\mathrm{N} + \mu_{i,\mathrm{eff},k}(\chi))\Big] \\ & - \frac{G_\omega}{3\pi^2}p^3 \sum_{i=p,n}\Big[n_\mathrm{F}(E_\mathrm{N} - \mu_{i,\mathrm{eff},k}(\chi)) - n_\mathrm{F}(E_\mathrm{N} + \mu_{i,\mathrm{eff},k}(\chi))\Big]\Big|_{p=k}^\Lambda. \end{aligned} \tag{4.126}$$

The expectation value of the background field ω_0 is therefore still determined by an equation similar to the mean-field equation (4.58). However, the baryon number must be computed for the effective action at the flow parameter k in order to keep the equations self-consistent. Hence, the nucleonic loop is integrated only from Λ down to the scale k, which gives the contribution of a Fermi gas with restricted momenta. Moreover, there is a boundary term (the second line), as a consequence of the cutoffs k and Λ in the infrared and ultraviolet, respectively. In the limit $\Lambda \to \infty$ and $k \to 0$, the boundary terms vanish

and for a fixed value of χ, the vector field ω_0 takes its mean-field value (4.58) – with $\chi = \frac{1}{2}\bar{\sigma}^2$ still understood as a free parameter –, namely

$$\omega_{0,k=0}(\chi) \xrightarrow{\Lambda\to\infty} \bar{\omega}_0(\chi)\,. \tag{4.127}$$

In this limit, all fluctuations with arbitrary momenta are taken into account. The flow parameter k is directly related to the momentum parameter p in the fermionic integral, which contributes to the mean field potential. The value of χ is determined as the minimum of the effective potential, which can differ from the mean-field solution, and the field $\bar{\omega}_0(\chi)$ then is evaluated at a different value. The field ρ_0^3 can be treated in exactly the same way with the analogous conclusions.

Recall from Sec. 4.1 that there are two different ways to introduce an additional chemical potential. We added different chemical potentials for protons and neutrons, respectively. Another strategy more in the spirit of chiral symmetry would have been to introduce an **isospin-chemical potential**, μ_{I}. The isospin-chemical potential is related to a rotation around the isospin-3 direction. As a consequence, μ_{I} couples to the kinetic term of π_1 and π_2, as can be read off from Eq. (4.13). Therefore, the bosonic part of the flow equation depends also on μ_{I}. As was shown in Ref. [200], the pions π_1 and π_2 are influenced by the isospin-chemical potential, and the energy E in the Bose distribution is replaced by $E \pm 2\mu_{\mathrm{I}}$. In the presence of vector bosons, ω_0 and ρ_0^3, the isospin chemical potential is shifted. Consequently, also the pion loops for π_1 and π_2 contribute to the flow of the vector bosons. It follows that the flow equations for ω_0 and ρ_0^3 are more complicated. Most importantly, the pionic loop depends explicitly on the potential U_k, and so do the flow equations of the vector bosons. For proton and neutron chemical potentials, the flow equations (4.122) and (4.123) are numerically very useful, as they do not depend on the potential U_k. Therefore, these equations can be solved first for a given temperature and chemical potentials μ_p and μ_n. The result is then inserted into the flow equation for the potential. This split into two processes does no longer work in the presence of an isospin-chemical potential. Either the full set of equations has to be solved at once, or ω_0 and ρ_0^3 are kept as free parameters, which have to be minimized in the end. As a consequence of the symmetry breaking $\mathrm{SO}(4) \to \mathrm{SO}(2) \times \mathrm{SO}(2)$, an additional complication is that the potential depends on two different invariants, as defined in Eq. (4.18). The flow equations have to be solved on a two-dimensional grid, which is much more demanding.

Luckily, this additional source of isospin breaking is not expected to be severe. First, it gives a correction of the order μ_{I}/μ to the pion loops, where μ is the baryon chemical potential. This ratio is at most about 0.15 for high-density neutron matter, and usually even smaller in our applications. Note that the pion loops themselves give only a correction to the leading nucleon part. In an explicit calculation in chiral effective field theory, the contribution of the isospin-breaking effects in the pion sector to the equation of state was found to be small [204].

4.3.3 *Fluctuations around the liquid-gas transition*

In the mean-field approximation, the effects of the bosonic quantum fluctuations are not implicitly included. Nevertheless, a certain amount of information is contained in the couplings of the higher powers in the fields. If the bosonic fields are integrated out, these terms are converted into contact interactions between two and more nucleons. The contact interactions then parametrize the unknown short-distance physics. The purpose of the model is to describe symmetric and asymmetric nuclear matter. As we have seen in Sec. 4.2.2, the parameters are determined in such a way that a good description of nuclear

matter around the liquid-gas phase transition at vanishing temperature is guaranteed. As a consequence, the fluctuations should also be systematically included around the liquid-gas transition at $T = 0$ and $\mu_p = \mu_n = \mu_c = 923\,\mathrm{MeV}$. Litim and Pawlowski gave a description how to include thermal fluctuations without infrared problems [196]. In the spirit of their approach, we study the flow equation of the chiral part of the effective potential relative to the potential at the liquid-gas transition, i.e.,

$$\bar{U}_{k,\chi}(T,\mu_p,\mu_n,\chi,\omega_0,\rho_0^3) = U_{k,\chi}(T,\mu_p,\mu_n,\chi,\omega_0,\rho_0^3) - U_{k,\chi}(0,\mu_c,\mu_c,\chi,\omega_{0,c},0)\,. \tag{4.128}$$

The flow equation is

$$k\frac{\partial \bar{U}_{k,\chi}}{\partial k}(T,\mu_p,\mu_n,\chi,\omega_{0,k}(\chi),\rho_{0,k}^3(\chi)) = \bar{f}_U(T,\mu_p,\mu_n,\chi,\omega_{0,k}(\chi),\rho_{0,k}^3(\chi))\,, \tag{4.129}$$

where

$$\begin{aligned}&\bar{f}_U(T,\mu_p,\mu_n,\chi,\omega_{0,k}(\chi),\rho_{0,k}^3(\chi))\\ &\quad = f_U(T,\mu_p,\mu_n,\chi,\omega_{0,k}(\chi),\rho_{0,k}^3(\chi)) - f_U(0,\mu_c,\mu_c,\chi,\omega_{0,c},0)\,.\end{aligned} \tag{4.130}$$

The subtracted term is

$$f_U(0,\mu_c,\mu_c,\chi,0,0) = \frac{k^5}{12\pi^2}\left\{\frac{1}{E_\sigma} + \frac{3}{E_\pi} - \frac{8[1-\theta(\mu_c - g_\omega\omega_{0,c} - E_\mathrm{N})]}{E_\mathrm{N}}\right\}, \tag{4.131}$$

where E_π and E_σ are evaluated at the potential at $T = 0$ and $\mu = \mu_c$. The value of $\omega_{0,c}$ was given in Eq. (4.63).

In the following, we describe the procedure to solve Wetterich's equation. First, temperature and the chemical potentials μ_p and μ_n are fixed as external parameters. The flow equations for the vector fields depend on χ but not on the potential $\bar{U}_{k,\chi}$. It is therefore possible to first compute the solutions $\omega_{0,k}(\chi)$ and $\rho_{0,k}^3(\chi)$ for each point on a χ-grid as a function of k, independent of the flow equation for the potential. These functions then are inserted into the flow equation for the potential $\bar{U}_{k,\chi}$. In a second step, the flow equation for the potential is solved with the grid method explained in Sec. 3.4. This way, the numerical cost is reduced significantly. Finally, the explicit symmetry breaking term $m_\pi^2 f_\pi(f_\pi - \sigma)$ and the term $U_{k,\chi}(0,\mu_c,\mu_c,\chi,0,0)$ are added to the potential and the minimum σ_min is determined. We define $\chi_\mathrm{min} = \frac{1}{2}\sigma_\mathrm{min}^2$. From Eq. (3.34), the grand-canonical potential is

$$U_\mathrm{gc}(T,\mu_p,\mu_n) = U_{k=0}\big(T,\mu_p,\mu_n,\boldsymbol{\pi}=0,\,\sigma_\mathrm{min},\,\omega_{0,k=0}(\chi_\mathrm{min}),\,\rho_{0,k=0}^3(\chi_\mathrm{min})\big). \tag{4.132}$$

All thermodynamic quantities follow from Eq. (3.35).

It is far from obvious that the flow equations reduce to the mean-field equations if the boson loops are turned off. Therefore, this is a useful consistency check, which we turn to in the following section.

4.3.4 *Renormalization group equations in the mean-field approximation*

In the mean-field approximation, not only the vector particles but all bosonic exchange particles are replaced by their expectation values. As a consequence, the bosonic loops do

not contribute to the flow equation. At the mean-field level, the flow equation simplifies to

$$k\frac{\partial \bar{U}_{k,\chi}}{\partial k}(T,\mu_p,\mu_n,\chi,\omega_{0,k}(\chi),\rho^3_{0,k}(\chi)) = \frac{k^5}{12\pi^2}\,\frac{4\sum_{i=n,p}\sum_{r=\pm1} n_{\mathrm{F}}(E_{\mathrm{N}}-r\mu_{i,\mathrm{eff},k}(\chi)) - 8\,\theta(\mu_c - g_\omega\omega_{0,c} - E_{\mathrm{N}})}{E_{\mathrm{N}}}. \tag{4.133}$$

The flow equation is a differential equation that requires an initial condition. Therefore, the potential has to be fixed at the ultraviolet cutoff scale Λ. We choose the scale

$$\Lambda = 1.4\,\mathrm{GeV}, \tag{4.134}$$

which is large enough that also for large chemical potentials (in the 1 GeV range) and higher temperatures (up to about 100 MeV) all relevant contributions to the partition function – such as fluctuations around the Fermi surface – are included.

The initial UV-potential is fixed at $T=0$ and $\mu_p=\mu_n=0$. To determine it, the flow equation is solved in the backward direction. In this case, the initial condition at $k=0$ is given by the mean-field potential (4.33). The ansatz for the potential at the ultraviolet cutoff Λ is

$$\begin{aligned}\bar{U}_{\Lambda,\chi}(\chi) &= U_{\mathrm{MF}}(0,0,\sqrt{2\chi},0,0) - m_\pi^2 f_\pi(f_\pi-\sigma)\\ &\qquad - U_{0,\chi}(0,\mu_c,\mu_c,\chi,\omega_{0,c},0) + \int_0^\Lambda dk\,\frac{\partial \bar{U}_{k,\chi}}{\partial k}(0,0,0,\chi,0,0)\\ &= U_{\mathrm{B},\chi}(\chi) - U_{0,\chi}(0,\mu_c,\mu_c,\chi,\omega_{0,c},0) - \int_0^\Lambda dk\,\frac{2k^4}{3\pi^2}\cdot\frac{\theta(\mu_c-g_\omega\omega_{0,c}-E_{\mathrm{N}})}{E_{\mathrm{N}}},\end{aligned} \tag{4.135}$$

where $U_{\mathrm{B},\chi}(\chi)$ is the chiral bosonic part (4.37) of the mean-field potential. We now show that if this potential is taken as a starting point, the flow provides us with the mean-field potential for any given T, μ_p, and μ_n. In fact, the effective potential is

$$\begin{aligned}U_{\mathrm{eff}}(T,\mu_p,\mu_n,\sigma) &= U_{k=0}(T,\mu_p,\mu_n,\boldsymbol{\pi}=0,\sigma,\bar{\omega}_0(\chi),\bar{\rho}^3_0(\chi))\\ &= \bar{U}_{0,\chi}(T,\mu_p,\mu_n,\chi,\omega_{0,0}(\chi),\rho^3_{0,0}(\chi)) + U_{0,\chi}(0,\mu_c,\mu_c,\chi,\omega_{0,c},0) + m_\pi^2 f_\pi(f_\pi-\sigma)\\ &= \bar{U}_{\Lambda,\chi}(\chi) + U_{0,\chi}(0,\mu_c,\mu_c,\chi,\omega_{0,c},0) + m_\pi^2 f_\pi(f_\pi-\sigma)\\ &\qquad - \int_0^\Lambda dk\,\frac{\partial \bar{U}_{k,\chi}}{\partial k}(T,\mu_p,\mu_n,\chi,\omega_{0,k}(\chi),\rho^3_{0,k}(\chi))\\ &= U_{\mathrm{B},\chi}(\chi) + m_\pi^2 f_\pi(f_\pi-\sigma) - \sum_{i=n,p}\sum_{r=\pm1}\int_0^\Lambda dk\,\frac{k^4}{3\pi^2}\cdot\frac{n_{\mathrm{F}}(E_{\mathrm{N}}-r\mu_{i,\mathrm{eff},k}(\chi))}{E_{\mathrm{N}}}.\end{aligned} \tag{4.136}$$

On the other hand, the mean field potential is given by

$$\begin{aligned}U_{\mathrm{MF}}(T,\mu_p,\mu_n,\sigma,\omega_0,\rho^3_0) &= -\frac{1}{2}m_\omega^2\omega_0^2 - \frac{1}{2}m_\rho^2(\rho^3_0)^2 + U_{\mathrm{B},\chi}(\chi) + m_\pi^2 f_\pi(f_\pi-\sigma)\\ &\qquad - \sum_{i=p,n}\sum_{r=\pm1}\int_0^\infty dp\,\frac{p^4}{3\pi^2}\cdot\frac{n_{\mathrm{F}}(E_{\mathrm{N}}-r\mu_{i,\mathrm{eff}})}{E_{\mathrm{N}}}.\end{aligned} \tag{4.137}$$

We replace the vector fields by their χ-dependent minima $\bar{\omega}_0$ and $\bar{\rho}_0^3$. If the cutoff Λ is large enough compared to the scales T and μ, the contributions from $p > \Lambda$ are suppressed by the Fermi distribution. Moreover $\omega_{0,k=0}(\chi) \to \bar{\omega}_0(\chi)$ in this case, according to Eq. (4.127). The mean field potential then is equal to

$$\begin{aligned} U_{\mathrm{MF}}(T, \mu_p, \mu_n, \sigma, \bar{\omega}_0, \bar{\rho}_0^3) = &-\frac{1}{2} m_\omega^2 \left[\omega_{0,0}(\chi)\right]^2 - \frac{1}{2} m_\rho^2 \left[\rho_{0,0}^3(\chi)\right]^2 + U_{\mathrm{B},\chi}(\chi) \\ &+ m_\pi^2 f_\pi (f_\pi - \sigma) - \sum_{i=p,n} \sum_{r=\pm 1} \int_0^\Lambda dp \, \frac{p^4}{3\pi^2} \cdot \frac{n_{\mathrm{F}}(E_{\mathrm{N}} - r\mu_{i,\mathrm{eff},0}(\chi))}{E_{\mathrm{N}}} \,. \end{aligned} \tag{4.138}$$

Note the different way that ω_0 enters U_{eff} and U_{MF}. While the value in the RG-calculation is calculated for each k self-consistently, in the mean-field approach ω_0 is minimized in the end. The effective chemical potential in the mean-field approximation does not depend on the momentum p. Also the interpretation of the integral is slightly different: In the mean field approach, the integral extends over all particles and all momenta p, whereas in the RG treatment, at a certain step k, fluctuations at this scale are integrated out. While the first integral is in momentum space, the second is along the RG-scale. To see that both potentials are the same, subtract U_{eff} from U_{MF}:

$$\begin{aligned} &U_{\mathrm{MF}}(T, \mu_p, \mu_n, \sigma, \bar{\omega}_0, \bar{\rho}_0^3) - U_{\mathrm{eff}}(T, \mu_p, \mu_n, \sigma) \\ &\quad = -\frac{1}{2} m_\omega^2 \left[\omega_{0,0}(\chi)\right]^2 - \frac{1}{2} m_\rho^2 \left[\rho_{0,0}^3(\chi)\right]^2 \\ &\qquad + \sum_{i=n,p} \sum_{r=\pm 1} \int_0^\Lambda dk \, \frac{k^4}{3\pi^2} \cdot \frac{n_{\mathrm{F}}(E_{\mathrm{N}} - r\mu_{i,\mathrm{eff},k}(\chi)) - n_{\mathrm{F}}(E_{\mathrm{N}} - r\mu_{i,\mathrm{eff},0}(\chi))}{E_{\mathrm{N}}} \\ &\quad = -\frac{1}{2} m_\omega^2 \left[\omega_{0,0}(\chi)\right]^2 \\ &\qquad + \sum_{r=\pm 1} \int_0^\Lambda dk \, \frac{k^4}{3\pi^2 E_{\mathrm{N}}} \int_{\omega_{0,0}(\chi)}^{\omega_{0,k}(\chi)} dy \, \frac{\partial}{\partial y} \Big[n_{\mathrm{F}}(E_{\mathrm{N}} - r(\mu_p - g_\omega y - g_\rho \rho_{0,k}^3(\chi))) \\ &\qquad\qquad + n_{\mathrm{F}}(E_{\mathrm{N}} - r(\mu_n - g_\omega y + g_\rho \rho_{0,k}^3(\chi))) \Big] \\ &\qquad - \frac{1}{2} m_\rho^2 \left[\rho_{0,0}^3(\chi)\right]^2 \\ &\qquad + \sum_{r=\pm 1} \int_0^\Lambda dk \, \frac{k^4}{3\pi^2 E_{\mathrm{N}}} \int_{\rho_{0,0}^3(\chi)}^{\rho_{0,k}^3(\chi)} dz \, \frac{\partial}{\partial z} \Big[n_{\mathrm{F}}(E_{\mathrm{N}} - r(\mu_p - g_\omega \omega_{0,k}(\chi) - g_\rho z)) \\ &\qquad\qquad - n_{\mathrm{F}}(E_{\mathrm{N}} - r(\mu_n - g_\omega \omega_{0,k}(\chi) + g_\rho z)) \Big] . \end{aligned} \tag{4.139}$$

The first two lines of the last expression cancel, as do the last two lines. We will show this explicitly for the first two lines, the second cancellation is analogous. The two integrals can be interchanged as shown in Fig. 8. Let $\omega_0(k)^{-1}$ be the inverse function with respect

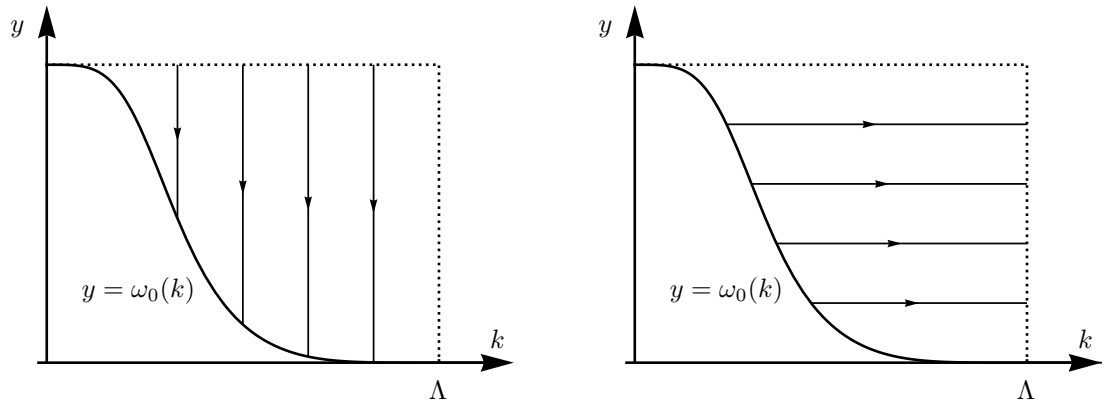

(a) Integrate along the arrowed line for each ω_0, then over ω_0.

(b) Integrate along the arrowed line for each k, then over k.

Figure 8: The order of the integrals is changed.

to k, such that $\omega_0^{-1}(y) = k$ (where we suppress the χ dependence for simplicity). With the help of Eq. (4.120) the first two lines can be written as

$$\begin{aligned}
&-\frac{1}{2}m_\omega^2\left[\omega_{0,0}(\chi)\right]^2 \\
&+\int_{\omega_{0,0}(\chi)}^{\omega_{0,\Lambda}(\chi)\equiv 0} dy \sum_{r=\pm 1}\int_{\omega_0^{-1}(y)=k}^{\Lambda} dk\, \frac{k^4}{3\pi^2 E_{\mathrm{N}}}\frac{\partial}{\partial y}\Big[n_{\mathrm{F}}\big(E_{\mathrm{N}} - r(\mu_p - g_\omega y - g_\rho \rho_{0,k}^3(\chi))\big) \\
&\qquad\qquad + n_{\mathrm{F}}\big(E_{\mathrm{N}} - r(\mu_n - g_\omega y + g_\rho \rho_{0,k}^3(\chi))\big)\Big] \\
&= -\frac{1}{2}m_\omega^2\left[\omega_{0,0}(\chi)\right]^2 - m_\omega^2\int_{\omega_{0,0}(\chi)}^{0} dy\; y = 0\,.
\end{aligned} \tag{4.140}$$

We have seen that the mass terms that explicitly appear in the mean-field potential are contained in the flow-equation in a intricate way through the k-dependent effective chemical potentials.

This concludes the proof of the equivalence between mean-field calculations and the RG flow without bosonic fluctuations.

4.4 SYMMETRIC NUCLEAR MATTER

We now include the bosonic loops in our calculation. The flow equations at the liquid-gas transition are subtracted. At vanishing temperature, the whole range of chemical potentials $\mu < \mu_c$ corresponds to a single physical state, namely the vacuum. The flow equation in this case is given by

$$\frac{\partial \bar{U}_k(\mu,\chi)}{\partial k} = \frac{2k^4}{3\pi^2}\frac{\theta\big(\mu - g_\omega\omega_{0,k} - \sqrt{k^2+2g^2\chi}\big) - \theta\big(\mu_c - \sqrt{k^2+2g^2\chi}\big)}{\sqrt{k^2+2g^2\chi}} + \text{bos. part}, \tag{4.141}$$

where the bosonic terms are not written down explicitly. The main contribution to the flow equation comes from the nucleonic term. For $\mu < \mu_c$ and for σ close to f_π, the vector field $\omega_{0,k}$ vanishes, and $\sqrt{2g^2\chi} \simeq m_{\mathrm{N}} = 939\,\mathrm{MeV}$. Therefore, for $\mu < \mu_c$ the theta functions both vanish and there is no nucleonic contribution to the flow equation. The

$a_3\,(\mathrm{MeV}^{-2})$	$a_4\,(\mathrm{MeV}^{-4})$	$m_\sigma\,(\mathrm{MeV})$	g_s	$G_\omega\,(\mathrm{fm}^2)$	$G_\rho\,(\mathrm{fm}^2)$
$5.55 \cdot 10^{-3}$	$8.38 \cdot 10^{-5}$	770	10	4.04	1.12

Table 3: List of all FRG parameters.

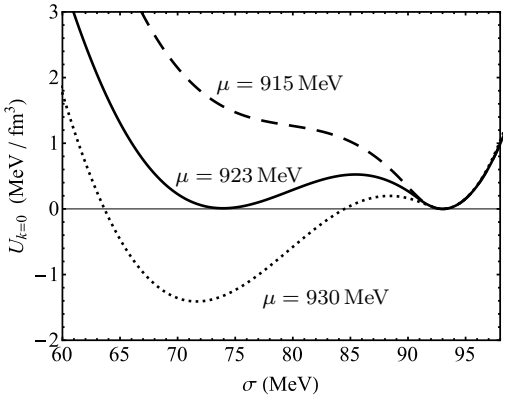

Figure 9: The σ-dependent effective potential for vanishing temperature at three different baryon chemical potentials.

solution of the remaining flow equation is $\bar{U}_k(\mu, \chi) = 0$ for σ close to f_π. The properties of the effective potential at its minimum – its value and the values of its derivatives – are not affected by the renormalization group equations. The pion mass and the pion decay constant are not altered and stay at their vacuum values. As a consequence, the vacuum constraints will not change.

In contrast, the fluctuations do influence the dependence of the potential on temperature and chemical potential. The higher powers in χ and the vector couplings have to be re-adjusted in order to reproduce a correct saturation density, surface tension, and symmetry energy. The new parameters are given in Table 3.

The full flow equations can now be solved with the grid method. For a given temperature and chemical potentials μ_p and μ_n, the effective potential (4.98) at $k = 0$ is computed as a function of σ. First we treat symmetric nuclear matter, where the chemical potentials are equal, i.e., $\mu \equiv \mu_p = \mu_n$. Most of the results of the following sections have been published in Refs. [205, 206].

4.4.1 *Liquid-gas transition*

In Fig. 9, the potential at $T = 0$ is shown for three different chemical potentials. Because the fluctuations are included around the liquid-gas transition as discussed in Section 4.3.3, the effective potential at $\mu = \mu_c$ looks similar to the mean-field potential from Fig. 6. The slight differences originate from the re-adjustment of the parameters. At smaller chemical potentials, the minimum of the effective potential is located at $\sigma = f_\pi$, and the system is still in its vacuum ground state. Therefore, in a T–μ phase-diagram, the μ-axis at $T = 0$ up to $\mu = \mu_c$ corresponds to a single physical state. At $\mu = \mu_c$, the two minima of the effective potential are degenerate. Vacuum and nuclear matter both have vanishing pressure and can coexist. The Fermi sea is filled and the system changes. Drops of nuclear liquid form and the density increases up to saturation density. The whole coexistence region up to saturation density corresponds to a single chemical potential, μ_c, and can

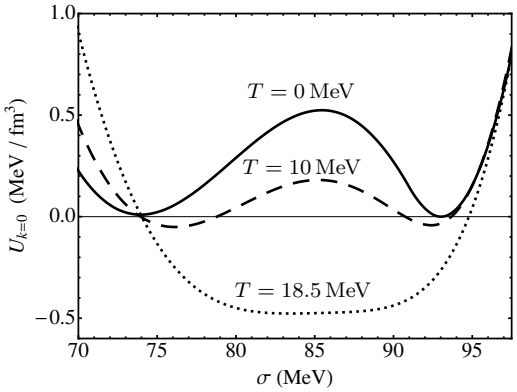

Figure 10: The σ-dependent effective potential at the liquid-gas phase transition for three different temperatures.

therefore not be resolved in our framework. Finally, for larger chemical potentials the system is characterized by a smaller expectation of the σ-field and the density increases.

Next, we study finite temperatures. In Fig. 10, we show the potential for three different temperatures at the first-order transition. The chemical potential is adjusted such that the two minima are degenerate. One observes that the minima move closer to each other as the temperature increases. At the **critical temperature**,

$$T_c = 18.3\,\text{MeV}, \tag{4.142}$$

and for $\mu = 913\,\text{MeV}$, the minima are no longer separated, and we have reached the second-order critical endpoint of the liquid-gas phase transition. For higher temperatures, there is a unique minimum.

In Fig. 11, the liquid-gas phase transition is shown in a T–μ phase diagram. The left-bending of the curve can be understood from a Clausius–Clapeyron type relation. Along the first-order line, the minima (corresponding to the gas and the liquid phase) must be degenerate. Therefore, the total differentials of the effective potentials agree for both phases, i.e.,

$$\frac{\partial U_{\text{liquid}}}{\partial \mu} d\mu + \frac{\partial U_{\text{liquid}}}{\partial T} dT = \frac{\partial U_{\text{gas}}}{\partial \mu} d\mu + \frac{\partial U_{\text{gas}}}{\partial T} dT\,. \tag{4.143}$$

The slope of the transition line then can be expressed as the ratio of differences between baryon number densitites, $n_{\text{liquid}} - n_{\text{gas}}$, and entropy densities, $s_{\text{liquid}} - s_{\text{gas}}$, i.e.,

$$\frac{dT}{d\mu} = -\frac{n_{\text{liquid}} - n_{\text{gas}}}{s_{\text{liquid}} - s_{\text{gas}}}\,. \tag{4.144}$$

In the limit of vanishing temperatures, the denominator vanishes as a consequence of Nernst's theorem. The slope diverges and the transition line hits the μ-axis at a right angle. For non-zero temperatures, particle-hole excitations around the Fermi surface contribute to the entropy in the liquid phase. The entropy is therefore larger in the liquid phase than in the gas phase. Moreover, the liquid phase is denser than the gas phase and the slope of the transition line is negative, as observed.

For comparison, we show the results obtained from a mean-field analysis [166]. Where necessary, we will in the following distinguish between the **MF-ChNM model** (at the mean-field level) and the **FRG-ChNM model** (with fluctuations included). The critical

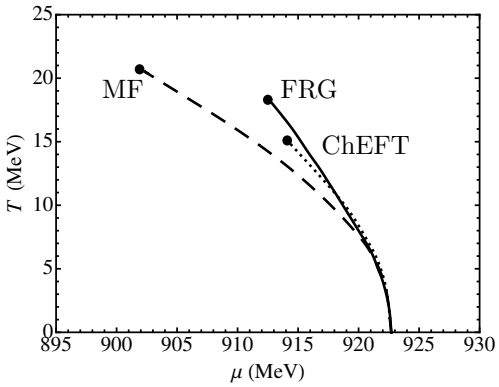

Figure 11: Liquid-gas phase transition. Dashed line: mean-field result of the ChNM model. Solid curve: FRG calculation including bosonic fluctuations. Dotted curve: in-medium chiral effective field theory calculation of Refs. [12, 13].

endpoint is situated at a larger temperature $T_c = 20.7\,\mathrm{MeV}$ and a smaller chemical potential $\mu = 901\,\mathrm{MeV}$. Fluctuations beyond the mean-field approximation bend the phase-transition boundary towards higher chemical potentials. The curvature of the boundary line is in good agreement with the ChEFT results of Refs. [12, 13]. These calculations were performed in a perturbative framework up to three-loop order. The free energy was computed including all possible one- and two-pion exchange processes in the medium. Moreover, three-body forces and Δ-isobar excitations were included. In our framework, pion and nucleon loops are resummed in a non-perturbative way. In addition, part of the effects that are treated explicitly in ChEFT are relegated to the parametrization of the effective potential. Nevertheless, the results are consistent. The critical temperature in our model is higher compared to the ChEFT result, $T_c = 15.1\,\mathrm{MeV}$ [12,13]. Our temperature is in excellent agreement with empirical data. The critical temperature can be deduced from nuclear reactions and multifragmentation experiments, which yield a critical temperature of $T_c = 17.9(4)\,\mathrm{MeV}$ [207, 208]. The surface tension of the nuclear droplets is related to the potential well between the two minima (see Eq. (4.75)). For increasing temperature, the surface tension therefore decreases, until it vanishes at the critical point, and liquid and gas phases are no longer separated. It is therefore easier to break the droplets at higher temperatures. Experimentally, one observes a larger amount of intermediate-mass fragments (multifragmentation). Likewise, the barrier for nuclear fission is smaller, and from a measurement of the fissility one can estimate the critical temperature. Our model nicely reproduces the temperature deduced in this way. It should be noted that in our idealized model surface effects as well as Coulomb repulsion are not taken into account. In order to make contact with experiments, the effects of light clusters have to be included at low densities. A study in the framework of relativistic mean field and microscopic quantum statistical models showed a moderate influence on the position of the critical endpoint [209].

In Fig. 12 we show the coexistence regions of the liquid-gas phase transition in a temperature-density plane. Again, ChEFT and FRG agree nicely at small temperatures, once the fluctuations are taken into account. Also the critical density comes out the same, at about

$$n = 0.33\, n_0 = 0.053\,\mathrm{fm}^{-3}. \tag{4.145}$$

This value for the critical density is again in excellent agreement with the experimental result of $n = 0.06(1)\,\mathrm{fm}^{-3}$ [207, 208].

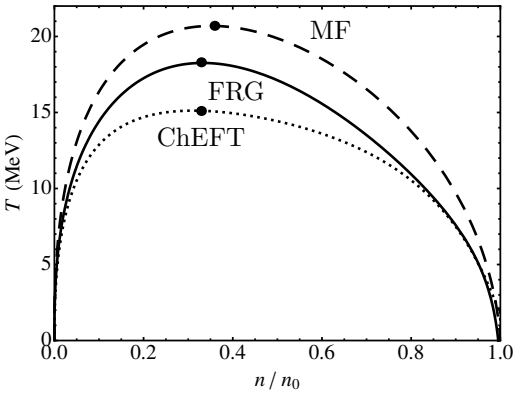

Figure 12: Coexistence regions. Solid line: FRG-ChNM model. Dashed: MF-ChNM model. Dotted: ChEFT [12,13]. The dots indicate the respective critical endpoints.

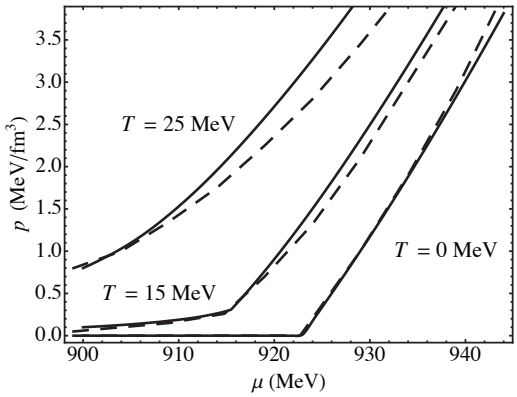

Figure 13: Pressure as a function of baryon chemical potential for three different temperatures. Solid line: FRG-ChNM model. Dashed: ChEFT [12,13].

The grand-canonical potential is obtained by evaluating the potential at its minimum, and the pressure as a function of the chemical potential can then be computed. The pressure obtained in our model is compared with the ChEFT results in Fig. 13. Because the effective potential was adjusted to reproduce the properties of nuclear matter at $\mu = \mu_c$ and vanishing temperature, the results agree very well in both approaches close to this point. Since both models are consistent with the empirical compressibility of nuclear matter, they also agree on the slope of the pressure, which is related to the compressibility. The equations of state are also consistent for larger chemical potentials. At higher temperatures, slight deviations appear, largely because the two models predict a different critical temperature.

The energy per particle is shown as a function of density in Fig. 14. For comparison, we show two equations of state obtained in different ways. The first one is the Akmal-Pandharipande-Ravenhall EoS [210], which is based on the phenomenological Argonne v_{18} two-nucleon interactions together with the Urbana IX three-nucleon interactions. Relativistic boost corrections were included in the calculation. The second equation of state was obtained in an auxiliary-field diffusion Monte-Carlo (AFDMC) framework. The FRG-ChNM model is in remarkable agreement with both equations of state up to densities as large as three times nuclear saturation density.

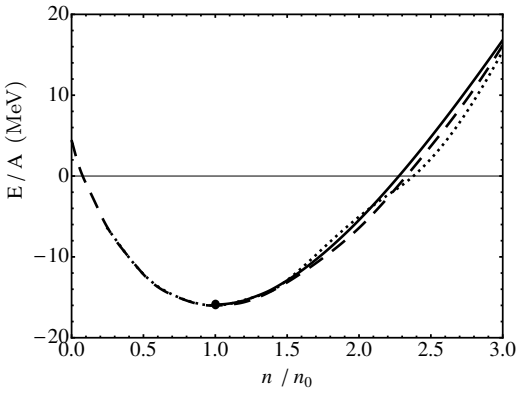

Figure 14: The energy per particle of symmetric nuclear matter. Solid line: FRG-ChNM model. Dotted: Akmal-Pandharipande-Ravenhall EoS [210]. Dashed: AFDMC [211].

4.4.2 *Chiral restoration*

The FRG-ChNM model nicely reproduces the liquid-gas transition and is also in agreement with realistic equations of state up to at least three times nuclear saturation density. Therefore, the model should be applicable at least up to about 100 MeV temperature and three times nuclear saturation density, which corresponds to a chemical potential of about 1 GeV. The model allows us to search for chiral restoration within this window. As we have seen in Sec. 2.5.2, chiral symmetry is restored in its Wigner-Weyl phase at high temperatures and high densities. Once the chiral symmetry is restored, a description based on hadronic matter is no longer applicable. Quarks and gluons start to play a role as one gets closer to the quark-gluon-plasma phase. All approaches to the QCD phase diagram based on hadronic matter rely on broken chiral symmetry. This is particularly the case for chiral perturbation theory, which takes chiral symmetry as its starting point; but also the ChNM model is restricted to the Nambu-Goldstone phase. The breaking of chiral symmetry is indicated by an order parameter, for instance the chiral condensate. As shown in Ref. [212], the chiral condensate can be computed in a systematic way from the Hellmann-Feynman theorem,

$$\frac{dE(\lambda)}{d\lambda} = \left\langle \phi(\lambda) \,\middle|\, \frac{dH(\lambda)}{d\lambda} \,\middle|\, \phi(\lambda) \right\rangle , \tag{4.146}$$

where E is the energy, H the Hamiltonian, λ some parameter of the theory, and $\phi(\lambda)$ a given normalized state. Let us write the Hamiltonian density of two-flavor QCD as

$$\mathcal{H} = \mathcal{H}_0 + m_u \bar{u}u + m_d \bar{d}d = \mathcal{H}_0 + m_q \bar{\psi}\psi + \frac{1}{2}\delta m_q (\bar{d}d - \bar{u}u), \tag{4.147}$$

with $\mathcal{H}_0$ the Hamiltonian in the chiral limit and

$$\bar{\psi}\psi = \bar{u}u + \bar{d}d\,, \qquad m_q = \frac{1}{2}(m_u + m_d)\,, \qquad \delta m_q = m_d - m_u\,. \tag{4.148}$$

The correction proportional to δm_q is small and can be ignored to leading order in the following. The Hellmann-Feynman theorem is now applied to $H = \int d^3x\, \mathcal{H}$ and $\lambda = m_q$,

$$\frac{d}{dm_q}\left\langle \phi(m_q) \right| \int d^3x\, \mathcal{H} \left| \phi(m_q) \right\rangle = \left\langle \phi(m_q) \right| \int d^3x\, \bar{\psi}(x)\, \psi(x) \left| \phi(m_q) \right\rangle . \tag{4.149}$$

The equations for nuclear matter at density n and for the vacuum are substracted, i.e., for $|\phi(m_q)\rangle = |n\rangle$ and $|\phi(m_q)\rangle = |0\rangle$, respectively. The integral $\int d^3x$ factors out as a consequence of homogeneity. Let us define $\langle\bar{\psi}\psi\rangle_n = \langle n|\bar{\psi}\psi|n\rangle$. Furthermore, let ϵ denote the energy density of nuclear matter at density n (normalized to the vacuum). Then one gets

$$\frac{d\epsilon}{dm_q} = \langle\bar{\psi}\psi\rangle_n - \langle\bar{\psi}\psi\rangle_0 \,. \tag{4.150}$$

The energy density of nuclear matter is in leading order in density n determined by the mass of the nuclei, i.e.,

$$\epsilon(n) = m_{\mathrm{N}}\, n \,. \tag{4.151}$$

Higher corrections from the kinetic energy of the nucleon as well as nucleon interactions can be neglected for low densities. In fact, the binding energy of nuclear matter is small compared to the nucleon mass. We get

$$n\,\frac{dm_{\mathrm{N}}}{dm_q} = \langle\bar{\psi}\psi\rangle_n - \langle\bar{\psi}\psi\rangle_0 \,. \tag{4.152}$$

The left-hand side can be evaluated further in terms of the **pion-nucleon sigma term**, σ_{N}. Let $|N\rangle$ be the one-nucleon state. The pion-nucleon sigma term can then be defined as [213]

$$\sigma_{\mathrm{N}} = m_q \int d^3x \Big(\langle N|\bar{\psi}\psi|N\rangle - \langle 0|\bar{\psi}\psi|0\rangle \Big) \,. \tag{4.153}$$

In this formulation, it can be interpreted as a measure of how the chiral condensate is distorted around the nucleon. From the Hellmann-Feynman theorem, the pion-nucleon sigma term is related to the quark-dependence of the corresponding energy, which for a nucleon at rest is the nucleon mass, so

$$\sigma_{\mathrm{N}} = m_q \frac{dm_{\mathrm{N}}}{dm_q} \,. \tag{4.154}$$

After integrating both sides from 0 to m_q, the pion-nucleon sigma term gets a new interpretation. It is the difference between the nucleon mass at physical quark masses, m_{N}, and the nucleon mass in the chiral limit, $m_{\mathrm{N}}^{(\chi)}$, i.e.,

$$\sigma_{\mathrm{N}} = m_{\mathrm{N}} - m_{\mathrm{N}}^{(\chi)} \,. \tag{4.155}$$

The value of the pion-nucleon sigma term is not extremely well determined. It can be obtained by an extrapolation of πN-scattering to the unphysical Cheng-Dashen point with $s = u = m_{\mathrm{N}}^2$ and $u = 2m_{\mathrm{N}}^2$. Results are typically of the order $\sigma_{\mathrm{N}} = 44\,\mathrm{MeV}$ (see, e.g., [214]). Similar results are obtained on the lattice, where the quark-mass can be varied directly, see for instance [215].

A combination of Eq. (4.152) and (4.154) gives us the leading order behavior of the chiral condensate as a function of density,

$$\frac{\langle\bar{\psi}\psi\rangle_n}{\langle\bar{\psi}\psi\rangle_0} = 1 + \frac{\sigma_{\mathrm{N}}}{m_q\,\langle\bar{\psi}\psi\rangle_0}\, n \,. \tag{4.156}$$

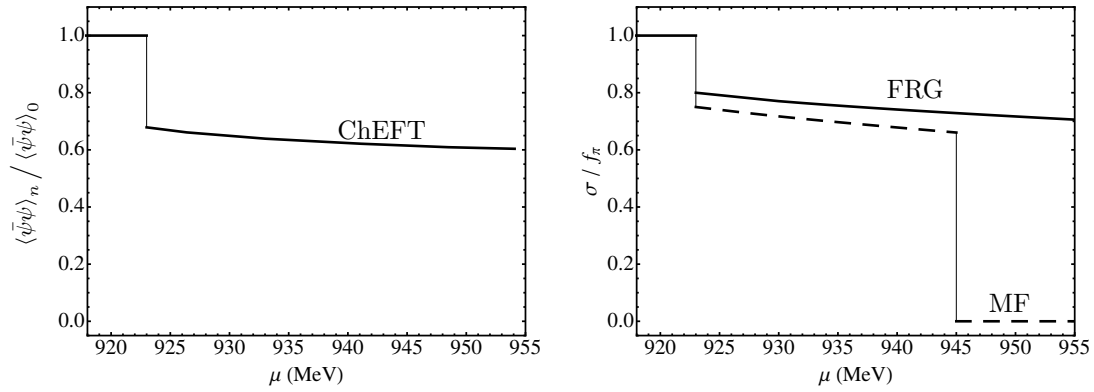

Figure 15: Symmetric nuclear matter at $T = 0$. Left: normalized chiral condensate computed in ChEFT [13]. Right: chiral order parameter in the MF-ChNM model (dashed) and the FRG-ChNM model (solid line).

The latter term can be expressed in terms of the pion mass and the pion decay constant using the Gell-Mann–Oakes–Renner relation (2.42):

$$\frac{\langle\bar{\psi}\psi\rangle_n}{\langle\bar{\psi}\psi\rangle_0} = 1 - \frac{n}{n_\chi}\,, \quad n_\chi = \frac{m_\pi^2 f_\pi^2}{\sigma_\mathrm{N}}\,. \tag{4.157}$$

To leading order, the chiral condensate vanishes at $n_\chi \simeq 3\,n_0$ and chiral symmetry is restored. Higher order corrections can be included by going beyond the linear-density approximation (4.151) for the energy density ϵ. Then, using the chain rule, the chiral condensate is

$$\frac{\langle\bar{\psi}\psi\rangle_n}{\langle\bar{\psi}\psi\rangle_0} = 1 + \frac{1}{\langle\bar{\psi}\psi\rangle_0}\frac{dm_\mathrm{N}}{dm_q}\frac{\partial\epsilon}{\partial m_\mathrm{N}} + \frac{1}{\langle\bar{\psi}\psi\rangle_0}\frac{dm_\pi}{dm_q}\frac{\partial\epsilon}{\partial m_\pi} + \dots\,. \tag{4.158}$$

The last term on the right-hand side can be evaluated from the Gell-Mann–Oakes-Renner relation, $\frac{dm_\pi}{dm_q} = \frac{m_\pi}{2m_q}$, such that

$$\frac{\langle\bar{\psi}\psi\rangle_n}{\langle\bar{\psi}\psi\rangle_0} = 1 - \frac{1}{n_\chi}\left(\frac{\partial\epsilon}{\partial m_\mathrm{N}} + \frac{m_\pi}{2\sigma_\mathrm{N}}\frac{\partial\epsilon}{\partial m_\pi}\right) + \dots\,. \tag{4.159}$$

The right-hand side can then be evaluated, for instance, in the framework of in-medium chiral perturbation theory [10–13]. The free-energy density is calculated up to three-loop order in a perturbative way. All one-pion and two-pion exchange processes in the medium are included. Moreover three-body forces and the Δ-isobar are included explicitly. An important finding is that the condensate decreases much slower as compared to the leading linear term. To explain the stabilization of the chiral condensate, a crucial role is played by two-pion exchange processes with the exchange of a virtual Δ-isobar.

In the ChNM model, the expectation value of the σ-field plays the role of an order parameter, as it vanishes in the chirally-restored phase. On the right-hand side of Fig. 15, the chiral order parameter (normalized to its vacuum expectation value) at vanishing temperature is shown as a function of baryon chemical potential. The first-order liquid-gas transition is also visible in the chiral order parameter, which shows a discontinuity at $\mu = \mu_c$. However, the chiral order parameter is still non-vanishing and chiral symmetry is not yet restored. In the mean-field approximation, a first-order transition to the chirally symmetric Wigner-Weyl phase already sets in at $\mu = 945\,\mathrm{MeV}$, corresponding to a baryon

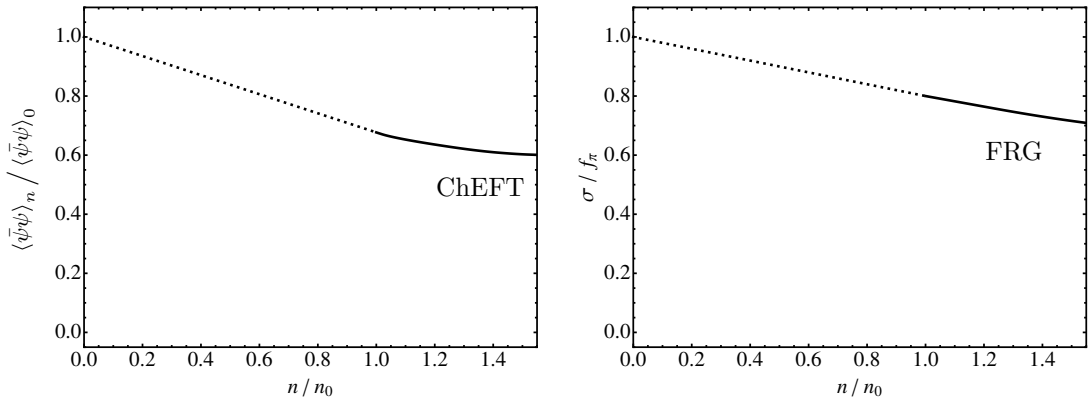

Figure 16: Left: normalized chiral condensate at $T = 0$ computed in ChEFT [13]. Right: chiral order parameter in the FRG-ChNM model (solid line). The dotted lines stem from a Maxwell construction.

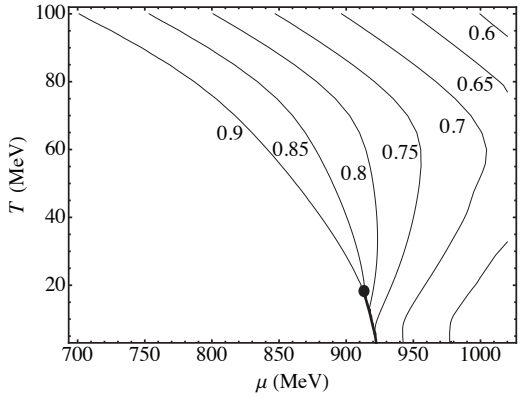

Figure 17: Contour plots of the chiral order parameter σ/f_π. Within the region of applicability ($\mu \lesssim 1\,\text{GeV}$, $T \lesssim 100\,\text{MeV}$) of the FRG-ChNM model, the order parameter is nonzero and chiral symmetry is not restored.

density of $1.5\,n_0$, which is an unphysical behavior. Once fluctuations are included, the chiral order parameter gets stabilized and decreases slowly up to larger chemical potentials. On the left-hand side, we show for comparison the chiral condensate as computed in ChEFT [13]. We see that both the condensate in ChEFT and the chiral order parameter σ run almost parallel. In both approaches, chiral restoration is postponed to higher densities, once fluctuations are included. Therefore, it is crucial to include fluctuations beyond the mean-field approximation to get a proper physical description at higher densities. Figure 16 shows the chiral condensate as a function of the density. At 2.5 times nuclear saturation density the chiral condensate has dropped only to about two thirds of its vacuum value. Of course, one has to keep in mind that the effective potential was fitted to the properties of nuclear matter around the liquid-gas transition. In particular, the χ-dependence was expanded around the vacuum value $\chi_0 = \frac{1}{2} f_\pi^2$. If the expectation value of σ becomes too small, the expansion breaks down and the model is no longer applicable. Consequently, the chiral restoration itself cannot be treated within the ChNM model. In contrast, the power of the ChNM model is to exclude a possible restoration to the Wigner-Weyl phase for a certain physical range.

Figure 17 shows contour lines of the normalized chiral order parameter σ/f_π at finite temperature and chemical potential. As long as $\mu \lesssim 1\,\text{GeV}$ and $T \lesssim 100\,\text{MeV}$, the chiral

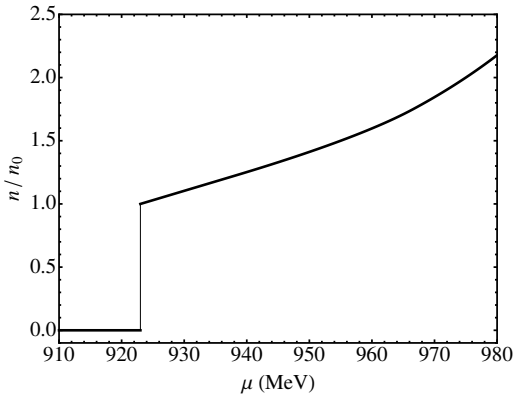

Figure 18: The density as an order parameter of the liquid-gas transition. It shows a discontinuity at μ_c.

order parameter stays above sixty percent of its vacuum value and the model is applicable. Chiral symmetry is broken for $T \lesssim 100\,\mathrm{MeV}$ and densities below at least twice the nuclear saturation density. We can now return to the original question about the relation between chiral restoration and chemical freeze-out. The chiral symmetry line lies well above the chemical freeze-out line, as in scenario B of Fig. 2, in agreement with the lattice findings. Scenario A is strongly disfavored by our calculations and the entanglement between chemical freeze-out and chiral restoration is realized only at small chemical potentials, whereas at larger chemical potentials, there is a clear separation.

4.4.3 *Fluctuations*

A mean-field approximation breaks down in the vicinity of the critical endpoint of a first-order phase transition. Fluctuations play an important role and cannot be ignored. As already discussed in Ref. [166], a detailed study of the critical endpoint of the liquid-gas transition can only be done once fluctuations are included. In the framework of the functional renormalization group, pionic fluctuations are treated in a systematic way. It is important to estimate the size of these fluctuations. Phase transitions are associated with a corresponding order parameter. In the case of the liquid-gas phase transition, the order parameter is the density, as can be seen in Fig. 18. Below μ_c the system is in the vacuum and the density vanishes, and at $\mu = \mu_c$, the density jumps to nuclear saturation density.

The magnitude of the fluctuations can be estimated from the **baryon-number susceptibility**,

$$\chi_n(T,\mu) = -\frac{\partial^2 U}{\partial \mu^2} = \frac{\partial n}{\partial \mu}\,, \tag{4.160}$$

associated with the baryon number density. In Fig. 19, plateau lines of constant χ_n are shown, both in the mean-field approximation and with fluctuations included with the functional renormalization group. The susceptibility diverges at the critical endpoint of the liquid-gas transition. In the mean-field approximation, the region where the susceptibility is large turns out to be relatively narrow, but long in extent. It is elongated along an extrapolation of the first-order transition line down to smaller chemical potentials and higher temperatures. In the FRG treatment, the region where the susceptibility is large and fluctuations are important is centered more around the critical endpoint. The region is broader but does not extend to small chemical potentials.

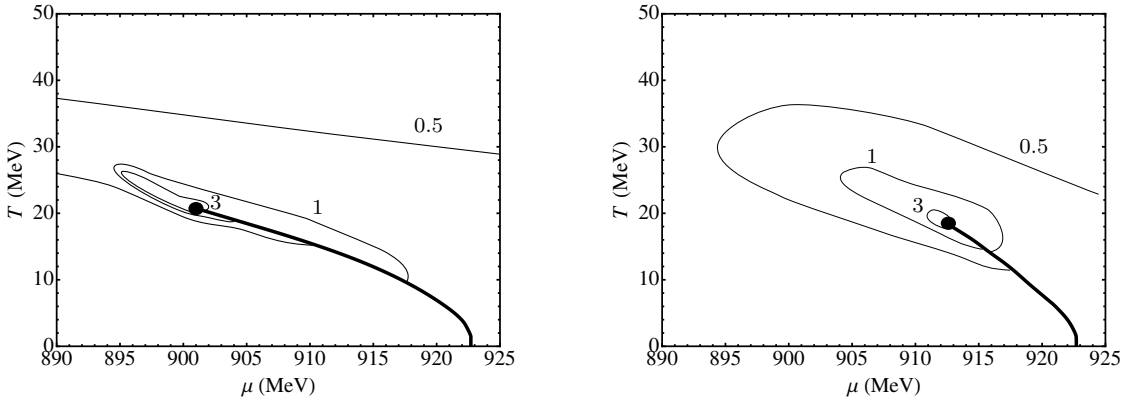

Figure 19: Contour plots of the baryon number susceptibility, $\chi_n = \frac{\partial n}{\partial \mu}$, in units of fm^{-2}. Left: mean-field, right: FRG-ChNM.

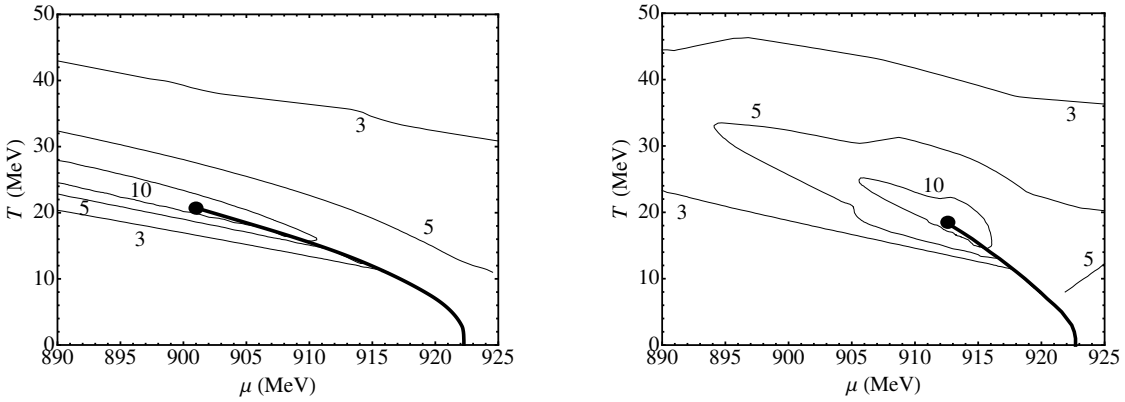

Figure 20: Contour plots of the normalized chiral susceptibility, $\chi_\sigma\, m^2_{\sigma,\mathrm{vac}}$. Left: mean-field, right: FRG-ChNM.

We have seen that the liquid-gas transition leaves its traces also in the order parameter of the chiral transition, namely the expectation value of σ. The corresponding **chiral susceptibility** is the inverse square of the σ-mass,

$$\chi_\sigma = \frac{1}{m_\sigma^2}\,. \tag{4.161}$$

Because the mass of the σ-boson is different in the mean-field approximation and in the FRG calculation, we multiply the chiral susceptibility with the respective square of the σ-mass in vacuum, $\chi_\sigma\, m^2_{\sigma,\mathrm{vac}}$. A comparison of these quantities is shown in Fig. 20. Again, a similar behavior is found as for the baryon number susceptibilities. A long but narrow region in the mean-field approximation turns into a broader but more centered region, once fluctuations are included.

A corresponding calculation was performed in a quark-meson model to study the critical region around the chiral critical endpoint (present in this model) [146]. The same conclusions were drawn in this study. Similar computations were also performed in the Polyakov-loop extended quark-meson (PQM) model [152, 201].

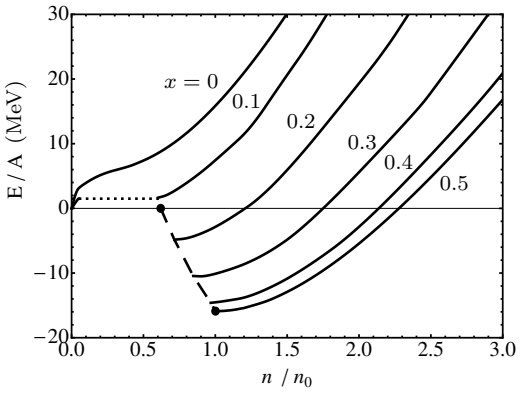

Figure 21: The equation of state for different proton fractions x at vanishing temperature. The dashed curve denotes the absolute minimum of the energy per particle. The dotted line results from a Maxwell construction.

4.5 ASYMMETRIC NUCLEAR MATTER

From now on, we allow the proton and neutron chemical potentials to be different. We can then study asymmetric nuclear matter with different proton density, n_p, and neutron density, n_n. Parts of the following sections have been published in Ref. [216].

4.5.1 *Phase coexistence and equation of state*

A measure for the asymmetry is the proton fraction

$$x = \frac{Z}{A} = \frac{n_p}{n_p + n_n} \,. \tag{4.162}$$

In Fig. 14 we have shown the energy per particle for symmetric nuclear matter, i.e., for $x = 0.5$. We now want to study how the equation of state changes as the proton fraction decreases. Figure 21 depicts the energy per particle for different proton fractions, ranging from symmetric nuclear matter ($x = 0.5$) to pure neutron matter ($x = 0$). For isospin-symmetric nuclear matter, the global minimum is located at nuclear saturation density, and the energy per particle equals the binding energy of $-16\,\mathrm{MeV}$. If we follow the dashed line, we see that the minimal energy per particle increases as x decreases, until it vanishes for $x \simeq 0.11$. For smaller values of x, the global minimum appears at vanishing density. The system is no longer self-bound and loses its saturation property. There appears however still a remnant of the first-order transition. In Fig. 22, the coexistence regions are shown for different proton fractions. For $x < 0.11$ there still is a coexistence region, but it starts already at a non-vanishing density, as can be seen for instance for $x = 0.1$. A first-order transition with a characteristic jump in density remains. Strictly speaking, the density is no longer an order parameter, since it does not vanish in one of the phases. In Fig. 21 the coexistence region for $x = 0.1$ corresponds to the dotted line, which can be obtained from a Maxwell construction. If x decreases even further, the coexistence region shrinks until it vanishes for $x = 0.045$. At this point, the energy per particle has a saddle point. For smaller x, it is a monotonously increasing function of density and the first-order transition disappears completely. As a consequence, the coexistence region is absent. From the coexistence regions one can read off the critical endpoint as a function of x, as indicated by the dotted line.

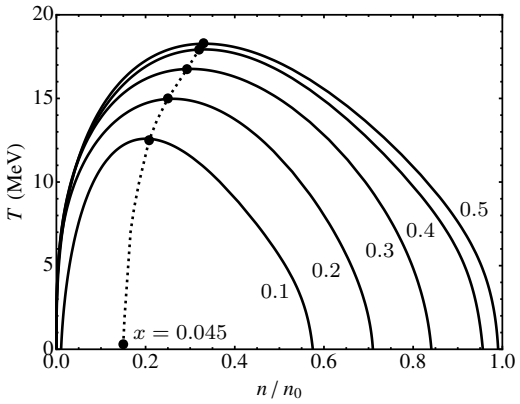

Figure 22: The liquid-gas coexistence regions for different proton fractions x.

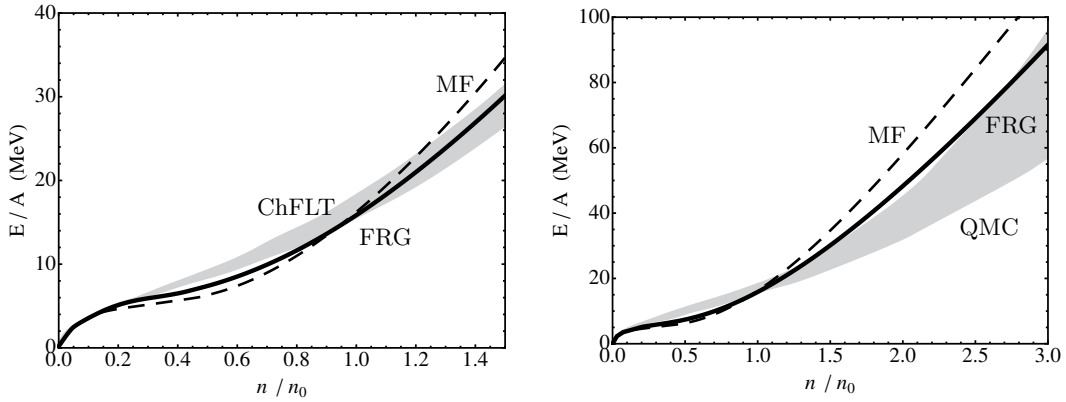

Figure 23: Equation of state. Left: at low densities, FRG (solid line) as compared to mean field (dashed line), and chiral Fermi liquid theory [217] (gray band, ChFLT). Right: at higher densities, FRG (solid line), as compared to mean field (dashed line), and QMC calculations [218] (gray band, with $32.0\,\mathrm{MeV} \leq E_{\mathrm{sym}} \leq 33.7\,\mathrm{MeV}$).

We now study the equation of state of pure neutron matter in more detail. In Fig. 23 we compare our results with a recent quantum Monte Carlo (QMC) study that includes realistic two- and three-nucleon interactions [218], as well as with chiral Fermi liquid theory at lower densities. Relativistic mean-field calculations typically have the problem that the equation of state is too soft at low densities, while it overshoots at higher densities. The same is true for the ChNM model in the mean-field approximation (dashed line). Once pionic fluctuations are incorporated (solid line), the equation of state improves considerably. Both at low and higher densities a good agreement with realistic models is achieved. The agreement is remarkable, given that there is only one additional adjustable parameter, namely the coupling strength of the ρ-boson, G_ρ. The coupling was fitted to reproduce the symmetry energy $E_{\mathrm{sym}} = 32\,\mathrm{MeV}$. There is some empirical uncertainty in the size of the symmetry energy (see Eq. (2.57)). In Fig. 24 we vary the coupling constant in the range $0.91\,\mathrm{fm}^2 \leq G_\rho \leq 1.46\,\mathrm{fm}^2$. The corresponding symmetry energies then lie within $29\,\mathrm{MeV} \leq E_{\mathrm{sym}} \leq 33\,\mathrm{MeV}$. A number of realistic equations of state are shown for comparison. The Akmal-Pandharipande-Ravenhall equation of state [210] was already discussed above for symmetric nuclear matter. Quantum Monte Carlo studies have been performed, based on both realistic potentials [211] and chiral potentials [219]. We also show results from chiral effective field theory [220]. Here, the equation of state was however fitted to the APR equation of state at medium and high densities. The FRG-ChNM model is found

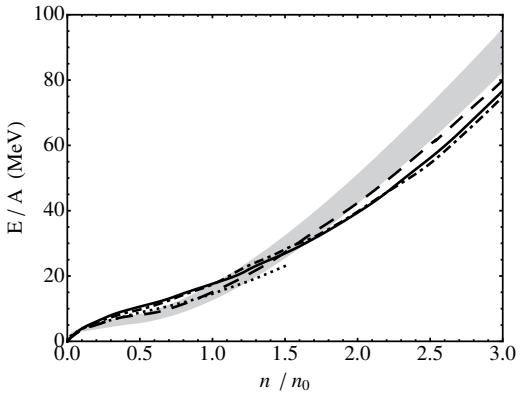

Figure 24: The equation of state for pure neutron matter. The gray band are our results with $29\,\mathrm{MeV} \leq E_{\mathrm{sym}} \leq 33\,\mathrm{MeV}$. For comparison, we show predictions from ChEFT (solid line, [220]), QMC based on realistic potentials (dashed, [211]), QMC based on chiral potentials (dotted, [219]) as well as the Akmal-Pandharipande-Ravenhall EoS (dashed-dotted, [210]).

to be in excellent agreement with all realistic equations of state, up to at least three times nuclear saturation density.

Another parameter which is empirically relatively well determined is the L-parameter related to the slope of the symmetry energy defined in Eq. (2.56). From numerous data, L is restricted to the range $40\,\mathrm{MeV} \leq L \leq 62\,\mathrm{MeV}$, see Eq. (2.57). For a symmetry energy of $E_{\mathrm{sym}} = 32\,\mathrm{MeV}$, we find in the FRG-ChNM model that

$$L = 66.3\,\mathrm{MeV}\,. \tag{4.163}$$

As can be seen also from the equation of state, the slope at nuclear saturation density is slightly too large compared to realistic equation of state. Nevertheless, the L-parameter is in reasonable consistence with the empirical constraints.

4.5.2 *In-medium pion mass*

Almost twenty years ago, extremely narrow and deeply-bound pionic atoms have been observed at the GSI [222]. Such states had been predicted earlier on the basis of pion-nucleus optical potentials [223]. The existence of these bound-states is a consequence of an intricate interplay between Coulomb attraction and s-wave repulsion. The pion-nucleus optical potential has been studied in chiral effective field theory and it was found that in addition to the linear-density approximation, an important role is played by a double-scattering process in the nuclear medium [224]. From the optical potential, one can deduce the effective in-medium pion mass. In Fig. 25 we show the effective pion mass as a function of density. On the left-hand side, the effective-pion mass in symmetric nuclear matter within the FRG-ChNM model is plotted[10]. For comparison, we show the result from the leading-order in density, as well as a recent chiral effective field-theory computation up to next-to-leading order [221]. At nuclear saturation density, the effective pion-mass is about ten percent larger as compared to the vacuum.

In pure neutron matter, the first-order transition is absent, and the pion mass is a continuous function of μ. The dependence on density turns out to be close to that of symmetric nuclear matter. In fact, in a fuller treatment, the masses of π^-, π^+ and

10 We note that densities below n_0 cannot be resolved, as they correspond to a single chemical potential.

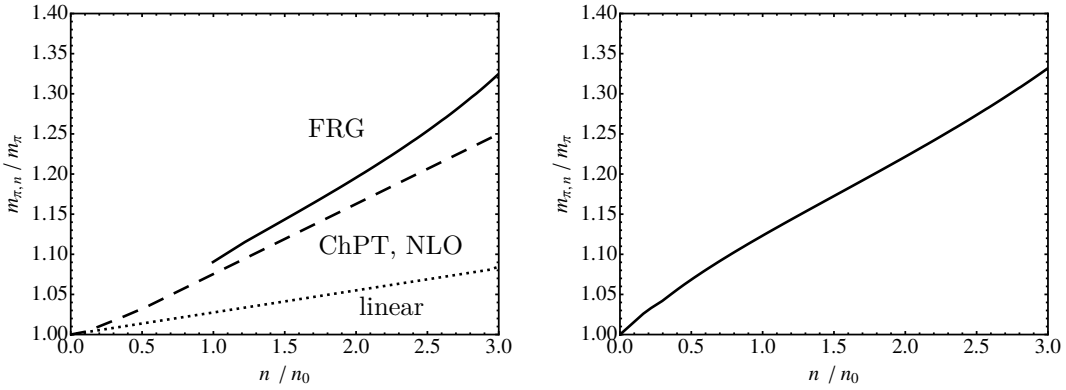

Figure 25: In-medium pion mass. Left: symmetric nuclear matter. The FRG-ChNM (solid line) is compared to ChEFT in leading and next-to-leading order [221]. Right: pure neutron matter.

π^0 behave differently. The main effect is due to the different coupling of the pions to the nucleons in the Weinberg-Tomozawa term. The mass of the π^- increases faster [225], whereas the π^0-mass increases slower, and the π^+-mass is even smaller at saturation density as compared to the vacuum [226]. These effects are not visible in our treatment, since we neglect isospin-breaking effects in the pion sector. However, as the influence on the pion mass is relatively modest, this approximation does not strongly affect the equation of state.

4.5.3 *Chiral restoration*

We extend the discussion of chiral restoration to pure neutron matter. Similarly to our discussion in Sec. 4.4.2, the chiral condensate for pure neutron matter can be computed in chiral effective field theory. In contrast to symmetric nuclear matter, the condensate is not stabilized in neutron matter. In Ref. [14], one-pion exchange, iterated one-pion and irreducible two-pion exchange was considered, including the Δ-isobar excitations, together with corrections from Pauli-blocking up to three-loop order. Still, the condensate drops almost linearly without larger deviations from the leading-order term. At a density of about $3\,n_0$, the condensate is only at twenty percent of its vacuum value. Because of Pauli blocking, certain diagrams that can appear in symmetric matter are absent for pure neutron matter. Therefore, it is possible to even include the effects of four-body forces. A full calculation at next-to-next-to-next-to-leading order ($\mathrm{N^3LO}$) was performed in Ref [15]. It is again found that the condensate decreases only slightly slower than the leading σ_N term of Eq. (4.157). As compared to next-to-next-to-leading order ($\mathrm{N^2LO}$), the decrease is even faster for $\mathrm{N^3LO}$. These results make it questionable whether chiral perturbation theory is still applicable to neutron matter at densities not much beyond nuclear saturation density. However, the uncertainty bands (which originate from the uncertainties of the cutoffs and low-energy constants) of $\mathrm{N^2LO}$ and $\mathrm{N^3LO}$ do not even overlap at densities above nuclear saturation density. This might be an indication that the perturbative expansion did not yet converge and higher orders can become important.

On the left-hand side, we show the chiral condensate computed in ChEFT [14,15] and for comparison also the leading-order linear behavior. On the right-hand side of Fig. 26, the chiral order parameter σ in the ChNM model is depicted, both in the mean-field approximation and with fluctuations included. We see that in the mean-field approximation the

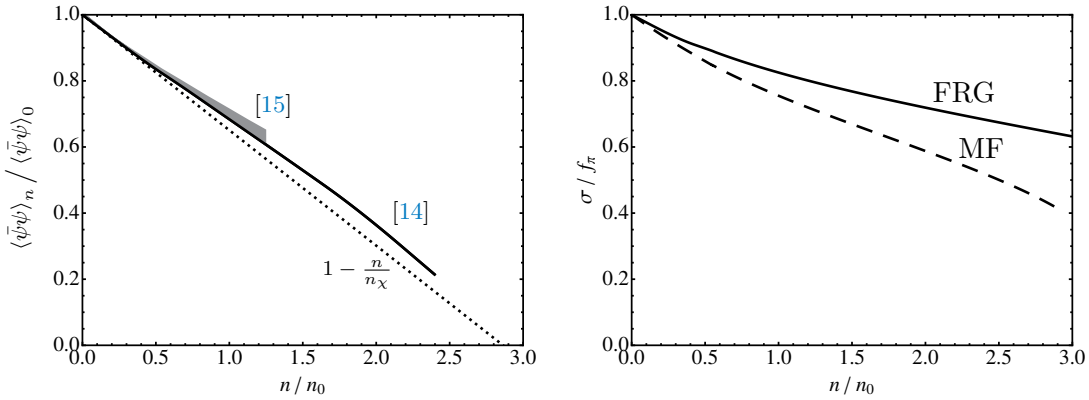

Figure 26: Pure neutron matter at $T = 0$. Left: normalized chiral condensate computed in ChEFT (solid line [14] and gray band [15]) as compared to the linear approximation (dotted line). Right: chiral order parameter in the MF-ChNM model (dashed) and the FRG-ChNM model (solid line).

order parameter decreases also at a relatively strong rate. Once fluctuations are included, the condensate is considerably stabilized. The flow equation generates higher powers in χ. The σ is coupled via a Yukawa-type interaction to the nucleons and if the σ is integrated out, effective many-body forces with three and more nucleons are generated. At increasing energies these many-body forces become more and more important and stabilize the condensate.

It is interesting to push the model to its limits and see when chiral symmetry gets restored. In Fig. 27, σ is shown for high densities. In the mean-field approximation (dashed-dotted curve), a first-order transition sets in at about 2.9 times nuclear saturation density. The effective potential develops a new minimum at a small but yet non-vanishing value of σ. The density also jumps discontinuously to about 3.9 times nuclear saturation density. If the chiral order parameter is plotted as a function of density one must therefore make a Maxwell construction as indicated by the dotted line. Chiral symmetry is only approximately restored, reflecting the explicit symmetry breaking of the original theory. The chiral order parameter decreases further at higher densities. In fact, also at very low densities, a small first-order transition can be observed (not visible in the plot), which is a remnant of the liquid-gas transition. Also for pure neutron matter there is a small coexistence region in the mean-field approximation.

In the FRG calculation, the coexistence region ceases to exist for a proton-fraction of $x = 0.045$, as was shown in Fig. 22. Therefore, no first-order transition exists for pure-neutron matter at low densities. But also the first-order transition to the (approximate) Wigner-Weyl phase at high densities disappears. The order parameter decreases slowly as a continuous function of density. Only at a density of about $7\,n_0$ the expectation value of σ drops significantly.

In our model, a vanishing σ implies also a vanishing in-medium nucleon mass, and in early models an abnormal **Lee–Wick phase** [227] was postulated. Later, one-loop corrections were included in the linear-sigma model, and the parameters were re-adjusted in order to avoid large corrections to three-body forces in contrast to experiments. Once these fluctuations beyond the mean-field approximation are included, it was found that the phase transition into the Lee-Wick phase sets in only at very large densities [228–230]. In accordance with our results, fluctuations can stabilize the order parameter.

In our model, at $5\,n_0$, the value of σ is still at half its vacuum value, at $6\,n_0$ at about forty percent. Consequently, chiral symmetry is broken and chiral models based on hadronic

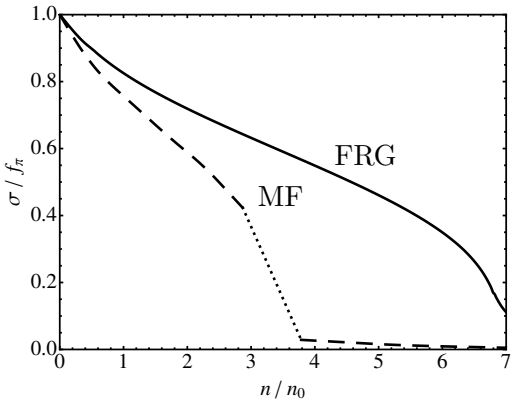

Figure 27: Pure neutron matter at $T = 0$: chiral order parameter in the MF-ChNM model (dashed) and the FRG-ChNM model (solid line). The dotted line stems from a Maxwell construction.

matter are applicable. In the following section we therefore take the equation of state from the FRG-ChNM calculation as a model for the interior of neutron stars.

4.6 NEUTRON STARS

It is so far impossible to study cold and dense matter in the laboratory. Fortunately, in the core of neutron stars these extreme conditions can be achieved. Therefore, observations of neutron stars are an excellent tool to extend our knowledge of nuclear matter at high densities. Different properties of neutron stars allow us to probe different physical aspects of dense matter, as will be explained in the following.

Neutron stars cool down because of the weak interaction. The mean free path of electrons inside the core of the neutron star is very small. As a consequence, only the surface electrons effectively contribute to the cooling process. Neutrinos, in contrast, can propagate almost freely even inside the neutron star and therefore are mainly responsible for the cooling of the neutron star. The heat capacity and the neutrino emissivity of dense matter can be extracted.

As neutron stars get older, their spin period decreases. The spin down depends strongly on the bulk and shear viscosity of dense matter. Spectacular phenomena related to the spin-down phenomenon are **neutron star glitches**. The spin frequency of the pulsar suddenly increases enormously and then slowly recovers. It is believed that glitches are related to a superfluid phase of neutrons close to the crust [231]: Vortices in the superfluid phase are pinned to the nuclei in the crust, which prevents them from spinning down. They lag with respect to the spinning of the star, and a Magnus force acts on the vortices and eventually breaks them free from the crust. Angular momentum is transferred from the vortices to the crust, resulting in a sudden increase in spin frequency (see also [232] for a recent review).

Most importantly for our purposes, observations of **neutron star masses and radii** can strongly constrain the equations of state of cold and dense matter. Although heavy neutron stars were already discussed earlier (see [233] for an overview), the uncertainties of the observations were rather large. This changed when in 2010 the microsecond pulsar J1614-2230 with mass $M = 1.97(4)\ M_\odot$ was observed, where $M_\odot$ is the mass of the sun. The exceptionally small uncertainty results from the almost edge-on configuration of the binary system with an inclination angle close to 90°. From the perspective of the earth,

the companion star passes directly behind its companion star during its orbit. The gravitational field of the companion star affects the signal (Shapiro delay). The mass of the companion can be deduced, and from a Keplerian analysis also the mass of the pulsar.

Subsequently, also a second star with $M = 2.01(4)\ M_\odot$ was discovered [9]. From a nuclear physics perspective, heavy neutron stars are extremely helpful as they provide constraints for any realistic theory of the interior of neutron stars. The equation of state has to be stiff enough to provide enough pressure to prevent the heavy star from collapsing into a black hole. A large class of speculative equations of state can be ruled out in this way.

The determination of neutron star radii is less straightforward and much more model-dependent. Typical masses of neutron stars are around $1.4\ M_\odot$. For these stars, the central density is not larger than a few times nuclear saturation density. Essentially the whole region of the equation of state needed to describe these stars is determined by the symmetry energy and L-parameter. These parameters are experimentally accessible as discussed in Sec. 2.6. Lattimer and Steiner performed a Monte Carlo analysis and computed the radius of a $1.4\ M_\odot$ neutron star to be [171]

$$R_{1.4} = 12.1(11)\,\mathrm{km}. \tag{4.164}$$

The radii can also be determined from the observation of X-ray burst oscillations. A neutron star accretes matter from its companion star and if the pressure is too high, nuclear burning is triggered. The subsequent X-ray bursts can be energetic enough to reach the Eddington limit. This means that gravity can be overcome and the photosphere of the star is expelled. The flux of these **photospheric radius expansion (PRE) bursts** can be measured. Under the assumption that the flux is close to the Eddington flux, the radius of the neutron star can be deduced. The radius determined in this way is smaller [171], since one gets

$$R = 10.77(65)\,\mathrm{km}. \tag{4.165}$$

Yet even smaller radii were deduced from measurements of quiescent low-mass X-ray binaries under the assumption that all neutron star have the same radius. The motivation was that most equations of state in general result in a mass-radius relation that is almost mass-independent for typical medium-mass neutron stars. The analysis of five neutron stars found an extremely small value [234]

$$R = 9.1^{+1.3}_{-1.5}\,\mathrm{km}. \tag{4.166}$$

A meta-analysis of different studies of X-ray burst oscillations, thermal emission, and stars with largest spin frequency was performed by Trümper [235]. A rhomboid-like region is then singled out in the mass-radius plane, which all realistic equations of state should intersect.

We will now provide an equation of state for the interior of the neutron star. At the surface the pressure is zero, and matter consists of a lattice of Fe^{56}, which is the most stable electrically neutral configuration. Going inwards, the density increases and the iron atoms become ionized. The relativistic electron gas dominates the equation of state, which is therefore well understood. Electron capture sets in at higher densities and the atoms become more and more neutron rich. After crossing the neutron drip-line, neutron-rich atoms are immerged in a (superfluid) neutron gas. In the coexistence region, exotic extended objects, the "pasta" phases, might exist [236]. The whole crust region can be well described by the **Skyrme-Lyon (SLy) equation of state** [237, 238]. Below the crust,

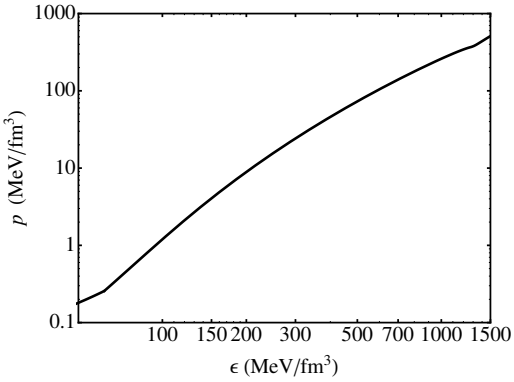

Figure 28: The equation of state (pressure versus energy density) of neutron star matter with $E_{\rm sym} = 32\,\text{MeV}$, taking beta equilibrium into account.

single atoms can no longer exist and the neutron star matter consists of a uniform fluid of mostly neutrons with a small admixture of protons, electrons, and muons. Hadronic models like the ChNM model then are applicable. We remark that the crust contributes only a small portion of the total mass of the neutron star.

Neutron stars are electrically neutral. To compensate for the admixture of protons, our model is extended by electrons and muons. The density of the positively charged protons equals the density of the negatively charged electrons and muons,

$$n_p = n_e + n_\mu \,. \tag{4.167}$$

The chemical potentials of the different particles are not independent, but related through the condition of chemical beta equilibrium involving the processes $n \leftrightarrow p + \mu^- + \bar{\nu}_\mu$ and $n \leftrightarrow p + e^- + \bar{\nu}_e$, i.e.,

$$\mu_n = \mu_p + \mu_e \,, \quad \mu_\mu = \mu_e \,, \tag{4.168}$$

where μ_e and μ_μ are the chemical potentials of electrons and muons, respectively. At zero temperature, the neutron chemical potential can be eliminated, because

$$\mu_n = \mu_p + \sqrt{(3\pi^2 n_p)^{2/3} + m_e^2} \,. \tag{4.169}$$

Finally, electrons and muons with energy $E_i = \sqrt{p^2 + m_i^2}$ contribute to the effective potential (negative pressure) as a Fermi gas,

$$U_{\text{e-}\mu} = -2 \sum_{i=e,\mu} \sum_{r=\pm 1} \int \frac{d^3p}{(2\pi)^3} \frac{p^2}{3E_i} n_{\rm F}(E_i - r\mu_i) \,, \tag{4.170}$$

where anti-particles do not contribute at zero temperature and the Fermi distribution turns into a step function. In Fig. 28, we show the equation of state of neutron star matter in beta equilibrium. The intersection point with the SLy EoS occurs at a density of $n \simeq 0.3\, n_0$. From this density onward we use the FRG-ChNM model EoS for the whole core of the neutron star.

This equation of state is then used as an input for the Tolman-Oppenheimer-Volkoff equations (2.8). The initial energy density at the surface that enters the ToV equations is that of iron, which is $\epsilon_{\rm Fe} = 4.4 \cdot 10^{-12}\,\text{MeV/fm}^3$. The TOV equations can be solved for a given density at the center of the neutron star. The radius is determined from $\epsilon(R) = \epsilon_{\rm Fe}$,

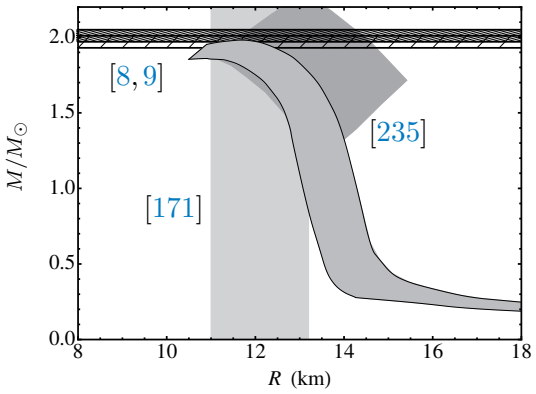

Figure 29: Mass radius relation for neutron star matter. The mass-radius constraints from reference [235], the radius constraint [171], and the two-solar-mass neutron stars [8, 9] are shown for comparison.

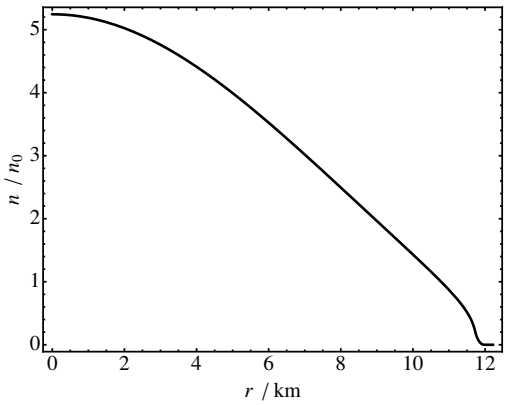

Figure 30: Density profile for a neutron star with mass $M = 1.97\,M_\odot$ and $R = 12.2$ km for $G_\rho = 1.46$ fm^{-2}.

and the mass can be computed from Eq. (2.11). Varying the central densities therefore results in a curve of possible masses and radii.

To account for the uncertain symmetry energy, we have varied the parameters of the model to reproduce symmetry energies in the range of $29\,\text{MeV} \leq E_{\text{sym}} \leq 37\,\text{MeV}$. Figure 29 shows the corresponding mass-radius relation as a band. The highest curve corresponds to the largest symmetry energy, as the equation of state then is stiffer (higher energy per particle for a given density). Correspondingly, the lower curve results from the smallest symmetry energy. We are consistent with the radius constaints (4.164) by Lattimer and Steiner (shown as a vertical band), and the constraints by Trümper (rhomboid). Within error bands, we are also consistent with the two-solar mass neutron star measurements. The maximum mass in our model is $1.97\,M_\odot$, which is a bit smaller than the results from other approaches based on conventional matter. For instance, the APR equation of state [210] supports neutron stars with masses as high as $2.2\,M_\odot$. For densities below $3\,n_0$, our equation of state is even slightly stiffer than APR or QMC calculations (see Fig. 24). However, at higher densities above about $3.5\,n_0$ the latter equations of state become stiffer. The behavior of the EoS at densities above $3.5\,n_0$ are in the end responsible for the highest-mass neutron stars. We have checked that if we take the APR EoS above the intersection point, the maximal mass is raised to $2.1\,M_\odot$.

Figure 30 shows the density profile for a neutron star with maximum mass $M = 1.97\,M_\odot$. The corresponding radius is 12.2 km. The central density is only five times nuclear saturation density. Therefore, we have *a posteriori* justified the validity of our assumption that the FRG-ChNM model can be used for the whole interior. At $5\,n_0$, the value of the condensate is still at 0.45 times its vacuum value and the model is applicable. Of course, the exact value for the maximum mass should be taken with a grain of salt. Since all hadronic models are fitted only to experimental data in the vacuum or at saturation density, the extrapolation to high densities is always speculative. A possible way to reduce the uncertainty is to use hadronic models only up to a certain density. Beyond, a polytropic ansatz $p \sim n^\Gamma$ is chosen, where Γ is varied in a certain range. The result is then a relatively broad band in the mass-radius plane [220, 239], with less predictive power.

It is a general observation that conventional models based on nuclei yield equations of state that are stiff enough to support two-solar-mass neutron stars. Many different extensions have been discussed, see, e.g., [240] for an overview. One possibility is an admixture of **hyperons** at higher densities. The low-energy Λ-nucleon interaction is repulsive, so it is in principle possible that Λ-hyperons appear in the interior of neutron stars. However, a significant admixture of Λ-hyperons considerably softens the equation of state and a two-solar mass pulsar can no longer be supported against gravitational collapse. Only if additional repulsion is added at high-densities, it is possible to be consistent with the observational constraints [241, 242].

Another possibility is the onset of **meson condensation**, like kaon or pion condensates, in the interior of the neutron stars [243]. Again, the equation of state is much too soft, unless the parameters at high-densities are fine-tuned [244].

The **strange matter hypothesis**, which goes back to Bodmer [245] and Witten [246], states that nuclear matter is only metastable and the true ground state in fact consists of a mixture of quasi-free up, down, and strange quarks. The masses of so-called quark stars or strange stars, which consist only of strange matter, are much too low and cannot serve as a model for high-mass pulsars.

At some unknown density, the phase changes from hadronic matter to quark matter, and therefore **quarks** can be important in the very core of the neutron star (see [247] and references therein). The transition can be studied in simplified models, with the finding that significant quark cores can only exist for large enough repulsive forces (see, e.g., [220, 248]).

It is certainly fair to say that the high-density regime of the QCD phase diagram is not yet fully understood. But the observations existing so far seem to indicate that conventional baryonic matter is prefered, even in the center of the heaviest neutron stars. More precise astrophysical observations are needed to pin down the equation of state even further.

5

SUMMARY AND OUTLOOK

In this thesis, a chiral nucleon-meson model has been studied in the framework of the functional renormalization group. This model is perfectly suited to explore the properties of dense nuclear matter at and around the nuclear liquid-gas phase transition. The physical behavior of nuclear matter is based on the strong force as described by Quantum Chromodynamics (QCD). We have given a concise overview of QCD with particular emphasis on its low-energy properties, which are governed by confinement and chiral symmetry breaking. An important task for both experimentalists and theoreticians is to improve the understanding of the behavior of QCD at finite temperatures and densities. One frequently discussed scenario is the existence of a first-order phase transition from a chirally broken phase to an unbroken phase at small temperatures and high chemical potentials. If this were the case, there would exist a second-order critical endpoint (CEP) at the end of the first-order line. Some models based on effective quarks predict a CEP at relatively low temperature and at chemical potentials close to the nuclear liquid-gas transition. However, in this region baryons cannot be ignored and they strongly influence the mechanism of chiral restoration. Therefore, we have discussed a model based on nucleonic degrees of freedom, with their long-range interaction dominated by pion exchange. The pions are combined with a scalar-isoscalar field in a chirally invariant way. Interactions of nucleons at shorter distances are modeled by an exchange of heavy vector particles. All free parameters of the model have been adjusted to low-energy pion dynamics as well as properties of nuclear matter at saturation density.

In the existing literature, the model has so far only been studied in a mean-field approximation, which does however not properly include the effects of pionic fluctuations. One approach to go beyond the mean-field approximation is the functional renormalization group (FRG) method. We have described the basic theoretical concepts of this approach, which is based on a fully non-perturbative flow equation for a renormalization-scale dependent effective action, which interpolates between the classical action and the full quantum effective action. Subsequently, we have applied the FRG methods to the nucleon-meson model and we have discussed its thermodynamic properties in detail. We have observed that the description of the nuclear liquid-gas phase transition is in excellent agreement with experimental data. We have in particular examined the influence of fluctuations close to the critical endpoint of the liquid-gas transition. Likewise, the equation of state of symmetric nuclear matter at vanishing temperature agrees nicely with sophisticated many-body computations up to at least three times saturation density.

Within the nucleon-meson model, a critical endpoint of a chiral first-order transition is excluded for symmetric nuclear matter in the range of applicability of the model. The chiral order parameter is well above zero for temperatures up to 100 MeV and densities at least up to three times nuclear saturation density. Consequently, chiral restoration takes place outside this physical window, which implies that a restoration close to the liquid-gas phase transition is strongly disfavored. At higher chemical potentials chiral restoration

and chemical freeze-out do not take place simultaneously. Whereas both transition temperatures agree at zero chemical potential, the interpolated chemical freeze-out line lies close to the liquid-gas transition, in contrast to the chiral restoration region.

Cold and dense baryonic matter cannot be probed directly in terrestrial experiments. However, high densities are naturally realized in the interior of neutron stars. To obtain a model for the interior of neutron stars, we have extended our studies to asymmetric nuclear matter with varying proton fractions. Similar to symmetric nuclear matter, the inclusion of fluctuations greatly improves the behavior of the equation of state of pure neutron matter in comparison with many-body calculations. In relativistic mean-field models, the equation of state is in general too soft at low densities and too stiff at high densities. Both effects are present also in the mean-field approach to the nucleon-meson model, but are strongly reduced by pionic fluctuations.

We have also studied chiral restoration in the case of pure neutron matter. In chiral effective field theory computations, the chiral condensate decreases almost linearly, which would indeed imply a restoration of chiral symmetry at densities of only about three times nuclear saturation density. Studies based on broken chiral symmetry then can no longer be trusted and it seems questionable if the interior of neutron stars can be described by conventional approaches based on nucleons and protons, extrapolated to higher densities. In the mean-field approximation of the nucleon-meson model, the chiral order parameter also decreases relatively strongly as a function of density. Once pionic fluctuations are included in a non-perturbative way, the chiral order parameter is stabilized up to densities of about seven times nuclear saturation density. Consequently, chiral symmetry is still broken below these densities and chiral models can be applied.

After this important consistency check, we have included electrons and muons to study beta-equilibrated neutron-star matter. Apart from the crust, which is modeled by a phenomenological equation of state, the FRG-improved nucleon-meson model describes the whole interior of the neutron star. Our model is in agreement with recent observational constraints, in particular the precise measurements of two-solar-mass neutron stars. We find that even for the heaviest stars, the central density is not much higher than five times nuclear saturation density, which justifies the applicability of the model. Our results confirm that conventional equations of state based on neutrons and protons describe the interior of neutron stars in an excellent way.

In view of future research, there are a number of possible extensions of our model: Concerning the technical implementation, the approximations made in the treatment of the flow equations could be relaxed, for instance by including running Yukawa couplings or higher derivative terms. From a physical perspective, one extension would be to go beyond the $N_f = 2$ case. Moreover, at sufficiently high temperatures the fluctuations of the massive bosons also start to play a role. Finally, it would be interesting to study the effects of an isospin chemical potential, which in particular allows a study of pion condensates. These extensions would certainly improve our understanding of dense matter and in particular the role of fluctuations.

To sum up, we have shown that it is important to include fluctuations beyond the mean-field approximation to get a solid understanding of hot and dense hadronic matter. The functional renormalization group is an excellent tool to study these effects in a systematic, non-perturbative way.

A

APPENDIX

A.1 CONVENTIONS

A.1.1 SU(2)

The fundamental representation of the Lie algebra $\mathfrak{su}(2)$ corresponding to the Lie group SU(2) is generated by $T^a = \frac{\sigma^a}{2}$, where σ^a, $a = 1, 2, 3$ are the Pauli matrices, given by

$$\sigma^1 = \begin{pmatrix} 0 & 1 \\ 1 & 0 \end{pmatrix}, \qquad \sigma^2 = \begin{pmatrix} 0 & -i \\ i & 0 \end{pmatrix}, \qquad \sigma^3 = \begin{pmatrix} 1 & 0 \\ 0 & -1 \end{pmatrix}. \tag{A.1}$$

They satisfy the important relation

$$\sigma^a \sigma^b = \delta^{ab} + i\epsilon^{abc}\sigma^c, \tag{A.2}$$

where ϵ^{abc} is the totally antisymmetric tensor with $\epsilon^{123} = 1$. In isospin space, the Pauli matrices are denoted by τ^a.

A.1.2 *Thermodynamical distributions*

Bose and Fermi distributions are defined as

$$\begin{aligned} n_{\mathrm{B}}(E) &= \frac{1}{\mathrm{e}^{\beta E} - 1}, \\ n_{\mathrm{F}}(E) &= \frac{1}{\mathrm{e}^{\beta E} + 1}, \end{aligned} \tag{A.3}$$

respectively, where $\beta = 1/T$ is the inverse temperature.

A.1.3 *Lorentzian signature*

The metric in Minkowski space is $g_{\mu\nu} = \mathrm{diag}(1, -1, -1, -1)$ and the Clifford algebra is

$$\{\gamma^\mu, \gamma^\nu\} = 2g^{\mu\nu}. \tag{A.4}$$

We choose the Weyl-representation of the Clifford algebra. In this representation the Dirac matrices γ^μ have the form

$$\gamma^\mu = \begin{pmatrix} 0 & \sigma^\mu \\ \bar{\sigma}^\mu & 0 \end{pmatrix}, \tag{A.5}$$

with $\sigma^\mu = (\mathbf{1}, \boldsymbol{\sigma})$ and $\bar{\sigma}^\mu = (\mathbf{1}, -\boldsymbol{\sigma})$, where $\boldsymbol{\sigma} = (\sigma^1, \sigma^2, \sigma^3)^T$ are the Pauli matrices of Eq. (A.1). In $3+1$ dimensions there is a fifth matrix which anticommutes with all γ^μ, namely $\gamma_5 = i\gamma^0\gamma^1\gamma^2\gamma^3$. In the Weyl-representation chosen above, γ_5 is diagonal,

$$\gamma_5 = \begin{pmatrix} -\mathbf{1} & \\ & \mathbf{1} \end{pmatrix}. \tag{A.6}$$

The projectors on right- and left-handed components are of the simple form

$$P_R = \frac{1}{2}(1+\gamma_5) = \begin{pmatrix} \mathbf{1} & \\ & \mathbf{0} \end{pmatrix}, \quad P_L = \frac{1}{2}(1-\gamma_5) = \begin{pmatrix} \mathbf{0} & \\ & \mathbf{1} \end{pmatrix}, \tag{A.7}$$

which is why this choice is also called the chiral representation.

All models we are interested in are based on fermions ψ, scalar fields φ and massive vector bosons A^μ. The scalars are coupled to the fermions via Yukawa-type interactions with strength g_φ. The vector bosons couple via a covariant derivative $D_\mu = \partial_\mu - ig_A A_\mu$. A generic action in Minkowski space has the following form:

$$S_{\mathrm{M}} = \int d^4x \left[\bar{\psi}(i\gamma^\mu D_\mu - g_\varphi\,\varphi)\psi + \frac{1}{2}\partial_\mu\varphi\,\partial^\mu\varphi - U(\varphi) - \frac{1}{4}F_{\mu\nu}F^{\mu\nu} + \frac{m_A^2}{2}A_\mu A^\mu\right]. \tag{A.8}$$

A.1.4 *Euclidean signature*

Finite temperatures require a continuation to imaginary times, realized by a Wick transformation. There are several different conventions and we take the one that is used in Ref. [29]. Euclidean coordinates are defined as

$$\tau \equiv x_{\mathrm{E}}^4 = ix^0, \quad x_{\mathrm{E}}^i = x^i. \tag{A.9}$$

As a consequence, the partial derivatives are given by

$$\frac{\partial}{\partial x_{\mathrm{E}}^4} = -i\frac{\partial}{\partial x^0}, \quad \frac{\partial}{\partial x_{\mathrm{E}}^i} = \frac{\partial}{\partial x^i}. \tag{A.10}$$

Indices are raised and lowered with the Euclidean metric, so there is no distinction between upper and lower indices. The integration measure is $\int d^4x_{\mathrm{E}} = i\int d^4x$. In order to get a compact form of the Dirac operator $\not{\partial}_{\mathrm{E}} = \gamma_{\mathrm{E}}^4\partial_4 + \gamma_{\mathrm{E}}^i\partial_{\mathrm{E},i}$ the Euclidean Dirac matrices are defined as

$$\gamma_{\mathrm{E}}^4 = \gamma^0, \quad \gamma_{\mathrm{E}}^i = -i\gamma^i. \tag{A.11}$$

As a consequence, the Euclidean Clifford algebra is

$$\{\gamma^\mu, \gamma^\nu\} = 2\delta^{\mu\nu}. \tag{A.12}$$

In particular, $\not{p}^2 = p^2$ for any vector p. The fifth anti-commuting matrix is defined as above, i.e., $\gamma_5^{\mathrm{E}} = i\gamma_{\mathrm{E}}^0\gamma_{\mathrm{E}}^1\gamma_{\mathrm{E}}^2\gamma_{\mathrm{E}}^3$. Also the vector fields can be put into a compact form by defining the Euclidean fields

$$A_{\mathrm{E}}^4 = -iA^0, \quad A_{\mathrm{E}}^i = -A^i. \tag{A.13}$$

With this definition, the Euclidean covariant derivative still has the form $D_\mu = \partial_\mu - ig_A A^{\mathrm{E}}_\mu$. The Euclidean action[11] is defined as $\mathrm{e}^{iS_{\mathrm{M}}} \to \mathrm{e}^{-S_{\mathrm{E}}}$ and the action (A.8) transforms into

$$S_{\mathrm{E}} = \int d^4x_{\mathrm{E}} \left[\bar\psi(\gamma^\mu_{\mathrm{E}} D^{\mathrm{E}}_\mu + g_\varphi\,\varphi)\psi + \frac{1}{2}\partial^{\mathrm{E}}_\mu\varphi\;\partial^\mu_{\mathrm{E}}\varphi + U(\varphi) + \frac{1}{4}F_{\mu\nu}F^{\mu\nu} + \frac{m_A^2}{2}A^{\mathrm{E}}_\mu A^\mu_{\mathrm{E}}\right]. \tag{A.14}$$

The above notation is very compact. However, from Eq. (A.13) it follows that if A^0 acquires a real expectation value, A^4_{E} is purely imaginary. In practice, it is easier to keep the original field A^0.

At finite temperature T, the $\tau = x^4_{\mathrm{E}}$ dimension is compactified on a circle with radius $\beta = 1/T$. In this case $\int d^4x_{\mathrm{E}} \to \int_0^\beta d\tau \int d^3x$.

A.1.5 *Fourier transformation*

To facilitate readability, in the following the momentum dependencies of the fields are indicated by a subscript:

$$\varphi_x \equiv \varphi(x)\,, \quad \psi_x \equiv \psi(x)\,, \quad \bar\psi_x \equiv \bar\psi(x)\,, \tag{A.15}$$

and likewise in momentum space. Moreover we define

$$\int_p \equiv \int \frac{d^4p}{(2\pi)^3}\,, \tag{A.16}$$

where p are the four-momenta corresponding to Euclidean space. The Fourier transformed fields in Euclidean space-time are defined as[12]

$$\varphi_x = \int_p \mathrm{e}^{ipx}\,\varphi_p\,, \quad \psi_x = \int_p \mathrm{e}^{ipx}\,\psi_p\,, \quad \bar\psi_x = \int_p \mathrm{e}^{-ipx}\,\bar\psi_p. \tag{A.17}$$

We want to compute the Fourier transform of the action (A.14) for constant vector fields. Therefore, we ignore the transformation of the field strength $F_{\mu\nu}$. The potential $U(\varphi)$ shall depend only on φ^2 and is expanded around a fixed value $\bar\varphi^2$:

$$U(\varphi) = \sum_n \frac{a_n}{n!}\Big(\frac{1}{2}\varphi^2 - \frac{1}{2}\bar\varphi^2\Big)^n. \tag{A.18}$$

The action in momentum space is given by

$$\begin{aligned} S_{\mathrm{E}} = {} & \int_p \bar\psi_p\, i\gamma^\mu_{\mathrm{E}}\, p_\mu\, \psi_p + \int_{p_1,p_2} \bar\psi_{p_1}\left[g_\varphi\,\varphi_{p_1-p_2} - ig_A\,\gamma^\mu_{\mathrm{E}}\,(A^{\mathrm{E}}_\mu)_{p_1-p_2}\right]\psi_{p_2} \\ & + \frac{1}{2}\int_p \varphi_{-p}\,p^2\,\varphi_p + \sum_n \frac{a_n}{n!}\int_x \Big[\frac{1}{2}\int_{p_1}\int_{p_2} \mathrm{e}^{i(p_1+p_2)x}\,\varphi_{p_1}\varphi_{p_2} - \frac{1}{2}\bar\varphi^2\Big]^n. \end{aligned} \tag{A.19}$$

The x-integral in the last term can in principle be performed, but for our purposes the present form is more useful. For the renormalization group equations, also the transpose of the integrand is needed in case of the fermionic fields. For transposing, be aware of

11 A different convention also often used is $\mathrm{e}^{iS_{\mathrm{M}}} \to \mathrm{e}^{iS_{\mathrm{E}}}$.

12 In Lorentzian signature (p.e. [249]), there appears an extra minus sign, since $p = (p^0, -\boldsymbol{p}) \to -p_{\mathrm{E}} = -(p_4, \boldsymbol{p})$.

the minus sign, when interchanging fermions. For the kinetic term this minus sign can be absorbed by a substitution $p \to -p$. The transposed version is

$$S_{\mathrm{E}} = \int_p \psi^T_{-p}\, i(\gamma^\mu_{\mathrm{E}})^T\, p_\mu\, \bar\psi^T_{-p} - \int_{p_1,p_2} \psi^T_{p_2} [g_\varphi\, \varphi_{p_1-p_2} - i g_A\, (\gamma^\mu_{\mathrm{E}})^T\, (A^{\mathrm{E}}_\mu)_{p_1-p_2}] \bar\psi^T_{p_1} + \frac{1}{2}\int_p \varphi_{-p}\, p^2\, \varphi_p + \sum_n \frac{a_n}{n!} \int_x \Big[\frac{1}{2}\int_{p_1}\int_{p_2} \mathrm{e}^{i(p_1+p_2)x}\, \varphi_{p_1}\varphi_{p_2} - \frac{1}{2}\bar\varphi^2\Big]^n . \tag{A.20}$$

At finite temperatures, the zero-component of the momentum has to be replaced by the discrete Matsubara frequencies, ω_l. Likewise, the integral is replaced by

$$\int_p \equiv T \sum_{\omega_l} \int \frac{d^3p}{(2\pi)^3} . \tag{A.21}$$

A.2 GEOMETRY

In this appendix, we elaborate a bit more on the underlying formalism of gauge theories. For more detailed introductions we refer to the textbooks, e.g., [250–252].

A.2.1 *Gravity*

Space-time is modeled by a $3+1$-dimensional pseudo-Riemannian manifold M. Manifolds are generalizations of $\mathbb{R}^n$ in the sense that locally they look like subsets of $\mathbb{R}^n$. The precise definition is as follows: An n-dimensional smooth **manifold** is a topological space M with local trivializations $\phi_a : U_a \to \mathbb{R}^n$, where $\{U_a\}_a$ is an open covering of M. The transition functions $\phi_b \circ \phi_a^{-1}$ have to be smooth on their overlap in the sense of functions from $\mathbb{R}^n$ to $\mathbb{R}^n$. In gravity, the manifold serves to distinguish between different space-time points. The specific parametrization, however, cannot have a physical meaning and the theory must be invariant under global diffeomorphisms[13].

Global information is important in gravity and in quantum field theory, as in the case of instantons, solitons, monopoles, domain walls, cosmic strings, or the appearance of Gribov copies in the BRST quantization procedure. However, the starting point often is a study of local properties. The linearized approximation of a manifold M at a point $p \in M$ is given by its **tangent space** T_pM, which is the union of all vectors $v_p : C^\infty(M) \to \mathbb{R}$ that are linear maps and satisfy

$$v_p(fg) = v_p(f)\, g(p) + v_p(g)\, f(p)\,. \tag{A.22}$$

The vectors can be thought of as derivatives acting on functions at p. Similarly, one defines the cotangent space $T^*(M) = (T(M))^*$ consisting of maps from $T_p(M)$ to $\mathbb{R}$.

Fiber bundles are very powerful generalizations of manifolds. A **fiber bundle** is characterized by a triple (E, π, M), where E and M are manifolds, the total space and the base space, respectively, and $\pi : E \to M$ is the projection map which projects from E down to M. For each point $p \in M$, its fiber F_p is defined as $\pi^{-1}(p)$. Often, one speaks of the fiber bundle E over M, or of the fiber bundle $\pi : E \to M$.

Since M looks locally like $U \subset \mathbb{R}^n$, a fiber bundle looks locally always like $U \times F$, with $U \subset \mathbb{R}^n$. Globally, the fibers can be glued together in a non-trivial twisted way, as in the case of the Möbius strip, shown in Fig. 31. If all transition functions can be chosen to be the identity map, a fiber bundle is said to be **trivial**.

A **section** of a fiber bundle $\pi : E \to M$ is a continuous map $s : M \to E$, such that $\pi(s(p)) = p$ for all $p \in M$. In this sense, sections are generalizations of graphs.

One example is the **tangent bundle** TM over M, which is the union of all tangent spaces $TM = \bigcup_{p\in M} T_p(M)$ with projection $\pi : T_pM \ni v_p \to p \in M$. A section is a smooth vector field. Other important examples of sections are scalar or spinor fields in quantum field theory.

In Yang-Mills theories, the fibers are Lie groups G, so think of a manifold M with a copy of G glued to each point. Conceptually, this is a **principal fiber bundle with structure group** G, namely a fiber bundle $\pi : P \to M$, with a continuous fiber-preserving right action $P \times G \to P$. The action is free (i.e., if $g.p = h.p$, then $g = h$, with $g, h \in G$ and $p \in P$) and transitive (i.e., for $p_{1,2} \in P$ there exists a $g \in G$ with $g.p_1 = p_2$).

13 As was shown by Élie Cartan, this notion of "general covariance" can also be applied to classical mechanics. What singles out general relativity is its "simplicity" in coordinate-free notation (see [17], Chapter 12), in contrast to classical mechanics, which looks only "simple" in local coordinates.

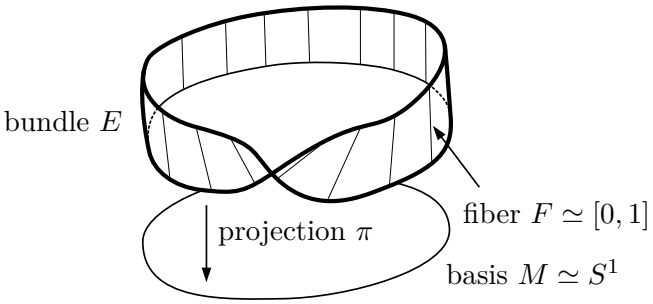

Figure 31: The Möbius strip as an example of a fiber bundle.

The fiber-preserving action therefore identifies the fiber with the Lie group G itself. Closely related is the concept of the associated fiber bundle. Let $\pi : P \to M$ be a principal vector bundle and V a k-dimensional vector space. Let ρ be a representation of a Lie group G on V. The **associated vector bundle** $P \times_\rho V$ is constructed from $P \times V$ by identifying $(u, v) \in P \times V$ with $(ug, \rho(g^{-1})v) \in P \times V$ for all $g \in G$.

If we denote the equivalence class of $(u, v) \in P \times V$ in $P \times_\rho V$ by $[u, v]$, then from the definition $[ug, v] = [u, \rho(g)v]$. Whereas the principal bundle was locally equivalent to $U \times G$, the associated bundle therefore is locally equivalent to $U \times V$. The transition functions of $P \times_\rho V$ which glue local trivializations together are $\rho(t_{ij})$, where t_{ij} are the transition functions of P. Intuitively, the principal fiber bundle and its associated vector bundle are twisted in the same way, but with different fibers G and V, respectively. Since G is a topologically complicated group and V is a linear vector space, the associated vector bundle is often easier to study.

We give an example. Let M be a four-dimensional Riemannian manifold with metric g. Let $\{e_I\}_{I=0,\dots,3}$ be a frame which consists of linearly independent vectors at $p \in M$, which in local coordinates is given by

$$e_I = e_I^\mu \partial_\mu \,. \tag{A.23}$$

An element $a^J{}_I$ of the group $\mathrm{GL}(n, \mathbb{R})$ acts on a frame via $e_I \to e_J a^J{}_I$. The action is transitive and therefore the union of the sets of all frames L_pM at all points $p \in M$ is a principal fiber bundle with structure group $\mathrm{GL}(n, \mathbb{R})$. It is called the **frame bundle** $LM = \bigcup_{p\in M} L_pM$. Its associated vector bundle is the tangent bundle [250]. If an orthogonality condition $g(e_I, e_J) = \eta_{IJ}$ is imposed on the frames, the structure group reduces to the group of Lorentz transformations $\mathrm{SO}(3, 1)$, since they preserve the orthogonality. If spinors are to be included in general relativity, one must lift the bundle to the so-called **spinor bundle** [253] with structure group $\mathrm{Spin}(3, 1)$.

Let us go back to gravity. Observers at two different points can in principle make different choices of reference frames. A change of reference frame (a local gauge transformation) corresponds to an element in the restricted Lorentz group

$$\mathrm{SO}^+_\uparrow(3, 1) = \{\Lambda \in \mathrm{O}(3, 1) \mid \det \Lambda = 1,\ \Lambda_0{}^0 > 0\}. \tag{A.24}$$

We associate therefore with every point a copy of the restricted Lorentz group $\mathrm{SO}^+_\uparrow(3, 1)$. The full set P of manifold plus groups glued to each point has mathematically the structure of a principal bundle over M with structure group $\mathrm{SO}^+_\uparrow(3, 1)$. Note that in contrast to a global symmetry, gauge symmetries are not related to conserved charges or new symmetries of nature [254].

It is easier to study the associated vector bundle $P \times_\rho V$ with metric η, where V is Minkowski space and ρ the representation of the Lorentz group on V. To get an intuitive

picture of $P \times_\rho V$, imagine that a copy of Minkowski space V is glued to each point $p \in M$ on which the group of Lorentz transformations acts on. In the following the indices μ, ν refer to curved space and I, J to flat Minkowski space attached to a given point. P is trivial in the sense that $P \times_\rho V$ admits a section X_I such that the metric is flat: $\eta(X_I, X_J) = \mathrm{diag}(1, -1, -1, -1)$. The physical interpretation follows from the equivalence principle, which lies at the heart of Einstein's theory: physical measurements of an observer in free fall will agree exactly with experiments in flat space-time. A free-falling observer is described by the so-called vierbein (or moving frame) e, which maps the tangent bundle TM to $P \times_\rho V$. The vierbein has components e^I_μ, so it converts tangent space indices μ and Lorentz space indices I into each other. The linearized neighborhood of a point – its tangent space – is therefore mapped to a Lorentz space (a system in free fall). Moreover, the vierbein equips the manifold M with a metric g via the pullback, namely

$$g(X, Y) = \eta\big(e(X),\, e(Y)\big), \tag{A.25}$$

for vector fields X and Y in TM. Two observers at different points want to know how to compare their measurements. The internal spaces can be related to each other with the spin-connection ω, a Lie-algebra $\mathfrak{so}(3,1)$-valued one-form with components $\omega_\mu{}^I{}_J$. Under a local gauge transformation h in the Lie group $\mathfrak{so}(3,1)$ acting on the vierbein e, the connection ω transforms as

$$\omega \to h^{-1}(d + \omega)h\,, \tag{A.26}$$

where d is the exterior derivative. The spin-connection defines a covariant derivative of an object X^I with an internal Minkowski index, namely[14]

$$D_\mu X^I = (\delta^I{}_J\, \partial_\mu + \omega_\mu{}^I{}_J) X^J\,. \tag{A.27}$$

The connection describes how the components in the internal Lorentz space change as we move along a section in $P \times_\rho V$. An object is transported parallely along a path γ in M if its covariant derivative vanishes along γ. In GR the connection ω has to be torsion-free and compatible with the metric. It gives rise to the curvature tensor

$$\Omega = d\omega + \omega \wedge \omega\,, \tag{A.28}$$

where $\wedge$ is the wedge-product. In local coordinates, Ω has components $\Omega_{\mu\nu}{}^I{}_J$.

The field equations follow now from an action principle. We start from the Palatini action,

$$S_{\mathrm{P}}[e, \omega] = \frac{1}{8\pi G} \int_M \epsilon_{IJKL} \eta^{LM}\, e^I \wedge e^J \wedge \Omega^K{}_M\,, \tag{A.29}$$

which depends on the vierbein e and on the connection ω, where G is the gravitational constant. The Palatini action describes the dynamics of gravity in the absence of matter. An action

$$S_{\mathrm{matter}} = \int d^4x\, \mathcal{L}_{\mathrm{m}} \tag{A.30}$$

14 Space-time and Lorentz indices are related via the vierbein e^I_μ and its inverse e^μ_I. From an object with Lorentz index X^I one can construct $X^\mu = e^\mu_I X^\mu$ with a space-time index. The covariant derivative of the latter reads $D_\mu X^\nu = (\delta^\nu{}_\sigma \partial_\mu - \Gamma^\nu_{\mu\sigma}) X^\sigma$. The Christoffel symbols $\Gamma^\nu_{\mu\sigma}$ can be computed from ω and the vierbein.

of matter described by a Lagrangian density $\mathcal{L}_{\mathrm{m}}$ can be added to the action. From the matter Lagrangian, one defines the energy-momentum tensor as follows:

$$T^{\mu\nu} = \frac{2}{\sqrt{-g}} \frac{\partial \mathcal{L}_{\mathrm{m}}}{\partial g_{\mu\nu}} , \tag{A.31}$$

where $g_{\mu\nu}$ are the components of the metric (A.25). The full action $S_{\mathrm{P}} + S_{\mathrm{matter}}$ is varied with respect to e and ω. Let $R_{\mu\nu} = g_{\nu\rho}\, \eta^{JK}\, e_K^{\sigma}\, e_I^{\rho}\, \Omega_{\mu\sigma}{}^I{}_J$ be the Ricci tensor and $R = g^{\mu\nu} R_{\mu\nu}$ the Ricci scalar. Einstein's field equations are then (see e.g. [17])

$$R_{\mu\nu} - \frac{1}{2} g_{\mu\nu} R = 8\pi G T_{\mu\nu} . \tag{A.32}$$

A.2.2 *Instantons*

As another application of the fiber bundle formalism, we describe how to construct **instantons**. These are special field configuations in Euclidean space-time with finite action. As a consequence, the field strength must vanish at a distance larger than a certain radius, say R, which defines a sphere $S^3 \subset \mathbb{R}^4$. Space-time gets compactifed to a four-sphere $\mathbb{R}^4 \cup \{\infty\} \cong S^4$ by an identification of the points at infinity. The origin is mapped to the south pole, $\{\infty\}$ to the north pole and the sphere S^3 to the equator of the four-sphere, as shown in Fig. 32. Instantons are now principal fiber bundles (gauge configurations) on S^4, which can be constructed via the clutching construction [250]. We start with trivial bundles with fibers $F \cong \mathbb{C}^3$ on the southern and northern hemispheres, D_- and D_+, respectively (i.e. the bundle is globally isomorphic to a simple product $D_\pm \times F$, see also Appendix A.2.1). The bundles overlap at the equator S^3. The fibers therefore have to be identified (possibly in some twisted way) along the equator with help of the clutching map $U : S^3 \to \mathrm{SU}(3)$. In local trivializations, the points $(x, v) \in D_+ \times F$ and $(x, U(x)\, v) \in D_- \times F$ are identified as shown in Fig. 32. We can still perform gauge transformations h_+ on D_+ and h_- on D_-. The function $U(x)$ is therefore defined only up to the equivalence relation

$$U(x) \sim h_+(x)\, U(x)\, h_-(x) . \tag{A.33}$$

Two functions $U(x)$ and $\widetilde{U}(x)$ defined on S^3 are called homotopic if $\widetilde{U}(x)\, U^{-1}(x)$ can be extended to a ball with boundary S^3. If this is the case, $h_+(x) := \widetilde{U}(x)\, U^{-1}(x)$ can be extended to a function on D_+ and can be taken as a gauge transformation. Therefore $U(x)$ and $\widetilde{U}(x)$ give rise to the same bundle (gauge field configuration up to gauge transformations). Hence, principle fiber bundles on S^4 are described by the equivalence classes obtained in this way. These equivalence classes build the third homotopy group $\pi_3(\mathrm{SU}(3))$ and gauge field configurations are divided into sectors according to

$$\pi_3\big(\mathrm{SU}(3)\big) \cong \pi_3\big(\mathrm{SU}(2)\big) \cong \pi_3(S^3) \cong \mathbb{Z} , \tag{A.34}$$

where any SU(2) subgroup was selected. In terms of the gauge bosons, the connection A_+ and A_- can be defined locally on D_+ and on D_-. We assumed that the field strength vanishes in the southern hemisphere. Since D_- is topologically trivial, the flat connection is unique and we can therefore choose the gauge $A_- \equiv 0$ on D_-. The whole topological information is now encoded in the transition function. On the overlap S^3, A_+ must satisfy

$$A_+(x) = U(x)^{-1} \Big(\frac{i}{g} d + A_-(x) \Big) U(x) = \frac{i}{g} U(x)^{-1}\, dU(x) . \tag{A.35}$$

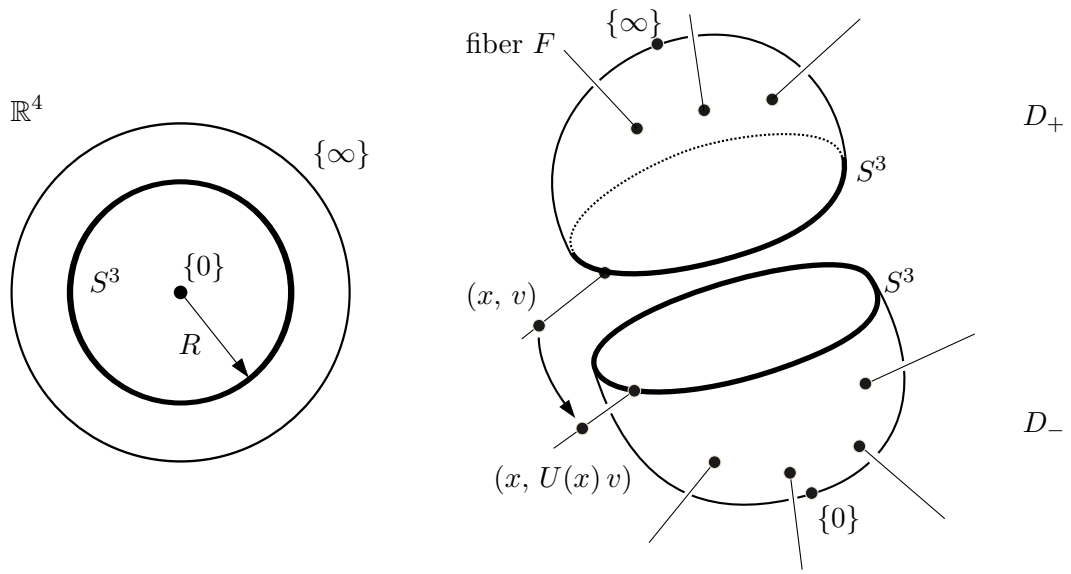

Figure 32: The original $\mathbb{R}^4$ on the left-hand side is compactified to a four-sphere. Instantons are principal bundles on the sphere S^4. They are constructed by gluing trivial bundles defined on the two hemispheres D^+ and D^- along the equator S^3 in a non-trivial way.

Translated back into the original $\mathbb{R}^4$, this is precisely the condition that the field strength vanishes at a distance R.

Gauge configuration can therefore be classified by integers, namely the second Chern class (which is a topological invariant) of the corresponding principal bundle, defined as

$$\begin{aligned} n &= \frac{g^2}{64\pi^2}\int d^4x\; \epsilon^{\mu\nu\rho\sigma} G^a_{\mu\nu} G^a_{\rho\sigma} = \frac{g^2}{32\pi^2}\int d^4x\; \partial_\mu J^\mu_{\mathrm{CS}} = \\ &= -\frac{i}{96\pi^2}\int_{S^3} d^3x\; f^{abc}\epsilon^{ijk}(U^{-1}\partial_i U)^a (U^{-1}\partial_j U)^b (U^{-1}\partial_k U)^c\,, \end{aligned} \tag{A.36}$$

with the Chern-Simons current

$$\begin{aligned} J^\mu_{\mathrm{CS}} &= \epsilon^{\mu\nu\rho\sigma}\Big(A^a_\nu G^a_{\rho\sigma} - \frac{g}{3} f^{abc} A^a_\nu A^b_\rho A^c_\sigma\Big) \\ &\xrightarrow{|x|\to\infty} \quad \frac{i}{3g^2} f^{abc}\epsilon^{\mu\nu\rho\sigma}(U^{-1}\partial_\mu U)^a (U^{-1}\partial_\rho U)^b (U^{-1}\partial_\sigma U)^c\,. \end{aligned} \tag{A.37}$$

The integrand of the last expression in Eq. (A.36) is identified as the Jacobian of the map U from S^3 to SU(3) and counts how often the configuration winds around an SU(2) subgroup of SU(3). The index n is therefore called **winding number**.

A.3 FLOW EQUATIONS

To compute the right-hand-side of Wetterich's flow equation, the effective action (4.97) with the ansatz (4.99) for the bosonic part of the potential is written in momentum space. The Fourier transformation is defined in Appendix A.1. The momentum dependence of the fields is indicated as an index. Moreover, we abbreviate

$$\int_p = \int \frac{d^4p}{(2\pi)^4} \tag{A.38}$$

The effective action then can be written down in momentum space:

$$\begin{aligned}\Gamma_k = &\int_p \bar{\psi}_p \, i\gamma_{\mathrm{E}}^{\mu} \, p_\mu \, \psi_p + \int_{p_1,p_2} \bar{\psi}_{p_1} g_s (\sigma_{p_1-p_2} + i\gamma_5 \, \boldsymbol{\pi}_{p_1-p_2} \cdot \boldsymbol{\tau}) \psi_{p_2} \\ &+ \int_p \bar{\psi}_p \gamma^0 (\boldsymbol{\mu} - g_\omega \, \omega_0 - g_\rho \, \rho_0^3 \tau^3) \psi_p \\ &+ \frac{1}{2} \int_p \phi^a_{-p} \, p^2 \, \phi^a_p + \sum_n \frac{a_{n,k}}{n!} \int_x \Big[\frac{1}{2} \int_{p_1} \int_{p_2} \mathrm{e}^{i(p_1+p_2)x} \, \phi^a_{p_1} \phi^a_{p_2} - \chi_0 \Big]^n \\ &+ \int_p \Big[m_\pi^2 f_\pi (f_\pi - \sigma_p) - \frac{1}{2} m_\omega^2 \omega_0^2 - \frac{1}{2} m_\rho^2 (\rho_0^3)^2 \Big].\end{aligned} \tag{A.39}$$

For simplicity, we do not write down the dependence of the coefficients $a_{n,k}$ on T, μ_p, μ_n, ω_0, and ρ_0^3 explicitly. In Wetterich's equation, the mixed derivatives of the effective action Γ_k with respect to both bosons and fermions are needed for the flow of the Yukawa couplings. Because this flow is neglected, only the diagonal terms in superspace (only bosonic or only fermionic derivatives) are needed. The matrix $\Gamma_k^{(1,1)}$ is diagonal, $\Gamma_k^{(1,1)} = \mathrm{diag}\,(\Gamma_{\mathrm{bos},k}^{(1,1)}, \Gamma_{\mathrm{fer},k}^{(1,1)})$, and can be inverted in bosonic and fermionic subspaces separately:

$$\begin{aligned}&\frac{1}{2} \operatorname{Tr} \left[k \frac{\partial R_k}{\partial k} \cdot \left(\Gamma_k^{(1,1)}[\Phi] + R_k \right)^{-1} \right] \\ &\quad = \frac{1}{2} \operatorname{Tr} \left[k \frac{\partial R_k^{\mathrm{bos}}}{\partial k} \cdot \left(\Gamma_{\mathrm{bos},k}^{(1,1)}[\Phi] + R_k^{\mathrm{bos}} \right)^{-1} \right] - \frac{1}{2} \operatorname{Tr} \left[k \frac{\partial R_k^{\mathrm{fer}}}{\partial k} \cdot \left(\Gamma_{\mathrm{fer},k}^{(1,1)}[\Phi] + R_k^{\mathrm{fer}} \right)^{-1} \right],\end{aligned} \tag{A.40}$$

where the fermionic loop comes with an additional minus-sign. The bosonic and fermionic loops are calculated in the following section.

A.3.1 *Bosonic part*

According to Eq. (3.50), the second derivative with respect to the bosonic fields is given by

$$\Gamma_{\mathrm{bos},k}^{(1,1)}(p,p') = \overrightarrow{\delta}_{\phi^a_{-p}} \, \Gamma_k \, \overleftarrow{\delta}_{\phi^b_{p'}}, \tag{A.41}$$

with $\phi^a = (\sigma, \boldsymbol{\pi})$. Inserting the effective action (A.39) gives

$$\begin{aligned}\Gamma^{(1,1)}_{\mathrm{bos},k}(p,p') = p^2\,\delta_{p-p'}\,\delta^a{}_b \\ + \sum_n \frac{a_{n+1,k}}{n!}\int_x \Big[\frac{1}{2}\int_{p_1}\int_{p_2} \mathrm{e}^{i(p_1+p_2)x}\,\phi^c_{p_1}\phi^c_{p_2} - \chi_0\Big]^n \cdot \mathrm{e}^{i(p'-p)x}\,\delta^a{}_b \\ + \sum_n \frac{a_{n+2,k}}{n!}\int_x \Big[\frac{1}{2}\int_{p_1}\int_{p_2} \mathrm{e}^{i(p_1+p_2)x}\,\phi^c_{p_1}\phi^c_{p_2} - \chi_0\Big]^n \\ \times \Big(\int_{p_3} \mathrm{e}^{i(p_3-p)x}\,\phi^a_{p_3}\Big)\cdot\Big(\int_{p_4} \mathrm{e}^{i(p_4+p')x}\,\phi_{b,p_4}\Big)\,.\end{aligned} \tag{A.42}$$

Because we are interested in the thermodynamics of nuclear matter, the fields are homogeneous. In momentum space they therefore have a sharp momentum and we set (by a slight abuse of notation) $\phi_p = \phi\cdot\delta_p$. Then, the effective action simplifies to

$$\begin{aligned}\Gamma^{(1,1)}_{\mathrm{bos},k}(p,p') &= p^2\,\delta_{p-p'}\,\delta^a{}_b \;+\; \sum_n \frac{a_{n+1,k}}{n!}\Big(\frac{1}{2}\phi^c\phi^c - \chi_0\Big)^n\cdot\delta_{p-p'}\,\delta^a{}_b \\ &\quad + \sum_n \frac{a_{n+2,k}}{n!}\Big(\frac{1}{2}\phi^c\phi^c - \chi_0\Big)^n\,\phi^a\phi_b\cdot\delta_{p-p'} \\ &= \Big[(p^2+U')\,\delta^a{}_b + U''\,\phi^a\phi_b\Big]\cdot\delta_{p-p'}\,.\end{aligned} \tag{A.43}$$

After adding the regulator $R^{\mathrm{bos}}_k = p^2 r_{\mathrm{bos}}$, the bosonic part can be diagonalized in complete analogy to the matrix $M^a{}_b$ in Eq. (4.44):

$$\begin{aligned}&(\Gamma^{(1,1)}_{\mathrm{bos},k} + R^{\mathrm{bos}}_k)(p,p') \\ &\qquad\cong \begin{pmatrix} p^2(1+r_{\mathrm{bos}}) + U' + 2\chi\,U'' & \\ & (p^2(1+r_b)+U')\cdot\mathbf{1}_{3\times3}\end{pmatrix}\cdot\delta_{p-p'}\,,\end{aligned} \tag{A.44}$$

where $\mathbf{1}_{3\times3}$ is the unit matrix in three dimensions. The inverse of the matrix (in a distributional sense) is given by

$$(\Gamma^{(1,1)}_{\mathrm{bos},k} + R^{\mathrm{bos}}_k)^{-1}(p,p') = \begin{pmatrix} \frac{1}{p^2(1+r_{\mathrm{bos}})+U'+2\chi\,U''} & \\ & \frac{\mathbf{1}_{3\times3}}{p^2(1+r_b)+U'}\end{pmatrix}\cdot\delta_{p-p'}\,. \tag{A.45}$$

According to Eq. (3.60), the optimal regulator at finite temperature is

$$R^{\mathrm{bos}}_k = p^2\,r_{\mathrm{bos}} = (k^2 - |\boldsymbol{p}|^2)\cdot\theta(k^2-|\boldsymbol{p}|^2)\,. \tag{A.46}$$

Moreover, the four-component is replaced by the discrete Matsubara frequencies $p_4 \to -\omega_l$ and the Euclidean integral $\int_p$ turns into a three-dimensional integral and a Matsubara sum. Taking the trace of the inverse propagator also yields a delta function evaluated at zero, which gives a volume factor βV. The bosonic contribution to Wetterich's equation is

$$\begin{aligned}&\frac{1}{2}\,\mathrm{Tr}\left[k\frac{\partial R^{\mathrm{bos}}_k}{\partial k}\cdot\Big(\Gamma^{(1,1)}_{\mathrm{bos},k}[\Phi] + R^{\mathrm{bos}}_k\Big)^{-1}\right] \\ &= \beta V\cdot T\sum_{\omega_l}\int\frac{d^3p}{(2\pi)^3}\,\frac{p^2k}{2}\,\frac{\partial r_{\mathrm{bos}}}{\partial k}\left[\frac{1}{p^2(1+r_{\mathrm{bos}})+U'+2\chi\,U''} + \frac{3}{p^2(1+r_{\mathrm{bos}})+U'}\right] \\ &= \beta V\cdot\int\frac{d^3p}{(2\pi)^3}k^2\cdot\theta(k^2-|\boldsymbol{p}|^2)\cdot T\sum_l\left[\frac{1}{\omega_l^2+k^2+U'+2\chi\,U''} + \frac{3}{\omega_l^2+k^2+U'}\right].\end{aligned} \tag{A.47}$$

With help of the identities

$$\begin{aligned}\sum_{l=-\infty}^{\infty} f(l) &= -\pi \sum_{\text{res } a_i} \text{Res}(f, a_i) \cdot \cot(\pi a_i)\,, \\ i\cot(ix) &= \coth(x) = 1 + \frac{2}{\mathrm{e}^{2x}-1}\,,\end{aligned} \tag{A.48}$$

the Matsubara sums over the momenta $\omega_l = 2l\pi T$ can be performed, with the result

$$T \sum_{l=-\infty}^{\infty} \frac{1}{\omega_l^2 + E^2} = \frac{1}{2E}\left[1 + 2n_{\mathrm{B}}(E)\right], \tag{A.49}$$

with the Bose distribution n_{B} defined in Appendix A.1. Finally, putting all parts together, one gets

$$\begin{aligned}&\frac{1}{2}\,\mathrm{Tr}\left[k\frac{\partial R_k^{\mathrm{bos}}}{\partial k} \cdot \left(\Gamma^{(1,1)}_{\mathrm{bos},k}[\Phi] + R_k^{\mathrm{bos}}\right)^{-1}\right] \\ &\qquad = \beta V \cdot \frac{k^5}{12\pi^2}\left\{\frac{1 + 2n_{\mathrm{B}}(E_\sigma)}{E_\sigma} + \frac{3\left[1 + 2n_{\mathrm{B}}(E_\pi)\right]}{E_\pi}\right\},\end{aligned} \tag{A.50}$$

with $E_\pi^2 = k^2 + U'$ and $E_\sigma^2 = k^2 + U' + 2\chi U''$.

A.3.2 *Fermionic part*

According to Eq. (3.50), the second derivative of the effective action with respect to the fermionic fields is the following matrix

$$\Gamma^{(1,1)}_{\mathrm{fer},k}(p,p') = \begin{pmatrix} \overrightarrow{\delta}_{\psi^T_{-p}} \Gamma_k \overleftarrow{\delta}_{\psi_{p'}} & \overrightarrow{\delta}_{\psi^T_{-p}} \Gamma_k \overleftarrow{\delta}_{\bar{\psi}^T_{-p'}} \\ \overrightarrow{\delta}_{\bar{\psi}_p} \Gamma_k \overleftarrow{\delta}_{\psi_{p'}} & \overrightarrow{\delta}_{\bar{\psi}_p} \Gamma_k \overleftarrow{\delta}_{\bar{\psi}^T_{-p'}} \end{pmatrix} \equiv \begin{pmatrix} 0 & A \\ B & 0 \end{pmatrix}, \tag{A.51}$$

where the diagonal terms vanish for the nucleon-meson model. They are non-vanishing only if higher powers in the fermionic fields are present. The matrix elements are computed from the effective action (A.39) and a version with transposed integrand, which was discussed in Eq. (A.20). First, we only consider one chemical potential, μ, and ignore the background fields ω_0 and ρ_0^3. In this case, the non-vanishing matrix elements are

$$\begin{aligned}A &= i(\gamma^\mu_{\mathrm{E}})^T p_\mu\, \delta_{p-p'} - g_s\left(\sigma_{p-p'} + i(\gamma_5)^T\, \boldsymbol{\pi}_{p-p'} \cdot \boldsymbol{\tau}^T\right) - (\gamma^0)^T\, \mu\, \delta_{p-p'}\,, \\ B &= i\gamma^\mu_{\mathrm{E}}\, p_\mu\, \delta_{p-p'} + g_s\left(\sigma_{p-p'} + i\gamma_5\, \boldsymbol{\pi}_{p-p'} \cdot \boldsymbol{\tau}\right) + \gamma^0\, \mu\, \delta_{p-p'}\,.\end{aligned} \tag{A.52}$$

The fields are again homogeneous, so we set

$$\phi_p = \phi \cdot \delta_p\,, \quad \psi_p = \psi \cdot \delta_p\,, \quad \bar{\psi}_p = \bar{\psi} \cdot \delta_p\,. \tag{A.53}$$

The regulator $R_k^{\mathrm{fer}} = \begin{pmatrix} 0 & ip_i(\gamma^i_{\mathrm{E}})^T \\ ip_i\gamma^i_{\mathrm{E}} & 0 \end{pmatrix} \cdot r_{\mathrm{fer}}$ is added and the matrix is inverted to yield

$$\left(\Gamma^{(1,1)}_{\mathrm{fer},k} + R_k^{\mathrm{fer}}\right)^{-1}(p,p') = \begin{pmatrix} 0 & C \\ D & 0 \end{pmatrix} \cdot \delta_{p-p'}\,, \tag{A.54}$$

where the matrix elements are

$$\begin{aligned} C &= \frac{-i(p_4 - i\mu)\gamma^0 - ip_i(1 + r_{\text{fer}})\,\gamma_{\text{E}}^i + g_s(\sigma - i\gamma_5\,\boldsymbol{\pi}\cdot\boldsymbol{\tau}) - \gamma^0\,\mu}{(p_4 - i\mu)^2 + |\boldsymbol{p}|^2(1 + r_{\text{fer}})^2 + 2g_s^2\chi}\,, \\ D &= \frac{-i(p_4 + i\mu)(\gamma^0)^T - ip_i(1 + r_{\text{fer}})\,(\gamma_{\text{E}}^i)^T - g_s(\sigma - i\gamma_5\,\boldsymbol{\pi}\cdot\boldsymbol{\tau}^T) + (\gamma^0)^T\mu}{(p_4 + i\mu)^2 + |\boldsymbol{p}|^2(1 + r_{\text{fer}})^2 + 2g_s^2\chi}\,. \end{aligned} \tag{A.55}$$

According to Eq. (3.60), the optimal Litim regulator at finite temperatures is

$$R_k^{\text{fer}} = \begin{pmatrix} 0 & ip_i(\gamma_{\text{E}}^i)^T \\ ip_i\gamma_{\text{E}}^i & 0 \end{pmatrix} r_{\text{fer}} = \begin{pmatrix} & ip_i(\gamma_{\text{E}}^i)^T \\ ip_i\gamma_{\text{E}}^i & \end{pmatrix} \left(\sqrt{\tfrac{k^2}{|\boldsymbol{p}|^2}} - 1\right)\theta(k^2 - |\boldsymbol{p}|^2)\,. \tag{A.56}$$

The fourth component of the momentum is again replaced by Matsubara frequencies, $p_4 \to -\omega_l$. A multiplication with $k\frac{\partial R_k^{\text{fer}}}{\partial k}$ and tracing over isospin space (factor two), Dirac space (factor 4), and momentum space (three infinite dimensions plus a Matsubara sum) yields the fermionic contribution to Wetterich's equation

$$\begin{aligned} &-\frac{1}{2}\,\text{Tr}\left[k\frac{\partial R_k^{\text{fer}}}{\partial k}\cdot\left(\Gamma_{\text{fer},k}^{(1,1)}[\Phi] + R_k^{\text{fer}}\right)^{-1}\right] \\ &\quad = -\beta V\cdot 2\cdot 4\cdot\frac{T}{2}\sum_{r=\pm1}\sum_l\int\frac{d^3p}{(2\pi)^3}\,|\boldsymbol{p}|^2(1 + r_{\text{fer}}) \\ &\qquad\qquad\qquad\qquad\times\frac{\partial r_{\text{fer}}}{\partial k}\,\frac{1}{(\omega_l + ri\mu)^2 + |\boldsymbol{p}|^2(1 + r_{\text{fer}})^2 + 2g_s^2\chi} \\ &\quad = -\beta V\cdot 2\cdot 4\cdot\int\frac{d^3p}{(2\pi)^3}k^2\theta(k^2 - |\boldsymbol{p}|^2)\cdot\frac{T}{2}\sum_{r=\pm1}\sum_l\frac{1}{(\omega_l + ri\mu)^2 + k^2 + 2g_s^2\chi}. \end{aligned} \tag{A.57}$$

Because the fermionic Matsubara frequencies $\omega_l = (2l+1)\pi T$ are summed over both positive and negative values and $r \to -r$ can be absorbed by $l \to -l$, the sum over $r = \pm1$ gives the same contribution twice. The Matsubara sum can be evaluated using Eq. (A.48) and

$$i\cot\left(\frac{\pi}{2} + ix\right) = \tanh x = 1 - \frac{2}{\mathrm{e}^{2x} + 1}\,, \tag{A.58}$$

which gives after a short computation

$$T\sum_l\frac{1}{(\omega_l + ri\mu)^2 + E^2} = \frac{1}{2E}\big[1 - n_{\text{F}}(E + \mu) - n_{\text{F}}(E - \mu)\big], \tag{A.59}$$

where the Fermi distribution n_{F} is defined in Appendix A.1. The nucleonic contribution to Wetterich's equation is given by

$$\begin{aligned} &-\frac{1}{2}\,\text{Tr}\left[k\frac{\partial R_k^{\text{fer}}}{\partial k}\cdot\left(\Gamma_{\text{fer},k}^{(1,1)}[\Phi] + R_k^{\text{fer}}\right)^{-1}\right] \\ &\qquad\qquad - \beta V\cdot\frac{k^5}{12\pi^2}\,\frac{2\cdot 4\big[1 - \sum_{r=\pm1} n_{\text{F}}(E_{\text{N}} - r\mu)\big]}{E_{\text{N}}}\,, \end{aligned} \tag{A.60}$$

with $E_{\text{N}}^2 = k^2 + 2g_s^2\chi$. Protons and neutrons enter in the same way. If the chemical potentials are different and the vector bosons are reinserted, the chemical potentials are

replaced by the effective chemical potentials $\mu_{i,\mathrm{eff}}$. Adding the bosonic contribution (A.50), the right-hand-side of Wetterich's equation is

$$\begin{aligned}\frac{1}{2}\,\mathrm{Tr}\left[k\frac{\partial R_k}{\partial k}\cdot\left(\Gamma_k^{(1,1)}[\Phi]+R_k\right)^{-1}\right]\\ =\beta V\cdot\frac{k^5}{12\pi^2}\Bigg\{\frac{1+2n_{\mathrm{B}}(E_\sigma)}{E_\sigma}+\frac{3\left[1+2n_{\mathrm{B}}(E_\pi)\right]}{E_\pi}\\ -\sum_{i=n,p}\frac{4\left[1-\sum_{r=\pm1}n_{\mathrm{F}}(E_{\mathrm{N}}-r\mu_{i,\mathrm{eff}})\right]}{E_{\mathrm{N}}}\Bigg\}.\end{aligned}\tag{A.61}$$

For an evaluation of the effective action as a Taylor expansion around the minimum, it is useful to work with the expression where the Matsubara sums are not yet computed. We define the threshold functions (because they describe the decoupling of modes as the renormalization group scale varies):

$$\begin{aligned}l_0^{\mathrm{bos}}(E)&=\frac{k^5}{6\pi^2}T\sum_l\frac{1}{\omega_l^2+E^2}\,,&&\omega_l=2l\pi T\,,\\ l_0^{\mathrm{fer}}(E,\mu)&=\frac{k^5}{6\pi^2}T\sum_l\frac{1}{(\omega_l+i\mu)^2+E^2}\,,&&\omega_l=(2l+1)\pi T\,.\end{aligned}\tag{A.62}$$

In terms of these threshold functions, the flow equation takes the form

$$\frac{1}{2}\,\mathrm{Tr}\left[k\frac{\partial R_k}{\partial k}\cdot\left(\Gamma_k^{(1,1)}[\Phi]+R_k\right)^{-1}\right]=\beta V\cdot\Big[l_0^{\mathrm{bos}}(E_\pi)+l_0^{\mathrm{bos}}(E_\sigma)-\sum_{i,n,p}l_0^{\mathrm{fer}}(E_{\mathrm{N}},\mu_{i,\mathrm{eff}})\Big].\tag{A.63}$$

BIBLIOGRAPHY

[1] L. D. Landau, "On the theory of stars," *Phys. Z. Sowjetunion* **1** (1932) 285.

[2] D. G. Yakovlev, *et al.*, "Lev Landau and the conception of neutron stars," *Phys. Usp.* **56** no. 3, (2012) 289–295, arXiv:1210.0682.

[3] J. Chadwick, "Possible Existence of a Neutron," *Nature* **192** (1932) 312.

[4] W. Baade and F. Zwicky, "Supernovae and Cosmic Rays," *Phys. Rev.* **45** (1934) 138.

[5] W. Baade and F. Zwicky, "On super-novae," *Proc. N. A. S.* **20** no. 5, (1934) 254–259.

[6] W. Baade and F. Zwicky, "Cosmic Rays from Super-Novae," *Proc. N. A. S.* **20** no. 5, (1934) 259–263.

[7] W. Baade and F. Zwicky, "Remarks on Super-Novae and Cosmic Rays," *Phys. Rev.* **46** no. 1, (1934) 76–77.

[8] P. B. Demorest, *et al.*, "A two-solar-mass neutron star measured using Shapiro delay," *Nature* **467** no. 7319, (2010) 1081–1083, arXiv:1010.5788.

[9] J. Antoniadis, *et al.*, "A Massive Pulsar in a Compact Relativistic Binary," *Science* **340** no. 6131, (2013) 1233232, arXiv:1304.6875.

[10] N. Kaiser, S. Fritsch, and W. Weise, "Chiral dynamics and nuclear matter," *Nucl. Phys. A* **697** no. 1-2, (2002) 255–276, arXiv:nucl-th/0406038.

[11] S. Fritsch, N. Kaiser, and W. Weise, "Chiral approach to nuclear matter: role of two-pion exchange with virtual delta-isobar excitation," *Nucl. Phys. A* **750** no. 2-4, (2005) 259–293, arXiv:nucl-th/0406038.

[12] S. Fiorilla, N. Kaiser, and W. Weise, "Chiral thermodynamics of nuclear matter," *Nucl. Phys. A* **880** (2012) 65–87, arXiv:1111.2791.

[13] S. Fiorilla, N. Kaiser, and W. Weise, "Nuclear thermodynamics and the in-medium chiral condensate," *Phys. Lett. B* **714** no. 2-5, (2012) 251–255, arXiv:1204.4318.

[14] N. Kaiser and W. Weise, "Chiral condensate in neutron matter," *Phys. Lett. B* **671** no. 1, (2009) 25–29, arXiv:0808.0856.

[15] T. Krüger, *et al.*, "The chiral condensate in neutron matter," *Phys. Lett. B* **726** (2013) 412, arXiv:1307.2110.

[16] C. Rovelli, "Why Gauge?," *Found. Phys.* **44** no. 1, (2014) 91–104, arXiv:1308.5599.

[17] C. W. Misner, K. S. Thorne, and J. A. Wheeler, *Gravitation*. W. H. Freeman, San Francisco, CA, 1973.

[18] R. M. Wald, *General Relativity*. University of Chicago Press, Chicago, 1984.

[19] G. Birkhoff, *Relativity and Modern Physics*. Harvard University Press, Cambridge, MA, 1923.

[20] R. C. Tolman, "Effect of inhomogeneity on cosmological models," *Proc. N. A. S.* **20** (1934) 169–176.

[21] R. C. Tolman, "Static Solutions of Einstein's Field Equations for Spheres of Fluid," *Phys. Rev.* **55** no. 4, (1939) 364–373.

[22] J. R. Oppenheimer and G. M. Volkoff, "On Massive Neutron Cores," *Phys. Rev.* **55** no. 4, (1939) 374–381.

[23] C. N. Yang and R. L. Mills, "Conservation of Isotopic Spin and Isotopic Gauge Invariance," *Phys. Rev.* **96** no. 1, (1954) 191–195.

[24] D. J. Gross and F. Wilczek, "Ultraviolet Behavior of Non-Abelian Gauge Theories," *Phys. Rev. Lett.* **30** no. 26, (1973) 1343.

[25] D. J. Gross and F. Wilczek, "Asymptotically Free Gauge Theories. I," *Phys. Rev. D* **8** no. 10, (1973) 3633.

[26] H. D. Politzer, "Reliable Perturbative Results for Strong Interactions?," *Phys. Rev. Lett.* **30** no. 26, (1973) 1346–1349.

[27] H. D. Politzer, "Asymptotic freedom: An approach to strong interactions," *Phys. Rep.* **14** no. 4, (1974) 129–180.

[28] J. Beringer, *et al.*, "Review of Particle Physics," *Phys. Rev. D* **86** no. 1, (2012) 010001.

[29] H. J. Rothe, *Lattice Gauge Theories: An Introduction*. World Scientific, Singapore, 3 ed., 2005.

[30] R. Alkofer and J. Greensite, "Quark Confinement: The Hard Problem of Hadron Physics," *J. Phys. G: Nucl. Part. Phys.* **34** (2007) S3, arXiv:hep-ph/0610365.

[31] G. S. Bali, "QCD forces and heavy quark bound states," *Phys. Rep.* **343** no. 1-2, (2001) 1–136, arXiv:hep-ph/0001312.

[32] G. 't Hooft, "Magnetic monopoles in unified gauge theories," *Nucl. Phys. B* **79** no. 2, (1974) 276–284.

[33] G. 't Hooft, "Topology of the gauge condition and new confinement phases in non-abelian gauge theories," *Nucl. Phys. B* **190** no. 3, (1981) 455–478.

[34] A. M. Polyakov, "Quark confinement and topology of gauge theories," *Nucl. Phys. B* **120** no. 3, (1977) 429–458.

[35] S. Mandelstam, "II. Vortices and quark confinement in non-Abelian gauge theories," *Phys. Rep.* **23** no. 3, (1976) 245–249.

[36] G. Ripka, *Dual superconductor models of color confinement*. No. 639 in Lecture Notes in Physics. Springer, Berlin, 2004. arXiv:hep-ph/0310102.

[37] N. Seiberg and E. Witten, "Monopole Condensation, And Confinement In $N = 2$ Supersymmetric Yang–Mills Theory," *Nucl. Phys. B* **426** (1994) 19–52, arXiv:hep-th/9407087.

[38] N. Seiberg and E. Witten, "Monopoles, Duality and Chiral Symmetry Breaking in $N = 2$ Supersymmetric QCD," *Nucl. Phys. B* **431** (1994) 484–550, arXiv:hep-th/9408099.

[39] T. Suzuki and I. Yotsuyanagi, "Possible evidence for Abelian dominance in quark confinement," *Phys. Rev. D* **42** no. 12, (1990) 4257–4260.

[40] H. Shiba and T. Suzuki, "Monopoles and string tension in SU(2) QCD," *Phys. Lett. B* **333** no. 3-4, (1994) 461–466, arXiv:hep-lat/9404015.

[41] A. D. Giacomo, *et al.*, "Colour confinement and dual superconductivity of the vacuum - I," *Phys. Rev. D* **61** no. 3, (2000) 034503, arXiv:hep-lat/9906024.

[42] A. D. Giacomo, *et al.*, "Colour confinement and dual superconductivity of the vacuum - II," *Phys. Rev. D* **61** no. 3, (2000) 034504, arXiv:hep-lat/9906025.

[43] K. Kondo, *et al.*, "Non-Abelian Dual Superconductor Picture for Quark Confinement," *Phys. Rev. D* **83** no. 11, (2011) 114016, arXiv:1007.2696.

[44] G. 't Hooft, "On the phase transition towards permanent quark confinement," *Nucl. Phys. B* **138** no. 1, (1978) 1–25.

[45] H. B. Nielsen and P. Olesen, "A quantum liquid model for the QCD vacuum: Gauge and rotational invariance of domained and quantized homogeneous color fields," *Nucl. Phys. B* **160** no. 2, (1979) 380–396.

[46] T. Kugo and I. Ojima, "Local Covariant Operator Formalism of Non-Abelian Gauge Theories and Quark Confinement Problem," *Prog. Theor. Phys. Suppl.* **66** (1979) 1–130.

[47] V. N. Gribov, "Quantization of non-Abelian gauge theories," *Nucl. Phys. B* **139** no. 1-2, (1978) 1–19.

[48] D. Zwanziger, "Fundamental modular region, Boltzmann factor and area law in lattice theory," *Nucl. Phys. B* **412** no. 3, (1994) 657–730.

[49] L. von Smekal, A. Hauck, and R. Alkofer, "Infrared Behavior of Gluon and Ghost Propagators in Landau Gauge QCD," *Phys. Rev. Lett.* **79** no. 19, (1997) 3591–3594, arXiv:hep-ph/9705242.

[50] J. M. Pawlowski, *et al.*, "Infrared behaviour and fixed points in Landau gauge QCD," *Phys. Rev. Lett.* **93** (2004) 152002, arXiv:hep-th/0312324.

[51] F. D. R. Bonnet, *et al.*, "Infrared Behavior of the Gluon Propagator on a Large Volume Lattice," *Phys. Rev. D* **62** no. 5, (2000) 051501, arXiv:hep-lat/0002020.

[52] J. Gattnar, K. Langfeld, and H. Reinhardt, "Signals of confinement in Green functions of SU(2) Yang–Mills theory," *Phys. Rev. Lett.* **93** no. 6, (2004) 061601, arXiv:hep-lat/0403011.

[53] A. Sternbeck, *et al.*, "Comparing SU(2) to SU(3) gluodynamics on large lattices," *PoS LAT2007* (2007) 340, arXiv:0710.1982.

[54] A. Cucchieri and T. Mendes, "What's up with IR gluon and ghost propagators in Landau gauge? A puzzling answer from huge lattices," *PoS LAT2007* (2007) 297, arXiv:0710.0412.

[55] A. Cucchieri, *et al.*, "Just how different are SU(2) and SU(3) Landau-gauge propagators in the IR regime?," *Phys. Rev. D* **76** no. 11, (2007) 114507, arXiv:0705.3367.

[56] J. Braun, H. Gies, and J. M. Pawlowski, "Quark confinement from colour confinement," *Phys. Lett. B* **684** no. 4-5, (2010) 262–267, arXiv:0708.2413.

[57] S. Weinberg, "Phenomenological Lagrangians," *Physica* **A96** (1979) 327–340.

[58] R. F. Streater, R. F. Streater, and A. S. Wightman, *PCT, Spin and Statistics, and All That*. Princeton University Press, Princeton, NJ, 1963.

[59] A. A. Belavin, *et al.*, "Pseudoparticle solutions of the Yang-Mills equations," *Phys. Lett. B* **59** no. 1, (1975) 85–87.

[60] R. Jackiw and C. Rebbi, "Vacuum Periodicity in a Yang-Mills Quantum Theory," *Phys. Rev. Lett.* **37** no. 3, (1976) 172—175.

[61] C. G. Callan, R. F. Dashen, and D. J. Gross, "The structure of the gauge theory vacuum," *Phys. Lett. B* **63** no. 3, (1976) 334–340.

[62] K. F. Freed, "Path Integrals and Semiclassical Tunneling, Wavefunctions, and Energies," *J. Chem. Phys.* **56** no. 2, (1972) 692–697.

[63] S. K. Donaldson, "Self-dual connections and the topology of smooth 4-manifolds," *Bull. Amer. Math. Soc.* **8** no. 1, (1983) 81–83.

[64] M. F. Atiyah, *et al.*, "Construction of instantons," *Phys. Lett. A* **65** no. 3, (1978) 185–187.

[65] S. Weinberg, *The Quantum Theory of Fields, Volume 2: Modern Applications*. Cambridge University Press, Cambridge, MA, 1996.

[66] C. A. Baker, *et al.*, "Improved Experimental Limit on the Electric Dipole Moment of the Neutron," *Phys. Rev. Lett.* **97** no. 13, (2006) 131801, arXiv:hep-ex/0602020v3.

[67] R. D. Peccei and H. R. Quinn, "CP Conservation in the Presence of Pseudoparticles," *Phys. Rev. Lett.* **38** no. 25, (1977) 1440–1443.

[68] R. D. Peccei and H. R. Quinn, "Constraints imposed by CP conservation in the presence of pseudoparticles," *Phys. Rev. D* **16** no. 6, (1977) 1791–1797.

[69] K. Fujikawa, "Path-Integral Measure for Gauge-Invariant Fermion Theories," *Phys. Rev. Lett.* **42** no. 18, (1979) 1195–1198.

[70] K. Fujikawa, "Path integral for gauge theories with fermions," *Phys. Rev. D* **21** no. 10, (1980) 2848–2858.

[71] T. Banks and A. Casher, "Chiral symmetry breaking in confining theories," *Nucl. Phys. B* **169** no. 1-2, (1980) 103–125.

[72] M. F. Atiyah and I. M. Singer, "The index of elliptic operators on compact manifolds," *Bull. Amer. Math. Soc.* **69** no. 3, (1963) 422–433.

[73] T. Schäfer and E. V. Shuryak, "Instantons in QCD," *Rev. Mod. Phys.* **70** no. 2, (1998) 323–425, arXiv:hep-ph/9610451v3.

[74] D. Trewartha, *et al.*, "Quark Propagation in the Instantons of Lattice QCD," *Phys. Rev. D* **88** no. 3, (2013) 034501, arXiv:1306.3283.

[75] L. Y. Glozman, C. B. Lang, and M. Schröck, "Symmetries of hadrons after unbreaking the chiral symmetry," *Phys. Rev. D* **86** no. 1, (2012) 014507, arXiv:1205.4887.

[76] G. 't Hooft, "Symmetry Breaking through Bell-Jackiw Anomalies," *Phys. Rev. Lett.* **37** no. 1, (1976) 8–11.

[77] C. Vafa and E. Witten, "Restrictions on symmetry breaking in vector-like gauge theories," *Nucl. Phys. B* **234** no. 1, (1984) 173–188.

[78] J. Goldstone, "Field theories with "Superconductor" solutions," *Nuov. Cim.* **19** no. 1, (1961) 154–164.

[79] J. Goldstone, A. Salam, and S. Weinberg, "Broken Symmetries," *Phys. Rev.* **127** no. 3, (1962) 965–970.

[80] M. Gell-Mann, R. J. Oakes, and B. Renner, "Behavior of Current Divergences under SU(3)×SU(3)," *Phys. Rev.* **175** no. 5, (1968) 2195–2199.

[81] P. Boucaud, *et al.*, "Dynamical Twisted Mass Fermions with Light Quarks," *Phys. Lett. B* **650** (2007) 304–311, arXiv:hep-lat/0701012.

[82] H. Fukaya, *et al.*, "Determination of the chiral condensate from QCD Dirac spectrum on the lattice," *Phys. Rev. D* **83** no. 7, (2011) 074501, arXiv:1012.4052.

[83] K. Fukushima and C. Sasaki, "The phase diagram of nuclear and quark matter at high baryon density," *Prog. Part. Nucl. Phys.* **72** (2013) 99, arXiv:1301.6377.

[84] J. Adams, *et al.*, "Experimental and theoretical challenges in the search for the quark-gluon plasma: The STAR Collaboration's critical assessment of the evidence from RHIC collisions," *Nucl. Phys. A* **757** no. 1-2, (2005) 102–183, arXiv:nuclex/0501009.

[85] K. Adcox, *et al.*, "Formation of dense partonic matter in relativistic nucleus-nucleus collisions at RHIC: Experimental evaluation by the PHENIX Collaboration," *Nucl. Phys. A* **757** no. 1-2, (2005) 184–283, arXiv:nuclex/0410003.

[86] B. Back, *et al.*, "The PHOBOS perspective on discoveries at RHIC," *Nucl. Phys. A* **757** no. 1-2, (2005) 28–101, arXiv:nuclex/0410022.

[87] I. Arsene, *et al.*, "Quark-gluon plasma and color glass condensate at RHIC? The perspective from the BRAHMS experiment," *Nucl. Phys. A* **757** no. 1-2, (2005) 1–27, arXiv:nuclex/0410020.

[88] R. J. Fries and C. Nonaka, "Evaluating Results from the Relativistic Heavy Ion Collider with Perturbative QCD and Hydrodynamics," *Prog. Part. Nucl. Phys.* **66** no. 3, (2010) 607–660, arXiv:1012.1881.

[89] T. Hirano, *et al.*, "Integrated Dynamical Approach to Relativistic Heavy Ion Collisions," *Prog. Part. Nucl. Phys.* **70** (2013) 108–158, arXiv:1204.5814.

[90] U. Heinz, "Towards the Little Bang Standard Model," *J. Phys.: Conf. Ser.* **455** no. 1, (2013) 012044, arXiv:1304.3634.

[91] P. F. Kolb and U. Heinz, "Hydrodynamic description of ultrarelativistic heavy-ion collisions," in *Quark-Gluon Plasma*, p. 634. World Scientific, Singapore, 2004. arXiv:nucl-th/0305084.

[92] U. W. Heinz and R. Snellings, "Collective flow and viscosity in relativistic heavy-ion collisions," *Ann. Rev. Nucl. Part. Sci.* **63** no. 1, (2013) 123–151, arXiv:1301.2826.

[93] H. Song and U. W. Heinz, "Extracting the QGP viscosity from RHIC data - a status report from viscous hydrodynamics," *J. Phys. G* **36** (2009) 064033, arXiv:0812.4274.

[94] H. Song, "QGP viscosity at RHIC and the LHC - a 2012 status report," *Nucl. Phys. A* **904-905** (2013) 114–121, arXiv:1210.5778.

[95] C. Gale, *et al.*, "Event-by-event anisotropic flow in heavy-ion collisions from combined Yang-Mills and viscous fluid dynamics," *Phys. Rev. Lett.* **110** (2013) 012302, arXiv:1209.6330.

[96] H. Song, S. A. Bass, and U. Heinz, "Elliptic flow in $\sqrt{s} = 200$ GeV Au+Au collisions and $\sqrt{s} = 2.76$ TeV Pb+Pb collisions: Insights from viscous hydrodynamics + hadron cascade hybrid model," *Phys. Rev. C* **83** no. 5, (2011) 054912, arXiv:1103.2380.

[97] P. K. Kovtun, D. T. Son, and A. O. Starinets, "Viscosity in Strongly Interacting Quantum Field Theories from Black Hole Physics," *Phys. Rev. Lett.* **94** no. 11, (2005) 111601, arXiv:hep-th/0405231.

[98] P. Braun-Munzinger, *et al.*, "Thermal Equilibration and Expansion in Nucleus-Nucleus Collision at the AGS," *Phys. Lett. B* **344** no. 1-4, (1995) 43–48, arXiv:nucl-th/9410026.

[99] J. Manninen and F. Becattini, "Chemical freeze-out in ultrarelativistic heavy ion collisions at $\sqrt{s_{NN}} = 130$ and 200 GeV," *Phys. Rev. C* **78** no. 5, (2008) 054901, arXiv:0806.4100v4.

[100] A. Andronic, P. Braun-Munzinger, and J. Stachel, "Thermal hadron production in relativistic nuclear collisions: The hadron mass spectrum, the horn, and the QCD phase transition," *Phys. Lett. B* **673** no. 2, (2009) 142–145, arXiv:0812.1186.

[101] F. Karsch, "Determination of freeze-out conditions from lattice QCD calculations," *Centr. Eur. J. Phys.* **10** no. 6, (2012) 1234–1237, arXiv:1202.4173.

[102] A. Bazavov, *et al.*, "Freeze-out Conditions in Heavy Ion Collisions from QCD Thermodynamics," *Phys. Rev. Lett.* **109** no. 19, (2012) 1292302, arXiv:1208.1220.

[103] A. Andronic, P. Braun-Munzinger, and J. Stachel, "Hadron production in central nucleus-nucleus collisions at chemical freeze-out," *Nucl. Phys. A* **772** (2006) 167–199, arXiv:nucl-th/0511071.

[104] A. Bazavov, *et al.*, "The chiral and deconfinement aspects of the QCD transition," *Phys. Rev. D* **85** (2012) 054503, arXiv:1111.1710.

[105] S. Borsányi, *et al.*, "Is there still any T_c mystery in lattice QCD? Results with physical masses in the continuum limit III," *JHEP* **2010** no. 9, (2010) 1–26, arXiv:1005.3508.

[106] P. Braun-Munzinger, J. Stachel, and C. Wetterich, "Chemical freeze-out and the QCD phase transition temperature," *Phys. Lett. B* **596** no. 1–2, (2004) 61–69, arXiv:nucl-th/0311005.

[107] J. Cleymans, *et al.*, "Comparison of chemical freeze-out criteria in heavy-ion collisions," *Phys. Rev. C* **73** no. 3, (2006) 034905, arXiv:hep-ph/0511094.

[108] S. Borsányi, *et al.*, "Freeze-out parameters: lattice meets experiment," *Phys. Rev. Lett.* **111** (2013) 062005, arXiv:1305.5161.

[109] P. Alba, *et al.*, "Freeze-out conditions from net-proton and net-charge fluctuations at RHIC," arXiv:1403.4903.

[110] L. McLerran and R. D. Pisarski, "Phases of Dense Quarks at Large N_c," *Nucl. Phys. A* **796** no. 1-4, (2007) 83–100, arXiv:0706.2191.

[111] A. Andronic, *et al.*, "Hadron production in ultra-relativistic nuclear collisions: Quarkyonic matter and a triple point in the phase diagram of QCD," *Nucl. Phys. A* **837** no. 1–2, (2010) 65—86, arXiv:0911.4806.

[112] B. Schaefer, J. M. Pawlowski, and J. Wambach, "The Phase Structure of the Polyakov–Quark-Meson Model," *Phys. Rev. D* **76** (2007) 074023, arXiv:0704.3234.

[113] T. K. Herbst, J. M. Pawlowski, and B. Schaefer, "The phase structure of the Polyakov-quark-meson model beyond mean field," *Phys. Lett. B* **696** no. 1-2, (2011) 58–67, arXiv:1008.0081.

[114] D. Nickel, "How Many Phases Meet at the Chiral Critical Point?," *Phys. Rev. Lett.* **103** no. 7, (2009) 072301, arXiv:0902.1778.

[115] K. Fukushima and P. A. Morales, "Spatial Modulation and Topological Current in Holographic QCD Matter," *Phys. Rev. Lett.* **111** no. 5, (2013) 051601, arXiv:1305.4115.

[116] O. Philipsen, "The QCD phase diagram at zero and small baryon density," *PoS LAT2005* (2005) 016, arXiv:hep-lat/0510077.

[117] C. Schmidt, "Lattice QCD at Finite Density," *PoS LAT2006* (2006) 021, arXiv:hep-lat/0610116.

[118] O. Philipsen, "Status of Lattice Studies of the QCD Phase Diagram," *Prog. Theor. Phys. Suppl.* **174** (2008) 206–213, arXiv:0808.0672.

[119] P. de Forcrand, "Simulating QCD at finite density," *PoS LAT2009* (2009) 010, arXiv:1005.0539.

[120] O. Kaczmarek, *et al.*, "Phase boundary for the chiral transition in (2+1)-flavor QCD at small values of the chemical potential," *Phys. Rev. D* **83** no. 1, (2011) 014504, arXiv:1011.3130.

[121] G. Endrodi, *et al.*, "The QCD phase diagram at nonzero quark density," *JHEP* **04** no. 001, (2011) 1–14, arXiv:1102.1356.

[122] F. R. Brown, *et al.*, "On the existence of a phase transition for QCD with three light quarks," *Phys. Rev. Lett.* **65** no. 20, (1990) 2491–2494.

[123] R. D. Pisarski and F. Wilczek, "Remarks on the chiral phase transition in chromodynamics," *Phys. Rev. D* **29** no. 2, (1984) 338–341.

[124] P. de de Forcrand and O. Philipsen, "The chiral critical point of $N_f = 3$ QCD at finite density to the order $(\mu/T)^4$," *JHEP* **0811** (2008) 012, arXiv:0808.1096.

[125] C. S. Fischer and J. Luecker, "Propagators and phase structure of $N_f = 2$ and $N_f = 2 + 1$ QCD," *Phys. Lett. B* **718** (2013) 1036–1043, arXiv:1206.5191.

[126] C. S. Fischer, *et al.*, "Polyakov loop potential at finite density," *Phys. Lett. B* **732** (2014) 273–277, arXiv:1306.6022.

[127] Y. Nambu and G. Jona-Lasinio, "Dynamical Model of Elementary Particles Based on an Analogy with Superconductivity. I," *Phys. Rev.* **122** no. 1, (1961) 345.

[128] Y. Nambu and G. Jona-Lasinio, "Dynamical Model of Elementary Particles Based on an Analogy with Superconductivity. II," *Phys. Rev.* **124** no. 1, (1961) 246.

[129] U. Vogl and W. Weise, "The Nambu and Jona-Lasinio model: Its implications for Hadrons and Nuclei," *Prog. Part. Nucl. Phys.* **27** (1991) 195–272.

[130] K. Fukushima, "Chiral effective model with the Polyakov loop," *Phys. Lett. B* **591** no. 3-4, (2004) 277–284, arXiv:hep-ph/0310121.

[131] C. Ratti, M. A. Thaler, and W. Weise, "Phases of QCD: Lattice thermodynamics and a field theoretical model," *Phys. Rev. D* **73** no. 1, (2006) 014019, arXiv:hep-ph/0506234.

[132] C. Ratti, *et al.*, "Thermodynamics of the PNJL model," *Eur. Phys. J. C* **49** no. 1, (2007) 213–217, arXiv:hep-ph/0609218.

[133] S. Rößner, C. Ratti, and W. Weise, "Polyakov loop, diquarks, and the two-flavor phase diagram," *Phys. Rev. D* **75** no. 3, (2007) 034007, arXiv:hep-ph/0609281.

[134] C. Sasaki, B. Friman, and K. Redlich, "Density Fluctuations as Signature of a Non-Equilibrium First Order Phase Transition," *J. Phys. G* **35** (2008) 104095, arXiv:0804.3990.

[135] K. Fukushima, "Isentropic thermodynamics in the Polyakov–Nambu–Jona-Lasinio model," *Phys. Rev. D* **79** no. 7, (2009) 074015, arXiv:0901.0783.

[136] M. Cristoforetti, *et al.*, "Thermodynamics and quark susceptibilities: A Monte Carlo approach to the Polyakov–Nambu–Jona-Lasinio model," *Phys. Rev. D* **81** no. 11, (2010) 114017, arXiv:1002.2336.

[137] T. Hell, *et al.*, "Dynamics and thermodynamics of a nonlocal Polyakov–Nambu–Jona-Lasinio model with running coupling," *Phys. Rev. D* **79** no. 1, (2009) 014022, arXiv:0810.1099.

[138] S. Klimt, M. Lutz, and W. Weise, "Chiral phase transition in the SU(3) Nambu and Jona-Lasinio model," *Phys. Lett. B* **249** no. 3–4, (1990) 386–390.

[139] C. Sasaki, B. Friman, and K. Redlich, "Quark Number Fluctuations in a Chiral Model at Finite Baryon Chemical Potential," *Phys. Rev. D* **75** (2007) 054026, arXiv:hep-ph/0611143.

[140] M. Kitazawa, *et al.*, "Chiral and Color-Superconducting Phase Transitions with Vector Interaction in a Simple Model," *Prog. Theor. Phys.* **108** no. 5, (2002) 929–951, arXiv:hep-ph/0207255.

[141] K. Fukushima, "Phase diagrams in the three-flavor Nambu–Jona-Lasinio model with the Polyakov loop," *Phys. Rev. D* **77** (2008) 114028, arXiv:0803.3318.

[142] N. M. Bratovic, T. Hatsuda, and W. Weise, "Role of Vector Interaction and Axial Anomaly in the PNJL Modeling of the QCD Phase Diagram," *Phys. Lett. B* **719** (2013) 131–135, arXiv:1204.3788.

[143] T. Hell, K. Kashiwa, and W. Weise, "Impact of Vector-Current Interactions on the QCD Phase Diagram," *Jour. Mod. Phys.* **04** no. 05, (2013) 644–650, arXiv:1212.4017.

[144] K. Fukushima, "Critical surface in hot and dense QCD with the vector interaction," *Phys. Rev. D* **78** (2008) 114019, arXiv:0809.3080.

[145] R. Friedberg and T. D. Lee, "Fermion-field nontopological solitons," *Phys. Rev. D* **15** no. 6, (1977) 1694–1711.

[146] B. Schaefer and J. Wambach, "Susceptibilities near the QCD (tri)critical point," *Phys. Rev. D* **75** (2007) 085015, arXiv:hep-ph/0603256.

[147] E. S. Bowman and J. I. Kapusta, "Critical points in the linear sigma model with quarks," *Phys. Rev. C* **79** no. 1, (2009) 015202, arXiv:0810.0042.

[148] B. Schaefer, M. Wagner, and J. Wambach, "Thermodynamics of (2+1)-flavor QCD: Confronting models with lattice studies," *Phys. Rev. D* **81** no. 7, (2010) 074013, arXiv:0910.5628.

[149] B. Schaefer and M. Wagner, "QCD critical region and higher moments for three flavor models," *Phys. Rev. D* **85** (2012) 034027, arXiv:1111.6871.

[150] J. Berges, D. Jungnickel, and C. Wetterich, "Quark and Nuclear Matter in the Linear Chiral Meson Model," *Int. J. Mod. Phys. A* **18** no. 18, (2003) 3189–3219, arXiv:hep-ph/9811387.

[151] V. Skokov, *et al.*, "Meson fluctuations and thermodynamics of the Polyakov-loop-extended quark-meson model," *Phys. Rev. C* **82** no. 1, (2010) 015206, arXiv:1004.2665.

[152] V. Skokov, B. Friman, and K. Redlich, "Quark number fluctuations in the Polyakov loop-extended quark-meson model at finite baryon density," *Phys. Rev. C* **83** no. 5, (2011) 054904, arXiv:1008.4570v1.

[153] T. K. Herbst, J. M. Pawlowski, and B. Schaefer, "On the Phase Structure and Thermodynamics of QCD," *Phys. Rev. D* **88** (2013) 014007, arXiv:1302.1426.

[154] H. Yukawa, "Interactions of elementary particles. Part I," *Pr. phys.-math. Soc. Japan* **17** (1935) 48–57.

[155] R. Machleidt, "The Meson Theory of Nuclear Forces and Nuclear Structure," *Adv. Nucl. Phys.* **19** (1989) 189–376.

[156] M. H. Johnson and E. Teller, "Classical Field Theory of Nuclear Forces," *Phys. Rev.* **98** no. 3, (1955) 783–787.

[157] I. Caprini, G. Colangelo, and H. Leutwyler, "Mass and Width of the Lowest Resonance in QCD," *Phys. Rev. Lett.* **96** no. 13, (2006) 132001, arXiv:hep-ph/0512364.

[158] R. Garcia-Martin, J. R. Pelaez, and F. J. Yndurain, "Experimental status of the $\pi\pi$ isoscalar S wave at low energy: $f_0(600)$ pole and scattering length," *Phys. Rev. D* **76** (2007) 074034, arXiv:hep-ph/0701025.

[159] J. Walecka, "A theory of highly condensed matter," *Ann. Phys.* **83** no. 2, (1974) 491–529.

[160] M. Gell-Mann and M. Lévy, "The axial vector current in beta decay," *Nuov. Cim.* **16** no. 4, (1960) 705–726.

[161] S. Weinberg, "Dynamical Approach to Current Algebra," *Phys. Rev. Lett.* **18** no. 5, (1967) 188–191.

[162] S. Scherer, "Introduction to Chiral Perturbation Theory," *Adv. Nucl. Phys.* **27** (2003) 277–538, arXiv:hep-ph/0210398.

[163] E. Epelbaum, H. Hammer, and U. Meißner, "Modern theory of nuclear forces," *Rev. Mod. Phys.* **81** no. 4, (2009) 1773–1825, arXiv:0811.1338.

[164] R. Machleidt and D. R. Entem, "Chiral effective field theory and nuclear forces," *Phys. Rep.* **503** (2011) 1–75, arXiv:1105.2919.

[165] J. W. Holt, N. Kaiser, and W. Weise, "Nuclear chiral dynamics and thermodynamics," *Prog. Part. Nucl. Phys.* **73** (2013) 35, arXiv:1304.6350.

[166] S. Floerchinger and C. Wetterich, "Chemical freeze-out in heavy ion collisions at large baryon densities," *Nucl. Phys. A* **890-891** no. 11, (2012) 11–24, arXiv:1202.1671.

[167] R. Hofstadter, "Electron Scattering and Nuclear Structure," *Rev. Mod. Phys.* **28** no. 3, (1956) 214–254.

[168] P. Moller, *et al.*, "Nuclear Ground-State Masses and Deformations," *Atomic Data and Nuclear Data Tables* **59** no. 2, (1995) 185–381.

[169] M. B. Tsang, *et al.*, "Constraints on the symmetry energy and neutron skins from experiments and theory," *Phys. Rev. C* **86** no. 1, (2012) 015803, arXiv:1204.0466.

[170] J. M. Lattimer and Y. Lim, "Constraining the Symmetry Parameters of the Nuclear Interaction," *ApJ* **771** no. 1, (2013) 51, arXiv:1203.4286.

[171] J. M. Lattimer and A. W. Steiner, "Constraints on the Symmetry Energy Using the Mass-Radius Relation of Neutron Stars," *EPJ A* **50** no. 2, (2014) 40, arXiv:1403.1186.

[172] L. D. Landau, "On the quantum theory of fields," in *Niels Bohr and the Development of Physics*, p. 52. Pergamon Press, New York, 1955.

[173] R. Fernandez, J. Fröhlich, and A. D. Sokal, *Random walks, critical phenomena, and triviality in quantum field theory*. Springer, Berlin, Heidelberg, 1992.

[174] B. S. DeWitt, *Dynamical theory of groups and fields*. Gordon and Breach, New York, 1965.

[175] M. L. Bellac, *Thermal Field Theory*. Cambridge University Press, Cambridge, MA, 1996.

[176] J. I. Kapusta and C. Gale, *Finite-Temperature Field Theory: Principles and Applications*. Cambridge University Press, Cambridge, MA, 2006.

[177] K. G. Wilson and J. Kogut, "The renormalization group and the ϵ expansion," *Phys. Rep.* **12** no. 2, (1974) 75–199.

[178] K. Huang, "A Critical History of Renormalization," *Int. J. Mod. Phys. A* **28** (2013) 1330050, arXiv:1310.5533.

[179] J. Polchinski, "Renormalization and effective lagrangians," *Nucl. Phys. B* **231** no. 2, (1984) 269–295.

[180] O. J. Rosten, "Fundamentals of the Exact Renormalization Group," *Phys. Rep.* **511** no. 4, (2012) 177–272, arXiv:1003.1366.

[181] C. Bagnuls and C. Bervillier, "Exact Renormalization Group Equations. An Introductory Review," *Phys. Rep.* **348** no. 1-2, (2001) 91–157, arXiv:hep-th/0002034.

[182] J. Polonyi, "Lectures on the functional renormalization group method," *Central Eur. J. Phys.* **1** (2003) 1–71, arXiv:hep-th/0110026.

[183] J. Berges, N. Tetradis, and C. Wetterich, "Non-Perturbative Renormalization Flow in Quantum Field Theory and Statistical Physics," *Phys. Rep.* **363** (2002) 223–386, arXiv:hep-ph/0005122.

[184] J. M. Pawlowski, "Aspects of the Functional Renormalisation Group," *Ann. Phys.* **322** (2007) 2831–2915, arXiv:hep-th/0512261.

[185] B. Schaefer and J. Wambach, "Renormalization group approach towards the QCD phase diagram," *Phys. Part. Nuclei* **39** no. 7, (2008) 1025–1032, arXiv:hep-ph/0611191.

[186] P. Kopietz, L. Bartosch, and F. Schütz, *Introduction to the Functional Renormalization Group*. Springer, Berlin, Heidelberg, 2010.

[187] H. Gies, "Introduction to the Functional RG and Applications to Gauge Theories," in *Renormalization Group and Effective Field Theory Approaches to Many-Body Systems*, no. 852 in Lecture Notes in Physics, pp. 287–348. Springer Berlin Heidelberg, 2012.

[188] B. Delamotte, "An Introduction to the Nonperturbative Renormalization Group," in *Renormalization Group and Effective Field Theory Approaches to Many-Body Systems*, no. 852 in Lecture Notes in Physics, pp. 49–132. Springer, Berlin, Heidelberg, 2012.

[189] J. Braun, "Fermion interactions and universal behavior in strongly interacting theories," *J. Phys. G: Nucl. Part. Phys.* **39** no. 3, (2012) 033001, arXiv:1108.4449.

[190] C. Wetterich, "Exact evolution equation for the effective potential," *Phys. Lett. B* **301** no. 1, (1993) 90–94.

[191] G. R. Golner, "Nonperturbative renormalization-group calculations for continuum spin systems," *Phys. Rev. B* **33** no. 11, (1986) 7863–7866.

[192] C. Wetterich, "Improvement of the average action," *Z. Phys. C* **60** no. 3, (1993) 461–469.

[193] J. F. Nicoll, T. S. Chang, and H. E. Stanley, "Approximate Renormalization Group Based on the Wegner-Houghton Differential Generator," *Phys. Rev. Lett.* **33** no. 9, (1974) 540–543.

[194] N. Tetradis and C. Wetterich, "Critical exponents from the effective average action," *Nucl. Phys. B* **422** no. 3, (1994) 541–592.

[195] D. F. Litim, "Optimised Renormalisation Group Flows," *Phys. Rev. D* **64** (2001) 105007, arXiv:hep-th/0103195.

[196] D. F. Litim and J. M. Pawlowski, "Non-perturbative thermal flows and resummations," *JHEP* **0611** (2006) 026, arXiv:hep-th/0609122.

[197] J. Blaizot, *et al.*, "Perturbation theory and non-perturbative renormalization flow in scalar field theory at finite temperature," *Nucl. Phys. A* **784** (2007) 376–406, arXiv:hep-ph/0610004.

[198] J. Adams, *et al.*, "Solving non-perturbative flow equations," *Mod. Phys. Lett. A* **10** (1995) 2367–2380, arXiv:hep-th/9507093.

[199] N. Strodthoff, B. Schaefer, and L. von Smekal, "Quark-meson-diquark model for two-color QCD," *Phys. Rev. D* **85** no. 7, (2012) 074007, arXiv:1112.5401.

[200] K. Kamikado, *et al.*, "Fluctuations in the quark-meson model for QCD with isospin chemical potential," *Phys. Lett. B* **718** no. 3, (2013) 1044–1053, arXiv:1207.0400.

[201] V. Skokov, *et al.*, "Vacuum fluctuations and the thermodynamics of chiral models," *Phys. Rev. D* **82** no. 3, (2010) 034029, arXiv:1005.3166.

[202] S. Coleman, "Fate of the false vacuum: Semiclassical theory," *Phys. Rev. D* **15** no. 10, (1977) 2929–2936.

[203] D. Jungnickel and C. Wetterich, "Effective action for the chiral quark-meson model," *Phys. Rev. D* **53** no. 9, (1996) 5142.

[204] N. Kaiser, "Isovector part of nuclear energy density functional from chiral two- and three-nucleon forces," *EPJ A* **48** no. 3, (2012) 1–9, arXiv:1203.6284v1.

[205] M. Drews, *et al.*, "Thermodynamic phases and mesonic fluctuations in a chiral nucleon-meson model," *Phys. Rev. D* **88** (2013) 096011, arXiv:1308.5596.

[206] M. Drews, *et al.*, "Dense nucleonic matter and the renormalization group," *EPJ web conf.* **66** (2014) 04008, arXiv:1307.6973.

[207] V. A. Karnaukhov, *et al.*, "Critical temperature for the nuclear liquid-gas phase transition (from multifragmentation and fission)," *Phys. Atom. Nuclei* **71** no. 12, (2008) 2067–2073, arXiv:0801.4485.

[208] J. B. Elliott, *et al.*, "Determination of the coexistence curve, critical temperature, density, and pressure of bulk nuclear matter from fragment emission data," *Phys. Rev. C* **87** no. 5, (2013) 054622.

[209] S. Typel, *et al.*, "Composition and thermodynamics of nuclear matter with light clusters," *Phys. Rev. C* **81** no. 1, (2010) 015803, arXiv:0908.2344.

[210] A. Akmal, V. R. Pandharipande, and D. G. Ravenhall, "Equation of state of nucleon matter and neutron star structure," *Phys. Rev. C* **58** no. 3, (1998) 1804–1828, arXiv:nucl-th/9804027.

[211] P. Armani, *et al.*, "Recent progress on the accurate determination of the equation of state of neutron and nuclear matter," *J. Phys.: Conf. Ser.* **336** (2011) 012014, arXiv:1110.0993.

[212] T. D. Cohen, R. J. Furnstahl, and D. K. Griegel, "Quark and gluon condensates in nuclear matter," *Phys. Rev. C* **45** no. 4, (1992) 1881–1893.

[213] R. L. Jaffe and C. L. Korpa, "The Pattern of Chiral Symmetry Breaking and the Strange Quark Content of the Proton," *Comments Nucl. Part. Phys.* **17** (1987) 163.

[214] J. Stahov, H. Clement, and G. J. Wagner, "Evaluation of the pion–nucleon sigma term from CHAOS data," *Phys. Lett. B* **726** no. 4–5, (2013) 685–690, arXiv:1211.1148.

[215] L. Alvarez-Ruso, *et al.*, "The nucleon mass and pion-nucleon sigma term from a chiral analysis of lattice QCD world data," *Phys. Rev. D* **88** no. 5, (2013) 054507, arXiv:1304.0483.

[216] M. Drews and W. Weise, "Functional renormalization group approach to neutron matter," arXiv:1404.0882.

[217] J. W. Holt, N. Kaiser, and W. Weise, "Chiral Fermi liquid approach to neutron matter," *Phys. Rev. C* **87** (2013) 014338, arXiv:1209.5296.

[218] S. Gandolfi, J. Carlson, and S. Reddy, "Maximum mass and radius of neutron stars, and the nuclear symmetry energy," *Phys. Rev. C* **85** no. 3, (2012) 032801, arXiv:1101.1921.

[219] A. Roggero, A. Mukherjee, and F. Pederiva, "Quantum Monte Carlo calculations of neutron matter with non-local chiral interactions," *Phys. Rev. Lett.* **112** (2014) 221103, arXiv:1402.1576.

[220] T. Hell and W. Weise, "Dense baryonic matter: constraints from recent neutron star observations," arXiv:1402.4098.

[221] S. Goda and D. Jido, "Pion properties at finite nuclear density based on in-medium chiral perturbation theory," *Prog. Theor. Exp. Phys.* **2014** no. 3, (2014) 33D03–0, arXiv:1312.0832.

[222] T. Yamazaki, *et al.*, "Discovery of deeply bound π^- states in the ^{208}Pb(d,^{3}He) reaction," *Z. Physik A* **355** no. 1, (1996) 219–221.

[223] H. Toki, *et al.*, "Structure and formation of deeply-bound pionic atoms," *Nucl. Phys. A* **501** no. 4, (1989) 653–671.

[224] M. Ericson and T. E. O. Ericson, "Optical properties of low-energy pions in nuclei," *Ann. Phys.* **36** no. 3, (1966) 323–362.

[225] T. Waas, R. Brockmann, and W. Weise, "Deeply bound pionic states and the effective pion mass in nuclear systems," *Phys. Lett. B* **405** no. 3–4, (1997) 215–218, arXiv:hep-ph/9704397v1.

[226] N. Kaiser and W. Weise, "Systematic calculation of s-wave pion and kaon self-energies in asymmetric nuclear matter," *Phys. Lett. B* **512** no. 3-4, (2001) 283–289, arXiv:nucl-th/0102062.

[227] T. D. Lee and G. C. Wick, "Vacuum stability and vacuum excitation in a spin-0 field theory," *Phys. Rev. D* **9** no. 8, (1974) 2291–2316.

[228] E. M. Nyman and M. Rho, "Abnormal nuclear matter and many-body forces," *Nucl. Phys. A* **268** no. 3, (1976) 408–444.

[229] E. M. Nyman and M. Rho, "Chiral symmetry and many-body forces in nuclei," *Phys. Lett. B* **60** no. 2, (1976) 134–136.

[230] E. M. Nyman and M. Rho, "Abnormal phase in dense neutron star matter," *Nucl. Phys. A* **290** no. 2, (1977) 493–500.

[231] G. Baym, C. Pethick, and D. Pines, "Superfluidity in Neutron Stars," *Nature* **224** no. 5220, (1969) 673–674.

[232] D. Page, *et al.*, "Stellar Superfluids," arXiv:1302.6626.

[233] J. M. Lattimer and M. Prakash, "What a Two Solar Mass Neutron Star Really Means," in *From Nuclei to Stars*, p. 275. World Scientific, Singapore, 2010. arXiv:1012.3208.

[234] S. Guillot, *et al.*, "Measurement of the Radius of Neutron Stars with High Signal-to-noise Quiescent Low-mass X-Ray Binaries in Globular Clusters," *ApJ* **772** no. 1, (2013) 7, arXiv:1302.0023.

[235] J. E. Trümper, "Observations of neutron stars and the equation of state of matter at high densities," *Prog. Part. Nucl. Phys.* **66** no. 3, (2011) 674–680.

[236] T. Tatsumi, N. Yasutake, and T. Maruyama, "Mixed phases during the phase transitions," in *Neutron Stars: The Aspect of High Density Matter, Equations of State and Observables*, pp. 199–231. Nova Science Publishers, 2012. arXiv:1107.0804.

[237] G. Baym, C. Pethick, and P. Sutherland, "The Ground State of Matter at High Densities: Equation of State and Stellar Models," *ApJ* **170** (1971) 299.

[238] F. Douchin and P. Haensel, "A unified equation of state of dense matter and neutron star structure," *Astron. & Astrophys.* **380** no. 1, (2001) 151–167, arXiv:astro-ph/0111092.

[239] K. Hebeler, *et al.*, "Equation of State and Neutron Star Properties Constrained by Nuclear Physics and Observation," *ApJ* **773** no. 1, (2013) 11, arXiv:1303.4662.

[240] J. Lattimer and M. Prakash, "Neutron Star Structure and the Equation of State," *ApJ* **550** (2001) 426–442.

[241] I. Bednarek, *et al.*, "Hyperons in neutron-star cores and a 2 $M_{\odot}$ pulsar," *Astron. & Astrophys.* **543** (2012) A157.

[242] S. Weissenborn, D. Chatterjee, and J. Schaffner-Bielich, "Hyperons and massive neutron stars: The role of hyperon potentials," *Nucl. Phys. A* **881** (2012) 62–77, arXiv:1111.6049.

[243] A. Ramos, J. Schaffner-Bielich, and J. Wambach, "Kaon Condensation in Neutron Stars," *Lect. Notes Phys.* **578** (2001) 175–202, arXiv:nucl-th/0011003.

[244] N. Gupta and P. Arumugam, "Role of higher order couplings in the presence of kaons in relativistic mean field description of neutron stars," *Phys. Rev. C* **85** no. 1, (2012) 015804, arXiv:1204.0101.

[245] A. R. Bodmer, "Collapsed Nuclei," *Phys. Rev. D* **4** no. 6, (1971) 1601–1606.

[246] E. Witten, "Cosmic separation of phases," *Phys. Rev. D* **30** no. 2, (1984) 272–285.

[247] M. Alford, *et al.*, "Astrophysics: Quark matter in compact stars?," *Nature* **445** no. 7125, (2007) E7–E8.

[248] K. Masuda, T. Hatsuda, and T. Takatsuka, "Hadron-quark crossover and massive hybrid stars," *Prog. Theor. Exp. Phys.* **2013** no. 7, (2013) 073D01, arXiv:1212.6803.

[249] M. E. Peskin and D. V. Schroeder, *An Introduction To Quantum Field Theory.* Perseus Books, Reading, MA, 1995.

[250] M. Nakahara, *Geometry, Topology and Physics.* Institut of Physics Publishing, Bristol, UK, 2003.

[251] J. C. Baez and J. P. Muniain, *Gauge Fields, Knots, and Gravity.* World Scientific, Singapore, 1994.

[252] V. G. Ivancevic and T. T. Ivancevic, *Applied Differential Geometry: A Modern Introduction.* World Scientific, Singapore, 2007.

[253] H. B. Lawson and M. Michelsohn, *Spin Geometry.* Princeton University Press, Princeton, NJ, 1990.

[254] D. J. Gross, "Gauge Theory—Past, Present and Future," *Chin. J. Phys.* **30** (1992) 955–972.